Development and Application of a Genetic Algorithm-based Tool for the Reduction and Optimization of Reaction Kinetic Mechanisms

Von der Fakultät für Ingenieurwissenschaften, Abteilung Maschinenbau und Verfahrenstechnik

der

Universität Duisburg-Essen

zur Erlangung des akademischen Grades

einer

Doktorin der Ingenieurwissenschaften

Dr.-Ing.

genehmigte Dissertation

von

Nejra Šikalo
aus
Sarajevo – Bosnien und Herzegowina

Gutachter: Univ.-Prof. Dr.-Ing. Andreas Kempf
Univ.-Prof. Dr. rer. nat. Tina Kasper

Tag der mündlichen Prüfung: 23.08.2017

Declaration of Authorship

I, Nejra Šikalo, declare that this thesis entitled, "Development and Application of a Genetic Algorithm-based Tool for the Reduction and Optimization of Reaction Kinetic Mechanisms" and the presented work are my own. This work was done while in candidature for a research degree at University Duisburg-Essen. This thesis has not been previously submitted for a degree or any other qualification at any oher institution. The published work of others has been referenced clearly.

Signed: Nejra Šikalo

Date: 24.05.2017

Abstract

An automatic method for the reduction and optimization of chemical kinetic mechanisms under specific physical or thermodynamic conditions has been developed and described in this work. The mechanism reduction method relies on the genetic algorithm (GA) search for a smallest possible subset of reactions from the detailed mechanism while still preserving the ability of the reduced mechanism to describe the overall chemistry at an acceptable error. Accuracy of the reduced mechanism is determined by comparing its solution to the solution obtained with the full mechanism under the same initial and/or physical conditions. For the reduction, not only the chemical accuracy and the size of the mechanism are considered but also the time for its solution which helps to avoid stiff and slow-converging mechanisms.

The (subsequent) optimization technique is based on a genetic algorithm that aims at finding new reaction rate coefficients to restore the accuracy which is usually decreased by the preceding reduction process. The accuracy is defined by an objective function that covers regions of interest where the reduced mechanism may deviate from the original mechanism. The objective function directs the search towards more accurate reduced mechanisms that are valid for a given set of operating conditions. The mechanism's performance is assessed for homogeneous-reactor or laminar-flame simulations against the results obtained from a given reference.

An additional term introduced to the objective function is a so-called penalty term that influences the reaction rates during the optimization. With the penalty term, the change to the reaction rates can be minimized, keeping them as close as possible to their nominal values. It is demonstrated that the penalty function can be used instead of defining the uncertainty bounds from the literature for each reaction in the mechanism, which can be a tremendous effort when dealing with large or insufficiently investigated mechanisms. The penalty term can also be used for further reduction of the mechanism by driving the reaction rates towards zero during the optimization. This approach is addressed in a greater detail in the final section of the thesis which shows the convergence behaviour of the integer-coded reduction, the real-coded optimization and reduction of the reduced mechanisms and the real-coded-optimization and reduction of the full mechanism. The convergence study shows that the real-coded optimization with the size-penalty function exhibits the fastest convergence towards one global optimum, which makes a good case for investigating and improving the real-coded reduction as a direct way to optimize and reduce the full mechanism at the same time. The GA-based reduction and optimization method has shown to be robust, flexible, and applicable to a range of operating conditions by using multiple criteria simultaneously.

Zusammenfassung

In dieser Arbeit wurde eine automatische Methode zur Reduktion und Optimierung von chemischen kinetischen Mechanismen unter spezifischen physikalischen oder thermodynamischen Bedingungen entwickelt und beschrieben. Die Reduktion des Mechanismus beruht auf dem genetischen Algorithmus (GA), der nach einer kleinstmöglichen Untermenge von Reaktionen aus dem detaillierten Mechanismus sucht, während er die Fähigkeit des reduzierten Mechanismus noch bewahrt, die Gesamtchemie bei einem akzeptablen Fehler zu beschreiben. Die Genauigkeit des reduzierten Mechanismus wird durch Vergleich seiner Lösung mit der Lösung, die mit dem vollständigen Mechanismus unter den gleichen Anfängsbedingungen und/oder physikalischen Bedingungen erhalten wird, bestimmt. Für die Reduktion werden nicht nur die chemische Genauigkeit und die Größe des Mechanismus berücksichtigt, sondern auch die Simulationszeit, die hilft, steife und langsam konvergierende Mechanismen zu vermeiden.

Die (nachfolgende) Optimierungstechnik basiert auf einem genetischen Algorithmus, der darauf abzielt, neue Koeffizienten der Reaktionsgeschwindigkeiten zu finden, um die Genauigkeit die üblicherweise durch den vorhergehenden Reduktionsvorgang verringert wird, wiederherzustellen. Die Genauigkeit wird durch eine Zielfunktion definiert, die Bereiche vom Interesse abdeckt, in denen der reduzierte Mechanismus von dem ursprünglichen Mechanismus abweichen kann. Die Zielfunktion lenkt die Suche nach genaueren reduzierten Mechanismen, die für einen bestimmten Satz von Betriebsbedingungen gültig sind. Die Leistung des Mechanismus wird für Simulationen von homogenem Reaktor oder laminaren Flammen gegenüber den Ergebnissen aus einer gegebenen Referenz bewertet.

Ein zusätzlicher Term, der in der Zielfunktion eingeführt wird, ist ein sogenannter Strafterm, der die Reaktionsgeschwindigkeiten während der Optimierung beeinflusst. Mit dem Strafterm kann die Änderung der Reaktionsgeschwindigkeiten minimiert werden, sodass sie so nah wie möglich an ihren Startwerten gehalten werden. Es wird gezeigt, dass der Strafterm verwendet werden kann, anstatt die Unsicherheitsgrenzen aus der Literatur für jede Reaktion im Mechanismus zu definieren. Der Strafterm kann auch zur weiteren Reduzierung des Mechanismus verwendet werden, indem die Reaktionsgeschwindigkeiten während der Optimierung auf Null gestellt werden. Dieser Ansatz wird im letzten Abschnitt der Arbeit näher erläutert.

Es wird das Konvergenzverhalten der ganzzahlig codierten Reduktion, der realcodierten Optimierung und Reduktion der reduzierten Mechanismen, sowie der realcodierten Optimierung und Reduktion des vollständigen Mechanismus analysiert. Die Konvergenzstudie zeigt, dass die realcodierte Optimierung mit dem Strafterm die schnellste Konvergenz zu einem globalen Optimum hat. Das bietet einige neue Möglichkeiten für die Erforschung und Verbesserung der realcodierten Reduktion, als direkten Weg zur gleichzeitigen Optimierung und Reduzierung des vollen Mechanismus.

Die GA-basierte Reduktions- und Optimierungsmethoden haben sich als robust, flexibel und anwendbar für eine Reihe von Betriebsbedingungen erwiesen, indem gleichzeitig mehrere Kriterien betrachtet werden sollen.

Acknowledgements

The present work was conducted during my PhD studies at the chair of Fluid Dynamics, Institute for Combustion and Gas Dynamics at the University of Duisburg-Essen.

I would like to thank my supervisor Prof. Dr.-Ing. Andreas Kempf for his guidance, many fruitful discussions and his support throughout my PhD study. I am also grateful for his enthusiasm for my work and encouragement to publish it.

I would like to thank Prof. Dr. Christof Schulz for enabling me to start my PhD at IVG and for his supervision during my first years at the IVG and also for his professional support in publishing my work in international journal.

My special gratitude goes to my co-examiner Prof. Dr. Tina Kasper for her interest in evaluating my thesis. I am grateful to Prof. Dr. Markus Winterer and Prof. Dr.-Ing. Alfons Fischer for serving as the members of my dissertation committee.

I wish to thank my group leader Dr.-Ing. Irenaeus Wlokas for his encouragement and thoughtful support with his knowledge and ideas from the beginning of my stay at the chair of Fluid Dynamics.

I am deeply grateful to Olaf Hasemann who generously offered me his expertise in software development and provided me with his extensive advice on optimization that were crucial to my work. He was never too tired for a good discussion on new ideas and results of my work and I have learned a lot from him.

I would also like to thank all my colleagues, former and present, for making my PhD years unforgettable: Sebastian Hardt, Claudia Weise, Thuong Minh Nguyen, Lei Deng, Peter Janas, Andreas Rittler, Fabian Proch, Miriam Rabaçal, Martin Rieth, Hossein Janbazi, Eray Inanc, Patrick Wollny, Johannes Sellmann, Timo Lipkowicz, Khadijeh Mohri, Vahid Sharifi, Pascal Gruhlke and Luis Cifuentes. I heartily thank Thuong for his friendship and everlasting positive attitude during our writing times. I thank Peter Janas for his detailed proof-reading of my thesis prior to the submission. My special thanks go to Sylvia Helwig for her administrative assistance and friendliness.

My warmest graditute goes to my parents and my sister who encouraged me to pursue my PhD in Germany and provided me with their love and support throughout my whole life. Finally, I thank my husband Amer for his love, encouragement and patience throughout the challenges of my research and life.

Contents

List of Figures

List of Tables

Abbreviations

CFD	**C**omputational **F**luid **D**ynamics
CSP	**C**omputational **S**ingular **P**erturbation
DRG	**D**irected **R**elation **G**raph
EFA	**E**lemental **F**lux **A**nalysis
GA	**G**enetic **A**lgorithm
ILDM	**I**ntristic **L**ow **D**imensional **M**anifolds
LOI	**L**evel of **I**mportance
MUM-PCE	**M**ethod of **U**ncertainty **M**inimization using **P**olynomial **C**haos **E**xpansions
NIST	**N**ational **I**nstitute of **S**tandards and **T**echnology
ODE	**O**rdinary **D**ifferential **E**quations
PEA	**P**artial **E**quilibrium **A**ssumption
PSR	**P**erfectly-**S**tirred **R**reactors
QSSA	**Q**uasi **S**teady **S**tate **A**ssumption
SA	**S**ensitivity **A**nalysis

Symbols

A_i	pre-exponential constant in Arrhenius expression	varies
A_0	low-pressure limit of pre-exponential constant	varies
A_∞	high-pressure limit of pre-exponential constant	varies
A	area	m^2
c_p	specific heat capacity of a mixture at constant pressure	J/(kg K)
c_{pk}	specific heat capacity at a constant pressure	J/(kg K)
c_{pk}^M	molar heat capacity at a constant pressure of the component k	J/(mol K)
c_v	specific heat capacity of a mixture at constant volume	J/(kg K)
c_{vk}	specific heat capacity at a constant volume	J/(kg K)
c_{vk}^M	molar heat capacity at a constant volume of the component k	J/(mol K)
D_{kj}	element of the matrix of ordinary multicomponent diffusion components	m^2/s
D'_{km}	mixture-averaged diffusion coefficient	m^2/s
$\mathcal{D}_{ij}$	binary mass diffusion coefficient	m^2/s
$\mathcal{D}_{kk}$	self-diffusion coefficient	m^2/s
$E_{a,i}$	activation energy in Arrhenius expression	J/mol
E_0	low-pressure limit of activation energy	J/mol
E_∞	high-pressure limit of activation energy	J/mol
e	specific internal energy	J/kg
e_s	specific sensible energy	J/kg
$\mathbf{F}$	force vector	N
$F(T, P_r)$	fall-off function	
f_ξ	normalization function for optimization target ξ	
f_{obj}	overall objective function	
$f_{obj,c}$	objective function for a single set of operating conditions	

$f_{\text{rot.}}$	rotational contribution to the thermal conductivity	
$f_{\text{trans.}}$	translational contribution to the thermal conductivity	
$f_{\text{vib.}}$	vibrational contribution to the thermal conductivity	
h	specific enthalpy of the mixture	J/kg
h	time step size	s
h_s	specific enthalpy of the mixture	J/kg
h_s^0	specific formation enthalpy of the mixture	J/kg
i	index for chemical reactions	
$\mathbf{J}$	Jacobian matrix	
$\mathbf{j}_k$	diffusive mass flux of species k	kg/(m^{2}s)
$K_{c,i}$	equilibrium constant in the concentration units	varies
$K_{p,i}$	equilibrium constant in the pressure units	
k_0	rate constant for low-pressure limit	varies
k_∞	rate constant for high-pressure limit	varies
$k_{\text{fwd},i}$	forward reaction rate constant	varies
$k_{\text{rev},i}$	reverse reaction rate constant	varies
M	total molar mass	kg/mol
M_k	molar mass of the individual component k	kg/mol
m	mass	kg
$\dot{m}''$	net mass flux	kg/s
m_{ij}	reduced mass of molecules i and j	
m_k	mass of the individual component k	kg
N	extensive variable in conservation equations	varies
N_R	number of reactions	
N_s	number of species in the mixture (mechanism)	
n	amount of substance	mol
n_k	amount of substance of the individual component k	mol
$\mathbf{P}$	momentum vector	kg m/s
p	pressure	Pa
p^0	standard-state pressure	Pa
p_k	partial pressure of species k	Pa
P_r	reduced pressure	
Q	heat flow into the system	W

q_i	rate of progress of reaction i	mol/(m^{3}s)
r	radial coordinate	m
R_{mk}	gas constant of the individual species k	J/(kg K)
$\mathbf{S}$	sensitivity matrix	varies
s	specific entropy of the mixture	J/(kg K)
s_k	specific entropy of the species k	J/(kg K)
s_k^0	standard-state specific entropy of the species k	J/(kg K)
s_L	laminar burning velocity	m/s
S	entropy	J/K
t	time	s
T	temperature	K
T_∞	environmental temperature	K
T	stress tensor	N/m^2
U	velocity function in axisymmetric stagnation flow	kg/(m^{2}s)
u	axial velocity	m/s
V	volume	m^3
$\mathbf{V}$	fluid velocity vector	m/s
$\mathbf{V}_k$	diffusion velocity vector of the species k	m/s
$\tilde{\mathbf{V}}_k$	average velocity vector of the species k	m/s
v	radial velocity	m/s
W	work done on the system	J
W	circumferenial velocity component scaled by radius	
X_k	mole fraction of the component k	
$[X_k]$	mole concentration of component k	mol/m^3
$[X_k]_{\text{equil}}^{\nu'_{k,i}}$	equilibrium value of the molar concentration, forward	mol/m^3
$[X_k]_{\text{equil}}^{\nu''_{k,i}}$	equilibrium value of the molar concentration, reverse	mol/m^3
Y_k	mass fraction of the component k	
y	solution of ODE	
α	heat transfer coefficient	W/(m^{2}K)
β_i	temperature exponent in Arrhenius expression	
β_0	low-pressure limit of temperature exponent	
β_∞	high-pressure limit of temperature exponent	

γ	adiabatic index	
ΔH_i^0	net change in enthalpy	J/mol
ΔS_i^0	net change in entropy	J/K
$\Delta h_{f,k}^0$	mass enthalpy of formation for species k	J/kg
$\Delta h_{f,k}^{0,M}$	molar enthalpy of formation for species k	J/mol
δ_{ij}	Kronecker delta	
δV	control volume	m^3
$\epsilon_{k,i}$	collision efficiency of third body k	
η	intensive variable in conservation equations	varies
ξ_{ref}	reference value of optimization target ξ	
ξ_{red}	value predicted by the reduced mechanism	
Λ_r	pressure curvature	N/m^4
λ	heat conductivity	W/(m K)
λ_k	pure species thermal conductivity	W/(m K)
μ	dynamic viscosity of the fluid	kg/(m s)
$\nu_{k,i}$	molar stochiometric coefficient difference	
$\nu'_{k,i}$	molar stochiometric coefficient, forward direction	
$\nu''_{k,i}$	molar stochiometric coefficient, reverse direction	
Φ	dissipation function	kg/(m s^3)
ρ	density	kg/m^3
ρ_k	density of the individual component k	kg/m^3
σ_{ij}	length scale in the two molecules interaction	m
τ	component of the stress vector	N/m^2
$\Omega_{ij}^{(1,1)*}$	collision integral	m^3/s
$\dot{\omega}_k$	rate of production of species k	mol/(m^3 s)

Physical Constants

Avogadro constant $N_A = 6.022140857 \cdot 10^{23}$ mol^{-1}

Bolzmann constant $k_B = 1.38064852 \cdot 10^{-23}$ JK^{-1}

Universal gas constant $R = 8.3144598$ $\text{JK}^{-1}\text{mol}^{-1}$

Chapter 1

Introduction

Combustion plays a significant role in almost every aspect of human lives and will continue as the technological demands and development evolve. Energy obtained from combustion is primarily needed for heat and power. For instance, the challenges we face today include conservation of energy, addressing the problem of global climate change, environmental concerns, and together these require more efficient and cleaner combustion. Beyond energy, combustion plays an important role in process technology and materials science.

Combustion encompasses a great variety of phenomena with wide application in industry, the science and its application is based on knowledge of physics, chemistry, and fluid mechanics; their interrelationship becomes particularly evident in treating flame propagation. The rapid development of computational capabilities enabled further fundamental studies and increased the confidence in predicting important combustion phenomena by integrating comprehensive chemical descriptions into reacting flow simulations [90]. Research on combustion phenomena has been growing rapidly since the early 1970s, being motivated by concerns for energy efficiency, safety and air pollution followed by fast advances in computational and experimental capabilities. Combustion research has grown in many aspects, for example, in chemical kinetics, both laminar and turbulent flames, explosions and heterogeneous combustion. It has been found that the research on laminar flames is of a particular importance because a wide range of combustion phenomena can be described by treating the laminar flames as their elemental unit [89]. Furthermore, technological advances demand further studies of complex fuels and fuel blends as they seem to be promising alternatives to oil-derived fuels. Combustion characteristics of these multi-component fuels are difficult to predict because of their composition complexity and lack of experimental data for large molecules these fuels are made of. Most of these complex molecules have a large number of isomers for which the transport and thermodynamic properties are still unknown. Chemical kinetics of

complex hydrocarbons and their blends is uncertain to a great extent, which makes the prediction and research on the combustion characteristics more difficult. For all these reasons, development of comprehensive reaction mechanisms for computational fluid dynamics (CFD) calculations is fundamental.

1.1 Motivation

Comprehensiveness of a detailed reaction mechanism is crucial for a reliable description of different combustion phenomena over a range of thermodynamic conditions. There is no theory which can indicate whether the given mechanism is complete in terms of its elementary reactions; the measure of its comprehensiveness is the ability of the mechanism to cover all possible combustion phenomena over all observed ranges of conditions [90]. Typical phenomena a comprehensive mechanism should cover include ignition (with and without the diffusion effects), laminar steady flames, flame quenching, premixed and non-premixed combustion, explosions, unsteady effects, pollutant chemistry, and all that under varying pressure, equivalence ratio and composition of the reacting mixture. The purpose of a detailed mechanism is not only to reproduce the available experimental results it was validated against, but also to predict chemical behavior of the system for which the experimental investigation is difficult, too expensive or impossible. Furthermore, detailed mechanisms also provide insight into chemical processes. The detailed chemical mechanisms are not only used for combustion modelling but also for other purposes, for example for atmospheric chemistry [10]. Increasing the comprehensiveness of the mechanism correspondingly increases the demand on the computational resources. However, because the comprehensiveness and size of a detailed mechanism are proportional to the number of phenomena and parameters the mechanism was developed for, the mechanism can be reduced if the range of conditions for which it will be used is limited. For example, if one is not interested in predicting emissions of NO_x, then the nitrogen kinetics may not be considered. However, a complete elimination of nitrogen chemistry might influence the catalysing effect of nitrogen in hydrocarbon species formation/consumption. Therefore, elimination of species and/or reactions from a mechanism is not a trivial task [90].

1.2 Objectives and Outline

The present work is dedicated to developing a software tool for the analysis, reduction and optimization of the reaction mechanisms on simple models (transient reactors and one-dimensional laminar flames) to make them less expensive for further application in

large-scale CFD simulations. The aim is to design a reduction and optimization method which is easy to use, does not require in-depth chemical knowledge from the user, robust, applicable to a wide range of reaction mechanisms and flexible in terms of a desired trade-off between the accuracy of the resulting mechanism and its computational cost. The present thesis is structured as follows: Chapter 1 introduces the significance of investigating chemically reacting flows and popular trends in combustion science. Then, the mathematical modelling of the reacting flows with specific attention to laminar flames and homogeneous reactors (which are used for mechanism evaluation in this work) followed with detailed description of finite-rate chemistry modelling and the need for mechanism simplification is described in Chapter 2. Chapter 3 gives an overview of the most popular existing methods for mechanism reduction and optimization. The reduction/optimization method developed in this work is described in Chapter 4 and its important aspects are then demonstrated for several different mechanisms in Chapter 5. A summary of the presented work and recommendations for the future work are outlined in Chapter 6.

Chapter 2

Modelling of Reacting Flows

The aim of this chapter is to provide an overview of mathematical representations of reacting flows, with specific attention to zero- and one-dimensional models as these are used in the present work. These models are often used as a base for approximating more complex systems as well.

Reacting flows are modelled using equations which govern fluid flows extended by additional terms to account for the chemistry. Unlike non-reacting flows, reacting flows must be described as a mixture of multiple components that react, thus contributing to variations in the composition and temperature of the mixture. Interactions between chemically reacting components (species) are usually described by a system of ordinary differential equations (ODEs). In the following sections, the mathematical modelling of reacting cases is explained in greater detail.

2.1 Thermodynamic Quantities of a Multicomponent Gas

For a complete understanding of the chemistry in a multicomponent gas consisting of N_s components, it is important to clarify basic relations between different measures of concentration for each component.

Mass-based Quantities

Mixture density ρ is the total mass m of the mixture per occupied volume V:

$$\rho = \frac{m}{V} \tag{2.1}$$

The total mass m of the mixture is the sum of masses m_k of its individual components:

$$m = \sum_{k=1}^{N_s} m_k, \tag{2.2}$$

therefore the mixture density in terms of partial densities ρ_k of the components is:

$$\rho = \frac{m}{V} = \frac{1}{V} \sum_{k=1}^{N_s} m_k = \sum_{k=1}^{N_s} \rho_k \tag{2.3}$$

The mass fraction of the individual component Y_k is the component mass m_k divided by the total mass of the mixture m:

$$Y_k = \frac{m_k}{m} = \frac{\rho_k}{\rho} \tag{2.4}$$

Therefore, $\sum_{k=1}^{N_s} Y_k = 1$.

Amount-of-Substance-based Quantities

Amount of substance is a quantity proportional to the number of entities (e.g. atoms, molecules, ions) in a given sample of substance. The standard unit of the amount of substance in the International System of Units is the mole, which is defined as the amount of substance that contains an equal number of elementary entities as there are atoms in 12 g of the isotope carbon-12 (^{12}C). This number is the numerical value of the Avogadro constant $N_A = 6.022140857 \cdot 10^{23}$ mol^{-1}.

Total molar mass M of the mixture is equal to its total mass m divided by the total amount of substance n of the mixture:

$$M = \frac{m}{n} \tag{2.5}$$

Analogously, the molar mass M_k of the component k is the mass m_k divided by the amount of substance n_k of the component:

$$M_k = \frac{m_k}{n_k} \tag{2.6}$$

Molar concentration $[X_k]$ of the component k, is the amount of substance of the component k contained in a unit volume of the mixture. Knowing the relation between the amount of substance of any species, n_k, its mass m_k and its molar mass M_k, mass

concentration of the species k is related to its molar concentration $[X_k]$ by:

$$[X_k] = \frac{\rho_k}{M_k} \tag{2.7}$$

Mole fraction X_k of the species k is the ratio of the amount of substance of the component k in a volume V to the total amount of substance n in the same volume:

$$X_k = n_k/n \tag{2.8}$$

Therefore, $\sum_{k=1}^{N_s} X_k = \sum_{k=1}^{N_s} n_k/n = 1$. The mean molar mass M of the mixture can be now defined as:

$$M = \sum_{k=1}^{N_s} M_k X_k \tag{2.9}$$

Thermal Equation of State for an Ideal Gas

If the observed multicomponent mixture is an ideal gas, relations between the mass terms and the molar terms are obtained using the ideal gas law:

$$\rho = \frac{pM}{RT}, \tag{2.10}$$

or in terms of the molar concentration of the components in the mixture

$$p = \sum_{k=1}^{N_s} [X_k] RT, \tag{2.11}$$

where p is the thermodynamic pressure, $R = 8.314\ \mathrm{J/(mol \cdot K)}$ is the universal gas constant, and T is the temperature of the gas. The mass and the mole fraction of the component k are related by:

$$Y_k = \frac{X_k M_k}{M} \tag{2.12}$$

Mean molecular mass of the mixture now can be expressed as:

$$M = \left(\sum_{k=1}^{N_s} \frac{Y_k}{M_k} \right)^{-1} \tag{2.13}$$

Molar concentration in terms of mass and mole fractions is

$$[X_k] = \frac{\rho Y_k}{M_k} \quad \text{and} \quad [X_k] = \frac{\rho X_k}{M} \tag{2.14}$$

For an ideal mixture of N_s gases, the total pressure p is the sum of the partial pressures p_k of the components k:

$$p = \sum_{k=1}^{N_s} p_k \quad \text{where} \quad p_k = \frac{\rho RT}{M_k} \tag{2.15}$$

Expressing the mixture composition as mass fraction Y_k yields:

$$p = \frac{1}{V} \sum_{k=1}^{N_s} n_k RT = \rho \frac{Y_k RT}{M_k} \tag{2.16}$$

The thermodynamic properties of the reacting gas change significantly with the temperature and the gas composition. Therefore, the energy expressions for reacting gases are more complex than those used in classical fluid dynamics. For ideal gases, the pressure dependence of thermodynamic properties is negligible [74]. The specific heat capacities of the component k at a constant volume c_{vk} and at a constant pressure c_{pk} are related by

$$c_{pk} - c_{vk} = R_{mk}, \tag{2.17}$$

where R_{mk} is the gas constant of the individual component k, $R_{mk} = R/M_k$.

The specific heat capacity c_{pk} is the quantity expressed per unit mass of the component k and is related to its molar heat capacity c_{pk}^M by $c_{pk} = c_{pk}^M/M_k$. Analogously, $c_{vk} = c_{vk}^M/M_k$ The specific heat capacity of the multicomponent mixture at a constant pressure can be expressed as:

$$c_p = \sum_{k=1}^{N_s} c_{pk} Y_k = \sum_{k=1}^{N_s} c_{pk}^M Y_k / M_k \tag{2.18}$$

and at a constant volume as:

$$c_v = \sum_{k=1}^{N_s} c_{vk} Y_k = \sum_{k=1}^{N_s} c_{vk}^M Y_k / M_k \tag{2.19}$$

Since the heat capacities are functions of the temperature and the mass fractions of the species in the reacting mixture, they may change significantly from one point to another. For practical purposes, specific heat capacities for single species are often represented in the form of temperature-dependent polynomials [27]. The ratio of the heat capacity at constant pressure to the heat capacity at constant volume is an adiabatic index $\gamma = c_p/c_v$.

Specific enthalpy of the mixture is

$$h = h_s + \sum_{k=1}^{N_s} \Delta h^0_{f,k} Y_k, \tag{2.20}$$

where h_s is the sensible specific enthalpy of the mixture expressed as:

$$h_s = \int_{T_0}^{T} c_p dT \tag{2.21}$$

and $h^0_{f,k}$ is the specific enthalpy of formation for species k at the reference temperature $T_0 = 298,15$ K, which is the standard-state temperature at which the experimental data for $h^0_{f,k}$ are obtained. The standard-state enthalpy of formation is sometimes available from theory. Alternatively, for many classes of species the enthalpies of formation can be estimated using "group additivity" rules [14–16]. Analogously to Eq. 2.20, the specific internal energy of the mixture is:

$$e = e_s + \sum_{k=1}^{N_s} \Delta h^0_{f,k} Y_k, \tag{2.22}$$

where the sensible energy is:

$$\begin{aligned} e_s &= h_s - p/\rho = \int_{T_0}^{T} c_p dT - RT/M = \int_{T_0}^{T} (c_v + R/M)\, dT - RT/M \\ &= \int_{T_0}^{T} c_v dT + \int_{T_0}^{T} (R/M)\, dT - RT/M \end{aligned}$$

Thus

$$e_s = \int_{T_0}^{T} c_v dT - RT_0/M \tag{2.23}$$

$$h_k = \int_{T_0}^{T} c_{pk} dT + \Delta h^0_{f,k} \tag{2.24}$$

The relation between the mass and the molar enthalpy of formation for species k is:

$$\Delta h^0_{f,k} = \Delta h^{0,M}_{f,k} / M_k$$

The total specific enthalpy of the system is:

$$h = \sum_{k=1}^{N_s} h_k Y_k = \sum_{k=1}^{N_s} \left(\int_{T_0}^{T} c_{pk} dT + \Delta h^0_{f,k} \right) Y_k = \int_{T_0}^{T} c_{pk} dT + \sum_{k=1}^{N_s} \Delta h^0_{f,k} Y_k \tag{2.25}$$

Enthalpy and energy are related by the specific work done by an applied pressure p by $e = h - p/\rho$. Therefore, it can be written:

$$\begin{aligned} e &= \sum_{k=1}^{N_s} \left(\int_{T_0}^{T} c_{pk} dT - RT/M_k + \Delta h^0_{f,k} \right) Y_k \\ &= \sum_{k=1}^{N_s} \left(\int_{T_0}^{T} c_{vk} dT - RT_0/M_k + \Delta h^0_{f,k} \right) Y_k \\ &= \int_{T_0}^{T} c_{vk} dT - RT_0/M + \sum_{k=1}^{N_s} \Delta h^0_{f,k} Y_k \end{aligned}$$

Thus

$$e = \sum_{k=1}^{N_s} e_k Y_k \tag{2.26}$$

Specific entropy of the species k is defined as:

$$s_k = s^0_k - \frac{R}{M_k} \ln X_k - \frac{R}{M_k} \ln \frac{p}{p^0} \tag{2.27}$$

where s^0_k is a standard-state specific entropy at standard pressure $p^0 = 101325$ Pa defined as:

$$s^0_k = \int_{T_0}^{T} \frac{c^0_{pk}}{T} dT + s_k(0) \tag{2.28}$$

The specific entropy of the mixture is therefore:

$$s = \sum_{k=1}^{N_s} \left(s^0_k - \frac{R}{M_k} \ln X_k - \frac{R}{M_k} \ln \frac{p}{p^0} \right) X_k \tag{2.29}$$

In practice, the specific entropy and the specific enthalpy for single species are, analogously to the specific heat capacities, usually represented as temperature-dependent polynomials [27]. The polynomial NASA parametrization is shown in section 2.5.1.

2.2 Conservation Laws - Low Mach Number Assumption

Conservation equations describe the fluid motion, heat and mass transport processes and consider the chemical reactions between the fluid components (if the fluid is a mixture of many different components). Derivation of these equations can be found in some standard books such as from Kee et al. [74], Kuo [82], Poinsot and Veynante [139], Williams [198] and Yeoh and Yuen [202]. The conservation equations considered in the present work are given as partial differential equations in the Eulerian framework

(i.e. the control volumes are "fixed" in space through which the fluid flows). Spatial coordinates and time are independent variables.

The conservation laws are quantitatively related to the fixed control volume (CV) by the substantial derivative as (here, density is constant):

$$\left(\frac{dN}{dt}\right)_{\text{system}} = \left[\rho\frac{D\eta}{Dt}\right]_{\text{CV}} \delta V, \tag{2.30}$$

where N is the extensive variable (e. g. total mass, momentum or energy), ρ is the fluid mass density and η is the intensive variable ($\eta = N/m$).

For the Eulerian control volume, the Reynolds transport theorem gives the momentum conservation as:

$$\left[\rho\frac{D\mathbf{V}}{Dt}\right]_{\text{control volume}} \delta V = \sum \mathbf{F} \tag{2.31}$$

where $\mathbf{V}$ is the fluid velocity vector. In general, the conservation law states that the rate of accumulation of an extensive property is equal to the net transport rate of the property across the surface bounding the system plus the net rate of internal generation of the property (creation minus destruction):

$$\left(\frac{dN}{dt}\right)_{\text{system}} = \left(\dot{N}_{\text{in}} - \dot{N}_{\text{out}}\right) + \dot{N}_{\text{gen}} \tag{2.32}$$

Mass Conservation (Continuity Equation)

The continuity law states that no mass can be created or destroyed within the observed control volume. Chemical reactions produce and destroy individual species, but the overall mass does not change, and is only transported by convection. Here, the extensive variable from Eq. 2.30 is mass ($N = m$) and the intensive variable is $\eta = 1$. The continuity equation in differential form can be written as:

$$\frac{D\rho}{Dt} + \rho\boldsymbol{\nabla}\cdot\mathbf{V} = 0 \tag{2.33}$$

Momentum Conservation (Navier-Stokes Equations)

The conservation of momentum is generally stated as:

$$\left(\frac{d\mathbf{P}}{dt}\right)_{\text{system}} = \sum \mathbf{F}, \tag{2.34}$$

where the momentum vector is $\mathbf{P}$, time is t and $\mathbf{F}$ are the forces acting on the system. The extensive variable (Eq. 2.30) is the momentum vector ($N = \mathbf{P}$) and intensive variable is the velocity vector $\eta = \mathbf{V}$, as the momentum is $\mathbf{P} = m\mathbf{V}$.

A general differential form of the Navier-Stokes equations for a constant density is:

$$\rho\frac{d\mathbf{V}}{dt} + \rho\left(\mathbf{V}\cdot\boldsymbol{\nabla}\right)\mathbf{V} = \rho\mathbf{g} + \boldsymbol{\nabla}\cdot\mathsf{T} + \mu\boldsymbol{\nabla}^2\mathbf{V} = \rho\mathbf{g} - \boldsymbol{\nabla}p + \boldsymbol{\nabla}\cdot\mathsf{T}' + \mu\boldsymbol{\nabla}^2\mathbf{V}, \tag{2.35}$$

where T is the stress tensor generally represented in terms of nine components of the stress vector τ as:

$$\mathsf{T} = \begin{pmatrix} \tau_{ii} & \tau_{ij} & \tau_{ik} \\ \tau_{ji} & \tau_{jj} & \tau_{jk} \\ \tau_{ki} & \tau_{kj} & \tau_{kk} \end{pmatrix} \tag{2.36}$$

The viscous tensor is formulated as:

$$\tau_{ij} = -\frac{2}{3}\mu\frac{\partial u_k}{\partial x_k}\delta_{ij} + \mu\left(\frac{\partial u_i}{\partial x_j} + \frac{\partial u_j}{\partial x_i}\right), \tag{2.37}$$

where μ is the dynamic viscosity of the fluid and δ_{ij} is the Kronecker symbol

$$\delta_{ij} = \begin{cases} 1 & \text{if } i = j \\ 0 & \text{otherwise.} \end{cases}$$

Although the Navier-Stokes equations are non-linear differential equations that cannot be solved analytically, there are situations that allow significant simplifications of the equations. In case of incompressible flows, the velocity divergence term can be neglected, i.e. $\boldsymbol{\nabla}\cdot\mathbf{V} \approx 0$ owing to the fact that the fluid density remains constant independent from changes in its velocity and pressure. Another criterion for compressibility is associated to the speed of sound throughout the fluid, which in case of liquids is very high. When the speed of sound is much higher than the fluid velocities, the fluid is considered incompressible. Although the gases are compressible, from the Navier-Stokes equations point of view, they behave as incompressible when their velocities are low as the pressure variations are small and the density remains constant. For the continuity equation 2.33, that means:

$$\boldsymbol{\nabla}\cdot(\rho\mathbf{V}) = \mathbf{V}\cdot(\boldsymbol{\nabla}\rho) + \rho\boldsymbol{\nabla}\cdot\mathbf{V} = 0 \tag{2.38}$$

The flow acts as incompressible when

$$|\mathbf{V}\cdot(\boldsymbol{\nabla}\rho)| \ll |\rho\boldsymbol{\nabla}\cdot\mathbf{V}| \tag{2.39}$$

Species Conservation

The continuity equation does not consider the composition of the flow, which may consist of multiple species. Furthermore, the mass continuity equation does not include the diffusion of molecules across the control surfaces and there is no creation nor destruction of the overall mass, which clearly does not apply to individual species taking part in chemical reaction. In the conservation equation for the individual species, the extensive variable is the mass m_k of the individual species k ($N = m_k$) and the intensive variable is its mass fraction $Y_k = m_k/m$ ($\eta = Y_k$). In a Eulerian framework, the differential form of the species conservation equation is given by:

$$\rho \frac{DY_k}{Dt} = -\boldsymbol{\nabla} \cdot \mathbf{j}_k + \dot{\omega}_k M_k, \tag{2.40}$$

where $\mathbf{j}_k$ is the diffusive mass flux and $\dot{\omega}_k$ is the rate of production of species k.

The diffusive mass flux is defined as:

$$\mathbf{j}_k = \rho_k \left(\widetilde{\mathbf{V}}_k - \mathbf{V} \right) = \rho_k \mathbf{V}_k = \rho Y_k \mathbf{V}_k, \tag{2.41}$$

where $\widetilde{\mathbf{V}}_k$ is the average velocity vector of species k relative to fixed coordinates, $\mathbf{V}$ is the mass average velocity vector, and $\mathbf{V}_k$ is the diffusion velocity vector for the species k. (The mass-flux vector is positive for the mass flux in the direction of increasing coordinate.) The diffusion velocity vector is defined as (Fick's formulation):

$$\mathbf{V}_k = -\frac{1}{X_k} D'_{km} \boldsymbol{\nabla} X_k, \tag{2.42}$$

where D'_{km} is a mixture-averaged diffusion coefficient for species k relative to the rest of the mixture. Employing Eq. 2.42 into Eq. 2.41 yields:

$$\mathbf{j}_k = -\rho \frac{Y_k}{X_k} D'_{km} \boldsymbol{\nabla} X_k = -\rho \frac{M_k}{M} D'_{km} \boldsymbol{\nabla} X_k \tag{2.43}$$

It is convenient to use the ratio of the molecular weights rather than X_k for the flow regions that do not contain species k, thus avoiding division with zero.

A more general formulation of the diffusion velocity is offered by the multicomponent approach [34]:

$$\mathbf{V}_k = \frac{1}{X_k M} \sum_{j \neq k}^{N_s} M_j D_{kj} \mathbf{d}_k - \frac{D_k^T}{\rho Y_k} \frac{1}{T} \boldsymbol{\nabla} T, \tag{2.44}$$

where D_{kj} is the matrix of ordinary multicomponent diffusion coefficients, $\boldsymbol{\nabla} X_k$ are the thermal diffusion coefficients and $\mathbf{d}_k$ is the vector of concentration gradients and pressure

fields:

$$\mathbf{d}_k = \boldsymbol{\nabla} X_k + (X_k - Y_k)\frac{\boldsymbol{\nabla} p}{p} \tag{2.45}$$

Energy Conservation

The energy equation is primarily used to determine the temperature fields of the fluid and is strongly coupled to the momentum equation through the convective terms and to the species equation as the chemical reactions and molecular transport significantly influence the thermal energy of the fluid. The energy equation is derived from the first law of thermodynamics which states that the rate of change of total stored energy E_t is equal to the rate of heat Q transferred to the system plus the rate of work W done on the system:

$$\frac{dE_t}{dt} = \frac{dQ}{dt} + \frac{dW}{dt} \tag{2.46}$$

The extensive variable in the energy equation is E_t and the intensive variable is the total specific energy $e_t = E_t/m$. The total energy equation in vector form is written as:

$$\rho\left(\frac{De}{Dt} + \mathbf{V}\cdot\frac{D\mathbf{V}}{Dt} - \mathbf{g}\cdot\mathbf{V}\right) = \boldsymbol{\nabla}\cdot(\lambda\boldsymbol{\nabla}T) - \sum_{k=1}^{N_s}\boldsymbol{\nabla}\cdot h_k\mathbf{j}_k + \boldsymbol{\nabla}\cdot(\mathbf{V}\cdot\mathsf{T}) \tag{2.47}$$

Summary of the Conservation Equations

In Cartesian coordinates, the conservation equations (for the constant density cases) can be summarized as follows [74]:
Overall mass conservation:

$$\frac{\partial\rho}{\partial t} + \boldsymbol{\nabla}\cdot(\rho\mathbf{V}) = 0 \tag{2.48}$$

Momentum (Navier-Stokes) conservation (constant density):

$$\begin{aligned}\rho\frac{D\mathbf{V}}{Dt} &= \rho\left[\frac{\partial\mathbf{V}}{\partial t} + (\mathbf{V}\cdot\boldsymbol{\nabla})\mathbf{V}\right]\\ &= \rho\left[\frac{\partial\mathbf{V}}{\partial t} + \boldsymbol{\nabla}\left(\frac{\mathbf{V}\cdot\mathbf{V}}{2}\right) + \mathbf{V}\times(\boldsymbol{\nabla}\times\mathbf{V})\right]\\ &= \mathbf{f} + \boldsymbol{\nabla}\cdot\mathsf{T} = \mathbf{f} - \boldsymbol{\nabla}p + \boldsymbol{\nabla}\cdot\mathsf{T}'\end{aligned} \tag{2.49}$$

Species conservation:

$$\rho\frac{DY_k}{Dt} = -\boldsymbol{\nabla}\cdot\mathbf{j}_k + \dot{\omega}_k M_k \tag{2.50}$$

Thermal energy conservation:

$$\rho\frac{Dh}{Dt} = \frac{Dp}{Dt} + \boldsymbol{\nabla}\cdot(\lambda\boldsymbol{\nabla}T) - \sum_{k=1}^{N_s}\boldsymbol{\nabla}\cdot h_k\mathbf{j}_k + \Phi \tag{2.51}$$

2.3 Molecular Transport

The molecular transport of species, momentum and energy in a multicomponent gas requires calculation of mass diffusion coefficients, viscosities, thermal conductivities and thermal diffusion coefficients. There are mainly two approaches to describing the transport properties of the mixture, depending on the application, namely the mixture-averaged and the multicomponent approach. A more detailed description of the transport phenomena and theories used for calculating the transport coefficients can be found in the books from Bird [19] or Curtiss and Hirschfelder [34]. In the following, a brief summary of the expressions used to evaluate the transport coefficients is presented.

2.3.1 Mass Diffusion

The mass diffusion coefficient is the proportionality constant relating the species concentration gradient to the mass flux and is derived from the kinetic theory of gases. Self-diffusion is a random displacement of the species molecules in the absence of a chemical potential gradient (i.e. no changes in chemical composition of the component). The self-diffusion coefficient expression is based on the kinetic gas theory [69]:

$$\mathcal{D}_{kk} = \frac{3}{8}\frac{\sqrt{\pi k_B^3 T^3/m_k}}{p\pi\sigma_k^2\Omega_{kk}^{(1,1)^*}} \tag{2.52}$$

The binary mass diffusion coefficient is described by the Chapman-Enskog theory [74] in terms of pressure and temperature as:

$$\mathcal{D}_{ij} = \frac{3}{16}\frac{\sqrt{2\pi k_B^3 T^3/m_{ij}}}{p\pi\sigma_{ij}^2\Omega_{ij}^{(1,1)^*}}, \tag{2.53}$$

where k_B is the Boltzmann constant, T is the absolute temperature, σ_{ij} is the length-scale in the interaction between the two molecules, m_{ij} is the reduced mass of molecules i and j

$$m_{ij} = \frac{m_i m_j}{m_i + m_j}$$

and $\Omega_{ij}^{(1,1)^*}$ is a collision integral which is a function of the temperature and the potential between the molecules.

In case of the mixture-averaged approach, three different expressions for the diffusion coefficient of species k into the mixture are used [74]:

1) a mixture-averaged diffusion coefficient D^*_{km} for calculating the molar flux $\mathbf{J}^*_k$ with respect to the molar average velocity as a function of the mole fraction gradient of the species k,
2) a mixture-averaged D_{km} for calculating the mass flux $\mathbf{j}_k$ with respect to the mass average velocity as a function of the mass fraction gradient of species k,
3) D'_{km} for calculating the mass flux $\mathbf{j}_k$ with respect to the mass average velocity as is a function of the mole fraction gradient.

The molar diffusive flux is related to the species mole fraction gradient by a Fickian expression [74]:

$$\mathbf{J}^*_k = [X_k]\left(\tilde{\mathbf{V}}_k - \mathbf{V}^*\right) = -cD^*_{km}\nabla X_k \tag{2.54}$$

where $\mathbf{V}^*$ is the molar average velocity:

$$\mathbf{V}^* = \frac{1}{c}\sum_{k=1}^{N_s}[X_k]\,\tilde{\mathbf{V}}_k = \sum_{k=1}^{N_s} X_k\tilde{\mathbf{V}}_k \tag{2.55}$$

and $\tilde{\mathbf{V}}_k$ is the average velocity of all molecules of species k at a fixed point in the fluid. The total molar concentration c of all species is $c = \sum_{k=1}^{N_s}[X_k]$. Therefore:

$$[X_k]\,\tilde{\mathbf{V}}_k - X_k\sum_{j=1}^{N_s}[X_j]\,\tilde{\mathbf{V}}_j = -cD^*_{km}\nabla X_k \tag{2.56}$$

Using the Stefan-Maxwell equation which relates the diffusion velocities to the field gradients:

$$\nabla X_k = \sum_{j=1}^{N_s}\frac{X_kX_j}{\mathcal{D}_{kj}}\left(\mathbf{V}_j - \mathbf{V}_k\right) + \left(Y_k - X_k\right)\left(\frac{\nabla p}{p}\right) + \sum_{j=1}^{N_s}\frac{X_kX_j}{\rho\mathcal{D}_{kj}}\left(\frac{D^T_j}{Y_j} - \frac{D^T_k}{Y_k}\right)\left(\frac{\nabla T}{T}\right), \tag{2.57}$$

where D^T_j and D^T_k are thermal diffusion coefficients, one can write (for isothermal and isobaric conditions):

$$\nabla X_k = -\sum_{j=1}^{N_s}\frac{X_kX_j}{\mathcal{D}_{kj}}\left(\tilde{\mathbf{V}}_k - \tilde{\mathbf{V}}_j\right) \tag{2.58}$$

By equating Eqs. 2.57 and 2.58 and assuming that the velocities of all species $j \neq k$ are equal, we obtain:

$$D^*_{km} = \frac{1 - X_k}{\sum_{j\neq k}^{N_s} X_j/\mathcal{D}_{kj}} \tag{2.59}$$

The mixture-averaged diffusion coefficient D_{km}, relating the mass flux $\mathbf{j}_k$ with respect to the mass average velocity as a function of the mass fraction gradient of species k:

$$\mathbf{j}_k = \rho\left(\tilde{\mathbf{V}}_k - \mathbf{V}\right) = \rho Y_k\mathbf{V}_k = -\rho D_{km}\nabla Y_k, \tag{2.60}$$

is calculated from:

$$D_{km} = \left(\sum_{j \neq k}^{N_s} \frac{X_j}{\mathcal{D}_{kj}} + \frac{X_k}{1 - Y_k} \sum_{j \neq k}^{N_s} \frac{Y_j}{\mathcal{D}_{kj}} \right)^{-1} \tag{2.61}$$

The mass flux $\mathbf{j}_k$ with respect to the mass average velocity a function of the mole fraction gradient is expressed as:

$$\mathbf{V}_k = -\frac{1}{X_k} D'_{km} \nabla X_k \tag{2.62}$$

Finally, the mixture-averaged diffusion coefficient D'_{km} is calculated from:

$$D'_{km} = \frac{1 - Y_k}{\sum_{j \neq k}^{N_s} X_j / \mathcal{D}_{kj}} \tag{2.63}$$

The multicomponent diffusion coefficients are computed from the solution of an equation system defined by the L matrix (see Appendix A). Since there is no reliable mixture-averaged theory for calculating the thermal diffusion coefficients D_k^T, the multicomponent approach is used to obtain D_k^T for cases where the thermal diffusion is considered.

2.3.2 Conductivity

The pure species thermal conductivities are required only for calculation of the mixture-averaged thermal conductivities as the mixture conductivity in the multicomponent approach does not depend on the conductivities of pure species. The pure species thermal conductivities λ_k are assumed to consist of translational, rotational, and vibrational contributions as given by [192]:

$$\lambda_k = \frac{\eta_k}{M_k} \left(f_{\text{trans.}} C_{v,\text{trans.}} + f_{\text{rot.}} C_{v,\text{rot.}} + f_{\text{vib.}} C_{v,\text{vib.}} \right), \tag{2.64}$$

where

$$f_{\text{trans.}} = \frac{5}{2} \left(1 - \frac{2}{\pi} \frac{C_{v,\text{rot.}}}{C_{v,\text{trans.}}} \frac{A}{B} \right), \tag{2.65}$$

$$f_{\text{rot.}} = \frac{\rho \mathcal{D}_{kk}}{\eta_k} \left(1 + \frac{2}{\pi} \frac{A}{B} \right), \tag{2.66}$$

$$f_{\text{vib.}} = \frac{\rho \mathcal{D}_{kk}}{\eta_k}, \tag{2.67}$$

$$A = \frac{5}{2} - \frac{\rho \mathcal{D}_{kk}}{\eta_k}, \tag{2.68}$$

$$B = Z_{\text{rot.}} + \frac{2}{\pi} \left(\frac{5}{3} \frac{C_{v,\text{rot.}}}{R} + \frac{\rho \mathcal{D}_{kk}}{\eta_k} \right) \tag{2.69}$$

The expressions for the individual molar heat capacities differ depending on the linearity of the molecule. If the molecule is linear, then:

$$C_{v,\text{trans.}} = \frac{3}{2}R, \quad C_{v,\text{rot.}} = R, \quad C_{v,\text{vib.}} = C_v - \frac{5}{2}R \tag{2.70}$$

If the molecule is not linear:

$$C_{v,\text{trans.}} = \frac{3}{2}R, \quad C_{v,\text{rot.}} = \frac{3}{2}, \quad C_{v,\text{vib.}} = C_v - 3R \tag{2.71}$$

If the species k is a single atom, there are no rotational and vibrational contributions to the molar heat capacity, hence:

$$\lambda_k = \frac{5}{2}\mu_k \frac{C_{v,\text{trans.}}}{M_k} \tag{2.72}$$

The thermal conductivity is calculated from the thermal conductivities of pure species and their mole fraction as [109]:

$$\lambda = \frac{1}{2}\left(\sum_{k=1}^{N_s} X_k \lambda_k + \frac{1}{\sum_{k=1}^{N_s} X_k/\lambda_k}\right) \tag{2.73}$$

The multicomponent thermal conductivities are calculated from the solution of the system of equations defined by the L matrix (Appendix A).

2.3.3 Viscosity

The single component (pure species) viscosities are given by the standard kinetic theory expression [69]:

$$\mu_k = \frac{5}{16}\frac{\sqrt{\pi m_k k_B T}}{\pi \sigma_k^2 \Omega^{(2,2)^*}}, \tag{2.74}$$

where σ_k is the Lennard-Jones collision diameter, m_k is the molecular mass, k_B is the Boltzmann constant, T is the temperature and $\Omega^{(2,2)^*}$ is the collision integral which depends on the reduced temperature T_k^*:

$$T_k^* = \frac{k_B T}{\varepsilon_k}, \tag{2.75}$$

and the reduced dipole moment:

$$\delta_k^* = \frac{1}{2}\frac{\mu_k^2}{\varepsilon_k \sigma_k^3} \tag{2.76}$$

In the above expression, ε_k is the Lennard-Jones potential well depth and μ_k is the dipole moment.

The mixture viscosity is evaluated using the pure species viscosity and binary diffusion coefficients. Wilke [197] proposed a semi-empirical formulation of the viscosity:

$$\mu = \sum_{k=1}^{N_s} \frac{X_k \mu_k}{\sum_{j=1}^{N_s} X_j \Phi_{kj}}, \tag{2.77}$$

where

$$\Phi_{kj} = \frac{1}{\sqrt{8}} \left(1 + \frac{M_k}{M_j}\right)^{-\frac{1}{2}} \left[1 + \left(\frac{\mu_k}{\mu_j}\right)^{\frac{1}{2}} \left(\frac{M_j}{M_k}\right)^{\frac{1}{4}}\right]^2 \tag{2.78}$$

2.4 Canonical Cases

Investigation and interpretation of chemical kinetics in a combustion regime is performed by employing several common experimental configurations: batch or static reactors, continuosly stirred reactors, shock tubes and laminar flames. These configurations are made in such way that facilitates both the measurements (temporal and/or spatial species concentrations, temperature, pressure, etc.) and the modelling, under a certain range of operating conditions. Such experiments and their corresponding models enable development and validation of reaction mechanisms [74, 193, 194]. In the following, the mathematical modelling of several typical canonical configurations (one- and zero-dimensional) are presented.

2.4.1 One-dimensional Laminar Flames

Propagation of premixed laminar flames is a phenomenon occuring in many practical combustion setups [67, 68], e.g. internal combustion engines, gas turbine combustors, and in laboratory enviroments to study chemical kinetics of combustion [113, 114]. Such flame configurations can be made very steady and effectively one-dimensional, which enables experimental measurements of the temperature and the species profiles [74, 77] and investigating the combustion of various fuel-oxidizer mixtures, thus understanding the combustion process itself [97, 166]. Modeling of laminar flames facilitates the interpretation of experimental findings, enables development and validation of kinetics for combustion and pollutant formation [75, 112, 115, 116].

A full mathematical description of the chemically reacting flow requires specification of temporal and spatial variations of pressure, temperature, density, velocity and the concentrations of the individual species at each point of the reacting system. Modelling of flames therefore has to consider all these properties as their variations are the result of different phenomena typically occuring in a flame (convection due to fluid flow, molecular

diffusion, heat conduction, chemical reactions and radiation). All the reacting systems are generally described by the conservation equations disscussed in Section 2.2 so that the main difference between the specific systems is the choice of their individual boundary and physiochemical conditions. Assumptions made for simplifying the complex nature of the general conservation laws when these are applied to the premixed flat flames are the following [192]:

- the reacting gas is considered ideal,
- effects of the external forces (e.g. gravity) are negligible,
- the flow is subsonic (low Mach number) which makes the pressure variations negligible,
- the kinetic energy of the flow is neglected,
- the reciprocal thermal diffusion effect is negligible,
- effects of radiation are negligible (which is valid for non-sooting flame),
- the system is continuous (the mean free path of molecules is small compared to the flame thickness),
- the flame is steady-state (no temporal variation of the properties),
- the system is in local thermal equilibrium,
- the chemical reactions, the convective and diffusive transport occur only in one spatial dimension.

All these assumptions yield the following simplified formulations of the conservation equations in z-direction:

Mass continuity:

$$\frac{\partial \rho}{\partial t} + \frac{\partial \rho u}{\partial z} = 0 \tag{2.79}$$

Axial momentum:

$$\rho \frac{\partial u}{\partial t} + \rho u \frac{\partial u}{\partial z} = -\frac{\partial p}{\partial z} + \frac{\partial}{\partial z}\left(\mu \frac{\partial u}{\partial z}\right) \tag{2.80}$$

Species conservation:

$$\rho \frac{\partial Y_k}{\partial t} + \rho u \frac{\partial Y_k}{\partial z} = -\frac{\partial j_{k,z}}{\partial z} + \dot{\omega}_k M_k \tag{2.81}$$

Thermal energy:

$$\rho c_p \frac{\partial T}{\partial t} + \rho u c_p \frac{\partial T}{\partial z} = \frac{\partial}{\partial z}\left(\lambda \frac{\partial T}{\partial z}\right) - \sum_{k=1}^{N_s} c_{pk} j_{k,z} \frac{\partial T}{\partial z} - \sum_{k=1}^{N_s} h_k \dot{\omega}_k M_k \tag{2.82}$$

Although the flame is considered steady-state, the transient terms are kept only for the purpose of the "hybrid" numerical solution [74]. Furthermore, the continuity equation

can be rewritten in terms of the net mass flux $\dot{m}''$ as:

$$\dot{m}'' = \rho u \tag{2.83}$$

Since the pressure is usually known (e.g. from the laboratory conditions) and the pressure variations are negligible compared to the pressure value, and the local density can be evaluated from the equation of state (with known temperature and mass fractions), the axial momentum equation is no longer necessary. Now the species equation becomes:

$$\rho\frac{\partial Y_k}{\partial t} + \dot{m}''\frac{\partial Y_k}{\partial z} = -\frac{\partial j_{k,z}}{\partial z} + \dot{\omega}_k M_k \tag{2.84}$$

and the energy equation:

$$\rho c_p\frac{\partial T}{\partial t} + \dot{m}'' c_p\frac{\partial T}{\partial z} = \frac{\partial}{\partial z}\left(\lambda\frac{\partial T}{\partial z}\right) - \sum_{k=1}^{N_s} c_{pk} j_{k,z}\frac{\partial T}{\partial z} - \sum_{k=1}^{N_s} h_k\dot{\omega}_k M_k \tag{2.85}$$

Boundary Conditions

The mass flux $\dot{m}''$ can either be specified at the burner inlet (burner-stabilized flame) or determined as part of the solution (adiabatic freely-propagating flame). The governing equations for both flames are the same, they differ only in their boundary conditions. For the burner-stabilized flame, values of the mass flux, the temperature at the burner inlet ($z = 0$) are explicitly given. The unburned gas composition (Y_k) is usually known as well, but due to the diffusive fluxes from the flame into the burner, it is not convenient to give the composition in terms of mass fractions. Instead, the following condition is given in order to preserve the balance of the species fluxes at the burner inlet:

$$\dot{m}''\epsilon_k = \dot{m}'' Y_k + \rho Y_k V_k, \tag{2.86}$$

where

$$\epsilon_k = Y_k + \frac{j_{k,z}}{\dot{m}''} \tag{2.87}$$

and the values of ϵ_k are specified. The mass fractions Y_k, diffusion velocities V_k and mass density ρ are computed as part of the solution [164]. The boundary condition after the flame is that all gradients are zero.

The burner-stabilized flame configuration is the most often used for analyzing species profiles in experiments. Such flames are stabilized on top of a porous metal cylindrical burner through which the reactants are fed with a known mass flow rate. In experimental setups, the operating pressure is usually low to distribute the reaction zone so that the spatial distributions of the temperature and the species can be measured [74].

For the adiabatic freely-propagating flame, the inlet mass flux is not known. The condition imposed to compensate the lack of the mass flux value is the temperature specified at some point of the grid so that Eq. 2.85 is satisfied, and the specified temperature must be equal to the resulting temperature at this point. All gradients must be zero at both boundaries to prevent diffusive losses of species or energy from the system. The laminar burning velocity for this type of flame is easily calculated from $s_L = \dot{m}''/\rho$ once the $\dot{m}''$ is found [165].

A freely-propagating flame model is normally used to determine the characteristic flame speed of the gas mixture at specified pressure and inlet temperature. This model does not consider heat losses, therefore the temperature is computed from the energy equation. Alternatively, if the heat losses are significant, the temperature profile can be obtained from the experiment and used as an input for the flame simulation. In this case, only the species transport equations are solved. Since the chemical kinetics strongly depends on the temperature, the accurate temperature profiles are important for specifying the chemical kinetics behavior. As the laminar flame speed partly depends on the heat transport, the temperature profile is essential for the flame speed calculation [77].

2.4.1.1 Parallel Flow

Parallel flows are the flows for which only one velocity component is different from zero, i.e. the flow is unidirectional. In these cases the governing equations can be reduced to linear ordinary or partial differential equations by exploiting physical situations that permit a significant simplification of the Navier-Stokes equations [74]. These simplifications and the flame models that are reduced to one-dimensional flames by employing the simplifications are described in the following.

2.4.1.2 Stagnation-Point Flow

Similarity assumptions are not the same as the approximations or assumptions made to simplify or neglect certain physical properties of the system, but they enable complete representation of two-dimensional behavior as one-dimensional for specific boundary conditions [74]. A basic principle of the similarity assumption is that there exists a viscous boundary layer in which the temperature and species composition depend on one independent variable only. This implies an infinite domain in directions orthogonal to the remaining independent variable. (Of course, no real problems have an infinite domain. Therefore it is important to identify the real problems for which the similarity assumptions are sufficiently valid.) The similarity assumptions that permit the problem to be treated as spatially one-dimensional are the following [74, 192]:

- there may be a circumferential velocity component w, but there are no variations of any variable in the circumferential direction,
- radial velocity varies linearly in the radial direction (the fluid properties are functions of the axial distance only),
- the solution is considered only along the stagnation stream line.

The one-dimensional system of conservation equations for axisymmetric steady-state stagnation flame is given in following [74]:

Continuity equation:

$$\frac{d(\rho u)}{dz} + 2\rho V = 0 \tag{2.88}$$

Radial momentum:

$$-2U\frac{d}{dz}\left(\frac{1}{\rho}\frac{dU}{dz}\right) + \frac{1}{\rho}\left(\frac{dU}{dz}\right)^2 - \rho\left(\frac{w}{r}\right)^2 = -\frac{1}{r}\frac{\partial p}{\partial r} - \frac{d}{dz}\left[\mu\frac{d}{dz}\left(\frac{1}{\rho}\frac{dU}{dz}\right)\right], \tag{2.89}$$

where it is convenient to write

$$\frac{1}{r}\cdot\frac{\partial p}{\partial z} = \Lambda_r = \text{constant} \tag{2.90}$$

and

$$\rho u = 2U, \quad \rho\frac{v}{r} = \rho V = -\frac{dU}{dz} \quad \text{and} \quad \frac{w}{r} = W \tag{2.91}$$

Therefore, the radial momentum can be written in a simpler form as:

$$\rho u\frac{dV}{dz} + \rho\left(V^2 - W^2\right) = -\Lambda_r + \frac{d}{dz}\left(\mu\frac{dV}{dz}\right) \tag{2.92}$$

Axial momentum:

$$4U\frac{d}{dz}\left(\frac{U}{\rho}\right) = -\frac{dp}{dz} + \frac{4}{3}\frac{d}{dz}\left[2\mu\frac{d}{dz}\left(\frac{U}{\rho}\right) + \frac{\mu}{\rho}\frac{dU}{dz}\right] - 2\mu\frac{d}{dz}\left(\frac{1}{\rho}\frac{dU}{dz}\right), \tag{2.93}$$

or in a simpler form:

$$\rho u\frac{du}{dz} = -\frac{dp}{dz} + \frac{4}{3}\frac{d}{dz}\left[\mu\frac{du}{dz} - \mu V\right] + 2\mu\frac{dV}{dz} \tag{2.94}$$

If there is a circumferential velocity component W, the circumferential momentum is:

$$2Ur\frac{dW}{dz} - r\frac{dU}{dz}\frac{\partial rW}{\partial r} - r\frac{dU}{dz}W =$$

$$= r\frac{\partial}{\partial z}\left(\mu\frac{\partial W}{\partial z}\right) + \frac{\partial}{\partial}\left[\mu\left(\frac{\partial rW}{\partial r} - W\right)\right] + \frac{2\mu}{r}\left(\frac{\partial rW}{\partial r}\right) \tag{2.95}$$

Dividing by r and eliminating any radial derivatives of W or ρ yields the desired stagnation-flow circumferential momentum equation:

$$\rho u \frac{dW}{dz} + 2\rho V W = \frac{d}{dz}\left(\mu \frac{dW}{dz}\right) \tag{2.96}$$

Assuming that the temperature and composition of the gas are functions of z alone, the thermal energy equation is:

$$\rho u c_p \frac{dT}{dz} = \frac{d}{dz}\left(\lambda \frac{dT}{dz}\right) - \sum_{k=1}^{N_s} \rho Y_k V_k c_{pk} \frac{dT}{dz} - \sum_{k=1}^{N_s} h_k M_k \dot{\omega}_k \tag{2.97}$$

and the species conservation:

$$\rho u \frac{dY_k}{dz} = -\frac{d}{dz}\left(\rho Y_k V_k\right) + M_k \dot{\omega}_k \tag{2.98}$$

The equation of state for a perfect gas gives the mass density when the mean pressure, the local temperature and the local composition is known:

$$p = \rho R T \sum_{k=1}^{N_s} \frac{Y_k}{M_k} \tag{2.99}$$

The axial momentum equation is no longer needed to calculate the velocity, temperature and composition, but it can be used to calculate the axial pressure gradient. The second-order equations (momentum, energy and species) require specifying boundary conditions at both ends of the z domain, particularly information about V, W, T and Y_k. The continuity equation requires specifying u on one boundary. In the following, two commonly used flame configurations are briefly presented, namely the impinging jet and the counterflow flame.

Impinging Jet

In the diffusion opposed-flames case, the fuel and the oxidizer flows are separated, impinging on each other and only mixing at the flame zone (shaded region in Fig. 2.1). Location of the flame depends on the stoichiometry of the fuel and the oxidizer and it does not neccessarily occur at the stagnation plane of the flow field. An opposed-flow diffusion flame configuration is illustrated in Fig. 2.1, right. Opposed flow configurations are used for both the premixed and nonpremixed (diffusion) flames in combustion experiments. The counterflow configuration, although physically two-dimensional (there are two velocity components), allows the flame to be treated as spatially one-dimensional by using the similarity assumptions thus enabling the researchers to model and study

the opposed flames with detailed chemical kinetics. Opposed-flow diffusion flames have been extensively used to test flammability of various fuel/oxidizer systems [33] and to evaluate fire suppressants where the fire suppression is approximated with an experimental configuration of fuel impinging upon air to which a suppression agent has been added [40, 133].

Flat flames can also be made to impinge onto surfaces. Such configurations can be used to study the effects of strain on the flame structure (important for investigating the fluid-mechanical effects encountered in turbulent flows) or to study the effect of a cold surface (an engine or furnace wall) onto the flame structure [47].

The following conservation equations mathematically describe one-dimensional impinging jets [74].

Continuity equation:

$$\frac{d(\rho u)}{dz} + 2\rho V = 0 \tag{2.100}$$

Radial momentum:

$$\rho\frac{dV}{dt} = \frac{d}{dz}\left(\mu\frac{dV}{dz}\right) - \Lambda_r - \rho u\frac{dV}{dz} - \rho V^2 \tag{2.101}$$

Energy equation:

$$\rho c_p\frac{dT}{dt} = -\rho c_p u\frac{dT}{dz} + \frac{d}{dz}\left(\lambda\frac{dT}{dz}\right) - \sum_{k=1}^{N_s}\rho Y_k V_k c_{pk}\frac{dT}{dz} - \sum_{k=1}^{N_s} h_k M_k\dot{\omega}_k \tag{2.102}$$

Species equation:

$$\rho\frac{dY_k}{dt} = -\rho u\frac{dY_k}{dz} - \frac{d}{dz}\left(\rho Y_k V_k\right) + M_k\dot{\omega}_k \tag{2.103}$$

Counterflow Flame

In the following, the steady-state description of an axisymmetric non-premixed flame occuring between two concentric, circular nozzles opposing to each other (Fig. 2.1, right) is given.

The stagnation plane is located between the nozzles, as a result of momentum balance of the two streams [76]. The flame is typically established on the oxidizer side of the stagnation plane, where the stoichiometry is reached (more oxidizer than fuel is needed by mass, for most of the fuels). The resulting flames are flat and are easily reduced from two-dimensional to one-dimensional problems by assuming that the flame properties are functions of the axial distance only (similarity assumptions), thus allowing for detailed study of the chemistry and flame structure in laboratories. The conservation equations

for the opposed-flow are the same as for the stagnation flow (Section 2.4.1.2) with the following boundary conditions:

$$z = 0: \quad U = \frac{\rho_{\mathrm{F}} u_{\mathrm{F}}}{2}, \quad \frac{dU}{dz} = 0, \quad T = T_{\mathrm{F}}, \quad \rho u Y_k + \rho Y_k V_k = (\rho u Y_k)_{\mathrm{F}} \tag{2.104}$$

$$z = L: \quad U = \frac{\rho_{\mathrm{O}} u_{\mathrm{O}}}{2}, \quad \frac{dU}{dz} = 0, \quad T = T_{\mathrm{O}}, \quad \rho u Y_k + \rho Y_k V_k = (\rho u Y_k)_{\mathrm{O}} \tag{2.105}$$

At the stagnation plane:

$$z = L/2: \quad U = 0, \quad \frac{dU}{dz} = 0, \quad \frac{dT}{dz} = 0, \quad \frac{dY_k}{dz} = 0, \tag{2.106}$$

where L is the distance between the inlets and indices F and O stand for fuel and oxidizer at the inlets, respectively.

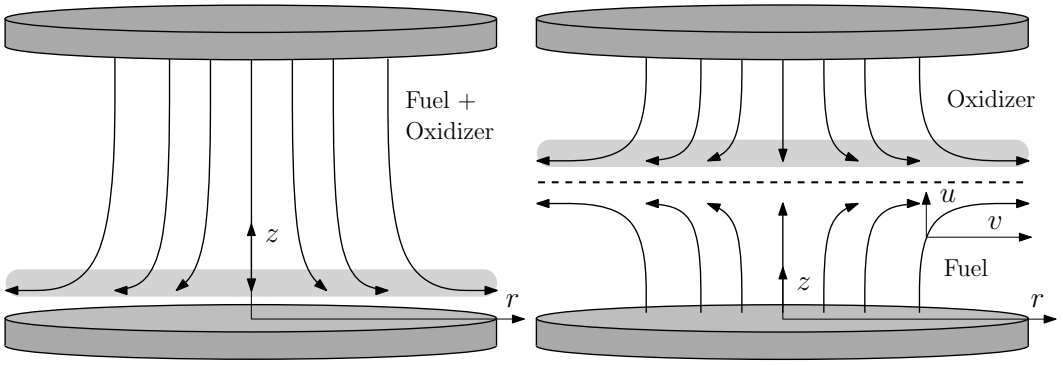

FIGURE 2.1: Axisymmetric stagnation premixed flame (left) and counterflow diffusion flame (right) configuration. The dashed line represents the stagnation plane and the shaded region depicts the flame.

The opposed-flow laminar diffusion flames are normally more complicated than the corresponding premixed flames due to difficulties associated with an adequate description of two- or three-dimensional flows with the detailed chemistry. However, one-dimensional treatment of the opposed-flow diffusion flames enable these systems to be regularly used for studying combustion chemistry [74].

2.4.2 Zero-Dimensional Reactors

The mixture composition of a well-stirred or homogeneous reactor is assumed to be spatially uniform, which means that the rate of conversion of reactants to products is controlled only by chemical kinetics and not by mixing processes. This assumption significantly simplifies the mathematical model thus enabling investigations of the kinetics

and computation of large detailed chemical reaction mechanisms with minimal computational demand. Conservation of mass, energy, and species for the homogeneous reactor include net generation of chemical species within the reactor volume, and net loss of species and mass to surfaces in the reactor. Examples of homogeneous systems widely used for the investigation of chemical kinetics are closed batch reactors, single-zone engine-cylinder models, perfectly-stirred reactors, and well mixed (low-pressure) plasma reactors. In the following, the conservation equations for zero-dimensional reactors are listed below.

Conservation of mass:

$$\frac{dm_k}{dt} = \dot{\omega}_k M_k V \tag{2.107}$$

Conservation of species:

$$\frac{dY_k}{dt} = \frac{\dot{\omega}_k M_k V}{\rho}, \tag{2.108}$$

where the mass density follows from equation of state for an ideal gas (for fixed pressure and temperature) as:

$$\rho = \frac{p}{RT \sum Y_k / M_k}$$

The rate of change of internal energy is balanced by the rate of heat transferred to the system and the rate of work done on the system:

$$\frac{dE}{dt} = \frac{dQ}{dt} + \frac{dW}{dt} \tag{2.109}$$

Energy Conservation for a Constant-volume Homogeneous System

A simple constant-volume reactor with no external work done on the system is considered. The heat can be transferred to the system at a rate given by Newton's law:

$$\frac{dQ}{dt} = \alpha A \left(T_\infty - T\right), \tag{2.110}$$

where α is the heat-transfer coefficient, A is the area of the surface through which the heat is transferred and T_∞ is the temperature of the environment. The net internal energy of the system in terms of a mass-weighted sum of the individual internal energies of the components is:

$$E = m \sum_{k=1}^{N_s} e_k Y_k \tag{2.111}$$

Substituting Eqs. 2.110 and 2.111 into Eq. 2.109, and representing the specific internal energy in terms of the temperature and the constant-volume specific heat yield the

energy equation:

$$\rho c_v \frac{dT}{dt} = -\sum_{k=1}^{N_s} e_k \dot{\omega}_k M_k + \frac{\alpha A}{V}(T_\infty - T) \tag{2.112}$$

Energy Conservation for a Constant-pressure Homogeneous System

The heat transfer to the system where the pressure is held fixed is represented with Eq. 2.110 and the work is done by the system as its volume expands (i.e., $dV/dt > 0$). Thus the work term in this case takes a negative sign (in Eq. 2.109, positive work means work done on the system):

$$\frac{dW}{dt} = -p\frac{dV}{dt} = -p\sum_{k=1}^{N_s} \frac{d(m_k v_k)}{dt} = -pm\sum_{k=1}^{N_s} Y_k \frac{dv_k}{dt} - pm\sum_{k=1}^{N_s} \frac{dY_k}{dt} \tag{2.113}$$

where $v_k = 1/\rho_k$ is the specific volume of the species k. Substituting Eq. 2.113 into Eq. 2.109, and representing the specific enthalpy in terms of the temperature and the constant-pressure specific heat, the energy equation becomes:

$$\rho c_p \frac{dT}{dt} = -\sum_{k=1}^{N_s} h_k \dot{\omega}_k M_k + \frac{\alpha A}{V}(T_\infty - T), \tag{2.114}$$

where the volume $V = m/\rho$ varies with time.

2.5 Modeling of Chemical Kinetics

A chemical reaction is essentially the exchange and/or rearrangement of atoms between colliding molecules [74, 192]. Chemical kinetics is the study of the rate at which the chemical reactions proceed. The rate at which a chemical species is formed (product) or consumed (reactant) is described by a rate expression that is usually empirically determined. For example, the observed rate r of the phenomenological (observed) reaction:

$$a\mathrm{A} + b\mathrm{B} \rightarrow \mathrm{P}$$

is represented in terms of concentrations of the reactants as:

$$r = k[\mathrm{A}]^a[\mathrm{B}]^b$$

where k is the rate constant, a is the reaction order with respect to reactant A and b is the reaction order with respect to reactant B. The overall order of the reaction is $a + b$. The order of reaction is a quantity that describes the dependence of the reaction rate

on the concentration of the reactants. The order of reaction is determined empirically. Often it is not an integer, and may or may not be related to the stoichiometric coefficients of the reactants. Introductory textbooks in chemical kinetics describe how to determine the reaction order of a reaction from experimental data [52, 74, 89].

Often the observed rate of destruction of the reactant species may be due to the net contribution of several (elementary) reactions taking place simultaneously. Therefore one must distinguish between the observed (also called macroscopic, empirical or phenomenological) chemical rate expressions and the rates of elementary reactions. For example, a global stoichiometric reaction for methane oxidation is:

$$CH_4 + 2O_2 \rightleftharpoons CO_2 + 2H_2O$$

The chemical conversion of reactants to products mainly depends on the temperature, the concentration of the reactants and the presence of a catalyst or inhibitor [52]. In a chemical reaction, the atoms are conserved (C, H and O), while the molecules are not (CH_4, O_2, CO_2 and H_2O). However, since the global reactions are valid only in a narrow range of conditions that cannot be extrapolated outside these conditions, the chemistry is rather described in a step-by-step manner. A few elementary reactions which take part in methane oxidation (GRI-Mech 3.0) are shown below as an example of step-by-step chemistry description along with the Arrhenius rate coefficients [163]:

$$\begin{aligned}
OH + CH_3 &\rightleftharpoons CH_2 + H_2O && \left(5.6 \cdot 10^7, 1.6, 5420\right) \\
OH + CH_4 &\rightleftharpoons CH_3 + H_2O && \left(1.0 \cdot 10^8, 1.6, 3120\right) \\
OH + CO &\rightleftharpoons H + CO_2 && \left(4.76 \cdot 10^7, 1.2, 70\right) \\
OH + HCO &\rightleftharpoons H_2O + CO && \left(5.0 \cdot 10^{13}, 0, 0\right)
\end{aligned}$$

In a reacting multicomponent mixture, interaction between the species can generally be represented as:

$$\sum_{k=1}^{N} \nu'_{k,i} \chi_k \Leftrightarrow \sum_{k=1}^{N} \nu''_{k,i} \chi_k \quad i = 1, \dots N_R \tag{2.115}$$

where $\nu'_{k,i}$ is the molar stoichiometric coefficient of reactant k of reaction i in forward direction, χ_k is symbol for reactant k, $\nu''_{k,i}$ is the molar stoichiometric coefficient of reactant k of reaction i in reverse direction and N_R is the total number of reactions. The conservation of mass gives:

$$\sum_{k=1}^{N} \nu'_{k,i} M_k = \sum_{k=1}^{N} \nu''_{k,i} M_k \quad i = 1, \dots N_R \tag{2.116}$$

The rate of progress q_i for the reaction i is defined as the difference between the forward and the reverse reaction rates:

$$q_i = k_{\text{fwd},i} \prod_{k=1}^{N_s} [X_k]^{\nu'_{k,i}} - k_{\text{rev},i} \prod_{k=1}^{N_s} [X_k]^{\nu''_{k,i}} \tag{2.117}$$

where $k_{\text{fwd},i}$ and $k_{\text{rev},i}$ are the forward and the reverse rate constants of the reaction i, respectively. The rate of progress can be positive or negative, depending on the direction (forward or reverse) in which the reaction is proceeding faster. The rate of production of species k is defined in terms of the rate of progress as:

$$\dot{\omega}_k = \sum_{k=1}^{N_R} \nu_{k,i} q_i \tag{2.118}$$

where

$$\nu_{k,i} = \nu''_{k,i} - \nu'_{k,i} \tag{2.119}$$

The forward rate constant is usually modelled by the modified Arrhenius temperature dependence:

$$k_{\text{fwd},i} = A_i T^{\beta_i} \exp \frac{-E_{a,i}}{RT} \tag{2.120}$$

where A_i is the pre-exponential constant, β_i is the temperature exponent and $E_{a,i}$ is the activation energy for the reaction i. When the reaction is in equilibrium, the forward reaction rate is equal to the reverse rate and $q_i = 0$, which gives:

$$k_{\text{fwd},i} \prod_{k=1}^{N_s} [X_k]^{\nu'_{k,i}} = k_{\text{rev},i} \prod_{k=1}^{N_s} [X_k]^{\nu''_{k,i}} \tag{2.121}$$

and the reverse rate constant can be expressed by:

$$k_{\text{fwd},i} = k_{\text{rev},i} \cdot \frac{\prod_{k=1}^{N_s} [X_k]_{\text{equil}}^{\nu''_{k,i}}}{\prod_{k=1}^{N_s} [X_k]_{\text{equil}}^{\nu'_{k,i}}} \tag{2.122}$$

where $[X_k]_{\text{equil}}^{\nu''_{k,i}}$ and $[X_k]_{\text{equil}}^{\nu'_{k,i}}$ are the equilibrium values of the molar concentrations of species k in reaction i.

Using Eq. 2.119, Equation 2.122 can be written as:

$$k_{\text{fwd},i} = k_{\text{rev},i} \prod_{k=1}^{N_s} [X_k]_{\text{equil}}^{\nu_{k,i}} \tag{2.123}$$

Furthermore, it is convenient to write:

$$K_{c,i} = \prod_{k=1}^{N_s} [X_k]_{\text{equil}}^{\nu_{k,i}} \tag{2.124}$$

which is the equilibrium constant in the concentration units. In pressure units, the equilibrium constant is defined as:

$$K_{p,i} = \prod_{k=1}^{N_s} \left(\frac{p_k}{p^0}\right)_{\text{equil}}^{\nu_{k,i}} \tag{2.125}$$

where p_k is the partial pressure of species k and p^0 is the standard-state pressure. For an ideal gas it holds that

$$p_k = [X_k]\, RT \tag{2.126}$$

Substituting the molar concentration $[X_k]$ from Eq. 2.126 into Eq. 2.124 yields:

$$K_{c,i} = \prod_{k=1}^{N_s} \left(\frac{p_k}{RT}\right)_{\text{equil}}^{\nu_{k,i}} \tag{2.127}$$

Relation between Eq. 2.127 and Eq. 2.125 is then

$$K_{c,i} = K_{p,i} \prod_{k=1}^{N_s} \left(\frac{p^0}{RT}\right)_{\text{equil}}^{\nu_{k,i}} \tag{2.128}$$

or

$$K_{c,i} = K_{p,i} \left(\frac{p^0}{RT}\right)^{\sum_{k=1}^{N_s} \nu_{k,i}} \tag{2.129}$$

On the other hand, the equilibrium constants can be expressed from reaction thermochemistry:

$$K_{p,i} = \exp\left(\frac{\Delta S_i^0}{R} - \frac{\Delta H_i^0}{RT}\right) \tag{2.130}$$

where the net change in entropy ΔS_i^0 and enthalpy ΔH_i^0 in the reaction i is given by:

$$\Delta S_i^0 = \sum_{k=1}^{N_s} \nu_{k,i} S_k^0 \tag{2.131}$$

and

$$\Delta H_i^0 = \sum_{k=1}^{N_s} \nu_{k,i} H_k^0 \tag{2.132}$$

Because the reverse rate constant $k_{\mathrm{rev},i}$ can be obtained from Eq. 2.123 as:

$$k_{\mathrm{rev},i} = \frac{k_{\mathrm{fwd},i}}{K_{c,i}} \tag{2.133}$$

it is more convenient to specify only the forward rate coefficients A_i, β_i and $E_{a,i}$ for each reaction in a reaction mechanism rather than specifying the rate coefficients in both directions. The reverse rate constants are then calculated from the Eq. 2.133 using the thermodynamic properties defined for each species in the mechanism (see 2.5.1). Although the rate coefficients in the mechanism can be given for both directions, one must ensure that the given thermodynamic properties of the species are fully consistent with the explicitly specified reverse rate coefficients, which can be rather complicated for complex reaction mechanisms [74].

2.5.1 Reaction Mechanisms

Chemical kinetics can be described by few different approaches depending on the complexity of the reacting system [74]. The fast chemistry approach (infinitely fast reactions and chemical equilibrium) assumes that the rate of chemical conversion is not controlled kinetically, i.e. the chemical reaction is instantaneous.

The finite rate chemistry approach (global reactions, analytically reduced reaction mechanisms and detailed reaction mechanisms) assumes that the conversion is kinetically controlled. The finite rate chemistry is described with a set of elementary reactions which represent the chemical process on a molecular level. An elementary reaction in most cases involves breaking or forming of only one chemical bond between the reacting atoms and it proceeds as it is written. The reaction order of an elementary reaction is integer. A collection of the elementary reactions with all the data necessary to solve differential equations related to chemical kinetics and thermodynamics represent a reaction mechanism.

Each species in the mechanism must be described by their transport (molecular weights, Lennard-Jones parameters, thermal conductivity, viscosity) and thermodynamic properties (heat of formation, enthalpy and heat capacity). For each elementary reaction, reactants, products and forward rate coefficients must be specified. In many reaction mechanisms, where only forward rate coefficients are given for reversible reactions, reverse rates are determined from the mass-action law (see Eq. 2.133). Alternatively, reversible reaction may be written in form of two irreversible reactions that proceed in forward directions each of them having explicitly specified rate coefficients. A carefully developed and well validated reaction mechanism provides the most accurate and reliable model for the finite rate chemistry [74].

Thermodynamic data for each species in a reaction mechanism are typically given as arrays of 14 coefficients for a polynomial fit [27, 28]. The first seven coefficients correspond to the low temperature range specified in the mechanism as $[T_{\text{min}}, T_{\text{mid}}]$ and the other seven correspond to the high temperature range $[T_{\text{mid}}, T_{\text{max}}]$. The first polynomial is fit for the low temperature region (typically $300 - 1000$ K) and the second polynomial is fit for the temperature region important for combustion (typically $1000 - 6000$ K). The two polynomial branches are "pinned" at T_{mid} and constrained to reproduce exactly the T_{mid} value (1000 K) to assure that the both branches will match at T_{mid} without discontinuity [27, 28]. The standard molar heat capacity for species k is then calculated as:

$$\frac{C_p^0(T)}{R} = a_1 T^{-2} + a_2^{-1} + a_3 + a_4 T^1 + a_5 T^2 + a_6 T^3 + a_7 T^4$$

The standard molar enthalpy and entropy are determined by integration of the specific heat in respect to the temperature:

$$\frac{H_p^0(T)}{RT} = a_1 + \frac{a_2}{2} T + \frac{a_3}{3} T^2 + \frac{a_4}{4} T^3 + \frac{a_5}{5} T^4 + \frac{a_6}{6}$$

and the entropy is calculated from

$$\frac{S^0(T)}{R} = a_1 \ln T + a_2 T + \frac{a_3}{2} T^2 + \frac{a_4}{3} T^3 + \frac{a_5}{4} T^4 + a_7$$

A typical definition of elementary chain reactions in a hydrogen oxidation mechanism [130] with defined forward rate coefficients A_i, β_i and $E_{a,i}$, respectively is given below. Units are cm^3, mol, s, kcal and K.

$$\begin{aligned}
&\text{H} + \text{O}_2 \rightleftharpoons \text{O} + \text{OH} && \left(1.91 \cdot 10^8, 0.0, 16.44\right) \\
&\text{O} + \text{H}_2 \rightleftharpoons \text{H} + \text{OH} && \left(5.08 \cdot 10^4, 2.67, 6.292\right) \\
&\text{OH} + \text{H}_2 \rightleftharpoons \text{H} + \text{H}_2\text{O} && \left(2.16 \cdot 10^8, 1.51, 3.43\right) \\
&\text{O} + \text{H}_2\text{O} \rightleftharpoons \text{OH} + \text{OH} && \left(2.97 \cdot 10^6, 2.02, 13.4\right)
\end{aligned}$$

To make a simulation of combustion processes as realistic as possible, equally realistic description of the reacting fluid flow, transport phenomena, chemical properties of the fuel and chemical reactions are mandatory. Development of comprehensive reaction mechanisms is motivated by capturing all the important chemical properties of the fuel over as many as possible operating conditions (temperature, pressure and the mixture composition). Furthermore, fuels that have been used in practical combustion engines in recent years consist of complex hydrocarbons or their blends (e.g. surrogates) and combustion of such fuels can only be described with complex reaction mechanisms. The comprehensiveness of the reaction mechanisms has the advantage to capture non-linear

and non-monotonic nature of combustion kinetics [89, 105] under different operating conditions. To demonstrate this complex behavior of chemical kinetics, an example of hydrogen combustion taken from Lu and Law (2009) [105] is cited below.

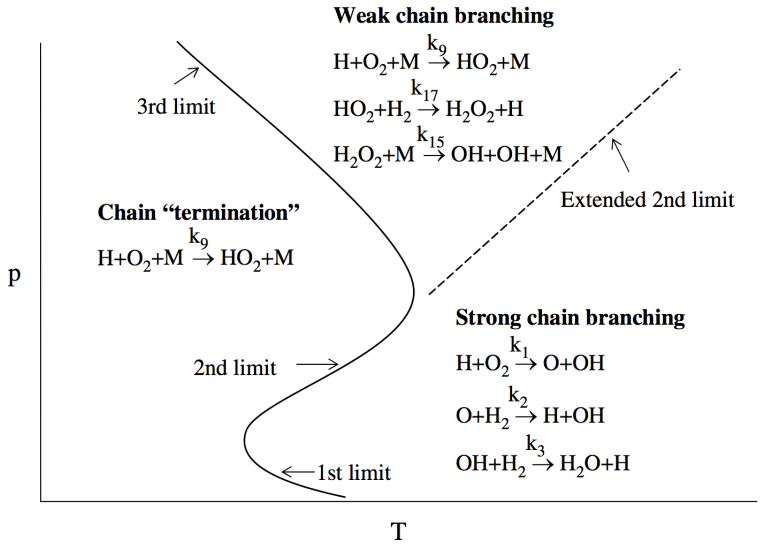

FIGURE 2.2: Schematic of the three explosion limits of homogeneous hydrogen-air mixtures, showing the non-monotonic system response. The controlling reactions in different regimes are also shown. Taken from Lu and Law, 2009 [105] and reprinted with permission.

Triple pressure-temperature explosion limits of a homogeneous hydrogen-oxygen mixture is illustrated in Fig. 2.2. Depending on the pressure-temperature values, the mixture exhibits explosive, non-explosive and again explosive behavior (at a moderate temperature, as the pressure increases). It has been found that such behavior is caused by different elementary reactions which occur in different temperature-pressure regions. Capturing such complex phenomena requires detailed kinetics modeling.

More detailed explanation and examples of the importance of comprehensiveness of reaction mechanisms are given by Law (2006) [89] and Lu and Law (2009) [105].

2.5.2 Types of Gas-Phase Reactions in a Mechanism

In a reaction mechanism, there are different types of the elementary reactions recognized. The individual reaction types typically occuring during combustion are presented in the following.

2.5.2.1 Temperature-dependent Reactions

In atmospheric kinetics, the temperature dependence of rate constant k is usually described by the so called original Arrhenius equation :

$$k = A \exp\left(\frac{-E_a}{RT}\right)$$

However, in the high-temperature gas-phase chemistry (combustion and pyrolysis), the modified Arrhenius equation is commonly used (Eq. 2.120).

$$k = AT^{\beta} \exp\left(\frac{-E_a}{RT}\right)$$

For reaction rate constants described by the modified Arrhenius equation, the activation energy changes with the temperature. Most of the gas-phase reactions in a combustion mechanims are of this type.

2.5.2.2 Third-body Reactions

For some reactions, specifically recombination or dissociation reactions, a so called "third body" is required to enhance the collision efficiency [74]. For example, in a reaction

$$\mathrm{H} + \mathrm{O_2} + \mathrm{M} \rightleftharpoons \mathrm{HO_2} + \mathrm{M},$$

the third body M is a collision partner which takes away the excess energy to stabilize the HO_2 molecule (forward direction) or supplies energy to break the HO_2 bond (reverse direction). Different species may be more or less effective in acting as the collision partner. A species that is much lighter than H and O_2 may not be able to transfer much of its kinetic energy, and so would be inefficient as a collision partner. When a third body is needed, the concentration of the effective third body must appear in the expression for the rate-of-progress variable:

$$q_i = \left(\sum_{k=1}^{N_s} \epsilon_{k,i} \left[X_k\right]\right) \left(k_{\mathrm{fwd},i} \prod_{k=1}^{N_s} \left[X_k\right]^{\nu'_{k,i}} - k_{\mathrm{rev},i} \prod_{k=1}^{N_s} \left[X_k\right]^{\nu''_{k,i}}\right), \tag{2.134}$$

where $\epsilon_{k,i}$ is collision efficiency of third body k in reaction i. If all the species in the reacting gas contribute equally to the reaction i as third bodies, then $\epsilon_{k,i} = 1$ for all the species and the total molar concentration of the mixture is then:

$$\sum_{k=1}^{N_s} \left[X_k\right] = \left[M\right] \tag{2.135}$$

Some species are more efficient as the collision partners then are others. For example, in the reaction example given above, water is much more efficient as a third body than nitrogen is, therefore the rate of this reaction is much higher when the third-body partner is H_2O [74].

2.5.2.3 Pressure-dependent reactions

Under certain conditions, the rate of some reaction types depend not only on temperature but on the pressure as well. Such behavior is characteristic for so-called unimolecular/recombination fall-off reactions (their rates increase with increasing pressure) and chemically activated bimolecular reactions (their rate decrease with increasing pressure), which are two types that are most frequently found in combustion mechanisms [138]. This section gives an overview of rate expressions for pressure-dependent reactions typically occuring in combustion mechanisms.

Unimolecular/Recombination Fall-off Reactions

As an example of a unimolecular/recombination fall-off reaction, methyl recombination is considered. In the high-pressure limit, the appropriate description of the reaction is:

$$CH_3 + CH_3 \rightleftharpoons C_2H_6$$

In the low-pressure limit, a third-body collision is required to provide the energy necessary for the reaction to proceed, therefore the appropriate description of this reaction is:

$$CH_3 + CH_3\,(+M) \rightleftharpoons C_2H_6\,(+M)$$

When such a reaction is at either limit, the (solely temperature-dependent) rate expressions discussed previously are applicable. However, when the pressure and temperature are such that the reaction is between the limits, the rate expressions are more complicated. To denote a reaction that is in this "fall-off" region, the reaction is written with the positive + M enclosed in parentheses.

The Arrhenius rate parameters are required for both the high- and low-pressure limiting cases, and the Lindemann form [96, 138] for the rate coefficient relates them in a pressure-dependent rate expression. In Arrhenius form, the parameters are given for the low-pressure limit (k_0) and the high-pressure limit (k_∞) as follows:

$$k_0 = A_0 T^{\beta_0} \exp\left(-E_0/RT\right)$$

and

$$k_\infty = A_\infty T^{\beta_\infty} \exp\left(-E_\infty / RT\right)$$

The rate constant at any pressure is then calculated as:

$$k = k_\infty \left(\frac{P_r}{1+P_r}\right) F\left(T, P_r\right),$$

where P_r is a so-called reduced pressure defined as:

$$P_r = \frac{k_0\left[M\right]}{k_\infty}$$

and $[M]$ is the concentration of the mixture, which can also include the third-body efficiencies. The fall-off function $F\left(T, P_r\right)$ proposed by Gilbert et al. [51] is:

$$\log F = \left[1 + \left(\frac{\log P_r + c}{n - d\left(\log P_r + c\right)}\right)^2\right]^{-1} \log F_{\text{cent}},$$

where the constants are [177, 178]:

$$\begin{aligned} c &= -0.4 - 0.67 \log F_{\text{cent}}, \\ n &= 0.75 - 1.27 \log F_{\text{cent}}, \\ d &= 0.14 \end{aligned}$$

and

$$F_{\text{cent}} = (1-A)\exp\left(-T/T_3\right) + A\exp\left(-T/T_1\right) + \exp\left(-T_2/T\right)$$

The parameters A, T_3, T_1 and T_2 are specified for each reaction of this type.

The approach taken at Stanford Research Institute (SRI International) [170] is somewhat similar to that explained above, but the blending function is approximated as:

$$F = d\left[a \cdot \exp\left(-b/T\right) + \exp\left(-T/c\right)\right]^X T^e,$$

where $X = \left[1 + \left(\log P_r\right)^2\right]^{-1}$ and the parameters a, b, c, d and e must be specified. Parameters d and e were not considered by Stewart et al. [170] but were added by Kee et al. [74, 77] to increase flexibility. Figure 2.3 illustrates the pressure dependent behavior of a fall-off unimolecular rate constant [32].

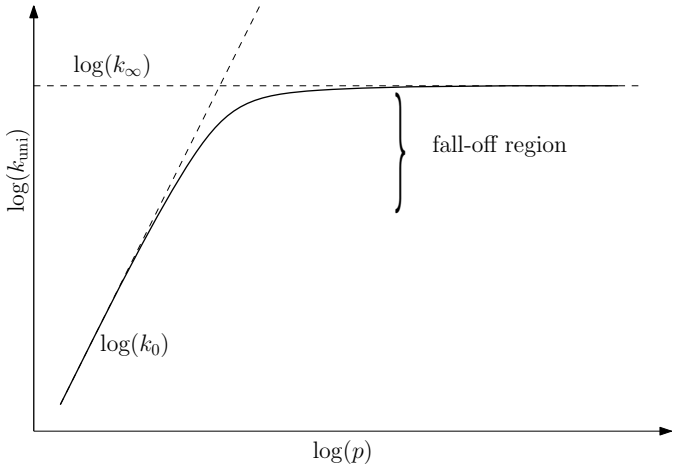

FIGURE 2.3: An illustration of a fall-off unimolecular rate constant as function of pressure

Chemically Activated Bimolecular Reactions

Total pressure also affects the rate constant for a class of bimolecular reactions called chemically activated reactions. A generic example is the reaction of molecules A and B to form products D and E, but where an alternate reaction is a recombination of the reactants to form the stable molecule C. An example of this type of chemical activation reaction is [74, 77]:

$$CH_3 + CH_3 \rightleftharpoons H + C_2H_5,$$

which competes with its alternative:

$$CH_3 + CH_3 \rightleftharpoons C_2H_6$$

Like fall-off reactions, chemically-activated reactions are described by blending between a low pressure and a high pressure rate expression. The difference is that the forward rate constant is written as being proportional to the low pressure rate constant:

$$k = k_0 \left(\frac{P_r}{1 + P_r} \right) F\left(T, P_r\right)$$

and the optional blending function $F\left(T, P_r\right)$ may be described by any of the parameterizations allowed for the fall-off reactions described above.

Pressure dependence using logarithmic interpolation (p-log reactions)

Apart from the unimolecular and chemically activated reactions, there are other reaction types that also display pressure dependence, such as radical-radical recombination,

addition of radicals to multiple bonds, dissociation and isomerization reactions, etc. [32]. The rate expression for some pressure-dependent reactions is often given by a so-called p-log formulation by interpolating logarithmically between Arrhenius expressions at different pressures for which the separate rate coefficients are given [182, 204]:

$$\ln k = \ln k_i + (\ln k_{i+1} - \ln k_i) \frac{\ln p - \ln p_i}{\ln p_{i+1} - \ln p_i}$$

Individual reaction rates are calculated using a modified Arrhenius rate expression using the rate coefficients individually listed with discrete pressures. At least two different pressures must be specified along with the corresponding rate coefficients. In some cases, more than one set of rate coefficients is given for one pressure point. The reaction rate for the given pressure is then calculated as the sum of the sets of rates. If the current pressure during the simulation is within 1% of one of the pressures for which the rate coefficients are given, then that set of rate parameters will be used directly [77]. However, if the current pressure falls in between the listed pressure values, then the rate will be evaluated using a linear interpolation of $\ln k$ as a function of $\ln p$. In case a pressure of interest is lower than any of the listed pressures, the rate coefficients for the lowest pressure are used. Likewise, if the current pressure is higher than any of the pressures provided, the rate coefficients for the highest pressure are used [55, 77].

Multiple-channel (Chebyshev Reactions)

A method for approximating the pressure- and temperature-dependent behavior of multiple-well reactions proposed by Venkatesh et al. [187, 188] uses Chebyshev expansions (instead of the modified Arrhenius) for approximating the rate coefficients. The Chebyshev expansions approximate the logarithm of the rate coefficient directly as a truncated bivariate Chebyshev series in the reverse temperature and logarithm of the pressure. Since the Chebyshev polynomials are only defined in the interval $[-1, +1]$, the temperature and pressure intervals $T_{\min} \leq T \leq T_{\max}$ and $P_{\min} \leq P \leq P_{\max}$ are mapped to an interval $[-1, +1]$:

$$\tilde{T} = \frac{2T^{-1} - T_{\min}^{-1} - T_{\max}^{-1}}{T_{\max}^{-1} - T_{\min}^{-1}}$$

and

$$\tilde{P} = \frac{2\log P - \log P_{\min} - \log P_{\max}}{\log P_{\max} - \log P_{\min}}$$

The logarithm of the rate coefficient is approximated by the Chebyshev expansions as:

$$\log k\left(\tilde{T}, \tilde{P}\right) \approx \sum_{t=1}^{N_T} \sum_{p=1}^{M_P} a_{tp} \phi_t\left(\tilde{T}\right) \phi_p\left(\tilde{P}\right),$$

where the Chebyshev polynomials of the first kind, of degree $n-1$ are given by $\phi(x) = \cos\left((n-1)\cos^{-1}(x)\right)$ with $n = 1, 2, \ldots$ and $-1 \leq x \leq 1$. The integers N_T and M_P are the number of basis functions along the temperature and the pressure axis, respectively, and a_{tp} are the coefficients of the matrix $N_T \times M_P$ determined from a least-squares fit to a set of rate coefficient data points $k\left(\tilde{T}, \tilde{P}\right)$ [77]. The Chebyshev expansions provide accurate approximations over any given temperature and pressure domain for single- and multiple-well reactions. However, these approximates should not be used for extrapolative studies outside their defined domain.

2.6 Sensitivity of Reaction Model to the Uncertainties of Thermodynamic and Transport Data

Due to the exponential dependence of the reverse rate constants on the thermodynamic properties of the species (see Section 2.5), any uncertainties in the thermodynamic data may cause significant uncertainties in reverse rate constants. Because the reaction rates are highly sensitive to thermodynamic data [183], many modelers prefer giving explicitly the rate coefficients for the reaction in both forward and reverse directions separately [11]. When the thermodynamic data are well known, the reaction can be given in its reversible form (with only forward rate coefficients), however, every attempt has to be made to ensure that the final model is internally consistent (the rate coefficents must be consistent with the thermodynamic properties of the species). The available thermodynamic data is collected in databases [11, 26–28, 149]. However, the thermodynamic data are not established for all important chemical species due to lack of available experimental methods and due to the enormous number of the species involved in real combustion systems (especially for complex hydrocarbons). In such cases, theoretical estimations may help completing the thermodynamic tables and correct inconsistencies in existing experimental values. There are two major theoretical methods to determine thermodynamic properties of chemical species [10]:

- ab initio calculations using quantum chemistry, where the chemical system is considered as an ensemble of atomic nuclei and electrons and the electronic Schrödinger equation is solved numerically using sophisticated techniques and approximations. Every molecule has to be calculated "from scratch" without any reference to the results obtained for related compounds.
- the group-additivity method which is based on summing the contributions of the functional groups constituting the molecule [15]. This method is empirical, thus restricting the applicability of each resulting additivity scheme to the range of compounds it has been made for.

A detailed overview of the methods used for determination of thermodynamic properties is given by Battin-Leclerc et al. [10].

For the combustion phenomena that take place in nonhomogeneous enviroments such as flames, accuracy of the transport properties of the species is equally important as the kinetics and the thermodynamic data. The transport properties of stable species are mostly well established, but there is a significant uncertainty in evaluating the transport properties of free radicals due to experimental limitations. The most significant radical in hydrocarbon combustion is the H atom [91]. For hydrocarbon flames the influence of the diffusion rate of the H atom was found to be comparable to the rate constant of the same chain branching process. Given the large sensitivity of laminar flame speeds with respect to the diffusion coefficients of the H atom [201], and recognizing that the discrepancy between experimental and computed laminar flame speeds of hydrogen-oxygen flames could be a result of uncertainties in H atom diffusion coefficients, a significant attention must be paid to the transport properties when developing detailed and reduced reaction mechanisms and both the experimental and theoretical efforts are required to improve their accuracy [2, 40].

2.7 Limitations of Detailed Kinetics Description

Realistic description of combustion phenomena required for combustion simulation requires a detailed description of the physics involved. All the given information, however, must be processed with an adequate accuracy and within the available computer memory and time. Detailed kinetics descriptions of realistic engine fuels frequently used in practice are too large for incorporating them into simulation codes for models that are more complex than zero- or one-dimensional cases. Figure 2.4 gives an overview of sizes of reaction mechanisms developed in the past decade. It can be seen that the number of species in mechanisms developed for complex hydrocarbons grows exponentially as the molecule size grows [105] and the mechanisms become more comprehensive as the research of reaction kinetics advances in time.

A graphic illustration of a detailed reaction mechanism for combustion of the simplest fuel (hydrogen) is given in Figure 2.5, showing a relatively large number of elementary reactions with respect to the molecule size.

In addition to a large number of species conservation equations to be solved, incorporating the mechanisms into computer simulations is impeded by chemical stiffness which frequently occurs due to large differences in time scales of species and reactions.

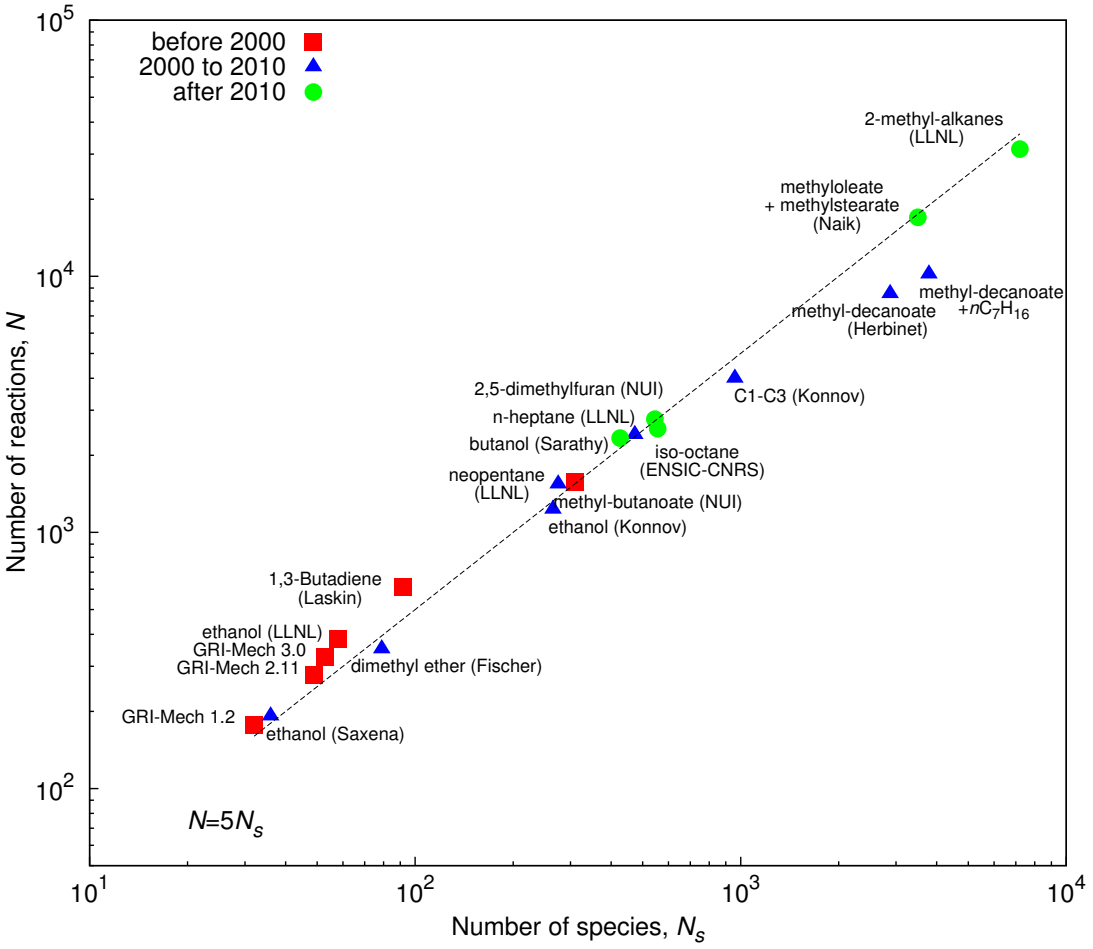

FIGURE 2.4: Overview of sizes of combustion mechanisms for some hydrocarbons and biofuels developed in last decade. This figure is made based on that from Lu and Law (2009) [105].

2.7.1 Stiffness in Combustion Problems

Numerical simulations of combustion problems are generally faced with issues of accuracy and stability during solution of differential equations. As previously stated, a general differential equation that governs the net rate of change of a species X due to an elementary reaction i can be written as:

$$\frac{d\,[\mathrm{X}]}{dt} = -k_i\,[\mathrm{X}]^x\,[\mathrm{Y}]^y\ldots \tag{2.136}$$

The overall net rate of change of molar concentration of reactant [X] results from the rates of all the reactions involving species X. These elementary reactions have different rate constants k_i, some of them being several orders of magnitude larger than the rate constants of other reactions involving X or other species. That leads to very large disparities in the time scales of the species concentration change, for example, time scales

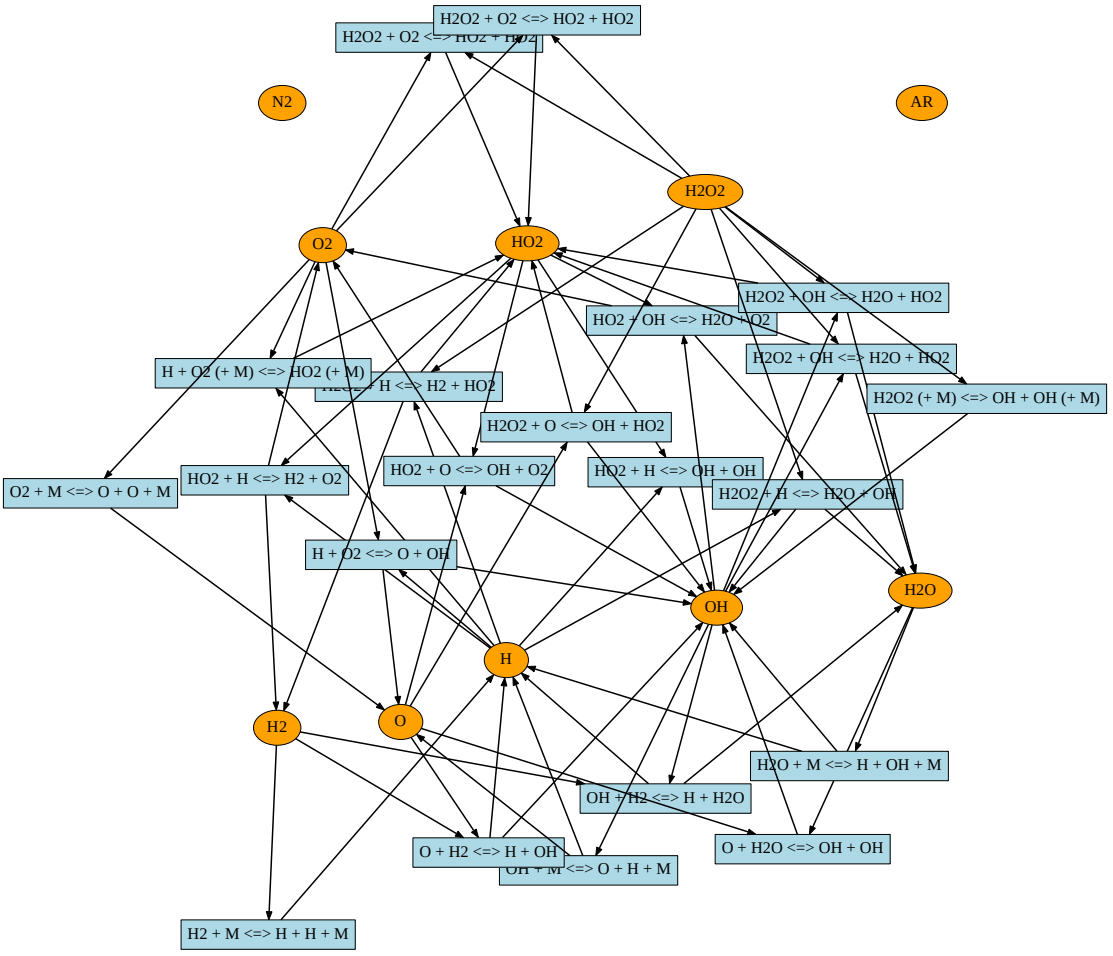

FIGURE 2.5: Bipartite representation of species and reactions in a detailed hydrogen oxidation mechanism [130].

for radicals are extremely small while the time scales for stable species are comparably large (Fig. 2.6).

In this chapter, the stiffness is only covered briefly. More detailed approaches to solving stiff equations can be found in books from Kee, Coltrin and Glarborg (2005) [74], Warnatz, Maas and Dibble (2006) [192] and work from Curtiss and Hirschfelder (1952) [35], Grcar et al. (1988) [57] and Hairer et al. (1996) [59].

Generally speaking, properties' changes in chemical kinetics may be represented with a simple linear so-called "test equation" [74]:

$$\frac{dy}{dt} = -\lambda y, \tag{2.137}$$

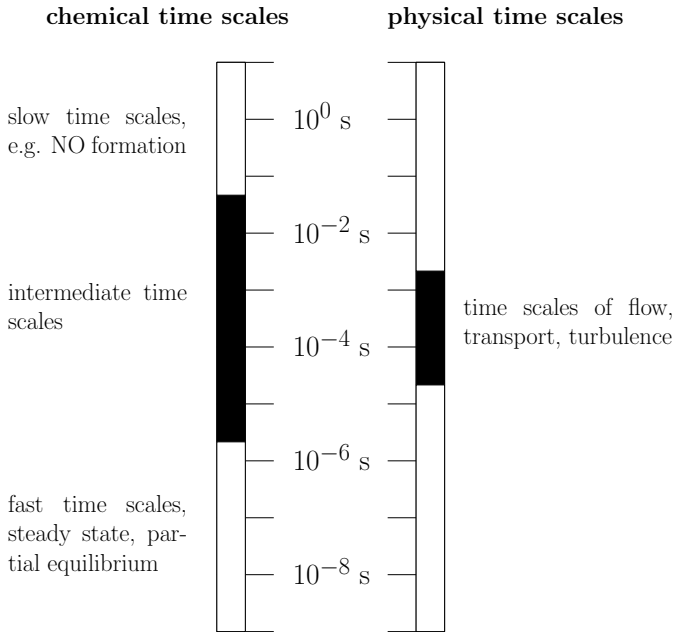

FIGURE 2.6: An illustration of the time scales governing a chemically reacting flow. This figure is based on that from Maas and Pope (1992) [106] and is reproduced with permission from Elsevier.

with $y(0) = 1$. As λ (e.g. in Eq 2.136, the rate constant) increases, the characteristic reaction time gets shorter. The general solution to this problem is obviously:

$$y(t) = e^{-\lambda t}. \tag{2.138}$$

The solution always reaches a steady state of $y = 0$, with λ determining how fast it gets there. Regardless of the value of y, the characteristic time scale of this model equation is $t = 1/\lambda$. Even at long time, when the solution is not changing at all ($y = 0$), the equation itself still has a characteristic time scale that can be quite short if λ is large. Stiffness occurs in regions where the solution is changing slowly (or not at all), yet the characteristic time scales are very small. In chemical kinetics, such behavior is exhibited by certain species, like the free radicals. After initial very rapid transients such as a combustion ignition, the free-radical concentrations often vary slowly, with their behavior controlled by steady-state or partial-equilibrium conditions. The faster the characteristic scales, the more rapidly the fast-time-constant species come into equilibrium with the major species (i.e., approach a slowly varying solution). Curtiss and Hirschfelder [35] first recognized the stiffness difficulty and showed that it could be resolved with implicit algorithms.

2.8 Need for Mechanism Reduction

A practical need for biofuels and complex fuel blends nowadays is a driving force for an extensive research of the combustion chemistry and development of comprehensive kinetics mechanisms to describe different combustion scenarios over a wide range of operating conditions. The comprehensiveness of the reaction mechanism grows with the number of different combustion phenomena and the range of operating conditions the mechanism can cover [91, 105].

Modelling of complex physical experiments (e.g. burners, turbines and engines), where not only the kinetics is being modeled, requires tremendous computational effort as each spatial dimension added to the model increases complexity and thus the computational demand. In such cases, the chemical source terms are only a sub-model within a larger more complex model. For example, for multidimensional CFD simulations that have a large number of computational cells rarely allow the calculation of detailed chemistry. Instead, global reactions or tabulated chemical source terms must be used. Figure 2.7 shows an example of a complex three-dimensional flame simulation where the combustion process is modelled with a flamelet-based tabulated chemistry approach, which assumes that the local turbulent flame structure can be described by an ensemble of wrinkled laminar flames. Instead of calculating the source terms from the reaction mechanism, tabulated values were used instead.

Therefore, on one side there are mathematically simple zero-dimensional reactors and one-dimensional laminar flame calculations where large detailed mechanisms can be studied with reasonable computational effort and, on the other side, there are complex multidimensional CFD simulations where only global reactions or tabulated values can be used. Inbetween, there are reduced mechanisms which are often derived from detailed calculations [10].

When using a mechanism in simulations, a modeler has to decide how much computational effort can be put into investigating the chemical kinetics. On the other hand, a constructed mechanism should be able to reproduce available experimental findings (validation) and, where these are not available, to predict the model behavior in not-yet observed scenarios. It should be noted that the validation alone does not mean that the model is realistic. The same combustion behavior can be achieved with different chemical models for the same fuel [147]. If a specific CFD simulation is done under a range of conditions narrower than those the detailed mechanism is validated for, the detailed mechanism is not needed for the simulation. Limiting the range of conditions the mechanism is used for is the key to applying reduction methods. Of course, there is

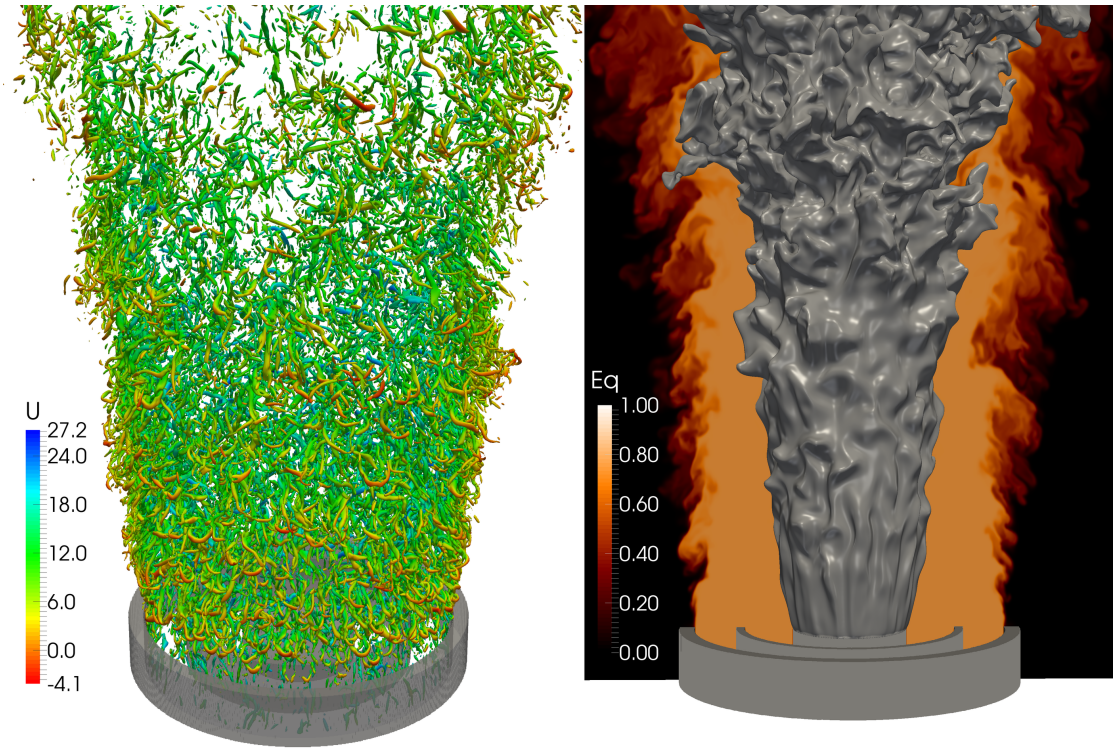

FIGURE 2.7: Results from a quasi-DNS simulation of the Cambridge/Sandia turbulent stratified burner on 1.6 billion cells with a resolution of 0.1 mm. The computation was run for for one week on 64000 processor cores at the JUQUEEN supercomputer in Jülich, Germany. Left: Turbulent structures visualized by the Iso-q-criterion. The coloring corresponds to the axial velocity component (U / (m/s)). Right: Contours of equivalence ratio in the mid-section of the burner. The isosurface for 50% of reaction progress gives the flame location [141]. Reprinted with permission.

always a trade-off between the desired comprehensiveness of the mechanism and physical accuracy of the model.

Chapter 3

State-of-the-art for Mechanism Reduction and Optimization

As previously stated, for a proper application of a chemical mechanism in CFD-based design of combustion devices, two important criteria should be met [10]: 1) a numerical solution that describes a complex combustion process should be found with affordable computational resources and 2) a mechanism should be accurate enough to provide reliable results for different operating conditions. Meeting these criteria requires development of different methods for making the mechanisms suitable for numerical simulations of combustion scenarios. This chapter presents the standard approaches for analysis, simplification and optimization of chemical reaction mechanisms.

3.1 Existing Approaches for Mechanism Reduction

There are several attractive strategies for simplifying the chemical reaction mechanisms; a comprehensive review of these approaches can be found in book chapters by Tomlin et al. [176], Law (2006) [89], Turanyi and Tomlin [182], and in several journal articles by Griffiths (1995) [58], Law et al. [90, 91] and Lu and Law (2009) [105]. In general, the mechanism reduction methods can be categorised into several groups: Elimination of unimportant reactions and/or species, time-scale analysis-based reduction, storage and tabulation methods and lumping of similar species of reactions [105].

Methods that involve selection and elimination of unimportant reactions and species are sensitivity analysis (SA), computational singular perturbation (CSP), element flux analysis (EFA), directed relation graph (DRG) and various optimization methods [4, 9, 18, 118, 122, 154, 210], for finding optimally reduced mechanisms from the corresponding

detailed mechanism. Time scale analysis and stiffness removal methods are dedicated to determining and thus decoupling fast reactions from slow reactions, which results in significant simplifications of the differential equations. Known among these methods are the so-called quasi-steady-state assumption (QSSA), partial equilibrium assumption (PEA) and intristic low-dimensional manifolds (ILDM). Lumping reduces the number of variables by combining similar reactions and species, for example, isomers that have similar thermal and transport properties. In the following, several standard reduction methods are summarized.

3.1.1 Sensitivity Analysis

As a method for elimination of unimportant reactions, sensitivity analysis is quite straightforward and simple although it may become time consuming. The concept of sensitivity analysis is to calculate the change in some global parameter, for example, in ignition delay time, the species concentrations or a laminar flame speed, due to a small change in the reaction rate [89, 151, 174, 176, 182].

Sensitivity is the dependency of the solution on the parameters of the system. If the system of reaction rate equations is formulated as:

$$\frac{d\mathbf{y}}{dt} = \mathbf{f}(\mathbf{y}, \mathbf{k}), \tag{3.1}$$

where $\mathbf{y}$ is the dependent variable vector that in this case consists of the reaction scalars such as the temperature and the concentrations of species, $\mathbf{f}(\mathbf{y}, \mathbf{k})$ is the production rate term, and $\mathbf{k}$ is the vector for the rate coefficient (preexponential factor).

The sensitivity matrix is then defined as:

$$\mathbf{S} = \frac{\partial \mathbf{y}}{\partial \mathbf{k}} \tag{3.2}$$

Time derivative of the sensitivity matrix is then

$$\frac{\partial \mathbf{S}}{\partial t} = \frac{\partial}{\partial t}\left(\frac{\partial \mathbf{y}}{\partial \mathbf{k}}\right) = \frac{\partial}{\partial \mathbf{k}}\left(\frac{\partial \mathbf{y}}{\partial t}\right) = \frac{\partial \mathbf{f}(\mathbf{y}, \mathbf{k})}{\partial \mathbf{k}} = \frac{\partial \mathbf{f}}{\partial \mathbf{k}} + \frac{\partial \mathbf{f}}{\partial \mathbf{y}} \cdot \frac{\partial \mathbf{y}}{\partial \mathbf{k}} = \frac{\partial \mathbf{f}}{\partial \mathbf{k}} + \mathbf{J} \cdot \frac{\partial \mathbf{y}}{\partial \mathbf{k}} \tag{3.3}$$

The term $\mathbf{J} = \partial \mathbf{f}/\partial \mathbf{y}$ is the Jacobian matrix of the Equation 3.2.

The sensitivity of a system response parameter $\mathbf{y}$ with respect to the perturbation of the reaction rate constant $\mathbf{k}$ of a reaction is defined as $\partial \mathbf{y}/\partial \mathbf{k}$. Thus its lognormal form, $\partial \ln \mathbf{y}/\partial \ln \mathbf{k}$, measures the relative error induced by the removal of this reaction. Reactions with sensitivity smaller than certain specified values can be considered to be

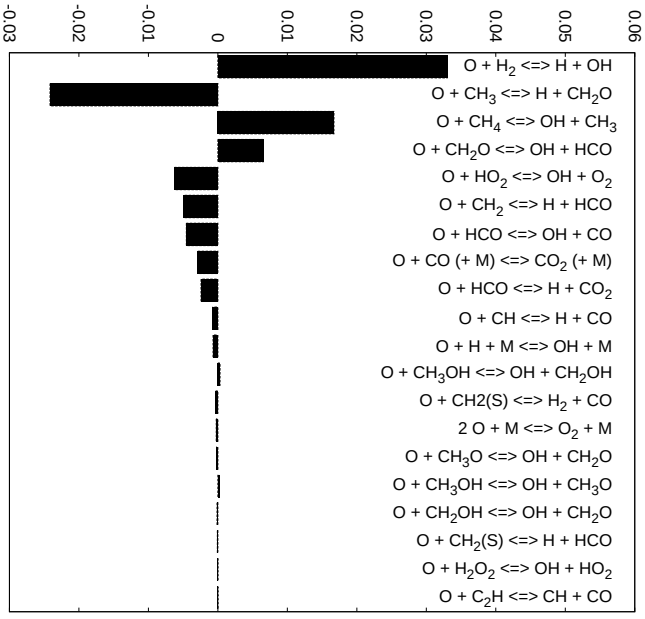

FIGURE 3.1: Ilustration of the sensitivity coefficients for the flame speed of an atmospheric stoichiometric methane flame in respect to arbitrarily chosen reactions from the mechanism.

unimportant and hence neglected. A graphical representation of sensitivity coefficients for the flame speed in respect to the reaction rates is illustrated in Fig. 3.1. The aim of the sensitivity calculation is to determine how the solution changes with the change of the reaction rates. Small changes in some elementary reactions may lead to significant changes of the solution, while changes in other reactions may not have any effect on the solution at all. This way, the sensitivity analysis shows which reactions are in quasi-steady state or in partial equilibria and which reactions are the rate-controlling steps. The sensitivity analysis is widely used for the investigation and analysis of chemical kinetics [80, 142, 173, 179, 180].

3.1.2 Quasi-Steady State and Partial Equilibrium Assumptions

The quasi-steady-state assumption (QSSA) and the partial equilibrium assumption (PEA) allow generating reaction-rate expressions that still can capture the details of the reaction chemistry with a minimum number of rate constants. One of the characteristic features of many chemically reacting systems is the widely disparate time scales at which elementary reactions occur. Complex reaction mechanisms usually contain rate constants that differ from each other by several orders of magnitude. For example, the concentrations of highly reactive intermediates (like radicals, atoms, ions and molecules

in excited states) may differ by orders of magnitude from the concentrations of relatively stable species.

These significantly different time and concentration scales introduce difficulties for accurate estimation of the rate constants, measurement of low concentration species and numerical solving of complex models. Usually these highly reactive and low-concentration intermediates, are identified as QSS-species [22, 182, 192]. This means that the production and destruction rates of these species can be considered zero in the kinetic system of ODEs. This allows algebraic solutions for the concentrations of the QSS-species from the concentrations of the other (non-QSS) species. The system of ODEs for the non-QSS-species and the system of algebraic equations for the QSS-species together form a coupled system of algebraic differential equations and their solution is close to that of the starting system of ODEs.

In some cases, the concentrations of all QSS-species can be calculated from (explicit) algebraic equations separately and then their concentrations can be used for solving the system of kinetic ODEs for the remaining species. In this way, the system of ODEs is transformed to a smaller system of ODEs having fewer variables. Very often, the concentrations of QSS-species are not relevant for the overall prediction ability of the kinetics scheme so that they can be eliminated, thus reducing the overall number of variables in the mechanism and consequently its stiffness (because the range of the remaining timescales has been reduced). Using the QSSA, the full mechanism is simplified based on rapidly equilibrating species rather than reactions as in the reaction equilibrium assumption.

Using the partial equilibrium assumption [182, 192], the mechanism simplification is made on the basis of fast and slow reactions. In a given complex mechanism, some reactions may be significantly faster than others, so that they equilibrate after any displacement from their equilibrium condition. The remaining, slower reactions then govern the rate at which the amounts of reactants and products change. If we consider the extreme case in which all reactions except one are assumed at equilibrium, this remaining slow reaction is called the rate-limiting step. Using PEA, a detailed mechanism can be divided in two subsets consisting of any number of slow and fast reactions, and make the equilibrium assumption for the subset of fast reactions. On the other hand, QSSA and PEA methods require considerable human effort and chemical knowledge for each fuel/oxidizer system. Another disadvantage of these classical methods is that they can only be applied to the conditions (ranges of compositions and temperatures) where it is aceptable to obtain the poor approximations of intermediate species concentrations [182, 192], which is typically not sufficient if a more detailed insight into kinetics

is desired, or if the prediction of the considered phenomena strongly depends on the intermediate species concentrations.

3.1.3 Jacobian Matrix Analysis

Computational Singular Perturbation

The concept of computational singular perturbation (CSP) was first proposed by Lam in 1985 [83], and further improved and used to simplify the kinetic model by decoupling the fast and slow reaction modes [56, 84–86, 88, 99, 107, 108, 132, 184, 185]. The CSP aims to computationally derive time-resolved simplified chemical models for complex chemical systems. The CSP method relies on the eigenvalues of the Jacobian matrix to determine the trial modes [106], and the subsequent refinement step improves the decoupling of the fast and slow trial modes. Unlike the QSSA and PEA, CSP and ILDM do not require any chemical knowledge and intuition, as the eigenvectors of the Jacobian matrix can always be used as the trial set. The CSP exploits the disparity of the time scales between the fast modes (exhausted) and the (currently active) slow modes. The output of the CSP is so-called CSP data and it contains the information on: the number of approximate equations of state (approximate algebraic relations between the species), which species are identified as radicals so that they can be computed from the approximate equations of state, which reactions are rate-controlling and what is the minimal reaction system that can yield the solution with a user-defined accuracy [84]. The CSP data can also be used to assess the sensitivity of solutions with respect to the input rate coefficients [87] as an alternative to the classical sensitivity analysis [203].

Intrinsic Low-Dimensional Manifold

This method is similar to the CSP method in identifying and decoupling fast and slow species by the Jacobian matrix analysis. The Intristic Low-Dimensional Manifold (ILDM) method searches for the low-dimensional manifold that represent a simplified description of the chemical model within the states space by identifying the fast time scales as those that reached the equilibrium [106]. Given that the chemical system composition is seen as a point in a multidimensional space, where each dimension represents a species concentration, the rate equations describes how that point moves in the scalar space [29, 78, 106, 145]. The ILDM analyses and simplifies these equations of the scalar-point motion by identifying attracting manifolds in the scalar space. Because of the wide range of time scales in a chemical system, the composition changes very rapidly in some directions and moves very slowly in other directions. Therefore the composition moves rapidly towards the attracting manifold, and then moves along that surface to the equilibrium point. The mechanism simplification is based on the assumption that the composition always lies on these manifolds.

The dimension of the manifold must be specified apriori. For example, a zero-dimensional manifold is the equilibrium point and a one-dimensional manifold is a line, on which the equilibrium point lies. One-dimensional manifold (a line in the scalar space) can therefore be parameterized by just one variable (a scalar, a combination of scalars or a thermodynamic property, known as the reference variable). The values of all the species in the detailed mechanism, including the intermediates as well, on the manifold are available as a function of the reference variable without increasing the mechanism complexity. The state properties can also be stored on the manifold and calculated taking into account all the minor species. The disadvantage of the ILDM method is that the tabulation of the manifolds in a database requires significant effort for each new detailed mechanism and requires a specialised computer program. The look-up tables for multivariate manifolds can become extremely large, and retrieval in the database can therefore be slow [182].

3.1.4 Flux Analysis

Element flux analysis is a species-oriented reduction technique based on quantification of atom fluxes of elements through all reactions in the mechanism. This way, the element contributions over the integrated time interval is determined and used as a basis for species selection. The method is proposed by Revel et al. (1994) [146] and later improved by Androulakis et al. (2004) [5], He et al. (2008 and 2010) [61, 62], Sun et al. (2010) [171] and Perini et al. (2012) [137]. The atom flux $\dot{A}_{ijk}$ during the reaction i from the species j to the species k is formulated as:

$$\dot{A}_{ijk}(t) = \left(|q_{fwd,i}(t)| + |q_{rev,i}(t)|\right) \frac{n_{A,j} n_{A,k}}{N_{A,i}}, \tag{3.4}$$

where $q_{fwd,i}$ and $q_{rev,i}$ are the atom fluxes during the reaction i in forward and reverse directions, respectively $n_{A,j}$ is the number of atoms of element A in species j, $n_{A,k}$ is the number of atoms of the same element in species k and $N_{A,i}$ is the overall number of atoms of the element A within the reaction i. The importance of the species is determined based on the contribution of the element fluxes A_{jk} to the overall flux A_{tot} which are defined as:

$$A_{tot} = \sum_{j,k} \dot{A}_{jk} \tag{3.5}$$

and

$$A_{jk} = \sum_{c=1}^{N_c} \left[\int_{\tau=0}^{\tau=t_c} \left(\sum_{i=1}^{N} \dot{A}_{ijk,c}(\tau) \right) d\tau \right], \tag{3.6}$$

where N_c is the number of conditions the mechanism is intended for and τ is the simulated time. Species that should remain in the mechanism are chosen according to a

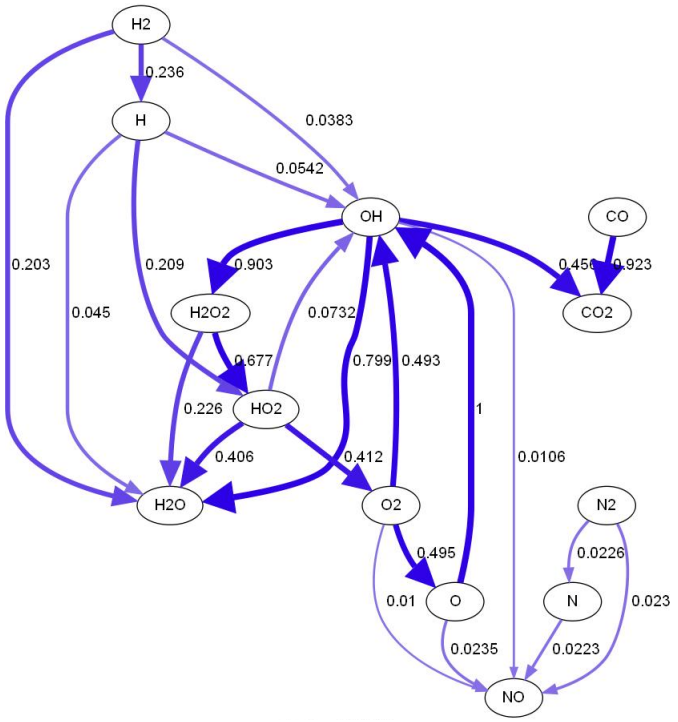

FIGURE 3.2: Ilustration of the elemental flux pathways between the reacting species

user-defined cut-off value (fraction of the overall atom flux to be kept in the reduced mechanism). Species (source-sink pairs) with element flux values above the cut-off value are kept in the mechanism, and those with fluxes below the cut-off value are eliminated. Consequently, a reaction is kept in the mechanism only if all its reacting species are kept. All the reactions with at least one of its species being eliminated from the mechanism are eliminated as well. Figure 3.2 illustrates the net elemental flux between the reacting species in the mechanism. The line thickness is proportional to the net elemental flux.

Wang et al. (2013) [191] combined the element flux analysis with CSP and QSSA to obtain a global reduced combustion mechanism for multicomponent kerosene surrogate. Zhang et al. (2013) [207] combined the dynamic flux-based "on-the-fly" reduction and the QSSA into a hybrid approach for the mechanism reduction.

3.1.5 Directed-Relation Graph

The directed relation graph (DRG) method is a species elimination-oriented reduction technique originally proposed by Lu and Law [100, 102]. Interaction and coupling between the species is represented as the edges of a directed graph whose nodes represent the species in the mechanism. The edges between the two nodes A and B exists if and only if the elimination of B directly causes significant error to the production rate of A,

and in that case B must be kept in the mechanism if the correct prediction of the production rate of A is important. This dependence between the two species is quantified in terms of a normalized contribution of, say, species B to the production rate of species A, r_{AB}:

$$r_{\mathrm{AB}} = \frac{\sum_{i=1}^{N_R} |\nu_{\mathrm{A},i}\omega_i\delta_{\mathrm{B},i}|}{\sum_{i=1}^{N_R} |\nu_{\mathrm{A},i}\omega_i|}, \tag{3.7}$$

where

$$\delta_{\mathrm{B},i} = \begin{cases} 1 & \text{if reaction } i \text{ involves species B} \\ 0, & \text{otherwise.} \end{cases} \tag{3.8}$$

Considered species are denoted with A and B, $\nu_{\mathrm{A},i}$ is the stoichiometric coefficient of species A in the reaction i and ω_i is the rate of reaction i. If the normalized contribution r_{AB} is smaller than a pre-defined threshold value ϵ, the edge from A to B is negligible and B can be removed. Otherwise, B must be kept. In general, for each species A in the detailed mechanism, there exists a set of species that significantly contribute to A and if A is important to be kept in the mechanism, its dependant species set must be kept as well. Figure 3.3, based on that from Lu and Law [100], illustrates relations between the species in DRG. Strongly coupled species should remain in the reduced mechanism.

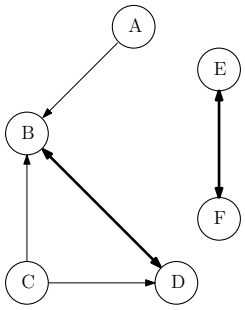

FIGURE 3.3: An example of DRG: If A must be kept, B and D must be kept as well. For the production rate of A, species C, E and F are not important and can be removed. Taken from [100] and reprinted with permission.

Prior to the reduction, a user-defined set of important species to be kept must be selected and a depth-first search of a relation graph is then performed to find the dependent set of the important species. The skeletal mechanism is constructed as a union of these dependant sets and the reactions not involving any of these sets are finally removed from the detailed mechanism. There are many variations and further enhancements of the DRG-based reduction method proposed in the literature [101, 104, 127–129, 135, 152, 208].

3.1.6 Lumping Methods

Despite significant reduction, some mechanisms may still be too expensive for complex CFD applications. This is especially true for pyrolysis and combustion mechanisms of complex hydrocarbons or atmospheric chemical models which contain a large number of isomers and intermediates and multiple-channel reactions between them. In such cases, when the reduction in terms of further elimination of species and reactions is no longer possible, the restructuring of the mechanism may be required [182]. This can be done either by species lumping or by reaction lumping methods briefly described in the following.

Species Lumping

Species lumping is done by representing a number of isomers of a specific species as one (lumped) component [24]. For applying the species lumping, the following steps are required: 1) identification of the species to be lumped, 2) definition of the lumping transformation (how the chosen species contribute to the lumped species) and 3) determination of the kinetic parameters for the reactions involving the lumped species. The reactions occuring between the lumped species are no longer elementary. Because of the same molecular weight and similar transport and thermodynamic properties, the isomers can be lumped and their transport equations combined into one if their chemical source term can be computed [103, 104].

Chemical lumping methods determine the lumping groups based on chemical structure of the species and rules for combining species and reactions. Such methods rely on a hierarchical manner in which the mechanisms are often developed [49, 134, 143, 144, 169, 182]. For complex hydrocarbons with many isomers, chemical lumping splits the main propagation reactions into few reaction classes [49, 144, 150] and the rate coefficients for each reaction class are defined based on the literature, similarity rules or fitting with respect to experimental data. Lumping isomers and intermediates results in a simplified reaction scheme with one pathway representing degradation to the average products of all the isomers. The chemical lumping requires extensive chemical expertise to organize the lumping structures. As an alternative, there are mathematically-based approaches for transforming the original species into lumped groups [71, 81, 92, 94, 175]. Since the chemical lumping yields lumped species whose concentrations are linear combinations of the original species, this approach can be mathematically defined as a transformation of the original vector of variables to a transformed variable vector using the transformation function [175, 182] which is not unique.

If the transformation function is linear, this lumping approach is termed linear species lumping. However, for highly nonlinear problems (e.g. ignition or oscillatory systems) where the lumping transformations may vary rapidly, approximate nonlinear lumping methods have been developed [93, 94, 182]. Although the nonlinear lumping methods may be more general and applicable over wider ranges of operating conditions than the linear methods are, the algebraic complexity is high due to nonlinear functions.

Reactions Lumping

Detailed reaction mechanism can also be simplified by lumping some of its elementary reactions based on their common reactants, for example [182]:

$$\begin{aligned} \mathrm{A} + \mathrm{B} &\rightarrow \mathrm{C} + \mathrm{D} \qquad (0.4k) \\ \mathrm{A} + \mathrm{B} &\rightarrow \mathrm{E} + \mathrm{F} \qquad (0.6k) \end{aligned}$$

This reaction is a multichannel reaction with two reaction channels, one resulting in products $\mathrm{C} + \mathrm{D}$ and the other in $\mathrm{E} + \mathrm{F}$ with the branching ratio $0.4 : 0.6$ and the overall rate constant of the reaction is k. The branching ratio is the ratio of the rate constant for one product of the multichannel reaction to the rate constant for the overall set of possible products [155]. The chemical equations above can therefore be written as [182]:

$$\mathrm{A} + \mathrm{B} \rightarrow 0.4\mathrm{C} + 0.4\mathrm{D} + 0.6\mathrm{E} + 0.6\mathrm{F} \qquad (k)$$

Despite the reduction in the number of reactions, the number of species is not changed. An alternative way to lump the reactions relies on a rate determining step [182]:

$$\begin{aligned} \mathrm{A} + \mathrm{B} &\rightarrow \mathrm{C} + \mathrm{D} \qquad (k_1[\mathrm{A}][\mathrm{B}]) \qquad slow \\ \mathrm{D} + \mathrm{E} &\rightarrow \mathrm{F} \qquad (k_2[\mathrm{D}][\mathrm{E}]) \qquad fast \end{aligned}$$

The rate-determining step is the first (slow) reaction, thus the rate of the resulting lumped reaction is $(k_1[\mathrm{A}][\mathrm{B}])$. The lumped reaction is now:

$$\mathrm{A} + \mathrm{B} \rightarrow \mathrm{C} + \mathrm{F} - \mathrm{E} \qquad (k_1[\mathrm{A}][\mathrm{B}])$$

Reactants A, B and E are consumed while C and F are produced. Since equal amounts of D are consumed and produced, D does not take part in the lumped reaction. Species E is consumed, but since it is not part of the rate-determining step, it appears on the right-hand side, with a negative stoichiometric coefficient. The reaction lumping decreased the number of reactions and removed species D, which may decrease the computational cost. The reactions lumping approach may also be combined with the local sensitivity analysis and the QSSA leading to significant reductions of complex hydrocarbon mechanisms [72].

3.2 Existing Approaches for Mechanism Optimization

Although the reduced mechanisms are computationally efficient, their accuracy may be lowered due to elimination of many reactions. In order to keep the reduced mechanism computationally inexpensive and to enhance its prediction quality at the same time, optimization approaches have been developed. In general, the optimization of a reaction mechanism is done by tuning its reaction rate coefficients to match the correct overall behavior of the detailed mechanism or the available experimental data. Rates of single reactions within a reaction mechanism are calculated from a rate expression which is at least a function of temperature (see Section 2.5). Coefficients for the rate expressions are available from chemical databases and are often consistent with measurements and theoretical calculations. In the following, a brief summary of the existing optimization approaches is presented.

3.2.1 Solution Mapping Method

Frenklach et al. (1992) [50] proposed a method of solution mapping to systematically optimize a dynamic model which is non-linear and its parameters are associated with their own uncertainties. Given a system of ODEs describing a dynamic system:

$$\frac{d\mathbf{y}}{dt} = \mathbf{g}\left(t, \mathbf{y}, \boldsymbol{\vartheta}\right), \tag{3.9}$$

where $\mathbf{y}$ is the vector of the state variables (concentration, temperature), t is the reaction time, $\boldsymbol{\vartheta}$ is the vector of rate coefficients and $\mathbf{g}$ functions express, for example, the mass-action law, energy balance, etc. The aim is to determine the values of $\boldsymbol{\vartheta}$ for given initial conditions $\boldsymbol{\zeta} = \mathbf{y}_{t=0}$ such that

$$\mathbf{y} = \mathbf{f}\left(\boldsymbol{\vartheta}, \boldsymbol{\zeta}, t\right), \tag{3.10}$$

which is the solution of Eq. 3.9, reproduces the experimental observations $\mathbf{y}^{\text{obs}}$. The extent of matching of Eq. 3.10 and $\mathbf{y}^{\text{obs}}$ is achieved by minimization of the objective function $\boldsymbol{\Phi}$ with respect to the rate coefficients $\boldsymbol{\vartheta}$:

$$\boldsymbol{\Phi}\left(\boldsymbol{\vartheta}\right) = \sum_{r=1}^{n} \omega_r \left[y_r^{obs} - y_r\left(\boldsymbol{\vartheta}\right) \right], \tag{3.11}$$

where n is the number of experiments (responses) and ω_r is the statistical weight of the response r. The minimum of the Eq. 3.11 can be found by a search algorithm in a straightforward manner, but that would require solving of differential equations to obtain $\mathbf{y}\left(\boldsymbol{\vartheta}\right)$ every time $\boldsymbol{\Phi}\left(\boldsymbol{\vartheta}\right)$ needs to be evaluated. To avoid the computational effort of numerical integrations, Eq. 3.10 is approximated with simple algebraic expressions

within a subspace of parameter space $\boldsymbol{\vartheta}$.

$$\mathbf{f}_t, (\boldsymbol{\zeta}\boldsymbol{\vartheta}) \approx \boldsymbol{\Psi}(\boldsymbol{\vartheta}). \tag{3.12}$$

The approximating functions $\boldsymbol{\Psi}(\boldsymbol{\vartheta})$ are obtained from a small number of numerical simulations (computer experiments) performed using a detailed chemical kinetics model with predefined parameters $\boldsymbol{\vartheta}$. These functions $\boldsymbol{\Psi}(\boldsymbol{\vartheta})$ are called response surfaces. The objective function (Eq. 3.11) now becomes

$$\boldsymbol{\Phi}(\boldsymbol{\vartheta}) = \sum_{r=1}^{n} \omega_r \left[\eta_r^{obs} - \boldsymbol{\Psi}_r(\boldsymbol{\vartheta})\right], \tag{3.13}$$

and does not require expensive numerical integration, thus decoupling the optimization process from numerical integration of differential equations. In general, there is no restriction in which mathematical expression to use for $\boldsymbol{\Psi}(\boldsymbol{\vartheta})$. In the work from Frenklach et al. [50], a polynomial form for $\boldsymbol{\vartheta}$ was used and its coefficients were obtained from computer experiments. It is not necessary to optimize all the reaction rate coefficients under a specific set of operation conditions, but only the so-called active parameters which are identified by screening sensitivity analysis. The method yields a number of indistinguishable solutions, giving evidence for the lack of solution-uniqueness. The method helps identifying parameter correlations and quantifying the model uncertainties as well.

3.2.2 Polynomial Chaos Expansion

A method that combines development of the chemical model and propagation and minimization of the chemical uncertainties is proposed by Sheen et al. [158–160] and is termed the Method of Uncertainty Minimization using Polynomial Chaos Expansions (MUM-PCE). The uncertainty is quantified using the stochastic spectral expansion (SSE) method [126] which is then combined with the solution mapping to calculate the prediction uncertainties of a simulation. The model is constrained by the data from the experimental databases and MUM-PCE quantifies the model uncertainties before and after optimization. First, an uncertainty factor UF_i is assigned to each input variable. This uncertainty factor UF_i is related to uncertainty parameter f, which is later discussed in Section 4.2, by $\mathrm{UF}_i = 10^f$. The rate coefficients are then normalised into factorial variables x_i as follows:

$$x_i = \frac{\ln\left(k_i/k_i^0\right)}{\ln \mathrm{UF}_i},$$

where k_i is the rate coefficient of reaction i and k_i^0 its nominal value. Therefore, $x_i = 0$ is the nominal value of the rate coefficient with an uncertainty bound $[-1, +1]$ based on evaluated data from chemical databases [11–13]. A response surface $\eta_r(\mathbf{x})$ of the model r is generated with respect to $\mathbf{x}$ as:

$$\eta_r(\mathbf{x}) = \eta_{r,0} + \sum_{i=1}^{m} a_{r,i} x_i + \sum_{i=1}^{m} \sum_{j \geq i}^{m} b_{r,i,j} x_i x_j + \dots$$

The uncertainty in x may be expressed as a polynomial expansion of basis random variables $\boldsymbol{\xi}$:

$$\mathbf{x} = \mathbf{x}^{(0)} + \sum_{i=1}^{m} \boldsymbol{\alpha}_i \xi_i + \sum_{i=1}^{m} \sum_{j \geq i}^{m} \boldsymbol{\beta}_{i,j} \xi_i \xi_j + \dots,$$

where $\boldsymbol{\alpha}$ and $\boldsymbol{\beta}$ are column vectors of the expansion coefficients, m is the number of the considered rate coefficients and $\mathbf{x}^{(0)}$ is a column vector of the normalised rate coefficients which is a zero vector for the nominal reaction model. If the x's are independent of each other and normally distributed, then the usual choice for the form of $\boldsymbol{\xi}$ would be a set of unit normal random variables. If $\ln \mathrm{UF}_i$ represents two times the standard deviation of $\ln k_i$, then $\boldsymbol{\alpha} = 1/2\mathbf{I}_m$, where $\mathbf{I}_m$ is the m-dimensional identity matrix and $\boldsymbol{\beta}$ and all higher-order terms are zero. In the general case, combining the above two equations and truncating the higher-order terms give [159, 182]:

$$\eta_r(\boldsymbol{\xi}) = \eta_r\left(\mathbf{x}^{(0)}\right) + \sum_{i=1}^{m} \hat{\boldsymbol{\alpha}}_{r,i} \xi_i + \sum_{i=1}^{m} \sum_{j \geq i}^{m} \hat{\boldsymbol{\beta}}_{r,i,j} \xi_i \xi_j + \dots,$$

with coefficients of $\hat{\boldsymbol{\alpha}}_r = 1/2\mathbf{I}_m \mathbf{a}_r$ and $\hat{\boldsymbol{\beta}}_r = 1/4\mathbf{I}_m^{\mathrm{T}} \mathbf{b}_r \mathbf{I}_m$. This equation shows that the overall model prediction is given by its nominal value plus the uncertainty contributions from each rate coefficient. The overall output variance is then expressed as the sum over terms involving the coefficients of the equivalent expansion:

$$\boldsymbol{\sigma}_r(\boldsymbol{\xi})^2 = \sum_{i=1}^{m} \hat{\boldsymbol{\alpha}}_{r,i}^2 + 2\hat{\boldsymbol{\beta}}_{r,i,j}^2 + \sum_{i=1}^{m} \sum_{j \geq i}^{m} \hat{\boldsymbol{\beta}}_{r,i,j}^2$$

This method is then combined with the solution mapping approach for the optimisation of the rate coefficients which are constrained depending on whether x's are uniformly or normally distributed. If x's are uniformly distributed, the optimization features a term in the objective function which constrains the rate coefficient change. If x's are normally distributed, this term is omitted and x is bounded by $[-1, +1]$ (normal distribution of the rate coefficient indicates that the parameter is carefully measured).

Later, relying on MUM-PCE, Cai and Pitsch [30, 31] used the rate rules to optimize the Arrhenius pre-exponential factors of the reaction classes instead of tuning individual

reactions. One set of rate coefficients is treated as one optimization object, which reduced the dimensionality of the optimization problem. Uncertainties of the rate rules in this work are considered to be large and the MUM-PCE method [159] was used for the model calibration and the uncertainty estimation.

Xin et al. 2015 [200] used MUM-PCE method to optimize skeletal reaction mechanisms for *n*-butane and *iso*-butane combustion obtained with DRG and DRGASA from USC Mech II [190]. They also investigated dependence of the model uncertainty on the model size indicating that the uncertainty increases with the model size. This approach underlines the necessity for a better quantification of the rate coefficients (experiments or theoretical calculations) to reduce the uncertainties. Furthermore, the uncertainty parameter f is only available for well-established models which is not the case for large and highly complex mechanisms (e.g. surrogates or biofuels).

Sheen and Wang 2011 [159] show that, when experimental results are the reference for the optimization, it is necessary that the experimental uncertainty be less than the model prediction uncertainty, which requires a rigorous uncertainty analysis. They stress that it is difficult (or impossible) to obtain a unique chemical model that can best reproduce the experimental measurements and suggest estimated or evaluated reaction rates as a reference for the optimization. As a mathematical tool, MUM-PCE can provide insight into couplings of the rate coefficients in a model and reduce prediction uncertainties inside and outside of the experimental conditions under which the fuel properties were studied.

3.2.3 Optimization Algorithms

Optimization methods for the reduction and/or the optimization of the mechanisms are based on minimising an objective function subject to a given set of constraints. Generally speaking, the objective function is based on the difference between the simulation results obtained using detailed and reduced mechanisms and the optimization method is aiming at minimising this difference (error). Many optimization techniques have been developed; some of them being gradient-based while others rely on heuristics and evolutionary algorithms. Gradient-based optimization methods direct the search in direction of the steepest gradient of the objective function to find its minimum [105, 176]. These methods are often extended by applying sensitivity analysis in order to identify the principal components of the system [174, 189]. However, the gradient-based methods capture only the local optimum of the objective function which is inconvenient for systems with multiple optima that are typical for chemical kinetics problems [17].

For handling complex objective functions over a multidimensional search space, genetic algorithms have shown to be particularly suitable and were used as an efficient tool for numerous optimization problems.

Polifke et al. [140] implemented genetic algorithms for optimizing a simplified two- and three-step methane-oxidation mechanism to match the heat release and net species production rates for premixed laminar flames. Harris et al. [60] used genetic algorithms to solve the inverse problem of determining the rate parameters that would match the measured species concentrations for hydrogen combustion. This approach was successful in retrieving rate coefficients that give accurate predictions for the investigated data set. Aiming to cover measurements different to those used in the optimization proposed in [60], Elliott et al. [42] extended the objective function of Harris' method to predict measurements of species concentration profiles for both laminar flames and perfectly-stirred reactors (PSR). Further on, to expand the validity range of the optimized mechanisms beyond the conditions used in the optimization, Elliott et al. [43, 44, 46] incorporated the predefined boundaries of the rate coefficients taken from the NIST (National Institute of Standards and Technology) chemical kinetics database.

Later, Elliott et al. [45] improved the multi-objective genetic algorithm to determine the Arrhenius coefficients and to recover observed species concentrations under different sets of operating conditions. Montgomery et al. 2006 [121] used a genetic algorithm to reduce a mechanism for methane-air combustion over a range of temperatures and stoichiometries by selecting the optimal set of QSS species based on the difference between the simulation results without and with the QSSA. The species set was found when the simulation error decreased below a certain threshold.

Aldawood et al. [1] used also a multi-objective genetic algorithm to optimize a model for homogeneous-charge compression ignition (HCCI) against twelve sets of experimental data. The mechanism was treated together with the model, i.e. three Arrhenius equation coefficients and four variables relevant for the simulated stochastic reactor model, were optimized at the same time. Constraints for the optimization variables were predefined to account for model uncertainties ($\pm 50\%$ for the Arrhenius coefficients and user-defined reasonable ranges for the model itself).

The genetic algorithm-based optimization method from Perini et al. [136, 137] employs the objective function adapted from [44] and optimizes both the pre-exponential factors and the activation energies allowing deviations of $\pm 15\%$ for the activation energy and $\pm 80\%$ for the pre-exponential factor. Temperature exponents were not optimized as most of them are equal to zero in many combustion mechanisms.

Optimization by Shaw et al. [157] considered chemical lifetime of each species in the large reaction mechanism, thus identifying the reactions to be optimized. The most relevant species are chosen based on the Level of Importance (LOI) technique [98] and the sensitivity analysis of the reactions in respect to important species helps identifying reactions to be optimized. Uncertainty of the reaction rates are not taken into account as the goal of the study was the optimization itself. However, certain constraints to altering the model were allowed and user-defined, with the maximum error being one order of magnitude for the reactions that were not well investigated. The resulting optimized mechanism had better predictability than the original one over a wide range of data from shock tube experiments.

The uncertainty of the rate parameters has been subject to numerous studies [63, 123–125, 156, 181, 186]. Although the consideration of the reaction rate uncertainties was not advocated by this work, it was made possible to constrain the individual reaction rates by their prescribed uncertainty factors. A preferred approach in this work is constraining the reaction rate alterations with the penalty function during the optimization. This approach is discussed in Section 4.2.3.

Chapter 4

Genetic Algorithm-based Mechanism Manipulation

This chapter explains the methodology of simplifying and optimizing the chemical kinetics mechanisms using the genetic algorithm adopted for this study. This section first explains the use of genetic algorithms for the elimination of reactions from the detailed reaction mechanism aiming to reduce the size of a reaction mechanism, ensuring a good accuracy for a certain application and preventing the excessive stiffness in the resulting reduced mechanisms. Following the reduction methodology, the use of the genetic algorithm to optimize the reduced mechanism by altering the rate coefficients of the remaining reactions is presented in the latter part of this section.

4.1 Mechanism reduction

The genetic algorithm-based methodology used in the present study for the mechanism reduction aims at finding the smallest possible mechanism (or one that is only slightly bigger, but easier to solve) from its detailed version which is still able to reproduce the simulation results of interest from the detailed mechanism with accuracy sufficient for the application and less computational effort. The accuracy and the size criteria for the reduced mechanism are user-defined within the objective function of the algorithm. The genetic algorithm is then searching for a solution (submechanism) for which the given objective function will be minimal. The reactions are gradually eliminated from the mechanism during the search by both the objective function containing the size criteria and the mutation operation adjusted to the reduction problem. The genetic algorithm can be summarized in the following steps [53, 117]:

1. Initialization of the first population of solutions by generating the initial chromosome population,
2. Evaluation of the performance of each chromosome (by using the chemical mechanism in a reacting case simulation),
3. Selection of the fittest chromosomes (parents) from the current population to yield the next generation of chromosomes,
4. Crossover of the selected chromosomes in order to exchange genes to produce new chromosomes (children) for the next generation,
5. Mutation by a small change to the children chromosomes which increases the diversity of the population and avoids falling into local minima.

Steps 2 to 5 are repeated until the pre-defined termination criteria are satisfied (Figure 4.1). The problem-specific genetic algorithm operations used in the present work are described in the following sections. For the GA-based reduction to be performed, a

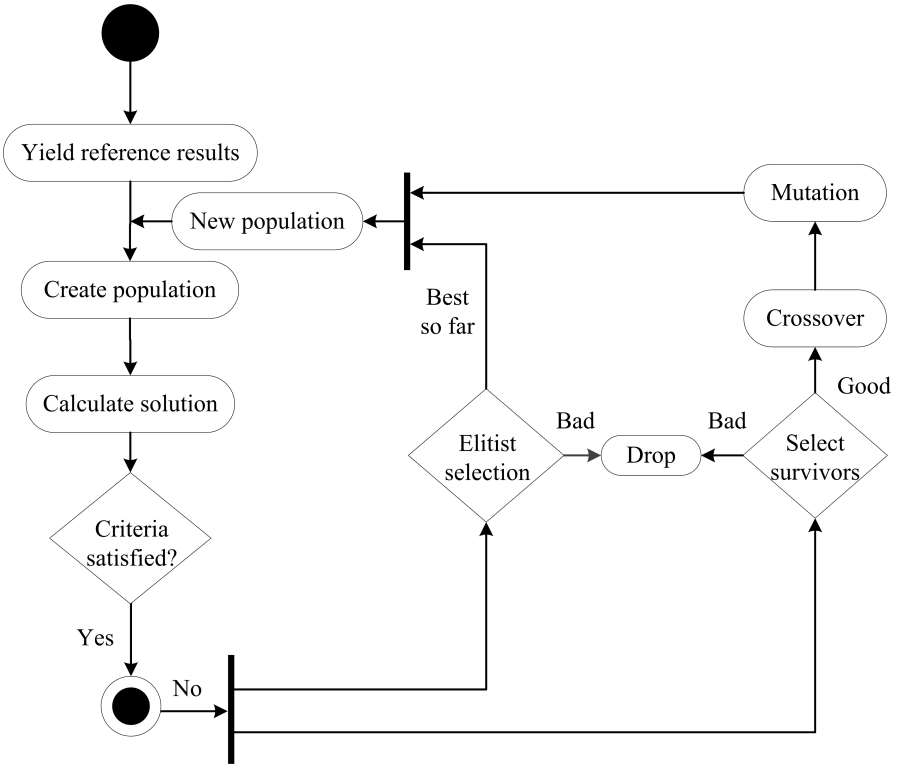

FIGURE 4.1: Activity chart of the genetic algorithm-based reduction [161]. Reprinted with permission.

reaction mechanism must first be translated into a form (chromosome) which can be easily operated by the GA. This step is called encoding and in this work, a reaction mechanism is encoded as a chromosome by representing its elementary reactions as

genes. Since this method aims at eliminating reactions, the encoding was done by representing the presence of a reaction by the gene value 1, while the gene value 0 stands for the eliminated reaction. For example, an eight-step mechanism with four reactions eliminated is presented as a chromosome (with eight genes) based on the presence of the reactions:

$OH + CH_3 \rightleftharpoons CH_2 + H_2O$	1
$OH + CH_4 \rightleftharpoons CH_3 + H_2O$	0
$OH + CO \rightleftharpoons H + CO_2$	0
$OH + HCO \rightleftharpoons H_2O + CO$	1
$OH + CH_2O \rightleftharpoons HCO + H_2O$	1
$OH + CH_2OH \rightleftharpoons H_2O + CH_2O$	1
$OH + CH_3O \rightleftharpoons H_2O + CH_2O$	0
$OH + CH_3OH \rightleftharpoons CH_2OH + H_2O$	0

The length of each chromosome is constant and corresponds to the number of reactions in the detailed mechanism, N_R, therefore the chromosome is formulated as:

$$\alpha = [\alpha_1, \alpha_2, ..., \alpha_{N_R}] \in \{0, 1\}^{N_R},$$

where the value of α_i indicates whether the reaction i is present in the reduced mechanism or not. This way of encoding is intuitive and easy to implement and allows a simple conversion of the optimal solution (resulting chromosome) to the reduced mechanism which can be later used for the simulation of the reacting case. Furthermore, for such a chromosome, the GA operators can easily be modified to enhance the reduction process, which is discussed in the following.

4.1.1 Initialization

In this work, the initial population of the chromosomes (the first generation of solutions) is created in a way that all the genes in all the chromosomes are set to $\alpha_i = 1$, i.e. the initial solutions are set to represent the detailed mechanism. Despite the absence of diversity among the initial chromosomes, the full-mechanism initialization is proven to be the safest starting point of the search and is preferred over the randomly generated initial population for the following reasons:

- The key reactions may be lost already in the first step if the initial population would be created randomly,

- The randomly generated mechanisms (chromosomes), although smaller than the detailed, can actually be more stiff or impossible to solve due to elimination of the key reactions (therefore it is preferred to start the search with the numerically stable first solutions).

Alternatively, the population can be initialized in a way that every initial chromosome just deactivates a single, randomly chosen reaction, such that

$$\sum_{i=1}^{N_R} \alpha_i = N_R - 1,$$

where the index i, for which $\alpha_i = 0$, is chosen randomly with a uniformly distributed probability:

$$P\left[\alpha_i = 0\right] = \frac{1}{N_R}.$$

This alternative initialization introduces a small diversity among the initial individual chromosomes (which avoids solving a complete population of identical chromosomes) while still maintaining (almost) nominal chromosomes thus avoiding losing the key-reactions. The subsequent crossover and the mutation increase the diversity among the chromosomes. The population size (number of chromosomes in the population) is user-defined; in this work it is adjusted according to the number of available computational cores that run in parallel. Figure 4.2 illustrates the initial population of four chromosomes representing eight-reaction mechanisms, as according to the two initialization types described above.

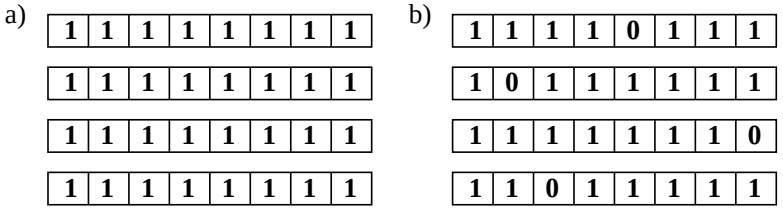

FIGURE 4.2: Initial populations of four mechanism representations (chromosomes) for a) a full-mechanism initialization and b) mechanisms with only one reaction missing [161]. Reprinted with permission.

After the initial population is generated, the chromosomes are evaluated, i.e. the corresponding submechanism is incorporated into the calculation of the reactive case (e.g., a perfectly stirred reactor or a laminar flame) and solved to provide information about how well the reduced mechanism performs compared to the full mechanism in respect to the desired criteria. The solution evaluation within the objective function is described in subsection 4.1.2.

Selection

Selection is the GA operation which chooses the fittest chromosomes to become parents to the new ones thus improving the quality of the population for the next generation. Selection is an important part of the evolution since it directs the algorithm towards better solutions. The probability of selecting a chromosome for the next generation depends on its fitness value so that the fittest chromosomes are usually preferred, whereas some less fit chromosomes can still contribute valuable diversity. Fit chromosomes are those with the lowest value of the fitness function, i.e. the lowest fitness, as the aim is to minimize the given fitness (objective) function.

There is a number of standard selection schemes [110, 117, 196]. For this work a tournament selection is applied [20, 54, 111]. The general concept of the tournament selection relies on a random selection of two or more chromosomes from the population, and choosing the fittest one among them. This is repeated n times, where n is the number of chromosomes in the population (population size). This way, the tournament selection gives a chance to all the individuals to be selected thus preserving the diversity. Tournament selection is among the most preferred selection schemes. In comparison to other standard selection schemes, the tournament selection is computationally more efficient and suitable for parallel implementation [117]. Its advantages are analysed and discussed by Goldberg and Deb [54], Blickle and Thiele [20, 21], and Zhong et al. [209] and they include simple implementation, efficiency (achieving best solution quality within short computation time) especially if implemented in parallel, no need for sorting of the individuals or fitness scaling, smallest loss of diversity and the highest selection variance, compared to other available selection schemes.

Due to the chromosomes alteration during the evolution (crossover and mutation), there is sometimes a risk of losing the good solution candidates when the children chromosomes are less fit than their parents. Although the GA is usually able to regenerate these lost improvements in a subsequent generation, there is no guarantee that this will happen. To make sure that the previously found good solutions do not get lost, a so-called elitism is used. Elitism was first introduced by Kenneth De Jong in 1975 [36]. Elitism preserves the fittest candidate found so far by copying it unchanged into the next generation. This way, the performance of GA is improved as the algorithm does not have to waste time rediscovering the previously lost good solutions. The unchanged candidates preserved by the elitism are available for selection as parents for the rest of the next generation.

Crossover

At the crossover stage, all of the chromosomes are paired up and their genes are exchanged with a previously defined probability (crossover probability or crossover rate). If the crossover rate is zero, then the children are exact copies of their respective parents. There are several ways to perform a crossover. For the present reduction method, the crossover of two chromosomes $\alpha, \beta \in \{0,1\}^{N_R}$ is accomplished by randomly choosing a single point at index $i \in \{1, ..., N_R\}$ from which the genes of the two chromosomes are swapped, yielding children

$$\gamma_1 = [\alpha_1, \alpha_2, ..., \alpha_i, \beta_{i+1}, \beta_{i+2}, ..., \beta_{N_R}]$$

and

$$\gamma_2 = [\beta_1, \beta_2, ..., \beta_i, \alpha_{i+1}, \alpha_{i+2}, ..., \alpha_{N_R}] .$$

This operation is known as a single-point crossover and is illustrated in Fig. 4.3. The crossover (recombination) is the crucial part of the evolution [70] as it leads the population to converge towards the best solution found so far (exploitation). However, with the crossover alone, the population may fall into the local optimum due to lack of diversity, which is why the crossover alone is not enough for the GA to find the global optimum. To avoid this premature convergence and to introduce some diversity, the mutation is employed after the crossover.

There are many types of crossover operators generally available in GAs, for example: the multiple-point crossover (analogous to the single-point crossover with multiple randomly chosen crossover points), uniform crossover (described in Section 4.2.2), arithmetic crossover (suitable only for real-valued chromosomes as the offspring chromosomes are the weighted arithmetic mean of the two parents), and the special crossovers that include permutation of the parental genes (e.g. partially mapped crossover, order-based crossovers, cyclic crossover). These types of crossovers are discussed to a greater detail in the book from Michalewitz (1996) [110].

The single-point crossover is a preferred crossover type for the mechanism reduction process in this work because it allows an easy parametrization of the algorithm by tuning the crossover and the mutation rates. For the results presented in this work, all the reduction runs use a single-point crossover for easier comparison and parameter study. The uniform crossover (described in Section 4.2.2) can also be used, but the user is then adviced to adjust the crossover and the mutation rate accordingly.

Mutation

After the formation of the children, a mutation operation takes place altering only a small number of randomly chosen genes in the chromosomes with a user-defined probability p_m:

$$(\forall i \in \{1, 2, ..., N_R\})\, P\left[\alpha_i = 0\right] = p_m.$$

The mutation probability (mutation rate) represents the likeness that randomly chosen genes of the chromosome will be altered. For example, if the integer-encoded chromosome consists of 100 genes, the mutation rate of 5% means that 5 randomly-chosen genes out of 100 will be altered (here, flipped to 0 or 1, depending on their initial values).

This operation is important as it introduces diversity and helps to avoid stagnation at local optima. However, the mutation probability should be fairly low, otherwise it might randomize the entire search and destroy a good solution. In this work, two mutation types are used: two-directional (the gene can be flipped to 0 or 1) and one-directional (regardless of the initial value, the gene is always flipped to 0). When the aim is to drive the solution towards smaller mechanisms quickly, the mutation can be done in one direction only, i.e. genes with a value 1 are converted to 0 while a value of 0 remains unchanged. This means that reactions are being gradually eliminated during the evolution beyond the elimination resulting from the evolution pressure applied by the fitness function. It must be stressed that for this particular goal, the mutation rate must be adjusted to the mechanism size (chromosome length) as the aggressive elimination of reactions might irreversibly eliminate important reaction paths and push the solution beyond an optimum. As the size of the mechanism is already a part of the evaluation function, the mutation should only provide a little help with the faster convergence towards the smaller mechanisms.

The effect of using a one-directional instead of a two-directional mutation operation is presented in Figs. 5.28, 5.29, 5.32, and 5.33 and discussed in Section 5.4. A general one-directional mutation scheme is illustrated on Fig. 4.3.

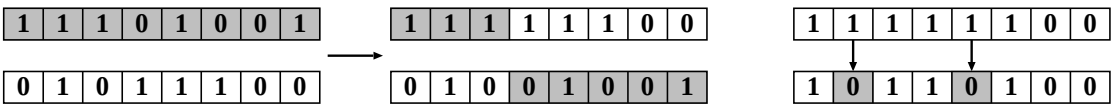

FIGURE 4.3: Single point crossover (left) and one-directional mutation (right)

Having completed the operations of crossover and mutation, a new population is created and evaluated once again for the next cycle of selection and reproduction (Fig. 4.1). Exploration means searching the search space as much as possible, while exploitation

means concentrating on one point (hopefully the global optimum). In GA, the mutation operators tend to provide exploration, and the crossover operators tend to lead the population to converge on the good solutions found so far (exploitation). Consequently, while the crossover tries to converge to a specific point in landscape, mutation does its best to avoid convergence and explore more areas.

The mutation alone, or too high mutation rate prevents the population convergence to any optimum solution. If the mutation rate is too small, the search relies on the crossover and fails to find a global optimum. Therefore, a proper balance between the exploitation and the exploration ability of the search/optimization algorithm should be accomplished. The optimal mutation rate is problem specific. Some recommendations for choosing the crossover and the mutation rates are reported in the literature. Numerous studies have shown that the crossover and the mutation rates are crucial to the success of GA evolution [7, 36–38, 65, 131]. The choice of the mutation and the crossover parameters is problem specific and will be discussed in Section 5.

4.1.2 Objective Function

The evaluation function (or objective or fitness function) is the essential part of any optimization technique and its proper definition is usually the trickiest part of setting up the optimization run. The goal of the search is defined through the objective function, i.e. the objective function contains the criteria a reduced mechanism must fulfil. It is therefore important to define the criteria in a way that a plausible trade-off between the size, stiffness and the accuracy of the resulting reduced mechanism can be achieved. For the mechanism reduction (and optimization), the objective function definition is typically based on the difference between the simulation results obtained from the detailed mechanism (taken as a reference) and its reduced version (candidate solution).

The evaluation of the mechanisms' performance can be based on any aspect of the simulation, in the present work for a homogeneous reactor or a laminar flame [55]. A homogeneous reactor and laminar flame models are used for the evaluation of the mechanism because of their moderate computational costs that enable detailed parameter studies even for large mechanisms. In general, the overall objective function for N_c different operating conditions, for a specific reacting case of interest, is formulated as:

$$f_{obj} = \frac{1}{N_c} \sum_{c=1}^{N_c} f_{obj,c} \tag{4.1}$$

where $f_{obj,c}$ is an objective function for a single set of operating conditions:

$$f_{obj,c} = \frac{\sum_{i=1}^{N_\xi} w_i f_\xi}{\sum_{i=1}^{N_\xi} w_i} \tag{4.2}$$

where N_ξ is the number of the optimization targets (criteria) and f_ξ is the optimization target with the corresponding weighting factor w_i. Generally, there are no restrictions in choice of mathematical expression for evaluating the difference between the target under consideration and its reference value. However, a proper evaluation of the performance of a reaction mechanism requires taking into account the relative importance and different orders of magnitudes for different chemical properties predicted by the mechanism. For example, the ignition delay time and the temperature which are usually defined as criteria in the same objective function must be normalized in a way to make them equally "visible" to the algorithm despite the difference in their orders of magnitudes. In case of multiple different criteria, an appropriate expressions for their evaluation must be chosen to avoid that some criteria significantly overweight the other criteria in the objective function. The simplest formulation of the difference between the reference value of property ξ_{ref} and the value predicted by the reduced mechanism ξ_{red} may be a linear expression (Eq. 4.3):

$$f_\xi = \left| \frac{\xi_{\text{red}} - \xi_{\text{ref}}}{\xi_{\text{ref}}} \right| \tag{4.3}$$

Although this type of difference evaluation is classical (Fig. 4.4, upper left), it is not particularly suitable for optimization in respect to multiple targets of different nature, relevance and orders of magnitude. However, it is incorporated into more complex functions listed below. Another rather intuitive formulation is a quadratic function (Fig. 4.4, upper right):

$$f_\xi = \left| \frac{\xi_{\text{red}} - \xi_{\text{ref}}}{\xi_{\text{ref}}} \right|^2 \tag{4.4}$$

This quadratic expression has been tested and discussed in Section 5, where it has been shown that Eq. 4.4 is not sufficient to provide the best fit to the criteria, especially when the overall objective function contains conflicting targets (accuracy and cost). Since the different targets may vary by several orders of magnitude, the evaluation approach preferred in this work is the logarithmic formulation (Fig. 4.4, bottom left):

$$f_\xi = \ln\left(1 + \sigma \cdot \left| \frac{\xi_{\text{red}} - \xi_{\text{ref}}}{\xi_{\text{ref}}} \right|\right) \tag{4.5}$$

A logarithmic formulation of the objective function is also advocated by the work of Perini [136, 137]. In the present thesis, the logarithmic scaling is usually chosen for the accuracy criteria, although several other expressions have also been adopted and tested,

depending on the nature and relevance of the desired targets. Another expression often used in this work is a sigmoid function (Fig. 4.4, bottom right). This function bounds the target values between 0 and 1. Furthermore, the sigmoid function increases the flexibility of the objective function because of its tunable slope and shift parameters. It is typically used for normalizing the cost parameters, as discussed in 5.4.

$$f_\xi = \left[1 + \exp\left(\sigma \cdot \left(1 - \frac{\xi_{\mathrm{red}}}{\lambda \cdot \xi_{\mathrm{ref}}}\right)\right)\right]^{-1} \tag{4.6}$$

Based on the sigmoid formulation, the expression typically used to normalize integral values of the profiles, or as a penalty function in the optimization (section 4.2) is formulated as:

$$f_\xi = 2 \cdot \left[1 + \exp\left(-\sigma \cdot |\xi_{\mathrm{red}} - \xi_{\mathrm{ref}}|\right)\right]^{-1} - 1 \tag{4.7}$$

The integral of the profile is calculated according to:

$$\xi_{\mathrm{profile}} = \frac{\int |\xi_{\mathrm{red}}(x) - \xi_{\mathrm{ref}}(x)|\, dx}{A_{\mathrm{ref}}} \tag{4.8}$$

where

$$A_{\mathrm{ref}} = (\xi_{\mathrm{ref,max}} - \xi_{\mathrm{ref,min}})\, \Delta x$$

is the bounding-box area spanned orthogonally by the reference mechanism's values ξ_{ref} along the simulation range Δx (time axis or flame coordinate). The area A_{ref} does not depend on the profile's shape but only on the minimal and maximal values of the reference target. The resulting values ξ_{profile} (Eq. 4.8) are relatively small so that they can be easily normalized (Eq. 4.9) and incorporated into the overall objective function (Eq. 4.2).

$$f_\xi = 2 \cdot \left[1 + \exp\left(-\sigma \cdot |\xi_{\mathrm{profile}}|\right)\right]^{-1} - 1 \tag{4.9}$$

The illustration of the normalization functions is shown in Fig. 4.4 for linear scaling (Eq. 4.3), square scaling (Eq. 4.4), logarithmic scaling (Eq. 4.5) and the sigmoidal normalization (Eq. 4.6).

The normalization from Eq. 4.7 restricts the error ξ_{profile} to the interval [0, 1], the steepness of the normalization function can be adjusted by the sharpening factor σ (Fig. 4.4). The sharpening factor dictates how strong the target ξ_{opt} is directed towards its optimal value ξ_{ref}. The value of σ is chosen based on the nature and the relevance of the optimization target ξ, therefore the choice of σ is always problem-dependent. Small values of σ for some targets are sufficient to continuously direct the targets to their reference value, while for other targets, a very strong directing towards their desired value may be necessary. The appropriate choice of σ is always made empirically, based

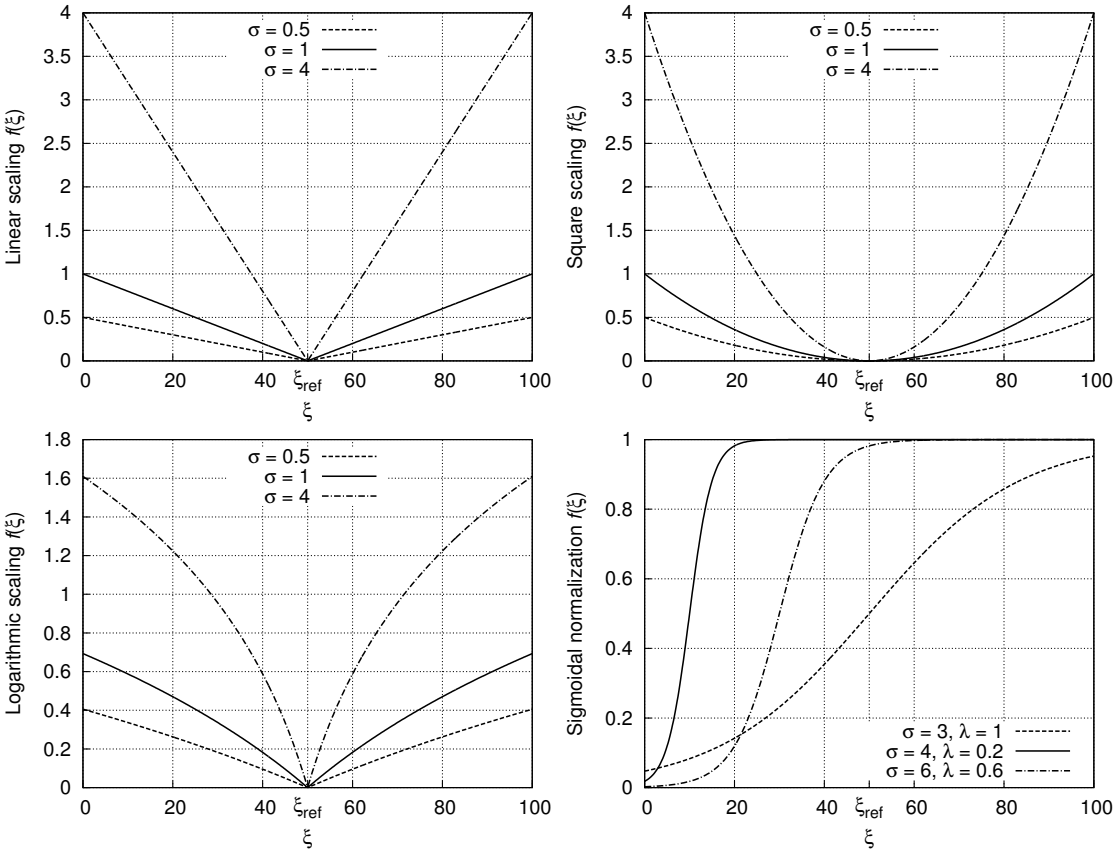

FIGURE 4.4: Scaling and normalization of optimization targets (objective function terms)

on the resulting values of ξ for a sample set of chromosomes, to make the optimization target weighting suitable for the overall objective function.

The overall evaluation function composed of the terms described above is found to provide a fast convergence towards the solution. These expressions are shown to preserve the important features observed during the evolution ensuring a good trade-off between the individual criteria and if necessary, weights for each part of the overall objective function can be introduced and controlled easily. The normalization enables flexible adjustment of the evolution pressure for any part of the objective function thus enabling an optimal combination of accuracy targets to be found in a transparent way.

4.2 Mechanism Optimization

As the reduction of the reaction mechanism may decrease its accuracy, the optimization of the mechanism is performed by altering its reaction rate coefficients to restore the mechanisms' accuracy with respect to its detailed version or some other mechanism whose overall behavior the optimized mechanism should match. In the present work,

the optimization targets only the forward pre-exponential factors of the elementary reactions. The reverse reaction rates are then calculated from the thermodynamic data (see section 2.5). In some cases, the reversible reactions are written explicitly in the form of two irreversible (forward and reverse) elementary reactions. When the thermodynamic data of the species involved in such reactions are known, altering the rate constants of both the reactions would violate the thermodynamics. To avoid this risk, the reactions listed in such manner are first converted into corresponding reversible reactions whose pre-exponential factors are then optimized. The process of the optimization is described in the following sections.

4.2.1 Encoding

In contrast to the mechanism encoding used for the reduction, where the mechanism-to-chromosome conversion was carried out based on the presence of the elementary reaction in the mechanism, the optimization of the real valued rate coefficients requires the operators appropriate for the real coded algorithm [64].

The starting point of the optimization process is the reduced mechanism with N_r reactions. The aim of the optimization is to alter its reaction-rate coefficients until the prediction quality of the mechanism, relative to its reference, has been improved. The chromosome that corresponds to this mechanism is a real-value ordered set of corresponding reaction-rate coefficients which are scaled against their original values such that $k_{i,\mathrm{opt}} = \alpha_i k_{i,\mathrm{ref}}$, where $k_{i,\mathrm{opt}}$ and $k_{i,\mathrm{ref}}$ are the optimized and the original forward rate-constants of the reaction i, respectively. For reversible reactions, the reverse rate constants are calculated by the law of mass action. Each scaled rate constant α_i $(i = 1, \ldots, N_r)$ is chosen from a continuous search space of dimension N_r. The scaling of the rate constant corresponds to the scaling of the pre-exponential factor of an Arrhenius rate expression. Normalizing the rate constants leads to an initial population with all scaling factors set to a real value of 1.0. Figure 4.5 illustrates how the reduced mechanism (integer-coded) is translated into a real-encoded mechanism suitable for reaction rate constants manipulation by GA. Using an unchanged mechanism in contrast to a random seed as a starting point of the optimization helps to avoid a purely random optimization search and ensures numerical stability of the first solutions. The rate constants are altered for the first time in the mutation step.

The selection scheme is the same as for the reduction process: the tournament selection.

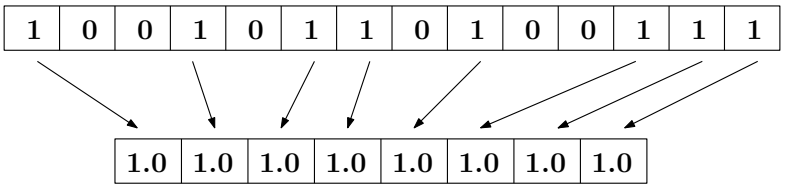

FIGURE 4.5: Encoding the integer-coded chromosome (reduced mechanism) as a real-coded chromosome. Genes of the real-coded chromosome correspond to the nominal values of its normalized forward reaction rate constants

The objective-function value for a single chromosome determines whether this chromosome will be selected for the next generation. The present approach employs a tournament selection [20, 54, 209] which randomly takes two or more chromosomes from the population of N_{pop} chromosomes and chooses the one with the smallest objective-function value amongst them. This is repeated N_{pop} times. The fittest chromosomes are generally preferred but some less fit chromosomes can contribute diversity. The tournament selection is described in Section 4.1.1.

It is the iterative combination of the crossover and the mutation which enables the genetic algorithm to find a global optimum. The mutation introduces a small variation to a randomly chosen subset of genes from one chromosome to maintain additional diversity. In the present mutation approach, these gene alterations are random normally-distributed variables $G(\mu, \sigma)$ with a mean μ and a standard deviation σ. This additive Gaussian mutation alters a gene x to a new value $\mathrm{x} + G(\mu, \sigma)$ (Figure 4.6). For non-negative genes x (scaling factors α) that can vary over several orders of magnitude, a multiplication with positive normally distributed random variables is more suitable, leading to a new gene $\mathrm{x}G(\mu, \sigma)$ after mutation, as the multiplication gives a log-normal distribution of the random-walk final values.

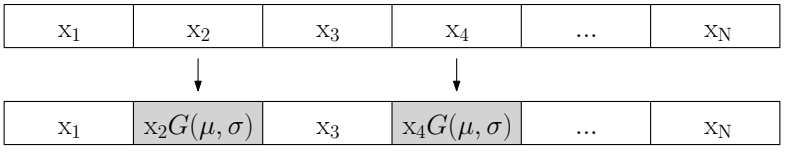

FIGURE 4.6: A multiplicative Gaussian mutation of real-coded genes.

The multiplicative mutation was chosen for the present study. Both additive and multiplicative Gaussian mutations are suitable for gene values within a highly dimensional search space [8, 48, 66]. Other types of crossover and mutation operators are available

as well, but the adopted ones have been shown to provide good robustness and convergence speed within the presented application. It should be noted that the choice of the operators does not affect the results, but only the convergence speed of the algorithm.

4.2.2 Crossover

The selected chromosomes pair up to exchange the information between each other by a uniform crossover chosen in this study where each gene has a 50% chance to be swapped between the mother and the father chromosome (Fig. 4.7). The uniform crossover is radically different to the single-point crossover described above. Each gene in the child chromosome results from copying the corresponding parent gene which is selected according to a randomly generated "crossover mask". A randomly created crossover mask has the same length as the individual chromosome and the parity of the bits in the mask determine which parent will supply the offspring with which bits. This means that, where there is 1 in the crossover mask, the gene is copied from the first parent, and where there is 0 in the mask, the gene is copied from the second parent, as shown in Figure 4.7. This process is repeated with the selected parents to produce the offspring. Then a new crossover mask is randomly generated for each pair of parents resulting in offspring that consists of a mixture of genes from each parent. The number of the crossover points is not fixed, but will average half of the chromosome length.

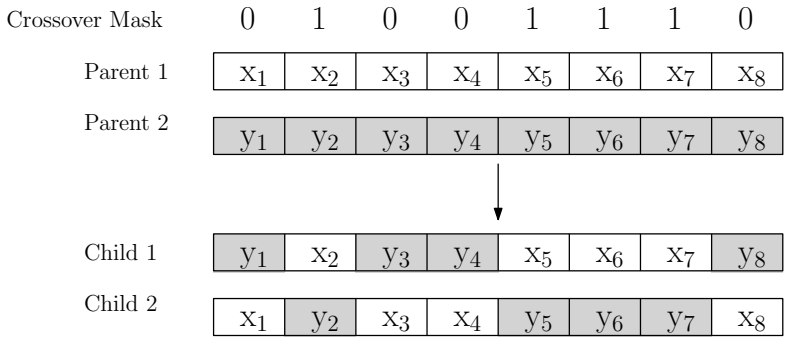

FIGURE 4.7: A uniform crossover between two parent chromosomes

There is a number of studies reporting the benefits of the uniform crossover [168, 172], one of them being that the uniform crossover is extremely useful when the search space is very large, which is the case for the reaction-rates optimization problem.

4.2.3 Objective Function

As disscussed in section 4.1.2, the role of the objective function is to evaluate the performance of the mechanisms from the population with respect to the reference. The search is directed towards the solution with the smallest possible value of the objective function. The general form of the overall objective function which covers N_c different physical conditions is given by Equation 4.1 in terms of the single objective functions f_{obj} corresponding to each condition (setup) c.

As explained in section 4.1.2, these evaluation terms are scaled and weighted to account for different orders of magnitude for different optimization targets (properties) and make the optimization flexible and easily adjustable to the desired output. The scaled terms are combined into one overall objective function (Eq. 4.2) for multiple conditions (Eq. 4.1). Different ways to scale or normalize the evaluation terms are disscussed in section 4.1.2 and are used for the optimization as well. Chosen expressions restrict the single error contributions to a comparable range and enable variable weighting of the optimization targets. These normalization expressions and their coefficients are problem-dependent. Thus, an appropriate choice of the function parameters can be made empirically, based on preliminary optimization runs consisting of only few generations.

The objective function for the purpose of the optimization has two aspects: accuracy of the optimized mechanism and the extent of altering of the reaction rates. This means that, besides the accuracy terms, the objective function can be used to constrain the modification of the reactions, which is not typical for classical use of the genetic algorithms. This aspect has been added to the optimization due to concern that established and well-defined reaction rates do not fall beyond their uncertainties for cases where the physical meaning of the reaction rates is important.

Accuracy Criteria

Optimization targets involving accuracy are normalized individually according to their order of magnitude and relevance. The deviation between the reference ξ_{ref} and the optimized mechanism ξ_{opt} is normalized using the expression introduced in section 4.1.2.

Penalty Function

The modifications to the model during the optimization can be constrained by introducing penalty terms into the objective function. In this work, the constraint is imposed

onto each gene (reaction rate constant) of the chromosome, to account for different goals of the optimization. The constraints are user-defined, depending of the optimization preferences, which may be minimal possible rate modifications, drawing certain rates towards zero or any other limiting value for certain reaction rates. In this work, the penalty function is mainly used to keep the reduced reaction coefficients close to their original values, but the penalty function is also applied for further reductions of the mechanisms. Both applications are discussed and tested below.

The term penalty function used here refers to a function that is an integral part of the objective function, alongside the accuracy criteria. The only difference is, that unlike the accuracy which is the output of the mechanism calculation, the penalty function affects the input parameters, i.e. the reaction rates in the mechanism. Athough it is not a standard definition of the penalty function, the term is used in this work to intuitively distinguish between the optimization targets associated with the performance of the solution (accuracy) and its properties (desired rate values).

Faithfulness to the original reaction mechanism

Some of the previous works on the mechanism optimization consider estimating and minimizing the uncertainty of the reaction rate coefficients that are experimentally and/or theoretically established and can be found in literature and kinetic databases. Although the uncertainty is an important issue in chemical kinetics modelling, it was not treated as the main goal of the present optimization technique, but rather as one possible aspect that can be taken into account upon the user's request.

The basic optimization of the (reduced) mechanism considers the rate coefficients of the original mechanism as an initial value, from which the optimization is started so that the values can be changed by a very large degree. This approach would hence neglect the chemical and physical knowledge that is already involved in these reaction coefficients, albeit with some (often large) uncertainty. To keep the reduced mechanism as faithful as possible to the nominal reaction rates, an additional component to the objective function is introduced. The penalty term penalizes large deviations of the reaction rates from their nominal values. A similar approach for constraining the change of the reaction rates was used in previous work by Sheen and Wang [159] and Cai and Pitsch [30].

Although the accuracy can be restored by tuning the rate coefficients of the reactions, there is a risk of exceeding the uncertainty ranges of the rate coefficients and of losing the chemical knowledge from the original mechanism. Instead of searching for the rate constraints from NIST database [195] and implementing each one of them into the optimization process, the changes imposed to the rates are constrained by the penalty

function (which is a part of the objective function). This approach is convenient as it does not require comprehensive search of the databases for each reaction, but constraints the changes automatically during the evolution.

Considering an uncertainty range for each reaction can also be done with the presented algorithm, but obtaining these ranges with a good accuracy for a large mechanism appears impractical. Work of Sheen and Wang [159] and later, Cai and Pitsch [30] use a penalty term as part of the objective function in order to account for the uncertainties of the reaction rate coefficients. The objective function minimized in the work from Cai and Pitsch [30] features a penalty term which is expressed as sum of weighted squared values of the optimized pre-exponential factors, aiming to constrain the modifications of these factors, if they are normally distributed. If the pre-exponential factors are uniformly distributed the penalty term is omitted and the modification is constrained by a pre-defined interval. They introduced this special term to ensure that the optimized factors differ as little as possible from their nominal values. This aspect is considered in the present study as one way of using the penalty term in the objective function.

In the present work, the following overall penalty function is applied on the reactions in the mechanism:

$$f_{\text{pen}} = \frac{1}{N_r} \sum_{i=1}^{N_r} f_{\text{pen},i} \tag{4.10}$$

where the penalty term $f_{\text{pen},i}$ is defined as:

$$f_{\text{pen},i} = \frac{2}{1 + \exp\left(-\sigma \left|\alpha_{i,\text{opt}} - \alpha_{i,\text{ref}}\right|\right)} - 1 \tag{4.11}$$

which is the expression already given by Eq. 4.7. In contrast to the square formulation of the penalty term used by Cai and Pitsch [30], the term from Eq. 4.11 provides a more general and more flexible way to constrain the model modification by adjusting the sharpness factor σ (Figure 4.9).

It should be noted that an ideal penalty function could be set for each reaction, with a weight scaled by the uncertainty of each specific reaction. The effort in obtaining a complete uncertainty vector can however be prohibitive, in particular, for more advanced and sizeable mechanisms. As a possible alternative to the penalty function advocated by this work, which is in an additive sense symmetric with respect to the nominal rate value, one can impose the multiplicative treatment of the rate constants. The additive symmetric treatment means that, by using the penalty from Eq. 4.11 with $\alpha_{\text{ref}} = 1.0$, a rate scaling factor of 0.5 is equally treated as the scaling factor of 1.5 (i.e. they have the same penalty). If preferred, the multiplicative treatment of the scaling factors can be achieved by logarithmic scaling of the normalized rate constants within the penalty

function as follows:

$$f_{\text{pen},i} = \frac{2}{1 + \exp\left(-\sigma \left|\ln\left(\frac{\alpha_{i,\text{opt}}}{\alpha_{i,\text{ref}}}\right)\right|\right)} - 1 \tag{4.12}$$

The shape of the logarithmic normalization (Eq. 4.12) compared to the one that is used in the present study (Eq. 4.11) for various sharpness values is illustrated in Fig. 4.9. The logarithmic normalization of the scaling factor α cannot be applied for the elimination of the reactions ($\alpha_{\text{ref}} = 0.0$), which limits the use of Eq. 4.12 to $\alpha_{\text{ref}} > 0$. For $\alpha_{\text{ref}} = 1.0$ with small sharpness factors σ, Eq. 4.12 can be preferred over Eq. 4.11 if, for example, scaling factors of 0.5 and 2.0 are to be treated equally. However, for higher values of σ (as used in this work), the difference between the two functions becomes negligible (Fig. 4.9, $\sigma > 4$), implying that, for the algorithm, there is no effective difference between the two functions. The logarithmic penalty function is used for several runs for optimization of the hydrogen mechanism in Section 5.1.

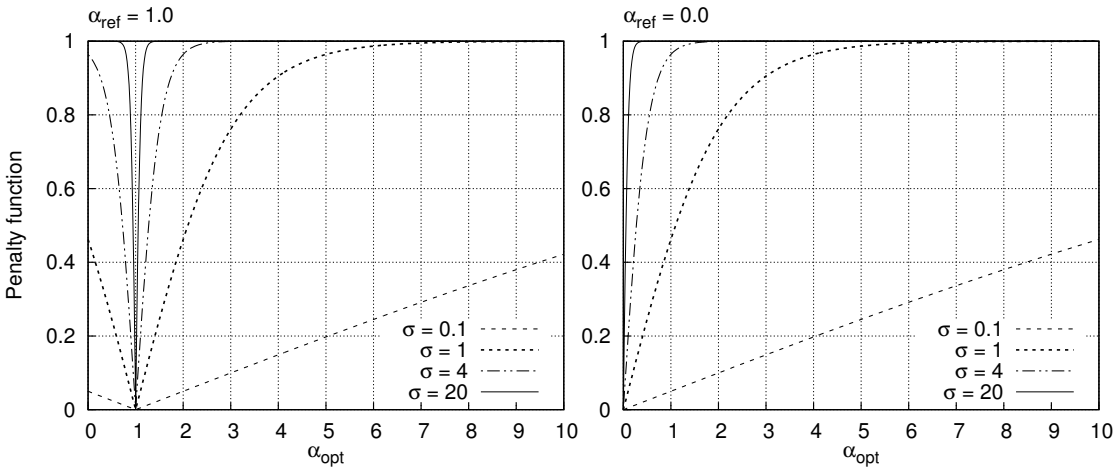

FIGURE 4.8: Penalty function for maintaining nominal values of the reaction rates ($\alpha_{\text{ref}} = 1.0$) and further reducing the mechanism ($\alpha_{\text{ref}} = 0.0$)

Elimination of reactions

The penalty function can also be used to help the further reduction of the mechanism during the optimization by driving very small reactions coefficients k towards zero, so that these reactions can be removed. The reduction of the reaction rates is forced by setting the value of $\alpha_{i,\text{ref}}$ in Eq. 4.11 to zero. The idea was to simplify and optimize the mechanism at the same time using the real-coded algorithm. With this approach, the only constraint imposed to the rate modifications was set on the GA side of the method, where the minimal and the maximal gene value (search space) were defined.

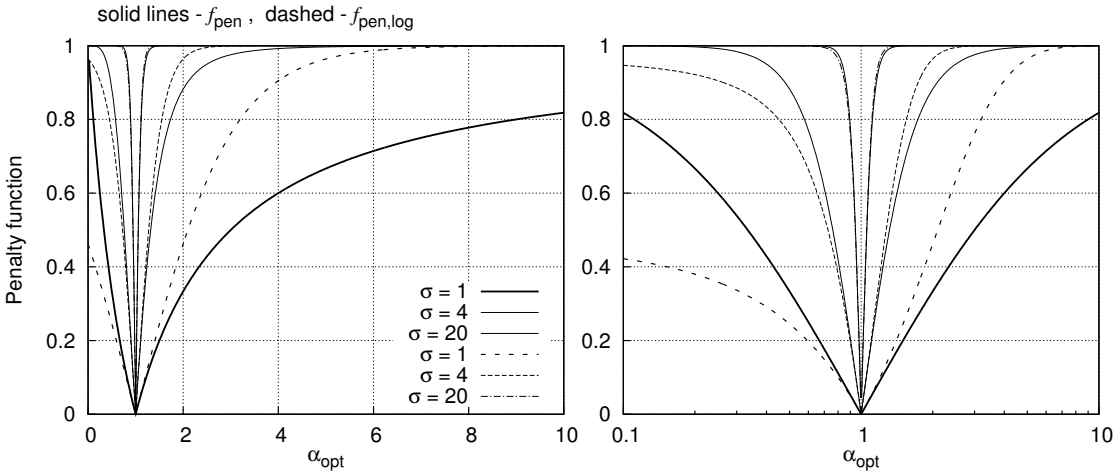

FIGURE 4.9: Comparison of the penalty functions with linearly and logarithmically scaled α

This allowed the algorithm to search freely for the new rate constants while directing the small rate values steeply towards zero.

The normalization expression (Eq. 4.11) is found to be convenient for the purpose of manipulating the alteration of the genes without imposing strict constraints to it. Figure 4.9 illustrates the function given by Eq. 4.11. One can notice that the gene values which fall near the desired gene value are steeply directed towards it, while those after the inflection point where the function reaches its plateau, have the same fitness values. This means that there are no maximal boundaries to the gene alterations (except those defined at the GA initialization step) once the gene value is in the plateau region, but when the values are decreased or negligible, then the algorithm is trying to draw them to zero (eliminate them). At this region, the differences in the fitness values are large. The accuracy is constantly observed, which avoids the risk of eliminating reactions essential for an accurate description of the target phenomena. The penalty function for helping the mechanism reduction during the real-coded optimization is demonstrated in Section 5.3 and its potential to reduce the mechanism during the real-coded optimization is further addressed in Section 5.4.4 in greater detail.

Rate uncertainty consideration

Although considering the rate uncertainties taken form the literature during the optimization is not primarily advocated by the present study, defining the uncertainty factor UF for each chosen reaction was tested for the Konnov [79] mechanism in Section 5.1. This approach may be used when optimizing small mechanisms for which the rate parameters are known with small uncertainty and/or if the physical meaning of the rate

coefficients is important for the resulting optimized mechanism. In the following, the definition of the rate uncertainty is explained. From the report by Westley (1980) [195] and the compilations of kinetic data from Baulch et al. [11–13], the uncertainty of the rate constant is defined by value f in the following way:

$$f = \log\left(\frac{k_i^0}{k_j^{\min}}\right) = \log\left(\frac{k_i^{\max}}{k_i^0}\right) = \frac{1}{\ln 10}\ln\left(\frac{k_i^{\max}}{k_i^0}\right) \tag{4.13}$$

where k_i^0, $k_i^{\min}$ and $k_i^{\max}$ are the recommended value, the possible minimal and the maximal value of the rate constant of the reaction i, respectively. Equation 4.13 is equivalent to

$$\frac{k_i^0}{k_j^{\min}} = 10^f = \frac{k_i^{\max}}{k_i^0} \tag{4.14}$$

Thus:

$$k_i^{\min} \cdot 10^f = \frac{k_i^{\max}}{10^f} \tag{4.15}$$

The reaction rate coefficient that falls outside the interval $\left[k_i^{\min}, k_i^{\max}\right]$ is considered very improbable by the evaluators [11–13]. The parameters f, k_i^0, $k_i^{\min}$ and $k_i^{\max}$ are evaluated at a given temperature, thus the uncertainty f is generally temperature-dependent. No attempt has been made to assign explicit error limits to the temperature coefficient of k [11–13]. The error limits in $\log k$ are assigned at the extreme values of the temperature range and indicate the variation of the data quality with the temperature but the form of this variation is not defined. The assignment of the error limits of the rate constant is a subjective assessment by the evaluators [11]. State-of-the-art measurement techniques under favorable conditions are able to determine the rate coefficients of some reactions with a standard deviation as small as 10%. On the other hand, the reaction rates of the same reaction obtained in different laboratories (and often by the same measurement methods) are often inconsistent with each other. Therefore, the minimum and the maximum values of the rate coefficients may differ by many standard deviations σ from the recommended value on a logarithmic scale, typically 3σ [25, 125, 183, 205, 206, 211, 212] or 2σ [125, 158, 160]. These deviations indicate systematic errors in experimental measurements, which are difficult to detect and estimate, and thus cannot be simply incorporated into the error limits of the reaction rate.

From Eq. 4.15, the range of values of k is determined by multiplication and division of k by a factor UF, where

$$\mathrm{UF} = 10^f.$$

The uncertainty factor UF therefore limits the change of the reaction rate constant k to a range

$$k/\mathrm{UF} < k < k\mathrm{UF}.$$

The optimization with predefined uncertainty factors is demonstrated in Section 5.1 for a hydrogen mechanism including a comparison between the penalty function approach and predefining the rate uncertainties.

Chapter 5

Application and Testing

This chapter demonstrates the application and properties of the reduction and optimization method described in Chapter 4 of this thesis. The presented results resemble different aspects of the mechanism manipulation and are organized as follows: Section 5.1 demonstrates the optimization of a reduced hydrogen mechanism for which the uncertainty bounds are known, so this mechanism is suitable for testing the penalty function for preventing that the reaction rates deviate too much from their nominal values or form their uncertainty bounds. The reduction method is then demonstrated for an ethylene combustion mechanism (Section 5.2) for a homogeneous constant-pressure reactor, and such a reduced mechanism was then optimized for the flame speed over a range of equivalence ratios.

In Section 5.3, the reduction was performed on a relatively large *tert*-butanol oxidation mechanism by Sarathy et al. (2012) [153] and then the subsequent optimization further reduced the mechanism with the help of the penalty function. A special attention was directed towards the penalty function and its parameters in Section 5.4.2. The choice of the operators for the integer-coded genetic algorithm used for elimination of the reactions from the detailed mechanism is justified in Section 5.4.1. An example of extrapolating the reaction mechanism outside of the conditions it was reduced for is demonstrated in Section 5.4.3.

N. Sikalo, O. Hasemann, C. Schulz, A. Kempf, and I. Wlokas. A genetic algorithm-based method for the optimization of reduced kinetics mechanisms. International Journal of Chemical Kinetics, 47(11):695-723, 2015.
Nejra Sikalo wrote most of the software, conducted all the simulations and wrote the papers. Olaf Hasemann contributed to software development, debugging and restructuring the code to run in parallel, contributed plots and adviced on the theory of optimisation. Irenäus Wlokas provided guidance, know-how on reaction mechanisms and supported the paper writing process. Christof Schulz supported the paper through advice on chemistry, detailed proof reading and background knowledge on the chemical kinetics. Andreas Kempf provided several key ideas to the papers, is the responsible supervisor of Nejra Sikalo, and contributed to writing, proof reading, revisions and rebuttals of the papers. The reused material is cited where appropriate.

5.1 Optimization with Predefined Uncertainties - Hydrogen Oxidation Mechanism

Hydrogen combustion is of a great significance for fundamental research of chemical kinetics due to its simplicity and practical importance for many applications (rocket propulsion, internal engines, fuel cells) [3, 41, 73, 74, 119, 167] and the adequate description of its elementary kinetics involving important radicals (H, O, OH, H_2O_2 and HO_2) that determine the radical kinetics for other complex hydrocarbon reaction systems [95]. The hydrogen reaction system is an integral part of any hydrocarbon combustion mechanism and it is extensively investigated by many research groups to help deriving elementary reaction rates. The chosen hydrogen mechanism from Konnov [79] is convenient for this particular study for several reasons: this mechanism is validated against a wide range of operating conditions, it was published with well-defined uncertainty factors UF for each elementary reaction, the hydrogen mechanism is small so that the resulting behavior can easily be analyzed and described in detail. The material from this particular section 5.1 has been published in International Journal of Chemical Kinetics [162] and reused with permission from Wiley.

5.1.1 Objectives

This section aims at comparing the optimization using the penalty function approach to predefining the rate uncertainties as fixed optimization constraints. The homogeneous reactor simulation was used to demonstrate the effect of differently constrained optimizations onto the resulting reaction rates. The optimization with predefined uncertainty

bounds for the reaction rates was tested for the hydrogen combustion mechanism by Konnov from 2008 [79] with 33 reactions. The uncertainty bounds for the reaction rate constants were defined by an uncertainty factor UF, so that the reaction rate constant is expected to lie between $k/\mathrm{UF} < k < k\mathrm{UF}$ [11, 79, 195].

5.1.2 Results

The reduction of the hydrogen combustion mechanism was conducted to introduce some perturbation to its accuracy so that the optimization runs involving different ways to constrain the rate alterations can be tested. Performed are several optimization runs to compare the effects of:

a) limiting the rate constants to their uncertainty range,
b) the penalty function approach, and
c) a combination of a) and b)

on the resulting reaction rates and the mechanism's accuracy. The optimization runs for the two reduced mechanisms aimed at restoring their accuracy with the following constraints to the rate modifications:

a) none,
b) with predefined UF,
c) with the penalty function f_{pen} (Eq. 4.11) only,
d) with a logarithmic penalty function $f_{\mathrm{pen,log}}$ (Eq. 4.9) only, and
e) with the combined constraints (uncertainty range defined with 2UF and f_{pen} and 2UF and $f_{\mathrm{pen,log}}$).

The reacting case used for the reduction was a homogeneous reactor model with an initial temperature of 1200 K and a constant pressure of 0.2 MPa. The initial fuel composition was a stoichiometric H_2/O_2 mixture diluted in Ar. Two reduced mechanisms were generated, one "strongly perturbed (S)" (reduced mechanism with lower accuracy) with 11 reactions and one "weakly perturbed (W)" (reduced mechanism with higher accuracy) with 12 reactions. The accuracy criteria for all optimization runs were the same and involved the ignition delay time, temperature history and mole fraction history of H_2O_2 as an additional target for an intermediate species (Table 5.1).

The genetic-algorithm operators for all the optimization runs are listed in Table 5.2.

The resulting reaction rate modifications from all the optimization runs for both mechanisms are presented in Fig. 5.1, together with the uncertainty ranges for each reaction taken from the original publication [79]. Uncertainty limits were considered in four

Property	w_i	Normalization	σ
τ_{ign}	1.0	Eq. 4.5	6
T_{profile}	1.0	Eq. 4.9	10
$X_{\text{H}_2\text{O}_2,\text{profile}}$	1.0	Eq. 4.9	10
f_{pen} ($\alpha_{\text{ref}} = 1.0$)	0.05	Eq. 4.7	4
$f_{\text{pen,log}}$ ($\alpha_{\text{ref}} = 1.0$)	0.05	Eq. 4.7	4

TABLE 5.1: Objective function parameters for optimization of reduced hydrogen mechanisms, including the penalty functions parameters for the runs where these were applied. The small values of the weighting factors w_i for the penalty terms are adjusted to the comparably small number of the remaining reactions.

GA parameter	Type	Value
Population size	-	48
Initialization	nominal gene values	-
Selection	tournament	-
Crossover	uniform	$p_{\text{cross}} = 0.5$
Mutation	Gaussian multiplicative	$p_{\text{mut}} = 0.02$

TABLE 5.2: Parameters of the genetic algorithm used for optimization of the perturbed hydrogen mechanisms.

optimization runs, all of them with the same numerical setup and the same accuracy criteria. The resulting reaction rate modifications for the UF-constrained cases and for one unconstrained run are presented in Fig. 5.1 (top).

The resulting reaction rates from UF-constrained runs are quite scattered within their given uncertainty bounds, although they follow the same trend of modifications. The unconstrained run has a similar behavior as UF-constrained runs in terms of rate modifications for both mechanisms, except for one reaction rate that exceeds the uncertainty bounds (S2 for the strongly perturbed and W4 for the weakly perturbed mechanism, see Fig. 5.1). The optimization results in terms of accuracy from these runs are shown in Figs. 5.2 and 5.3 for both mechanisms. Despite the different reaction rates for UF-constrained runs, the extent of accuracy restoration is identical for their corresponding mechanisms (Fig. 5.2 center, Fig. 5.7 and Fig. 5.3 center, Fig. 5.8). However, the extent of accuracy restoration was not the same for both reduced mechanisms using the constrained optimization. The constrained optimization did not fully restore the accuracy of the strongly perturbed mechanism (Fig. 5.2 center, Fig. 5.7), indicating that this mechanism was already distorted to an extent where some of the reactions (e.g., S2) must be modified beyond their uncertainty limits to fully restore the accuracy against the detailed mechanism. On the other hand, the unconstrained run (Fig. 5.2 left) fully restored the accuracy for this mechanism at the cost of exceeding the uncertainty of the reaction S2. The accuracy of the weakly perturbed mechanism was fully restored

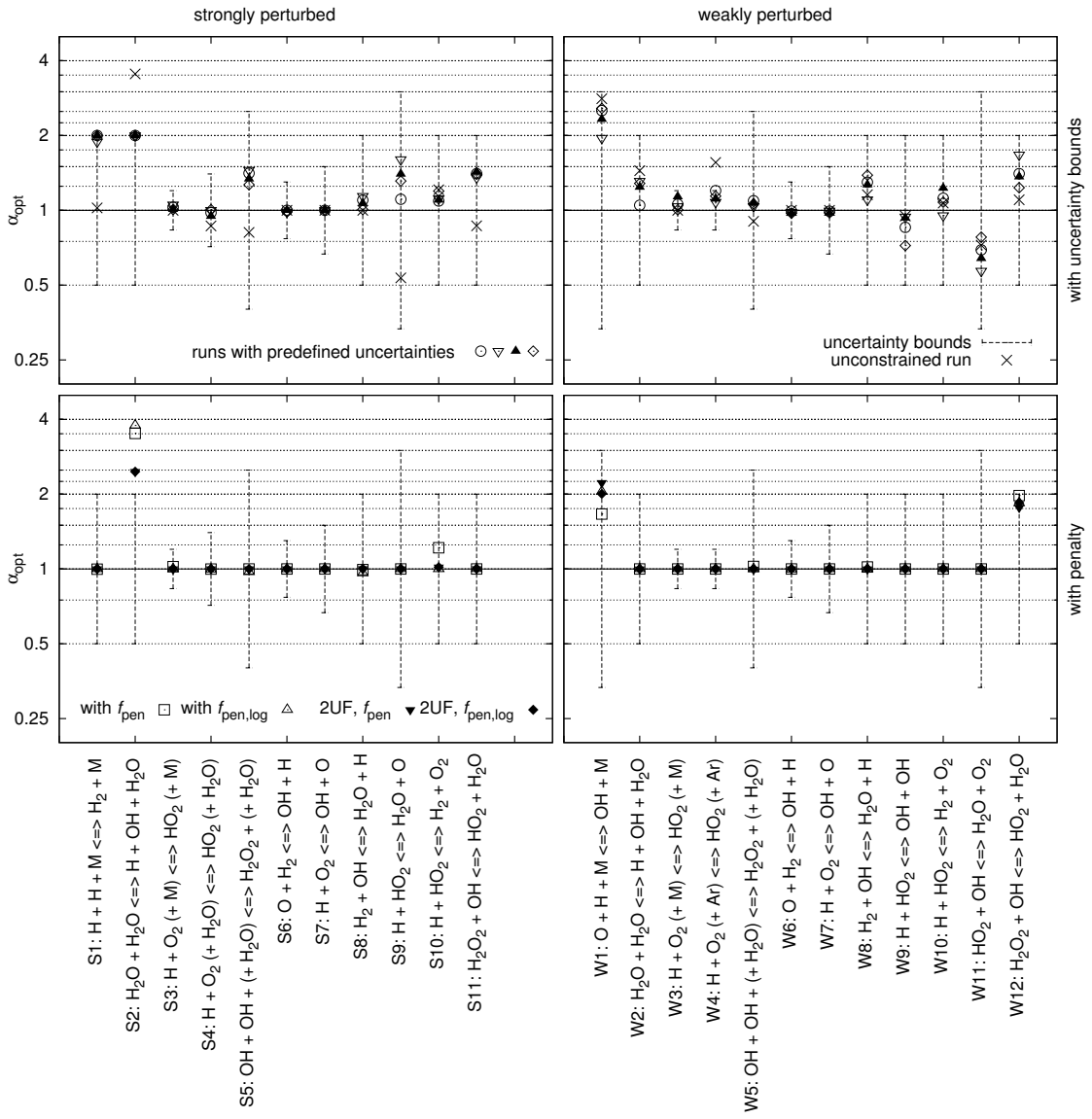

FIGURE 5.1: Extent of reaction rate modifications in comparison to their uncertainty bounds for optimization runs performed on two reduced mechanisms with different degrees of perturbation. Top: one unconstrained and four UF-constrained runs. Bottom: with a penalty function f_{pen} only, with a logarithmic penalty function $f_{\text{pen,log}}$ only, with 2UF and f_{pen}, with 2UF and $f_{\text{pen,log}}$. Left: a strongly perturbed (11 step) reduced mechanism. Right: a weakly perturbed (12 step) reduced mechanism.

for the UF-constrained and the unconstrained runs without exceeding the predefined uncertainty bounds (Fig. 5.3 left, Fig. 5.8).

The resulting reaction rate modifications for the optimization runs including penalty functions is presented in Fig. 5.1 (bottom) for both mechanisms. In comparison to the previous runs (Fig. 5.1, top), the reaction rates mostly remained close to their nominal values with exception of few reactions recognized as those that tend to exceed their uncertainties as seen in Fig 5.1 (top) to improve the accuracy. Specifically, one reaction

(S2) deviates from its nominal value and uncertainty bounds for the strongly perturbed mechanism, while all the other reactions remained close to their original coefficients or within their uncertainties (although these were not considered in runs with penalty functions). For the weakly perturbed mechanism, the behavior of the rate modifications for runs including penalty functions is similar to the previous case, with somewhat bigger deviation of the rate constants for reactions W1 and W12 which, however, do not exceed their uncertainty bounds. The penalty function managed to restore the accuracy for both mechanisms as seen in Figs. 5.2-5.5.

Combined constraints were imposed to test the effect of the penalty functions on the reaction rates in case when the uncertainty range is predefined but doubled (2UF). The idea behind this strategy was to evaluate if the penalty function would still bring the coefficients back into their original uncertainty bounds (UF) and restore the accuracy. The results of these tests in terms of accuracy are shown in Figs. 5.4 and 5.5 for two considered mechanisms.

The accuracy of the mechanism that was strongly perturbed during the reduction was not fully restored for runs with combined constraints (Fig. 5.4 center and right), as the penalty functions strongly pushed all the reaction rates towards their nominal values and the reaction S2 towards its uncertainty bounds. However, the combined constraints gave better accuracy than simple UF-constraints for this mechanism (Fig. 5.4). For the weakly disturbed mechanism, all the runs successfully restored the accuracy and the reaction rates remained within their prescribed uncertainty bounds. This implies that, for strongly or inappropriately reduced mechanisms, the accuracy can be largely restored for a chosen parameter range at the cost of violating the physical reaction rate uncertainties. For well-posed or appropriately reduced mechanisms, the penalty function is able to keep the reactions close to their original values or within their uncertainty ranges, while still obtaining a plausible accuracy for a given range of optimization parameters.

To get a better insight into the behavior of the reactions that exceed their uncertainty limits, a sensitivity analysis for temperature and H_2O_2 in respect to the remaining reactions of two reduced mechanisms was performed; the results are shown in Fig. 5.6. Sensitivity coefficients were calculated as $\frac{A_i}{T}\frac{\partial T}{\partial A_i}$ for the temperature, and $\frac{A_i}{Y_{H_2O_2}}\frac{\partial Y_{H_2O_2}}{\partial A_i}$ for H_2O_2, respectively [74].

Figure 5.1 shows that the most sensitive reactions (Fig. 5.6) remain unchanged (e.g., S7 (W7): $H + O_2 \rightleftharpoons OH + O$) for both reduced mechanisms through all the optimization runs. The reactions that tend to fall outside their uncertainty bounds (S2 for the strongly perturbed, W1 and W12 for the weakly perturbed mechanism) show small sensitivity relative to other reactions. In addition to Figs. 5.2-5.5, the accuracy of the remaining optimization runs with predefined uncertainty factors UF repeated for the

same conditions and criteria are shown in Figs. 5.7 and 5.8. The extent of modifications of the reaction rates for these runs is reported in Fig. 5.1 top (strongly perturbed and weakly perturbed reduced mechanism, respectively).

Different reaction rate modifications resulted from each successive UF-constrained run for the corresponding mechanism (Fig. 5.1 top) but their prediction abilities were the same for the chosen optimization targets.

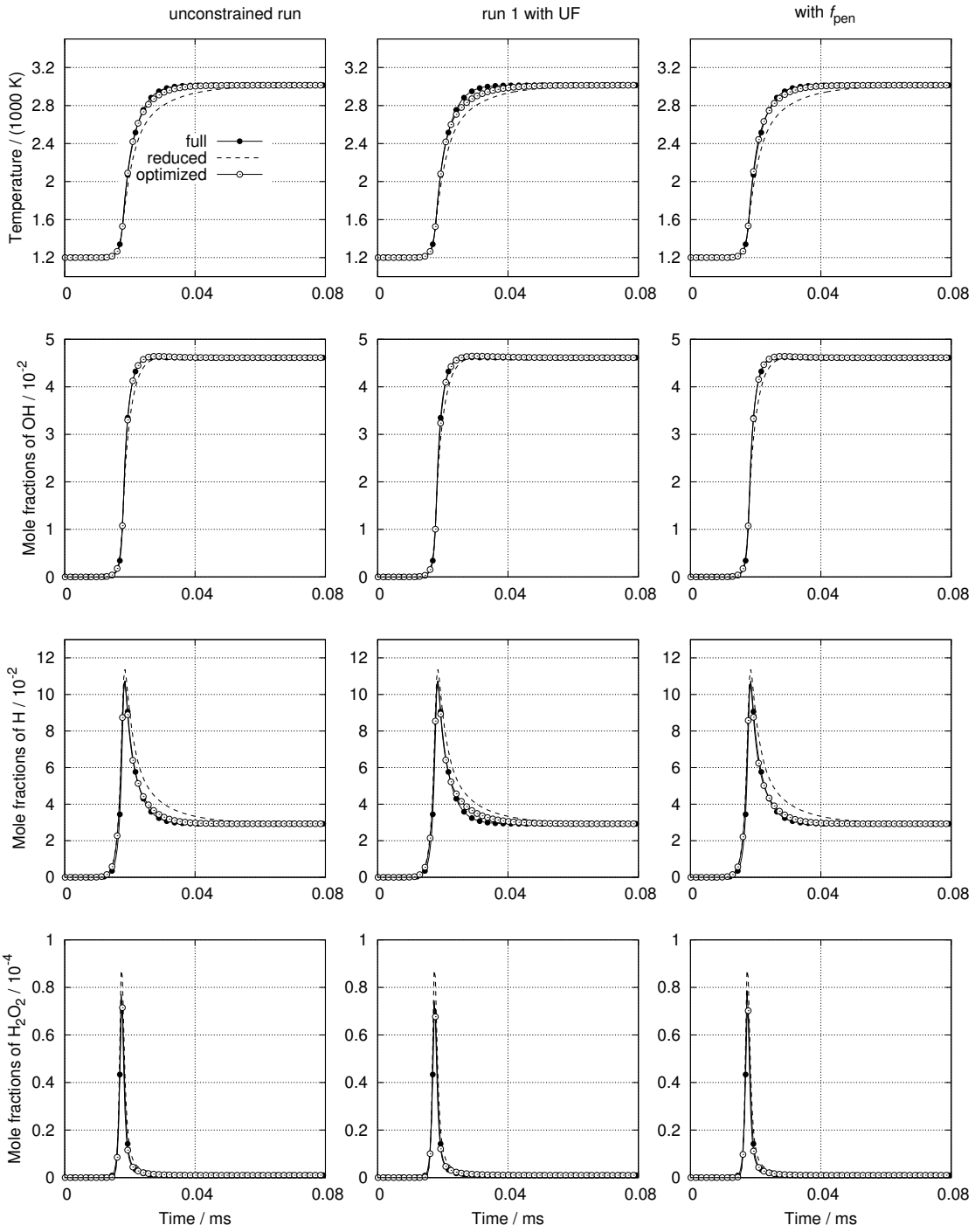

FIGURE 5.2: Auto ignition for full, reduced and optimized hydrogen mechanism resulting from three optimization runs with the same numerical setup and the accuracy criteria but different constraints imposed to reaction rate modifications: no constraints (left), with predefined uncertainty factor UF (center) and with penalty function f_{pen} ($\alpha_{\text{ref}} = 1.0$) to minimize the modification (right). The input mechanism was reduced with strong perturbation. .

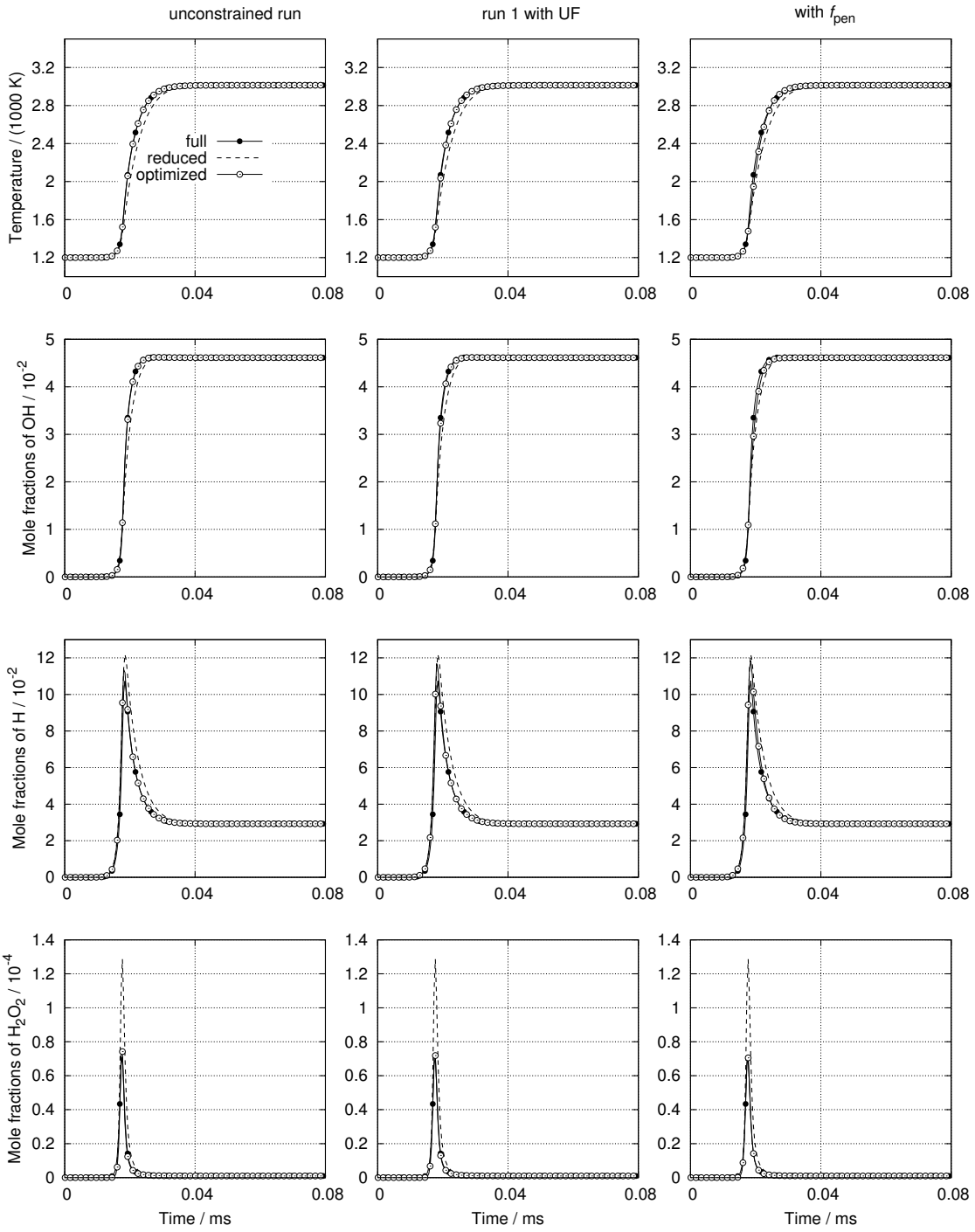

FIGURE 5.3: Auto ignition for full, reduced and optimized hydrogen mechanism resulting from three optimization runs with the same numerical setup and the accuracy criteria but different constraints imposed to reaction rate modifications: no constraints (left), with predefined uncertainty factor UF (center) and with penalty function f_{pen} ($\alpha_{\text{ref}} = 1.0$) to minimize the modification (right). The input mechanism was reduced with weak perturbation.

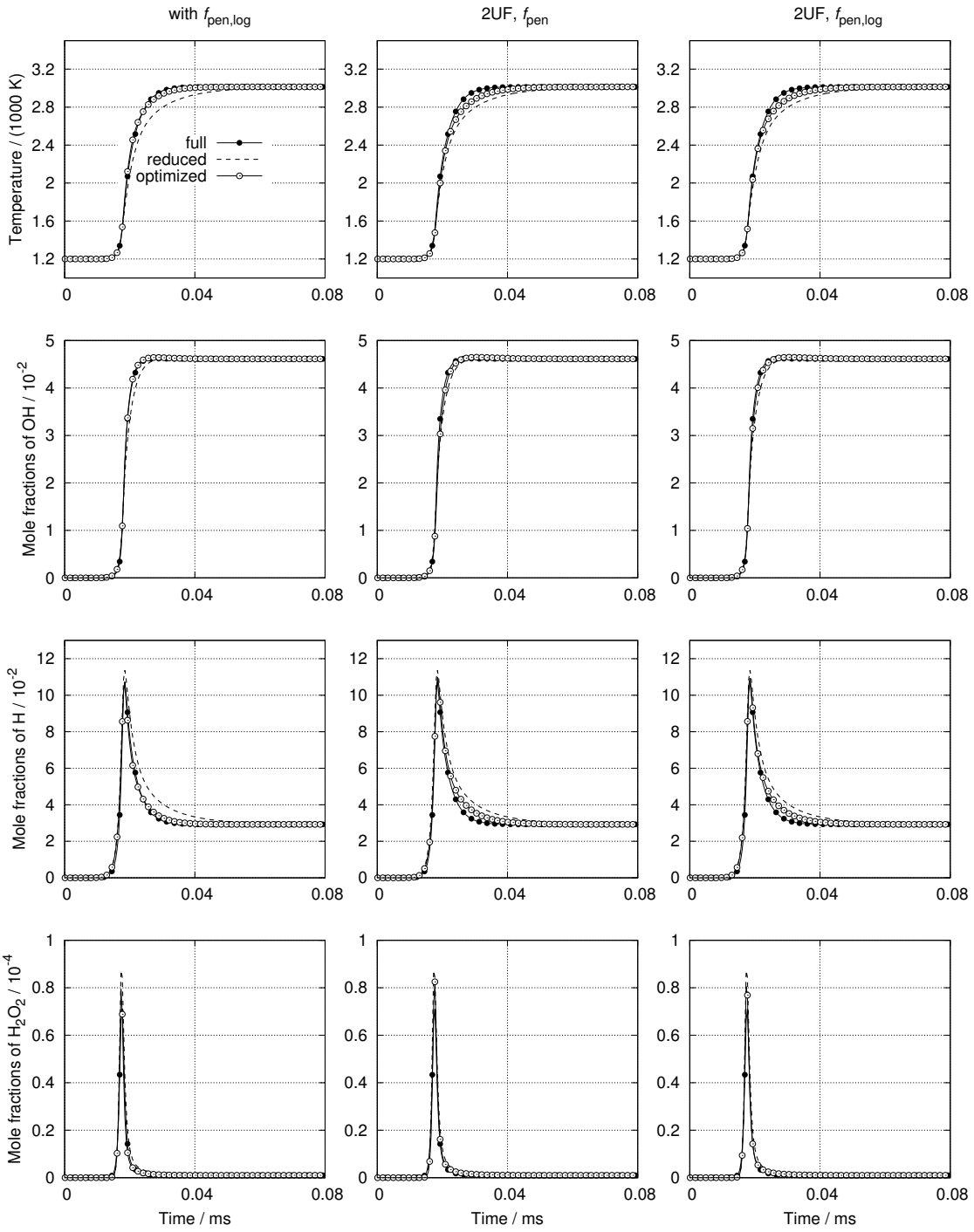

FIGURE 5.4: Auto ignition for full, reduced and optimized hydrogen mechanism resulting from three optimization runs with the same numerical setup and the accuracy criteria but different constraints imposed to reaction rate modifications: penalty function $f_{\mathrm{pen,log}}\,(\alpha_{\mathrm{ref}} = 1.0)$, with doubled UF and $f_{\mathrm{pen}}\,(\alpha_{\mathrm{ref}} = 1.0)$ (center) and with doubled UF and $f_{\mathrm{pen,log}}\,(\alpha_{\mathrm{ref}} = 1.0)$ (right). The input mechanism was reduced with strong perturbation.

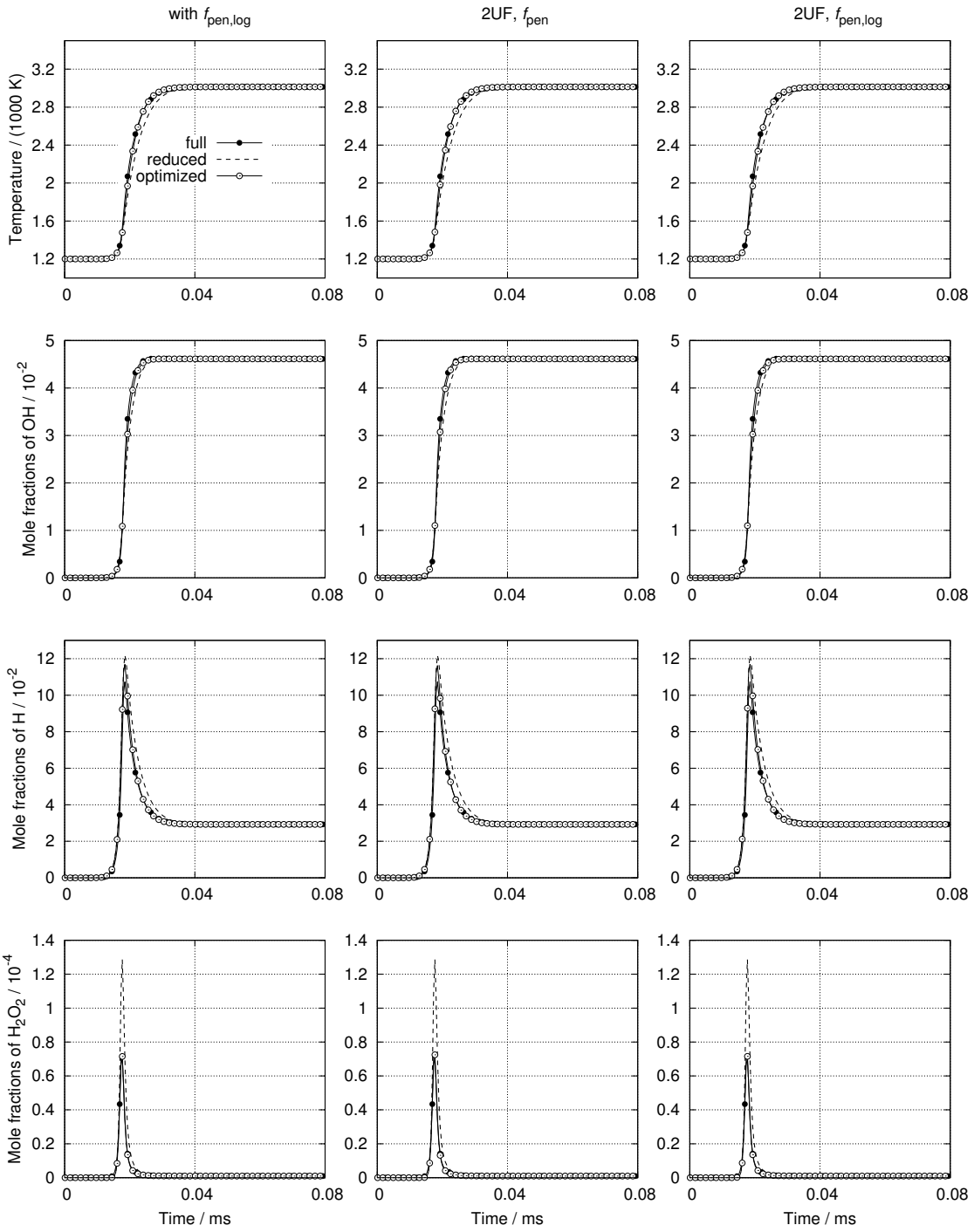

FIGURE 5.5: Auto ignition for full, reduced and optimized hydrogen mechanism resulting from three optimization runs with the same numerical setup and the accuracy criteria but different constraints imposed to reaction rate modifications: penalty function $f_{\text{pen,log}}$ ($\alpha_{\text{ref}} = 1.0$), with doubled UF and f_{pen} ($\alpha_{\text{ref}} = 1.0$) (center) and with doubled UF and $f_{\text{pen,log}}$ ($\alpha_{\text{ref}} = 1.0$) (right). The input mechanism was reduced with weak perturbation.

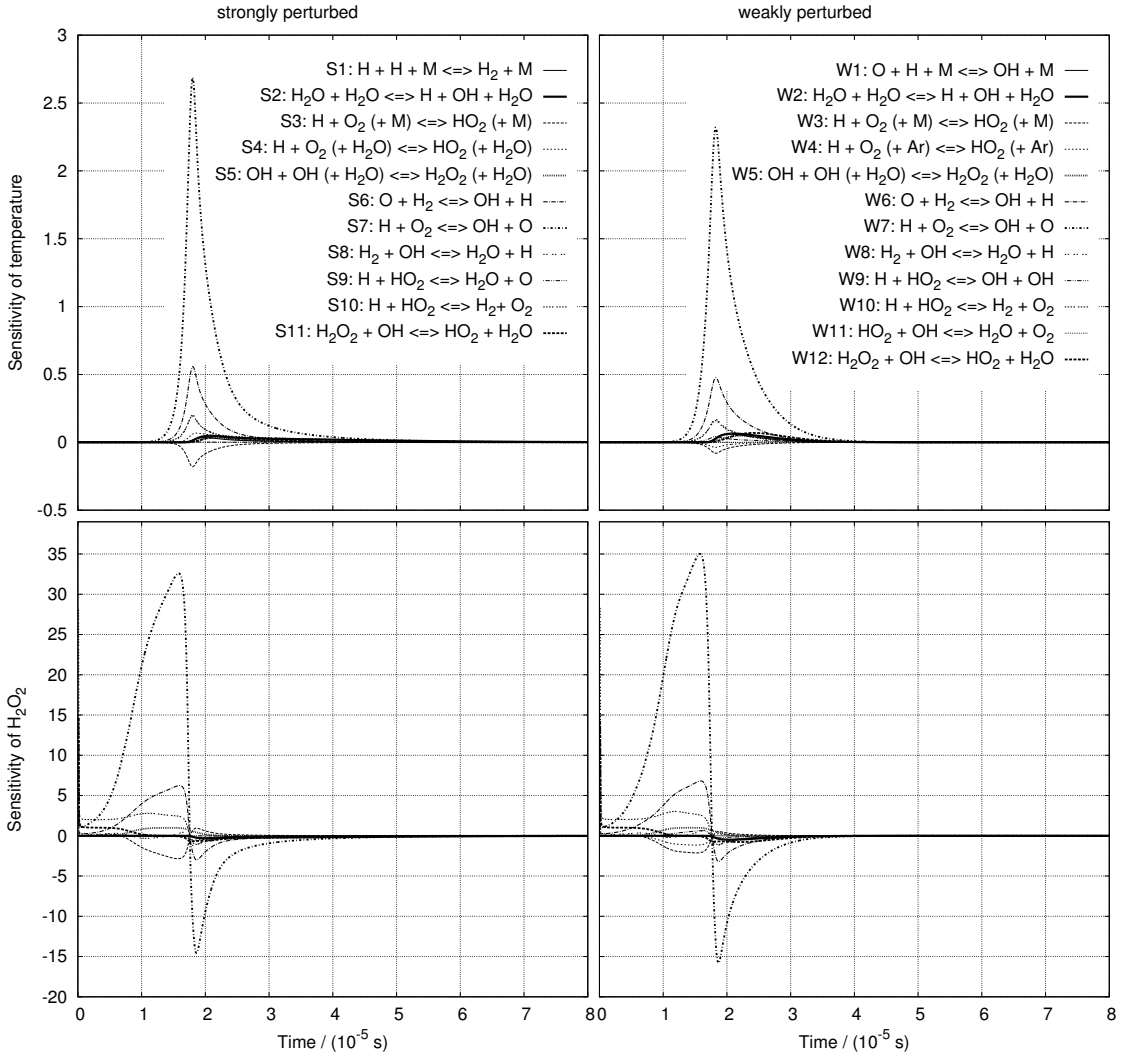

FIGURE 5.6: Normalized sensitivities of the temperature (top) and H_2O_2 (bottom) in respect to the remaining reactions in two reduced mechanisms.

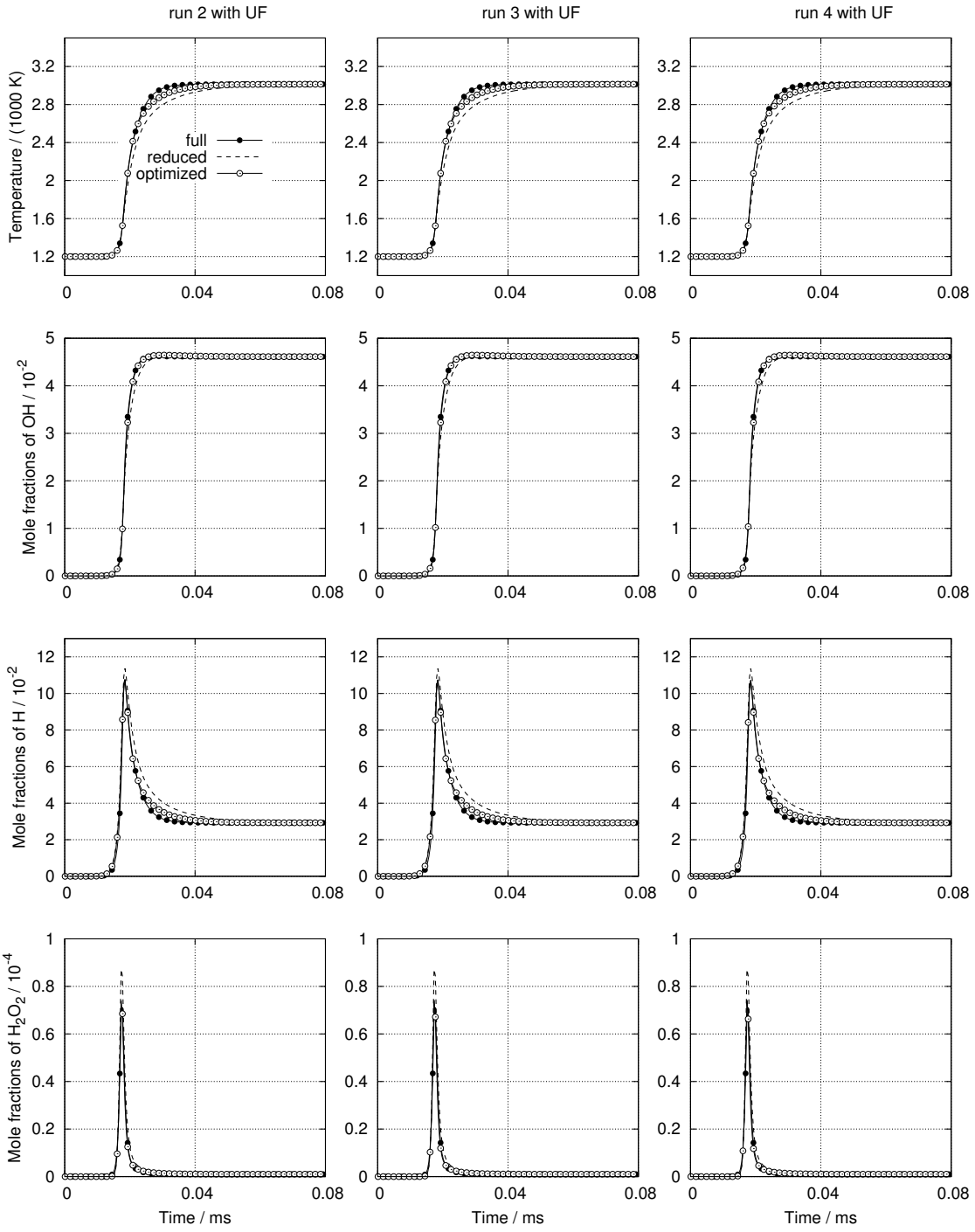

FIGURE 5.7: Auto ignition for full, reduced and optimized hydrogen mechanism resulting from three optimization runs with the same numerical setup, the accuracy criteria and predefined uncertainty factors UF. The input mechanism was reduced with strong perturbation.

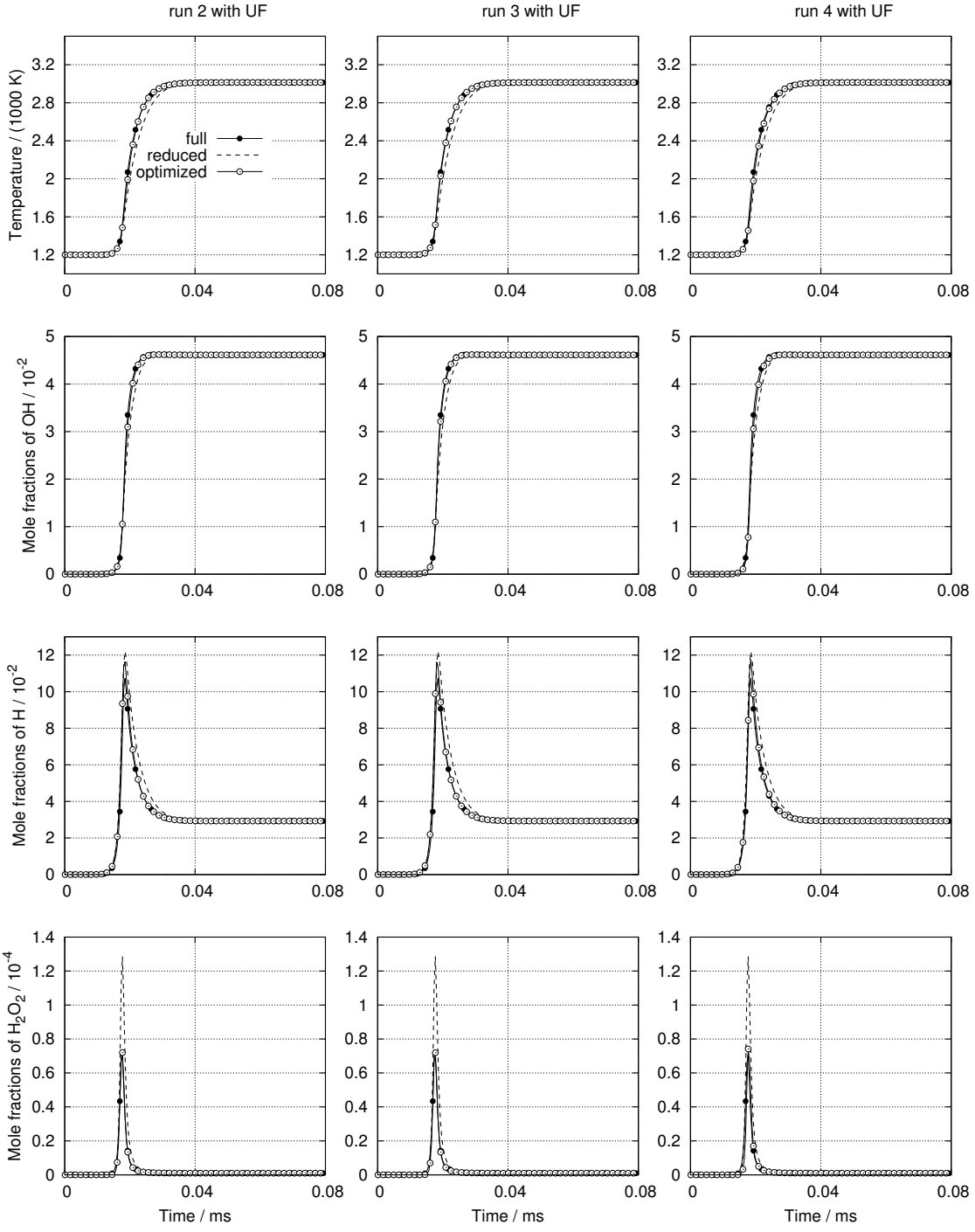

FIGURE 5.8: Auto ignition for full, reduced and optimized hydrogen mechanism resulting from three optimization runs with the same numerical setup, the accuracy criteria and predefined uncertainty factors UF. The input mechanism was reduced with weak perturbation.

5.2 Reduction and Subsequent Optimization - Ethylene Oxidation Mechanism

Aim of this section is to demonstrate the optimization of a mechanism that was previously reduced for a reactor, for laminar flame under multiple operating conditions. A moderately-sized mechanism was reduced for a simple model (homogeneous rector) over a range of different equivalence ratios and subsequently optimized for predicting the flame speed over the same range of conditions. The original mechanism considered here is USC Mech Version II [190], a high-temperature combustion mechanism of H_2/CO/C1-C4 compounds which consists of 111 species and 784 reactions. In the following, the reduction and the optimization results of the ethylene combustion mechanism are presented.

Reduction

The reduction was performed for the constant-pressure homogeneous reactor at atmospheric pressure, initial temperature $T_{\text{in}} = 1300$ K and six different equivalence ratios for ethylene/air mixture, $\phi = [0.6, 0.8, 1.0, 1.2, 1.4 \text{ and } 2.0]$. The criteria defined within the objective function for the elimination of reactions are listed in Table 5.3, the genetic algorithm parameters used for the mechanism reduction are given in Table 5.4.

Property	w_i	Normalization	σ	λ
N_{r}	4.0	Eq. 4.6	6.0	0.75
t_{CPU}	1.0	Eq. 4.6	6.0	4.0
τ_{ign}	1.0	Eq. 4.5	6.0	-
T_{profile}	2.0	Eq. 4.9	25.0	-
$X_{\text{H,profile}}$	2.0	Eq. 4.9	25.0	-

TABLE 5.3: Objective function parameters for reduction of the ethylene mechanism for a homogeneous constant-pressure reactor.

GA parameter	Type	Value
Population size	-	96
Selection	tournament	-
Crossover	single-point	$p_{\text{cross}} = 0.4$
Mutation	one-directional	$p_{\text{mut}} = 0.01$

TABLE 5.4: Parameters of the genetic algorithm used for reduction of the ethylene mechanism.

The convergence of the GA-based search for the smallest possible submechanism that satisfies the given criteria within the objective function is shown in Fig. 5.9 and the evolution of the remaining number of reactions is shown in Fig. 5.10.

The convergence plots show the best fitness within a generation (the minimum) and the statistical distribution of the fitnesses for all the individuals, represented by quantiles (Q25, Q50 and Q75).

For a given set of fitnesses within a generation, ascendingly sorted according to the fitness value, the median is the value separating the higher half of fitnesses from the lower half. It is often described as the "middle" value. For a given generation, the quantile Q50 is the median of the fitnesses within the generation (i.e. 50% of the individual fitnesses do not exceed the value denoted by Q50). The quantile Q25 is the median of the subset of fitnesses that are between the minimum fitness and Q50. Analogously, the quantile Q75 is the median of the subset of fitnesses that are between Q50 and the maximum fitness.

The best performing reduced mechanism is found in generation 690 and has 114 reactions (Fig. 5.10). This way the ethylene mechanism was reduced from 111 species and 784 reactions to 63 species and 114 reactions.

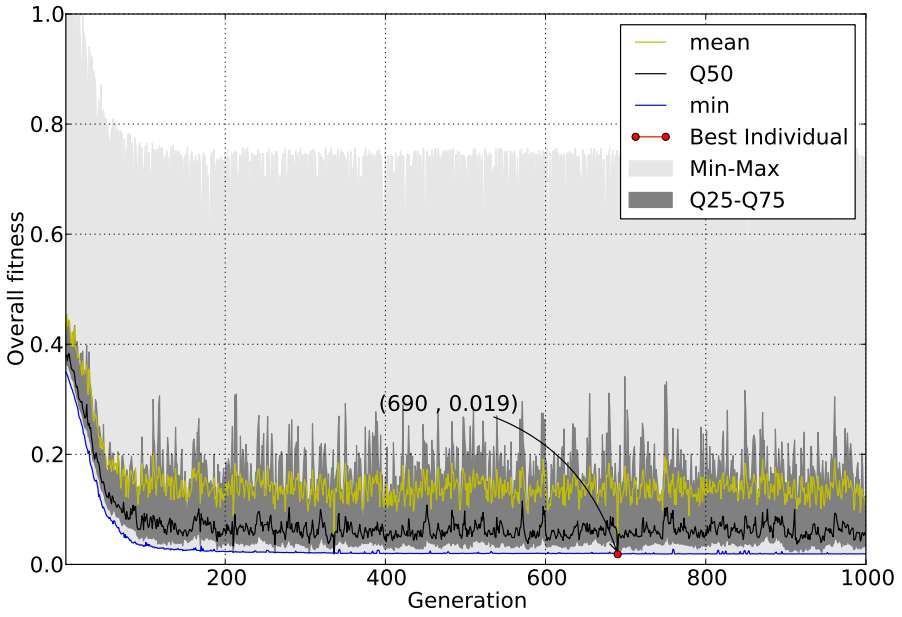

FIGURE 5.9: Overall fitness evolution for the USC-Mech mechanism reduction for ethylene/air combustion

The aim of reducing this mechanism for a simple reacting case (reactor) is to evaluate its performance for a more complex model (laminar flame) and to optimize such a reduced mechanism to predict the laminar flame speed. For the optimization, the adiabatic laminar freely propagating flame model with the following operating conditions was chosen: pressure $p = 10^5$ Pa, temperature at the burner $T_b = 300$ K and the flame lenght of

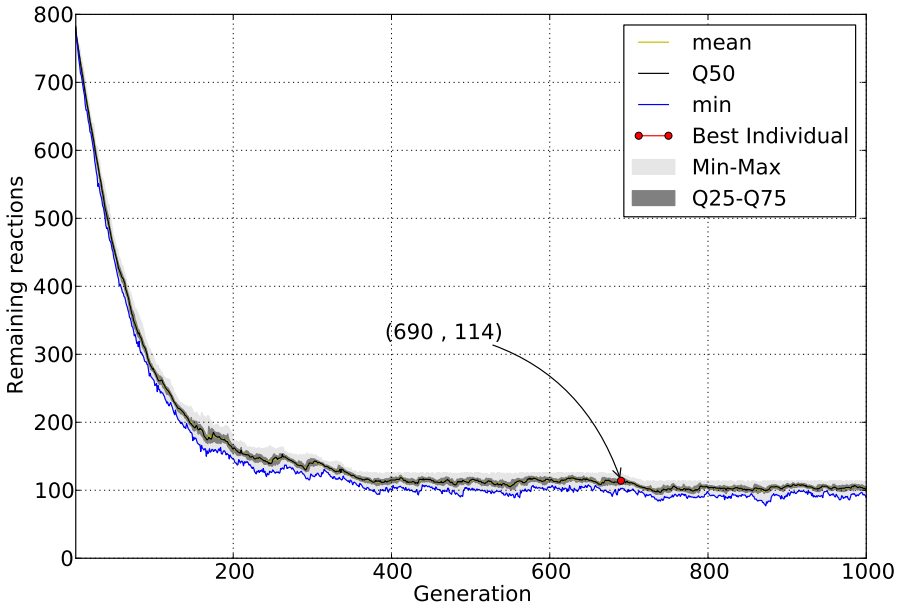

FIGURE 5.10: Evolution of the number of remaining reactions for the USC-Mech mechanism reduction for ethylene/air combustion

0.01 m. The equivalence ratios of the ethylene/air mixture were the same as for the reactor case, $\phi = [0.6, 0.8, 1.0, 1.2, 1.4 \text{ and } 2.0]$. The criteria (objective function terms) for the optimization are listed in Table 5.5. The penalty function was used to avoid that the resulting rate coefficients deviate too much from their nominal values.

Property	w_i	Normalization	σ
T_{profile}	1.0	Eq. 4.9	25
s_{L}	2.0	Eq. 4.5	6
$f_{\text{pen}}\,(\alpha_{\text{ref}} = 1.0)$	1.0	Eq. 4.7	6

TABLE 5.5: Objective function parameters for optimization of reduced ethylene mechanism for a freely-propagating flame.

The parameters of the genetic algorithm for the optimization of the reduced ethylene mechanism for the flame speed are given in Table 5.6.

The optimal solution was found in generation 946 with the overall fitness of 0.078, as shown in Fig. 5.11.

The performance of the optimized reduced ethylene mechanism is presented in terms of the temperature profiles for a freely propagating flame for $\phi = [0.6, 0.8, 1.0, 1.2, 1.4, 1.6, 1.8 \text{ and } 2.0]$ in Fig. 5.12 and the flame speeds in Fig. 5.13 showing that the reduced

GA parameter	Type	Value
Population size	-	48
Initialization	nominal gene values	-
Selection	tournament	-
Crossover	uniform	$p_{\text{cross}} = 0.5$
Mutation	Gaussian multiplicative	$p_{\text{mut}} = 0.02$

TABLE 5.6: Parameters of the genetic algorithm used for optimization of the reduced ethylene mechanism for a freely propagating flame.

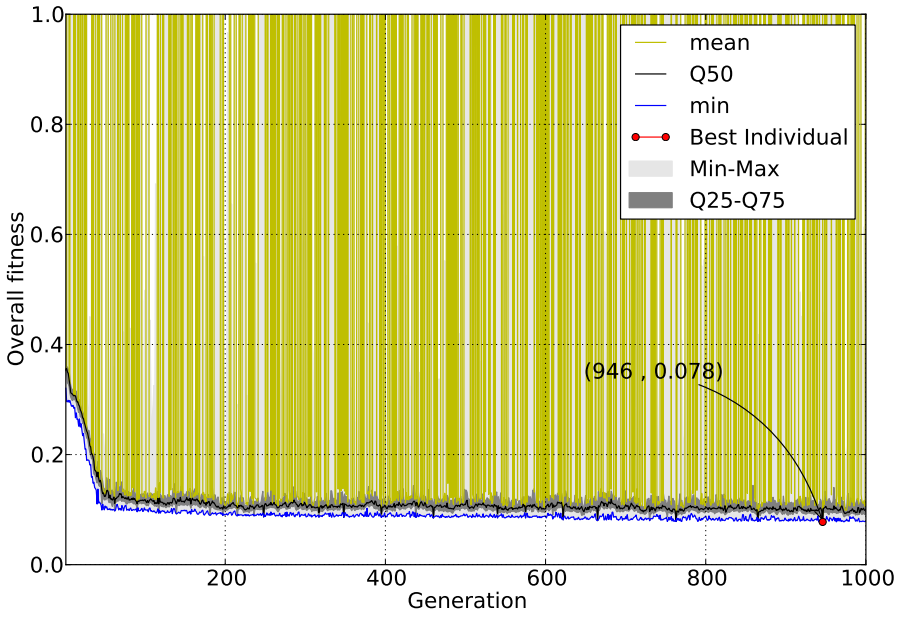

FIGURE 5.11: Overall fitness evolution for the reduced USC-Mech mechanism optimization for ethylene/air combustion in a freely propagating flame

optimized mechanism performs as well as its detailed version for the given operating conditions and the criteria.

The influence of the penalty function on the resulting reaction rates of the optimized mechanism is illustrated in terms of the discrete probability density of the normalized rate constants Fig. 5.14, with the mean value $\mu = 1.102$ and the standard deviation $\sigma = 0.478$, indicating that the accuracy of the chosen targets was fully restored without significant alteration of the reaction rates. The figure shows how most values were retained or mildly changed, and only two were increased/decreased significantly.

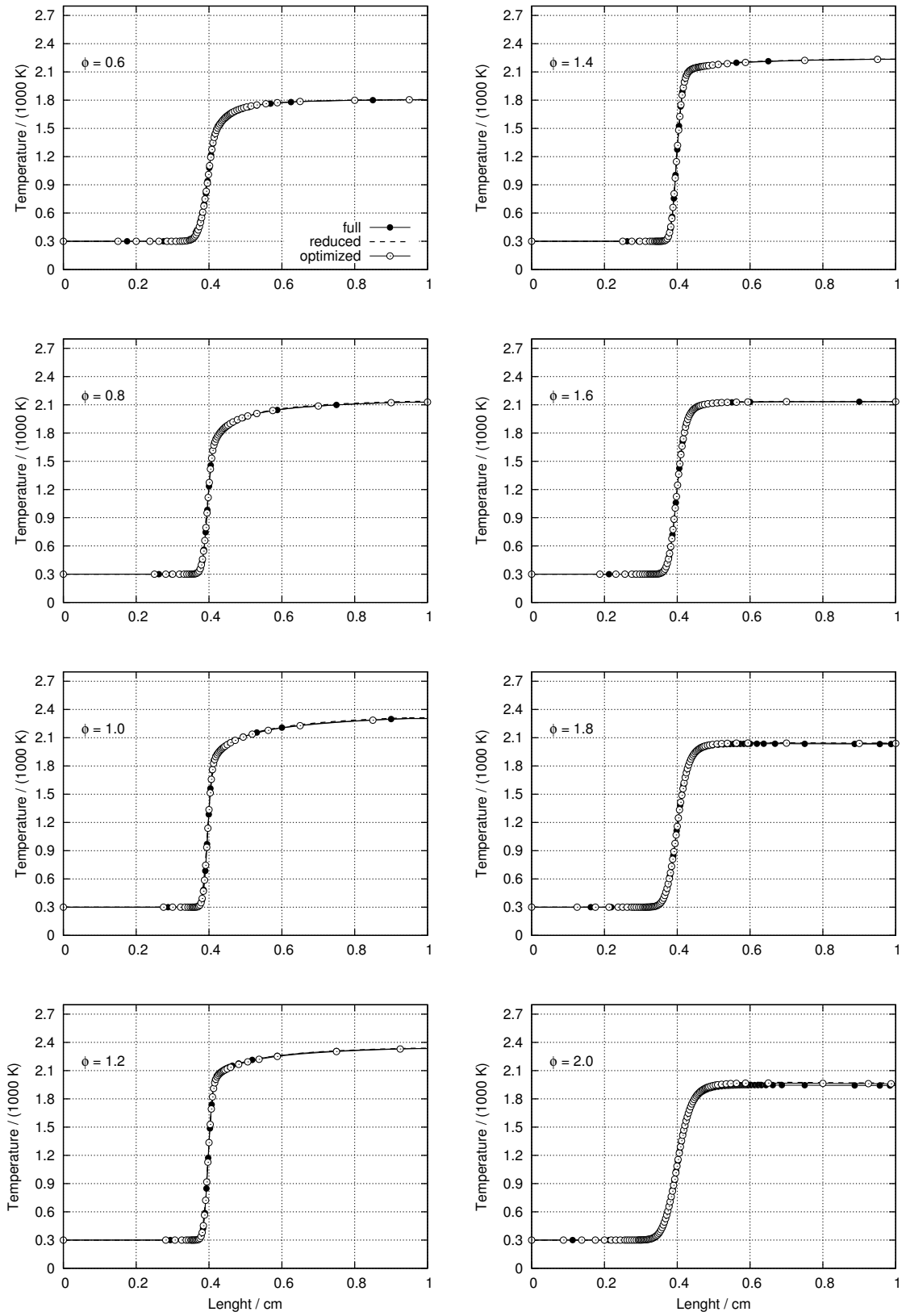

FIGURE 5.12: Temperature profiles for the full, reduced and optimized USC-Mech for a freely propagating flame for $\phi = [0.6, 0.8, 1.0, 1.2, 1.4, 1.6, 1.8 \text{ and } 2.0]$. Two points ($\phi = 1.6$ and $\phi = 1.8$) were not considered for the optimization.

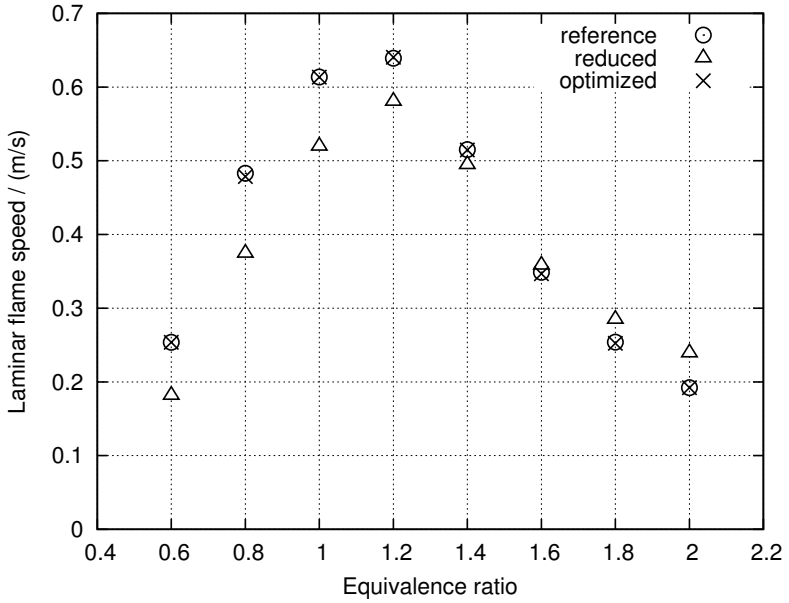

FIGURE 5.13: Laminar flame speeds for different equivalence ratios for which the reduced ethylene mechanism was optimized. Two points ($\phi = 1.6$ and $\phi = 1.8$) were not considered for the optimization.

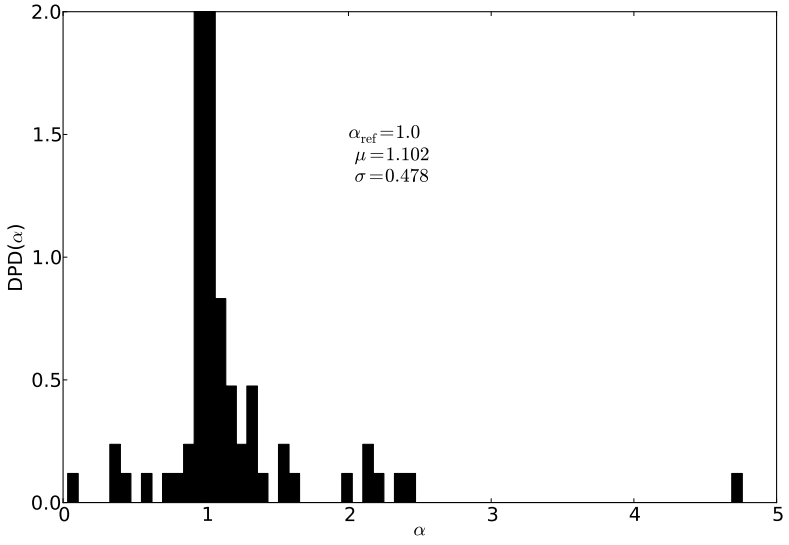

FIGURE 5.14: Discrete probability density of the normalized rate constants for the best individual from the ethylene mechanism optimization.

5.3 Further Reduction with the Penalty Function - *tert*-Butanol Oxidation Mechanism

The *tert*-butanol mechanism from Sarathy et al. 2012 [153] was chosen as an example of a large mechanism (2336 reversible reactions and 431 species) to demonstrate the usage of the penalty function for the further elimination of reactions during the optimization. Prior to the optimization, this mechanism was first reduced with the GA-based elimination procedure to 204 reactions and 144 species. The reduction was performed for a constant-pressure homogeneous reactor at pressure $p = 1.5$ atm, initial temperature $T_{\text{in}} = 1250$ K and stoichiometric *tert*-butanol/air mixture. The objective function terms are listed in Table 5.7.

Property	w_i	Normalization	σ	λ
N_{r}	4.0	Eq. 4.6	6.0	0.75
t_{CPU}	1.0	Eq. 4.6	6.0	4.0
τ_{ign}	1.5	Eq. 4.5	6.0	-
T_{profile}	1.5	Eq. 4.9	10.0	-

TABLE 5.7: Objective function parameters for reduction of *tert*-butanol mechanism for a homogeneous constant-pressure reactor simulation.

The parameters of the genetic algorithm used for reaction elimination are listed in Table 5.8.

GA parameter	Type	Value
Population size	-	96
Initialization	one-reaction-missing	-
Selection	tournament	-
Crossover	single-point	$p_{\text{cross}} = 0.5$
Mutation	one-directional	$p_{\text{mut}} = 0.004$

TABLE 5.8: Parameters of the genetic algorithm used for reduction of *tert*-butanol mechanism.

5.3.1 Objectives

The reduced *tert*-butanol mechanism was further optimized for the same operating conditions against its detailed version taking into account the criteria listed in Table 5.9. The aim of this optimization run is to restore the accuracy and reduce the mechanism further with the penalty function.

The parameters of the genetic algorithm used for reaction-rate optimization are listed in Table 5.10.

Property	w_i	Normalization	σ
τ_i	1.0	Eq. 4.5	6.0
T_{profile}	1.0	Eq. 4.9	10.0
$X_{\text{H,max}}$	1.5	Eq. 4.5	4.0
$X_{\text{H2,profile}}$	1.0	Eq. 4.9	15.0
$X_{\text{O,max}}$	1.0	Eq. 4.5	4.0
$X_{\text{CH3,max}}$	1.0	Eq. 4.5	4.0
$X_{\text{CH3,profile}}$	1.5	Eq. 4.9	15.0
$X_{t\text{C4H9OH,profile}}$	1.0	Eq. 4.9	15.0
$f_{\text{pen}}(\alpha_{\text{ref}} = 0.0)$	6.0	Eq. 4.7	25.0

TABLE 5.9: Terms of the objective function for the optimization of *tert*-butanol mechanism.

GA parameter	Type	Value
Population size	-	96
Initialization	nominal gene values	-
Selection	tournament	-
Crossover	uniform	$p_{\text{cross}} = 0.5$
Mutation	Gaussian multiplicative	$p_{\text{mut}} = 0.02$

TABLE 5.10: Parameters of the genetic algorithm used for optimization of the reduced *tert*-butanol mechanism.

5.3.2 Results

The butanol combustion mechanism of Sarathy et al. from 2012 [153] was first reduced with the reduction procedure from 2336 reversible reactions and 431 species to 204 reactions and 144 species. The overall fitness evolution during the integer-coded reduction of the mechanism is shown in Fig. 5.15, finding the optimal solution in generation 1291. The number of reactions decrease during the evolution is shown in Fig. 5.16. Evolution of the computational time criterion (Fig. 5.17) shows that the algorithm discarded the computationally expensive solutions. Further reduction to 136 reactions and 104 species was achieved with the optimization using the penalty function $f_{\text{pen}}\,(\alpha_{\text{ref}} = 0.0)$. Figure 5.18 shows the overall fitness behavior during the optimization run. Late convergence was reached because of the penalty function. The penalty function was aiming to decrease the rate constants as much as possible (goal oposed to the accuracy citeria) so it never reached its minimal value (Fig. 5.19). The accuracy of the reduced and the optimized *tert*-butanol mechanism is presented in Fig. 5.20 showing a good agreement between the detailed mechanism and the significantly reduced optimized mechanism for all the optimization targets.

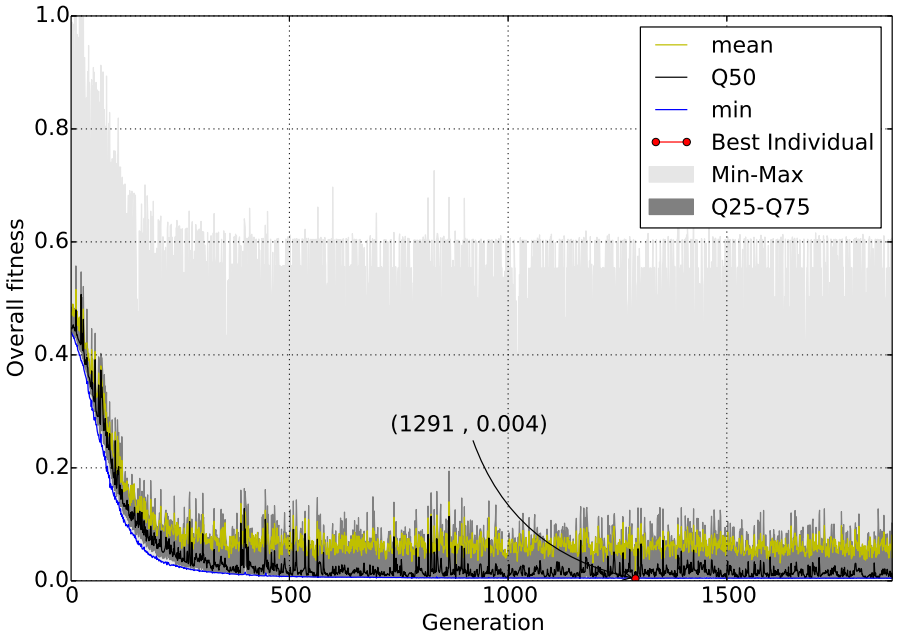

FIGURE 5.15: Overall fitness evolution for the tert-butanol mechanism reduction

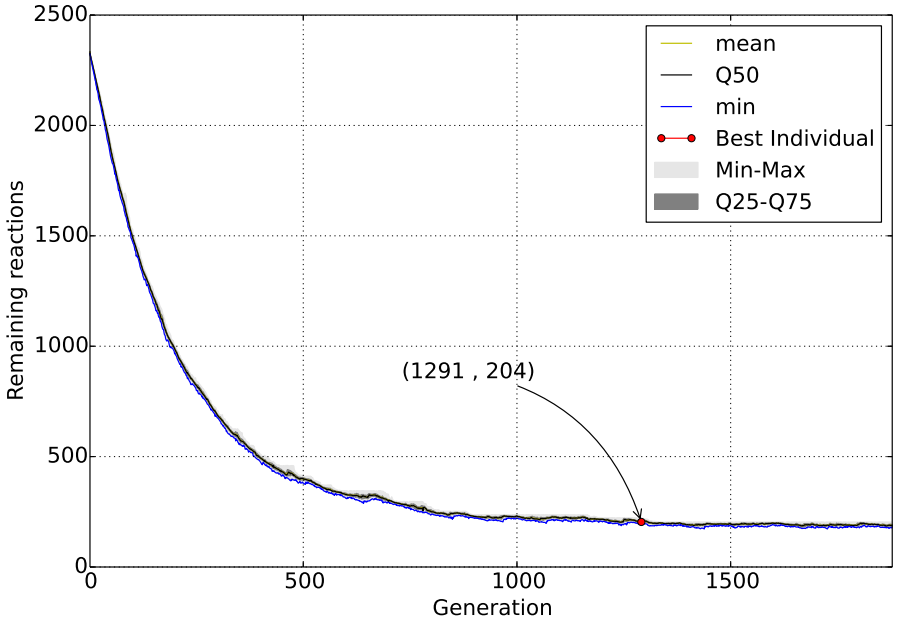

FIGURE 5.16: Evolution of the number of remaining reactions during the tert-butanol mechanism reduction

To illustrate the evolution of the reaction rates modifications and their correlation to the overall fitness and the penalty function, three different values of the resulting rates are shown in a scatter plot (Fig. 5.25).

Scatter plots 5.22, 5.23 and 5.24 show the visibility of the objective function terms to the overall objective function, indicating that the choice of the normalization functions

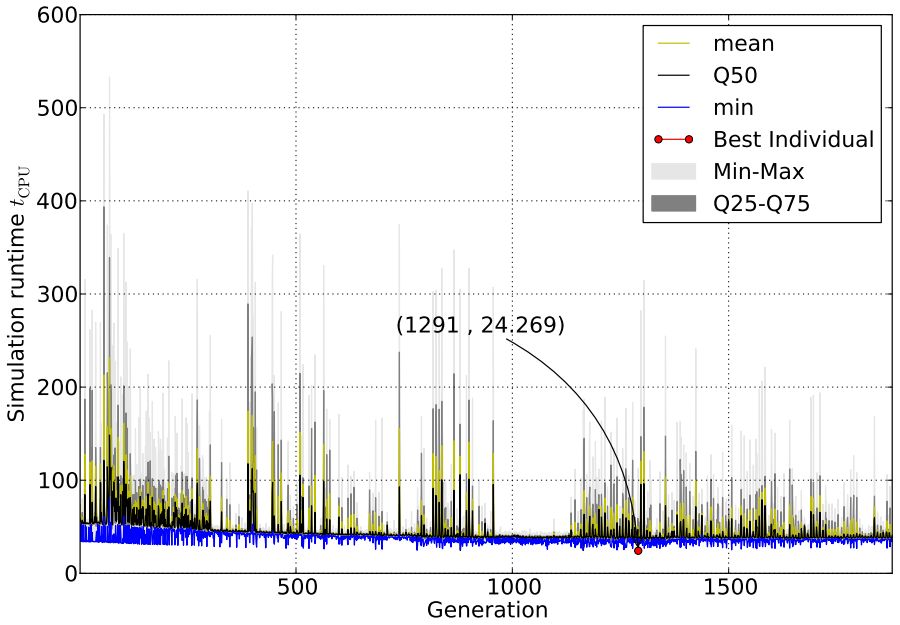

FIGURE 5.17: Evolution of the reactor simulation runtime during the tert-butanol mechanism reduction

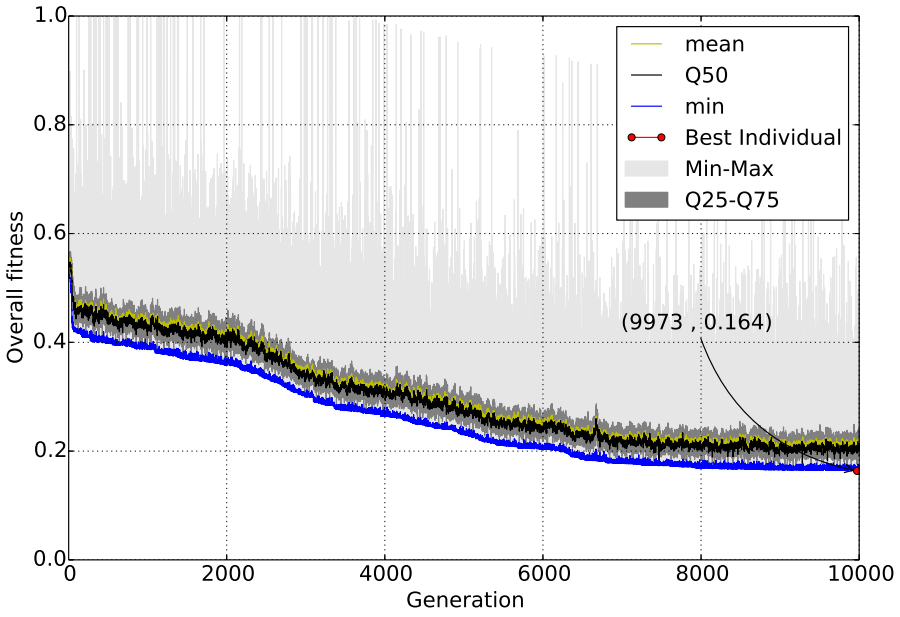

FIGURE 5.18: Overall fitness evolution for the reduced tert-butanol mechanism optimization with penalty function for $\alpha_{\text{ref}} = 0.0$

and their coefficients was appropriate for the desired optimization outcome (Fig. 5.20). This means that the optimization targets do not outweigh each other after scaling and are equally treated within the objective function. The scatter plots are colored by the overall fitness. The data on the scatter plots are logaritmically normalized (to the base 10) so that the changes across disparate scales can clearly be seen. Blue indicates minimal (desired) value, red indicates the maximal value (bad solutions) of the observed

target. Dark red points represent the candidate mechanisms with the highest fitness function value (caused either by a poor numerical behavior of these mechanisms or their inaccuracy) indicating that the optimization method is robust with respect to numerically unstable or inaccurate mechanisms that may occur during the search. Such solutions are successfully discarded. To obtain an insight into reaction rates behavior due to the penalty function, three illustrative reaction rate values are plotted against the penalty function and the overall fitness on Fig. 5.25.

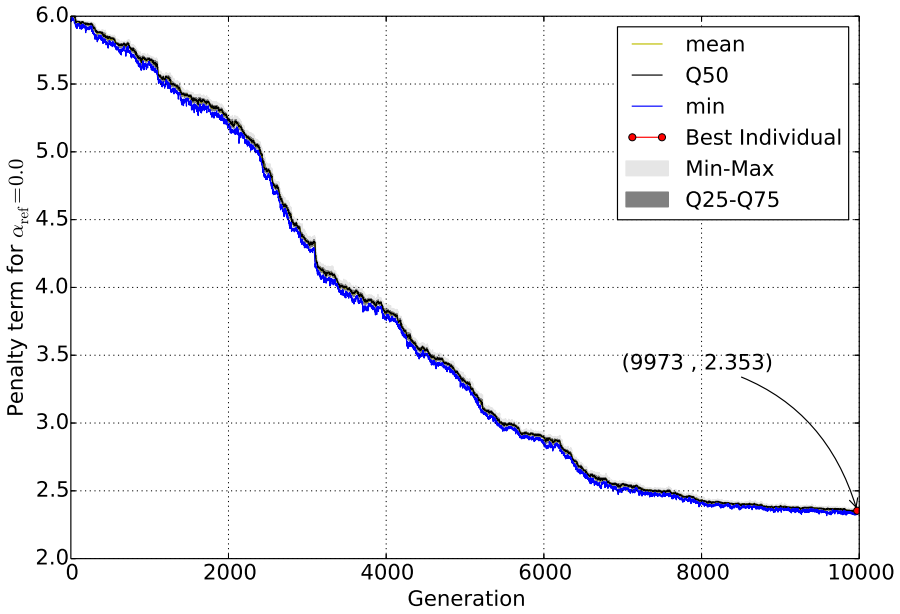

FIGURE 5.19: Penalty function evolution for thre reduced tert-butanol mechanism optimization for $\alpha_{\text{ref}} = 0.0$

Reactions rate values (genes) from Fig. 5.25 have different resulting values. Reaction 16 (gn00016) did not change its nominal value, i.e. $\alpha_{\text{opt}}(\text{gn00016}) = 1.0$. Reaction 21 (gn00021) was significantly modified $\alpha_{\text{opt}}(\text{gn00021}) = 7.6$ indicating that its value has fallen into the plateau region of the penalty function (see Fig. 4.8 in Section 4) so no constraints to this reaction rate were imposed (maximal allowed gene value was 8.0). Reaction 140 (gn00140) was eliminated from the mechanism by sharply directing its rate towards zero with the penalty function.

This way, the penalty function helped eliminating 68 reactions from the mechanism with the improvement of its accuracy (Fig. 5.20). As the consequence of eliminating these reactions, 40 species were further removed from the mechanism.

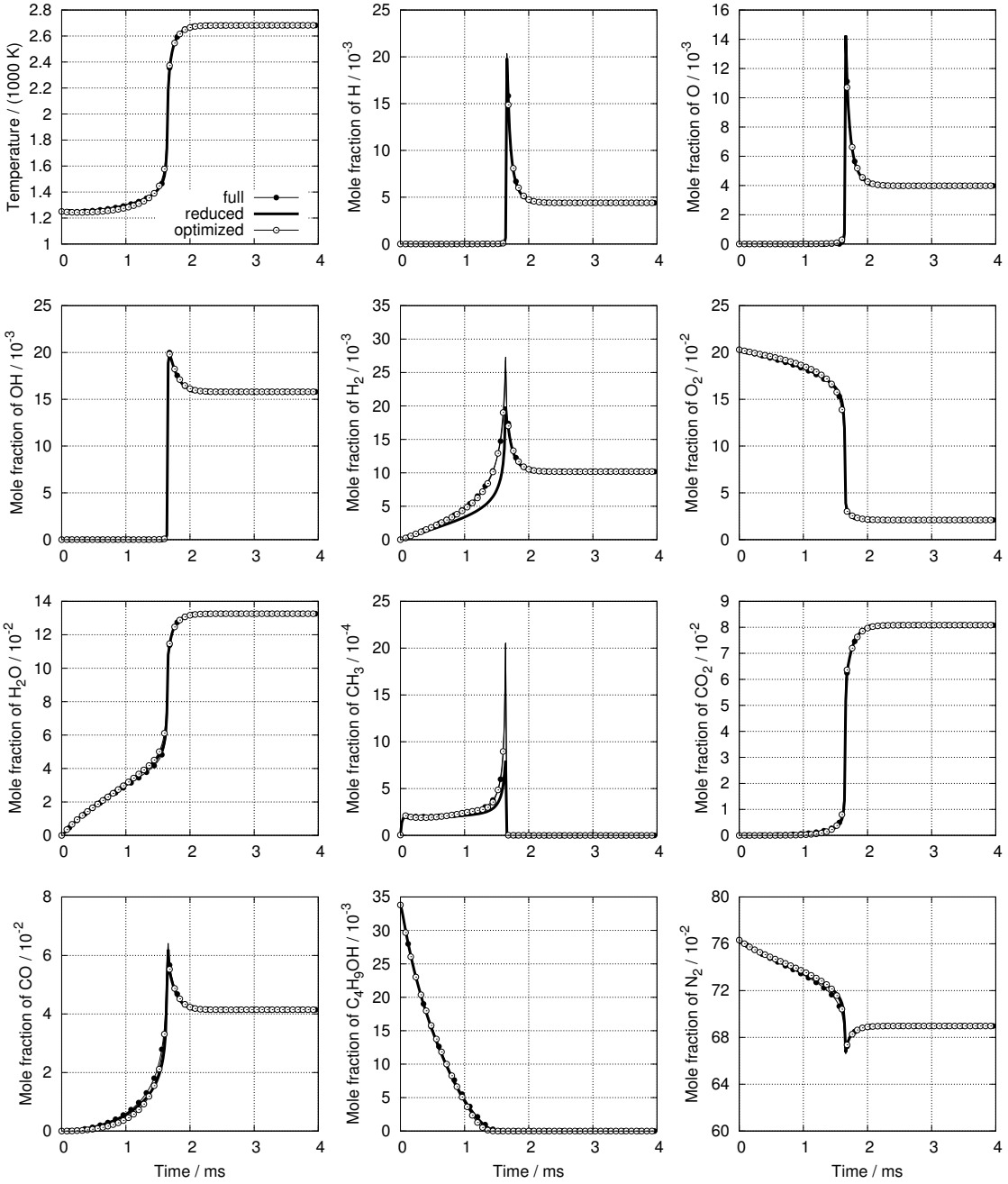

FIGURE 5.20: Auto-ignition with the full, reduced and optimized tert-butanol mechanism for a homogeneous constant-pressure reactor. The optimization reduced the mechanism further.

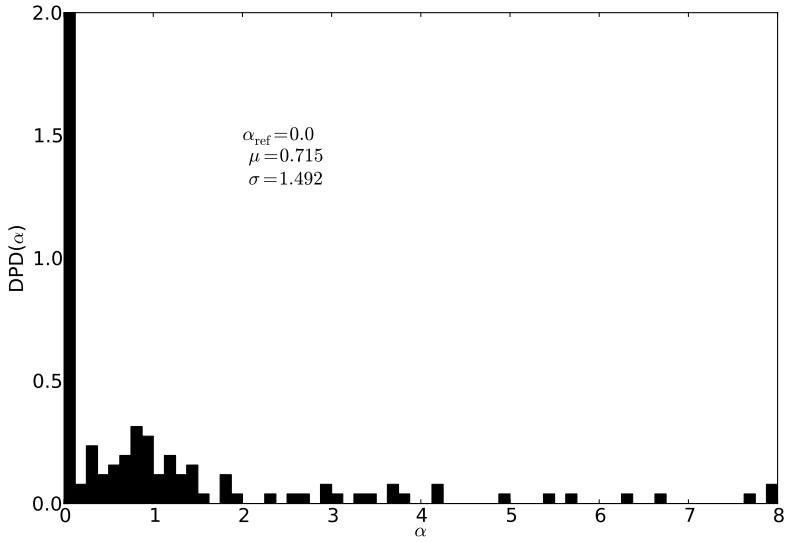

FIGURE 5.21: Discrete probability density of the normalized rate constants for the best individual from the *tert*-butanol mechanism optimization. The left-most bar relates to removed reactions.

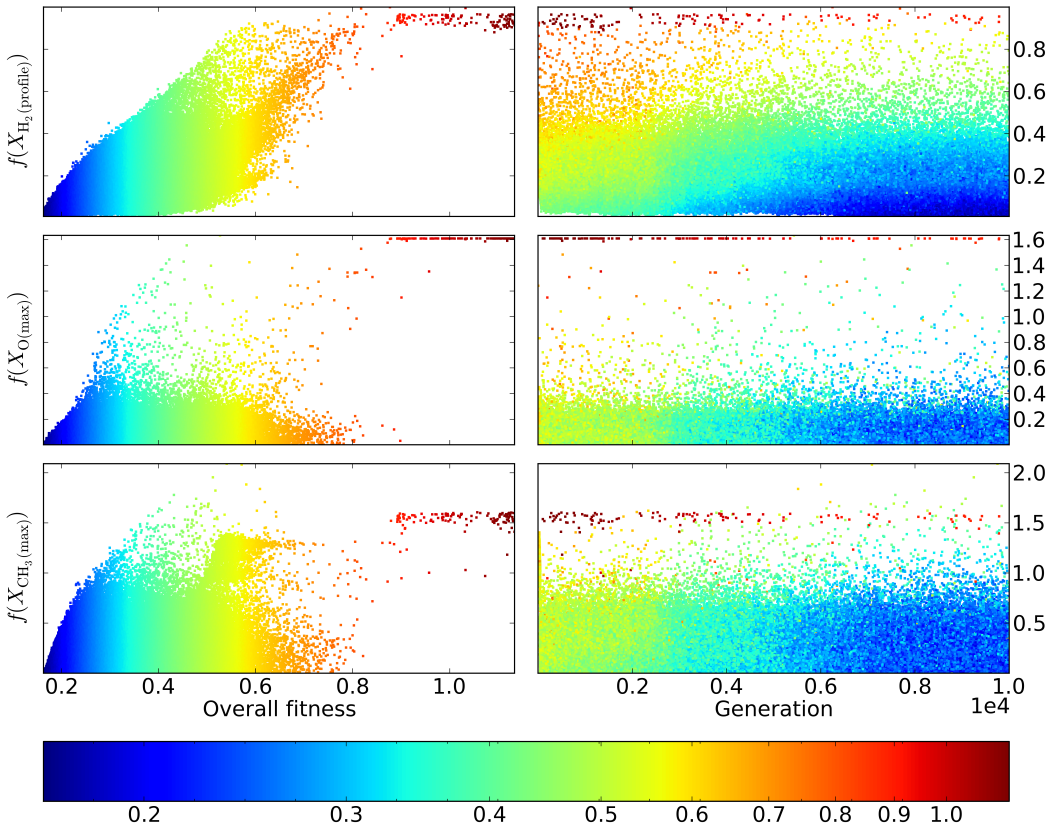

FIGURE 5.22: Scatter plots show the values of the objective function terms for each individual during the optimization colored by the overall fitness value, indicating the correlation between the normalized optimization targets and the overall fitness.

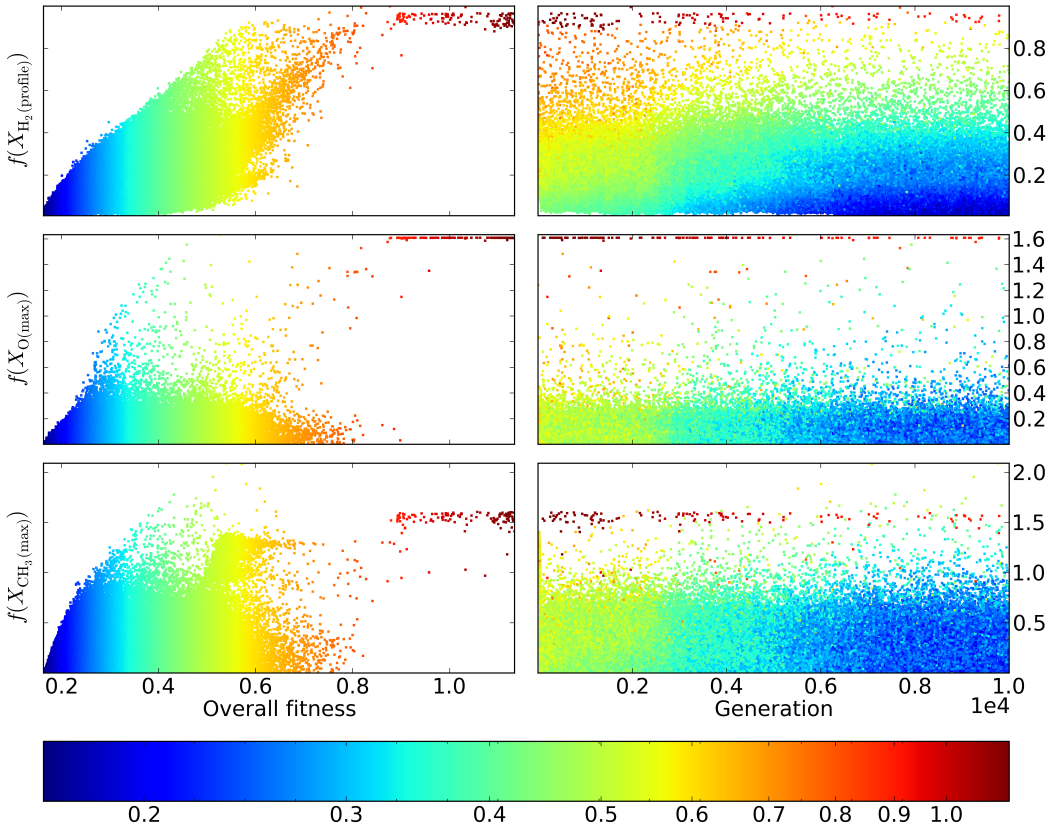

FIGURE 5.23: Scatter plots show the values of the objective function terms for each individual during the optimization colored by the overall fitness value, indicating the correlation between the normalized optimization targets and the overall fitness.

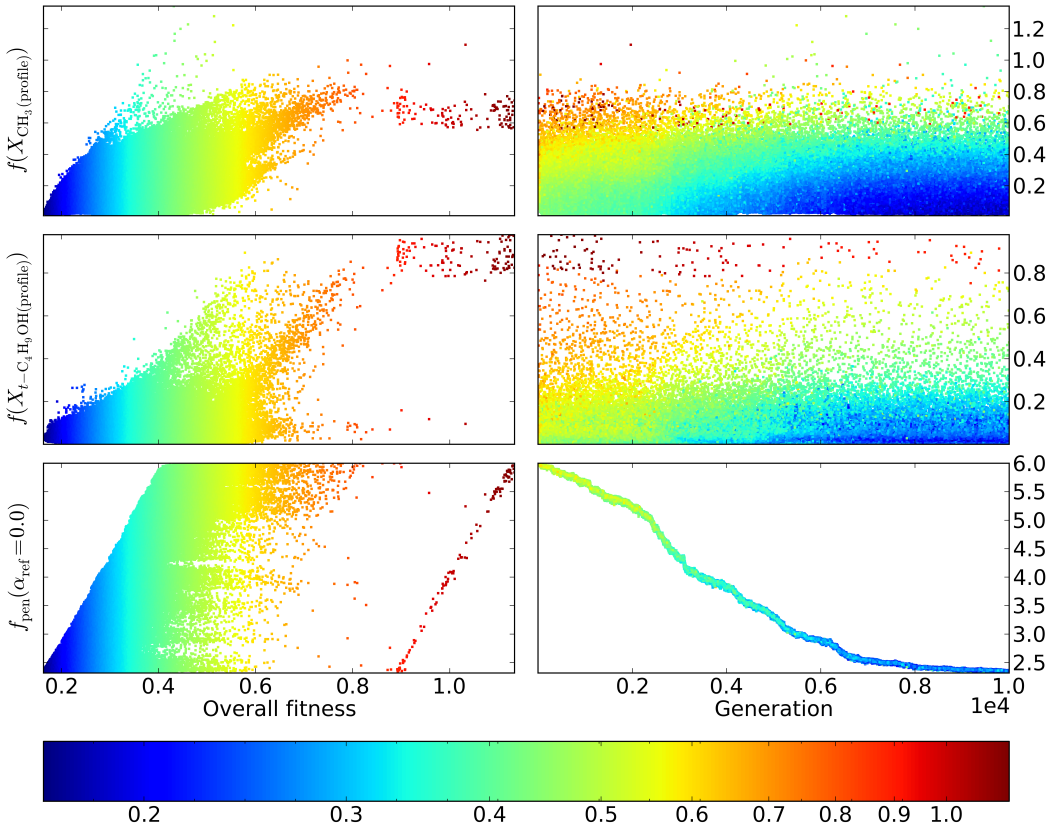

FIGURE 5.24: Scatter plots show the values of the objective function terms for each individual during the optimization colored by the overall fitness value, indicating the correlation between the normalized optimization targets and the overall fitness.

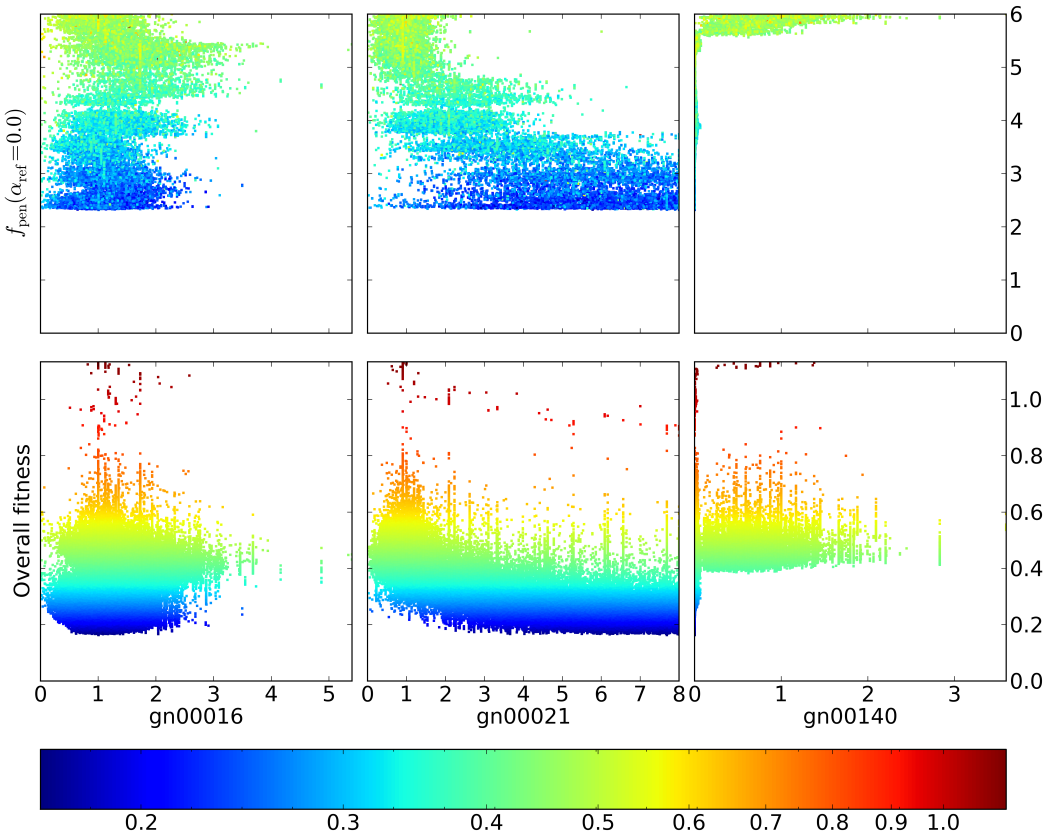

FIGURE 5.25: Scatter plots for each of the tested mechanisms during the optimization, indicating the correlation between the normalized rate constants of reactions 16, 21 and 123 in the mechanism and the penalty function and the overall fitness. Colored by the overall fitness.

5.4 Parameters Study

This section addresses the choice of the genetic algorithm operations and their parameters depending on the problem. Most important aspects of parameters for both the integer-coded (reduction) and the real-coded (optimization) genetic algorithm used in this work are discussed to provide help with chosing the appropriate functions and parameters for a given problem. The material from Sections 5.4.1, 5.4.2 and 5.4.3 has been published in International Journal of Chemical Kinetics [161, 162] and reused in this work with permission from Wiley.

5.4.1 Genetic Algorithm Parameters Study - Reduction

This section covers the crucial aspects of the specific method used for the reduction (see Section 4.1): initialization, mutation, evaluation function, the crossover rate and the population size. Specific operators and recommendations for their values are applicable only within the scope of the reduction method presented in this work.

Effect of initialization

The effect of different initializations was studied, comparing an initialization with the full mechanism to an initialization where one reaction was deactivated in every chromosome. Figures 5.26 and 5.27 show the evolution of the overall fitness over the generations, indicating that the type of initialization only affects the very first generations. For this case, the setup starting from the full mechanism has surpassed the incomplete initialization after approximately fifty generations, but the latter has converged faster initially. For relatively small or moderate mechanisms, the full-initialization does not slow the search process down significantly, but for large mechanisms, the "one-reaction-missing initialization" is preferred as it saves time for calculating the whole initial population of the same chromosomes with the full length.

Effect of one-way vs. two-way mutation

A mutator was chosen to create additional evolution pressure towards smaller mechanisms by only permitting mutations to remove reactions, but not to add them again. Where this approach involves the risk that a key reaction might be lost forever, we have found this approach to be generally beneficial, as can be seen by the faster convergence in Figures 5.28 and 5.29 as compared to Figures 5.32 and 5.33. The overall fitness and the remaining reactions over 500 generations for the sigmoid normalization of the

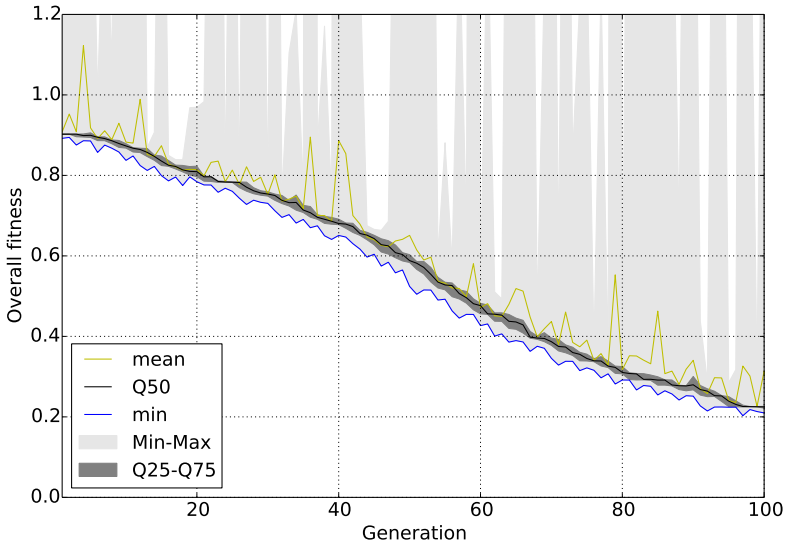

FIGURE 5.26: Evolution of the objective function within the first 100 generations using full mechanism initialization

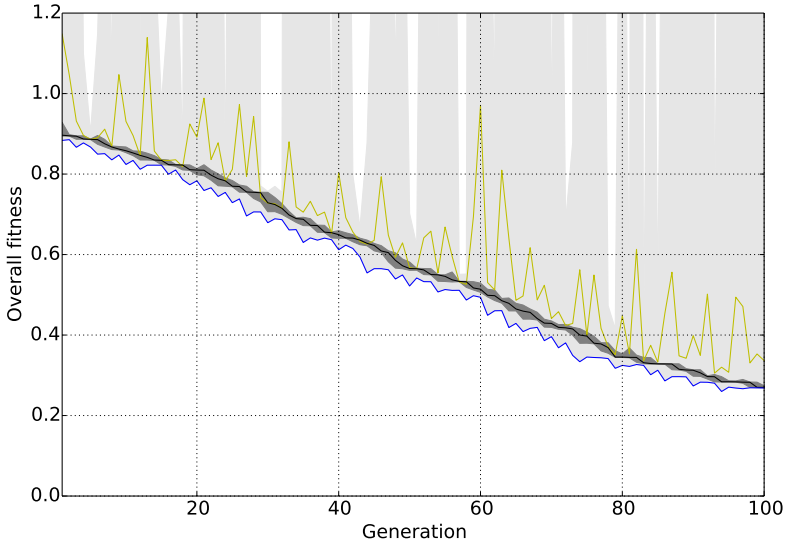

FIGURE 5.27: Evolution of the objective function within the first 100 generations using "one reaction missing" initialization

runtime and the number of reactions are shown for the two-directional mutation with the mutation rate 0.002 (Figures 5.28 and 5.29), the two-directional mutation with the mutation rate 0.003 (Figures 5.30 and 5.31) and the one-directional mutation with the mutation rate 0.002 (Figures 5.32 and 5.33).

The two-directional mutation results in somewhat slower convergence and many previous tests have shown that it may lead to a slightly bigger mechanism, as would be expected, since this mutator shifts the evolutionary pressure towards small mechanisms, but the overall effect is small. However, this must be tested statistically for a large number of

repeated runs (see Section 5.4.4). Nevertheless, the mutation rate for both mutators must be carefully chosen to prevent the solution to fall beyond the optimum.

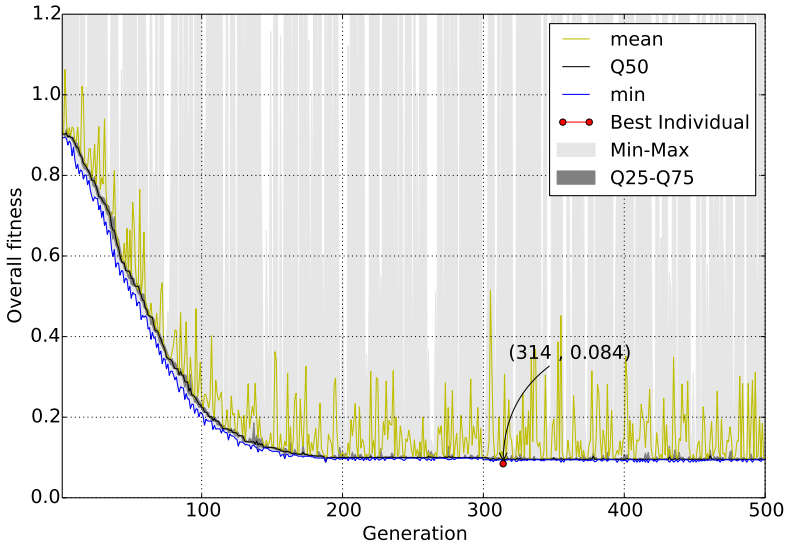

FIGURE 5.28: Overall convergence with the two-directional mutation ($p_m = 0.002$, sigmoid normalization of the runtime and the number of reactions): Objective function evolution

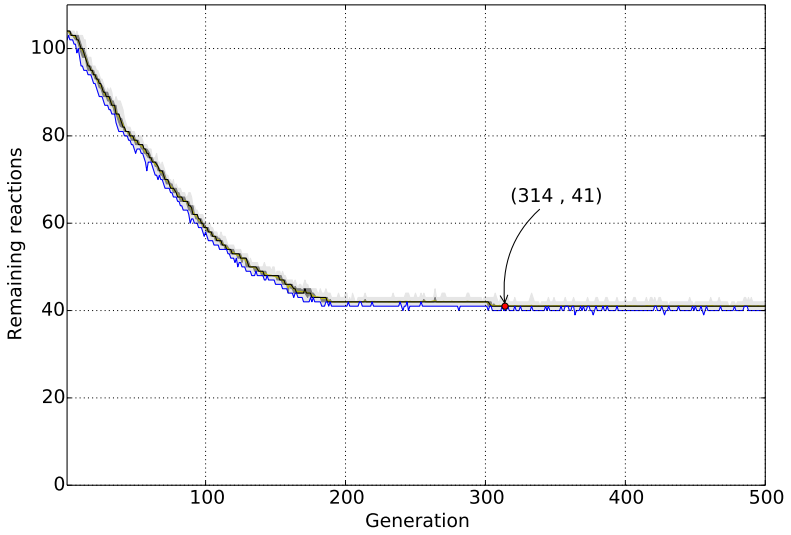

FIGURE 5.29: Overall convergence with the two-directional mutation ($p_m = 0.002$, sigmoid normalization of the runtime and the number of reactions): Evolution of the number of remaining reactions

Effect of the choice of evaluation functions

In order to examine the effect of the functions used for targets scaling on the overall convergence of the algorithm (here, the integer-coded), a mechanism containing 104 reactions ([148] combined with the mechanism from [130]) was taken as a test case.

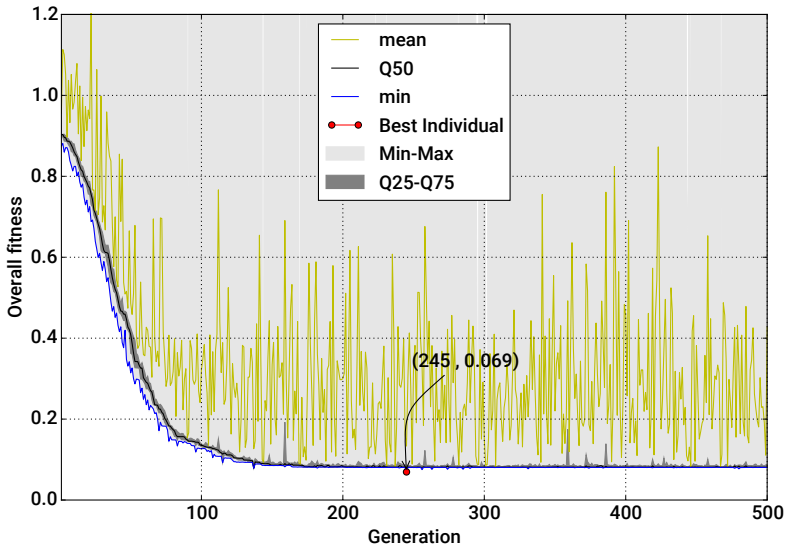

FIGURE 5.30: Overall convergence with the two-directional mutation ($p_m = 0.003$, sigmoid normalization of the runtime and the number of reactions): Objective function evolution

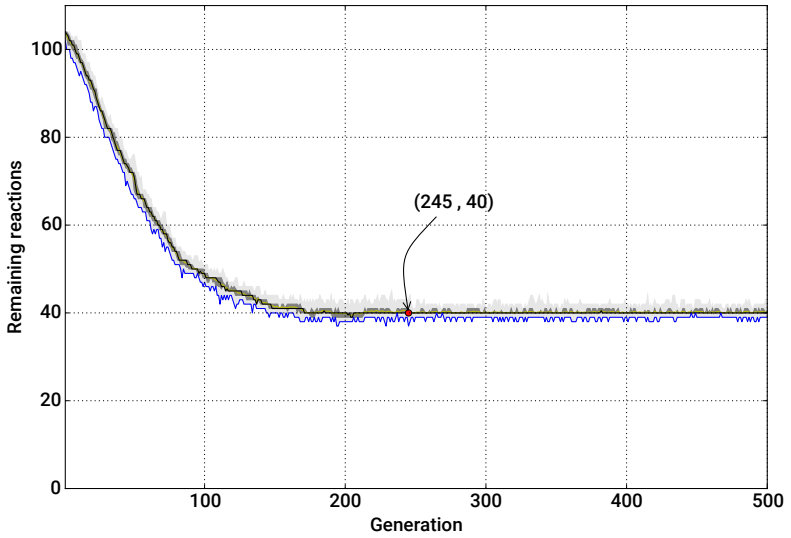

FIGURE 5.31: Overall convergence with the two-directional mutation ($p_m = 0.003$, sigmoid normalization of the runtime and the number of reactions): Evolution of the number of remaining reactions

This section considers few different forms of evaluation functions commonly used for the cost parameters (runtime and number of reactions). While the accuracy terms aim to direct the potential solution towards the correct solution calculated from the detailed mechanism, the cost evaluation terms work in "opposite direction" aiming to direct the potential solution towards the smallest possible cost value. In order to achieve a satisfactory trade-off between these two usually conflicting parts of the overall evaluation function, the cost criteria must be designed carefully to avoid outweighing the accuracy criteria. Numerous experiments were done with different shapes and weighting

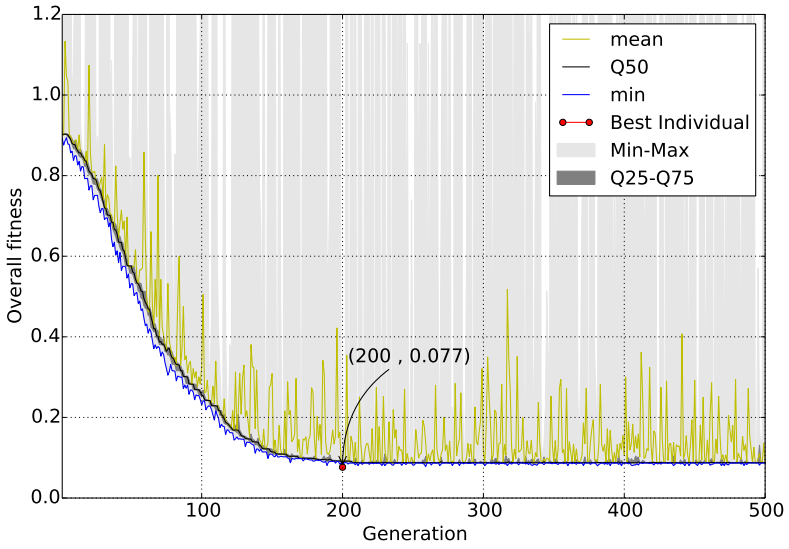

FIGURE 5.32: Overall evolution with one-way mutation ($p_m = 0.002$, sigmoid normalization of the runtime and the number of reactions): objective function evolution

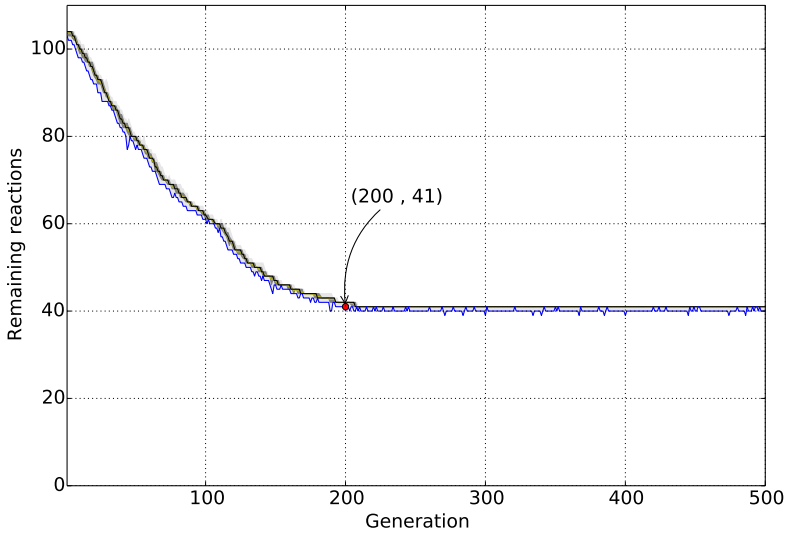

FIGURE 5.33: Overall evolution with one-way mutation ($p_m = 0.002$, sigmoid normalization of the runtime and the number of reactions): evolution of number of reactions

factors for the functions. In the following, behavior of three types of functions were presented, namely linear, square and sigmoid normalization functions shown in Fig. 5.34 is presented. To make them comparable, these functions were weighted to correspond to the best-performing sigmoid function (Eq. 4.6) adopted for the cost criteria (CPU time and number of remaining reactions). The linear function for the computational time is $f(\text{CPU}) = 0.125(t_{\text{CPU, red}}/t_{\text{CPU, ref}})$ whereas the number of reactions are normalized linearly as $f(N_\text{r}) = 0.667(N_\text{r}/N_\text{R})$. Square normalizations are, for the computational time $f(\text{CPU}) = 0.03125(t_{\text{CPU, red}}/t_{\text{CPU, ref}})^2$ and for the number of reactions $f(N_\text{r}) = 0.889(N_\text{r}/N_\text{R})^2$.

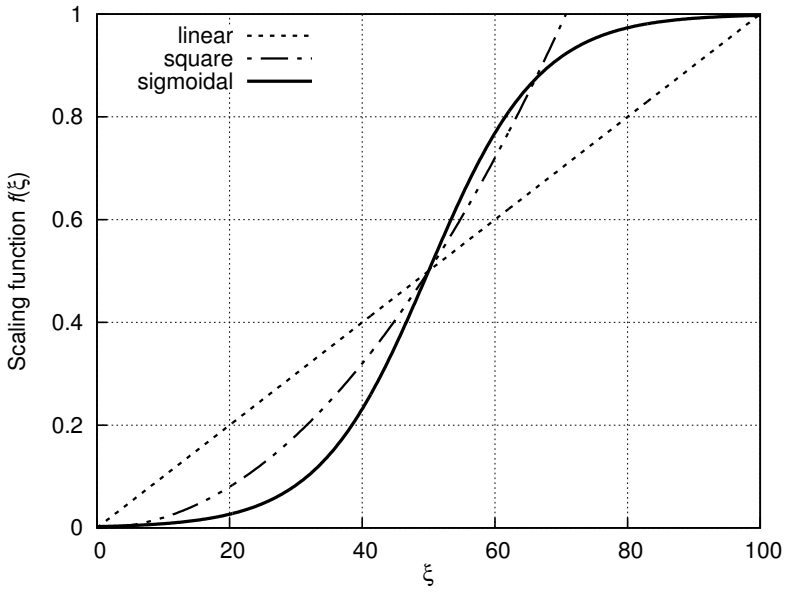

FIGURE 5.34: Linear, sigmoid and square normalization function $f(\xi)$ where ξ stands for the cost parameter

All the runs have the same accuracy terms, namely the ignition delay time, the steady-state temperature and the iron oxide mole fractions all logarithmically normalized (Eq. 4.5). A homogeneous constant-pressure reactor model is used for the evaluation. The full-mechanism initialization, one-directional mutation with the mutation rate 0.002, the single-point crossover with a probability of 0.4, the tournament selection and a population size of 48 were applied for the genetic algorithm-based reduction within 500 generations. The effects of linear, square, and sigmoid normalization on the overall fitness and the size of the resulting reduced mechanism are shown in Figs. 5.35, 5.36, 5.37, 5.38, 5.32 and 5.33.

In comparison to the linear normalization (Figs. 5.35 and 5.36), the square normalization functions give better algorithm convergence behavior as shown in Figs. 5.37, and 5.38. The algorithm did not manage to reach the stagnation within 500 generations using linear functions, whereas the square and the sigmoid functions (Figs. 5.32 and 5.33) did. Not only was the convergence influenced by the choice of the normalization functions, but the accuracy as well, as the algorithm managed to find the best perfoming individual within the given number of generations. In these cases, and in the most other numerical tests made with different functions, the sigmoid form of the cost functions gave the best accuracy-cost balance.

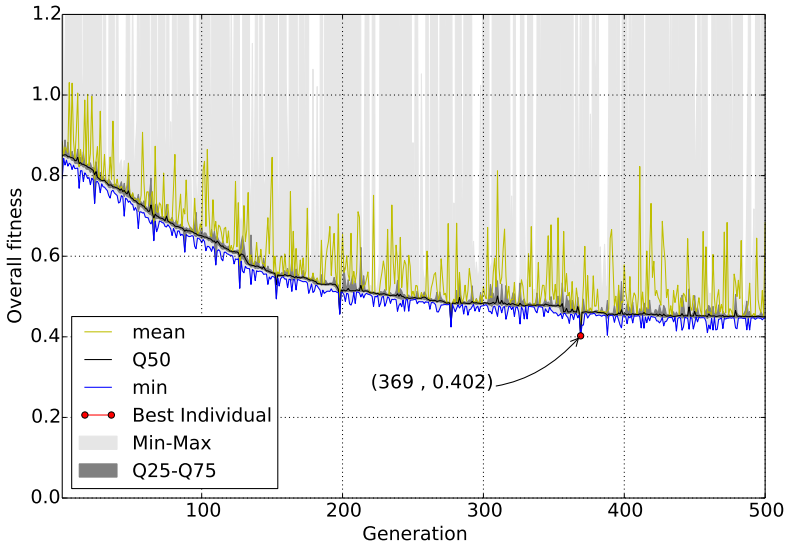

FIGURE 5.35: Overall convergence with linear scaling of the cost parameters: objective function evolution

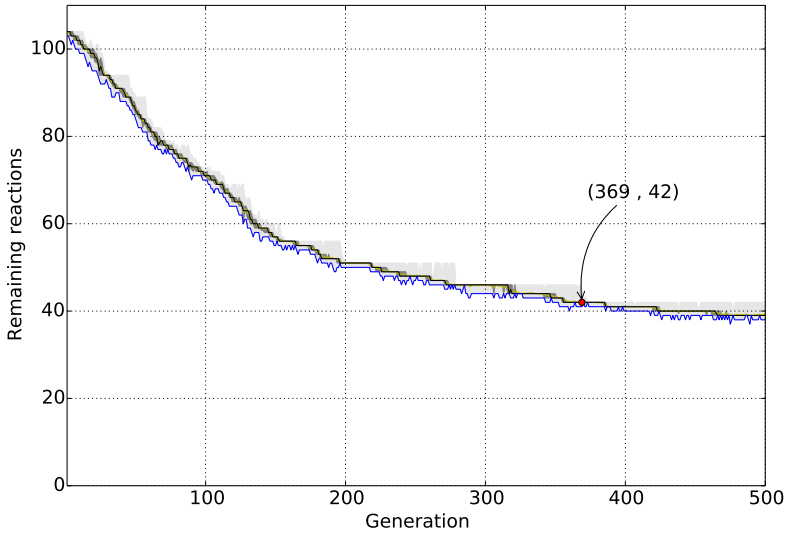

FIGURE 5.36: Overall convergence with linear scaling of the cost parameters: evolution of the number of remaining reactions

Effect of the crossover rate

For a constant population size of 48 individuals used in the analysis above, the crossover rate was varied to examine its influence on the overall convergence of the algorithm within 500 generations. Figure 5.39 shows the behavior of the minimal value of the overall error for runs with different crossover rates. The crossover rate has a small impact on the convergence of the algorithm within 500 generations, but a good compromise between the convergence speed and the minimal error value is achieved for a crossover

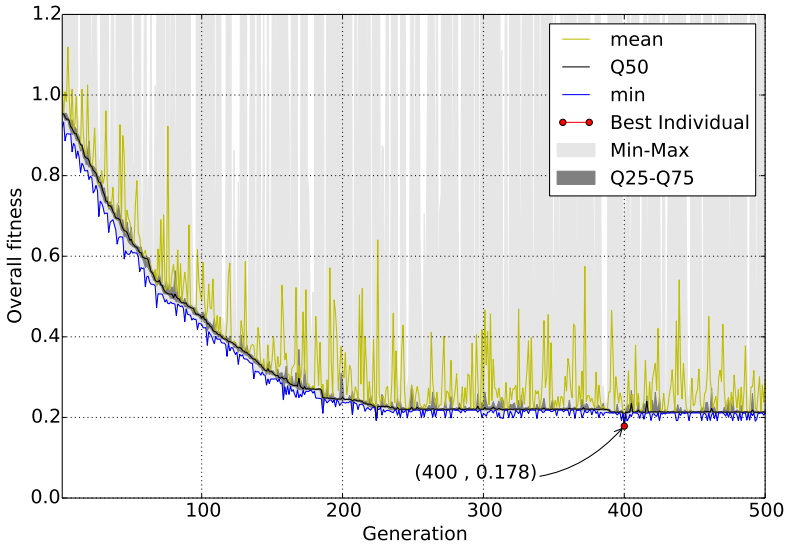

FIGURE 5.37: Overall convergence with square scaling of the cost terms: objective function evolution

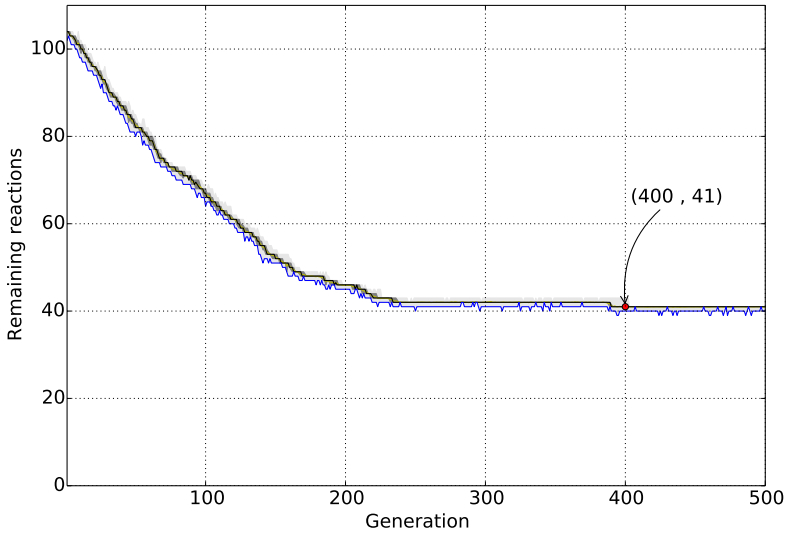

FIGURE 5.38: Overall convergence with square scaling of the cost terms: evolution of number of reactions

rate of 0.4 which is consistent with the "rule of thumb" for different genetic algorithm applications. The mutation rate for all the runs was constant, $p_m = 0.001$.

Effect of the population size

The effect of population size on the rate of convergence was investigated at a constant crossover rate of 0.4 and the mutation rate $p_m = 0.001$. Figure 5.40 shows the expected behavior of faster convergence with a bigger population size, but it must be noted that the effort for the solution of a single generation increases with the size of the population,

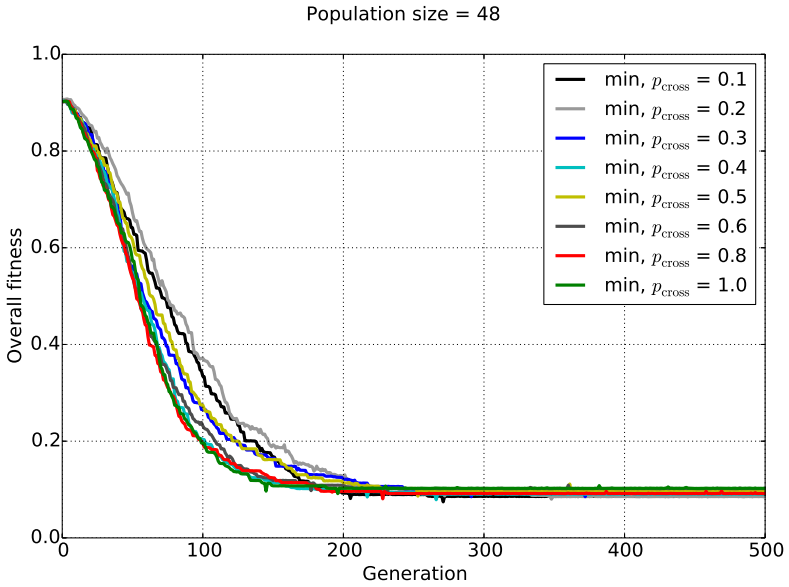

FIGURE 5.39: Minimal value of the objective function over 500 generations for runs with the constant population size of 48 individuals and variable crossover rate p_{cross}

as well as the variance of the population. This is illustrated on Figure 5.41, where the overall error distribution in terms of its minimum and the median (Q50) is shown along the entire sampling space. The number of samples is the number of the genomes in the population multiplied with the number of generations.

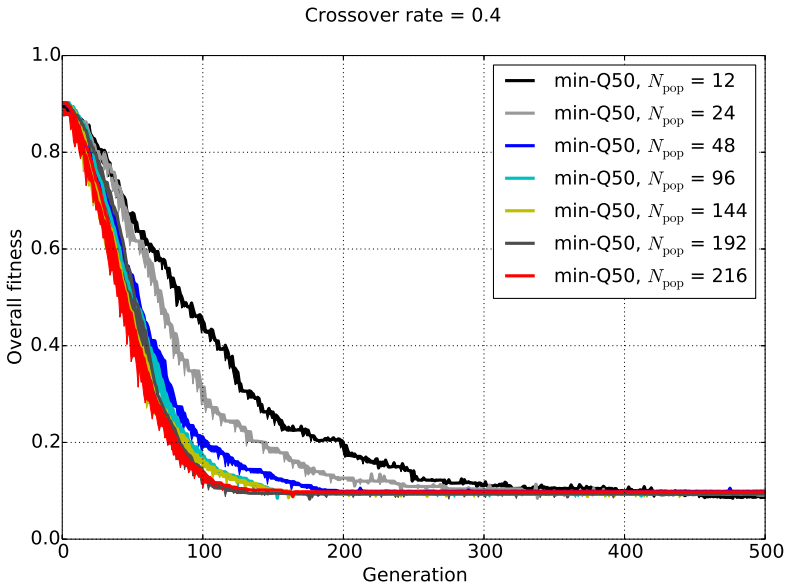

FIGURE 5.40: Distribution of the minimum and the median of the objective function value over 500 generations for runs with the constant crossover rate of 0.4 and variable population size

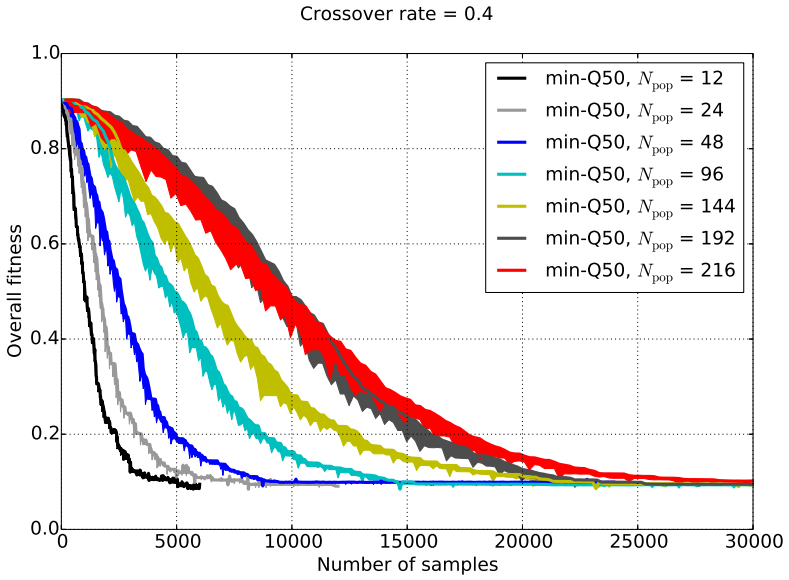

FIGURE 5.41: Distribution of the minimum and the median of the objective function value over the overall number of samples ($N_{pop} \cdot N_{generations}$) within 500 generations, constant crossover rate of 0.4 and variable population size

5.4.2 Parameter Study of the Penalty Terms - Optimization

The effect of the penalty terms onto the optimization outcome is demonstrated for the *tert*-butanol mechanism [153], which serves as an example of a chromosome with a large number of genes due to a relatively large number of reactions even after the reduction. The detailed mechanism was first reduced to 248 reactions and 198 species and then optimized with differently defined penalty terms. The objective function for the reduction included the ignition delay time, final temperature, the number of reactions and the computational cost (CPU time). For the objective function, stoichiometric *tert*-butanol/air combustion was simulated for a constant pressure (atmospheric) homogeneous reactor with an initial temperature of 1200 K. Operating conditions of the reactor simulation were the same for both the reduction and the optimization. The optimization criteria were the ignition delay time, the temperature (maximal value and the temporal variation), and the mole fractions of the important radicals (H, OH, and CH_3). The reference was the original mechanism [153]. Table 5.11 lists the considered properties and their normalization functions used as the accuracy terms within the objective function used for the optimization.

To provide an insight into the influence of differently defined penalty terms onto the overall results, ten optimization runs all with the same operating conditions and the accuracy criteria but different penalty terms are performed. Values of the single penalty function terms for the optimization runs 1-10 are listed in Table 5.12.

Property	w_i	Normalization	σ
τ_i	1.0	4.5	4
$t(T_{\max})$	1.0	4.5	4
$T_{\max}$	1.0	4.5	4
T_{profile}	1.0	4.9	25
$X_{\text{H,max}}$	1.0	4.5	4
$X_{\text{OH,profile}}$	1.0	4.9	25
$X_{\text{CH3,profile}}$	1.0	4.9	25

TABLE 5.11: Accuracy terms of the objective function for the optimization of the reduced *tert*-butanol mechanism

Run	$\alpha_{i,\text{ref}}$	w_i	σ
1	–	–	–
2	1.0	1.0	4
3	1.0	1.0	20
4	0.0	1.0	20
5	0.0	1.0	50
6	0.0	4.0	25
7	0.0	6.0	25
8	0.0; 1.0	0.5; 0.5	20; 4
9	0.0; 1.0	0.5; 0.5	20; 20
10	0.0; 1.0	6.0; 1.0	20; 4

TABLE 5.12: Parameters of the Penalty Function for *tert*-Butanol Mechanism Optimization Runs. Preferred values of the rate constant are $\alpha_{i,\text{ref}}$, weighting of penalty terms is w_i and σ is the sharpness of the penalty term normalization (Eq. 4.7)

The runs in Table 5.12 are listed in the first place according to the choice of preferred reaction rate values (α_{ref}) within their penalty terms:

- the run without the penalty function (run 1),
- the runs with penalties aiming to preserve the nominal α values (runs 2 and 3),
- the runs aiming to eliminate reactions (runs 4-7),
- and the runs combining the conflicting penalty terms (runs 8-10).

Weighting factors and the corresponding sharpness of the penalty function terms vary from small to large values and only one run per optimization setup is performed to indicate the influence that the weights and the sharpness values have on the penalty terms.

The conflicting penalty terms (runs 8, 9, and 10) were set to test their influence on the accuracy, and to gain a better understanding about how the penalty function affects the modification of the reaction constants. As the mechanism was reduced and optimized under the same conditions, all runs show significant improvement in terms of

accuracy (Fig. 5.43 and partially Fig. 5.42), indicating that the optimization can still enhance the mechanisms performance even if the constraints imposed on the reaction rate modifications are differently defined.

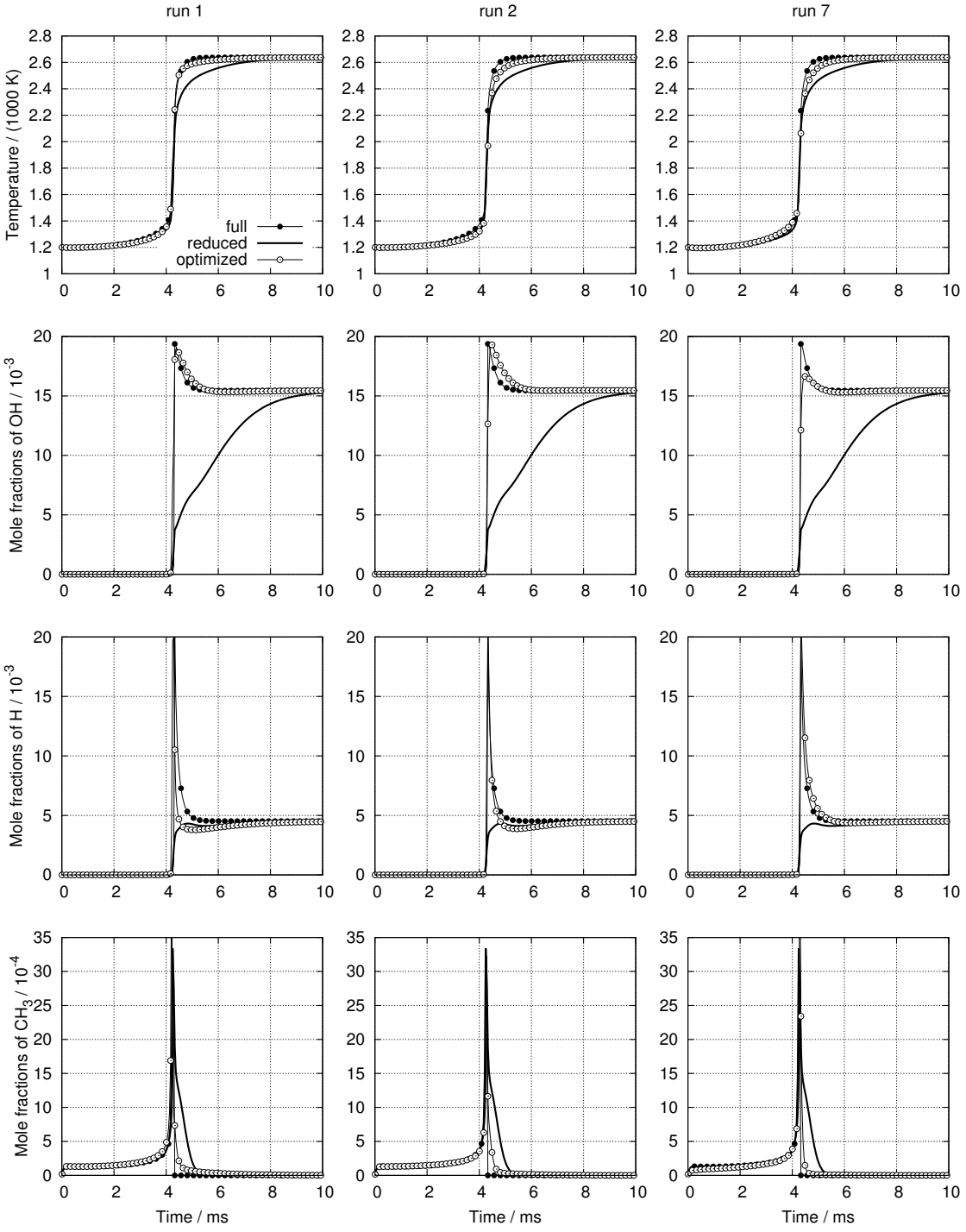

FIGURE 5.42: Auto ignition for full, reduced, and optimized *tert*-butanol mechanisms for a homogeneous constant-pressure reactor for runs 1, 2 and 7.

The standard deviation and the mean of the normalized rate coefficients for all runs are shown in Table 5.13. It can be seen from Tables 5.12 and 5.13 that the standard

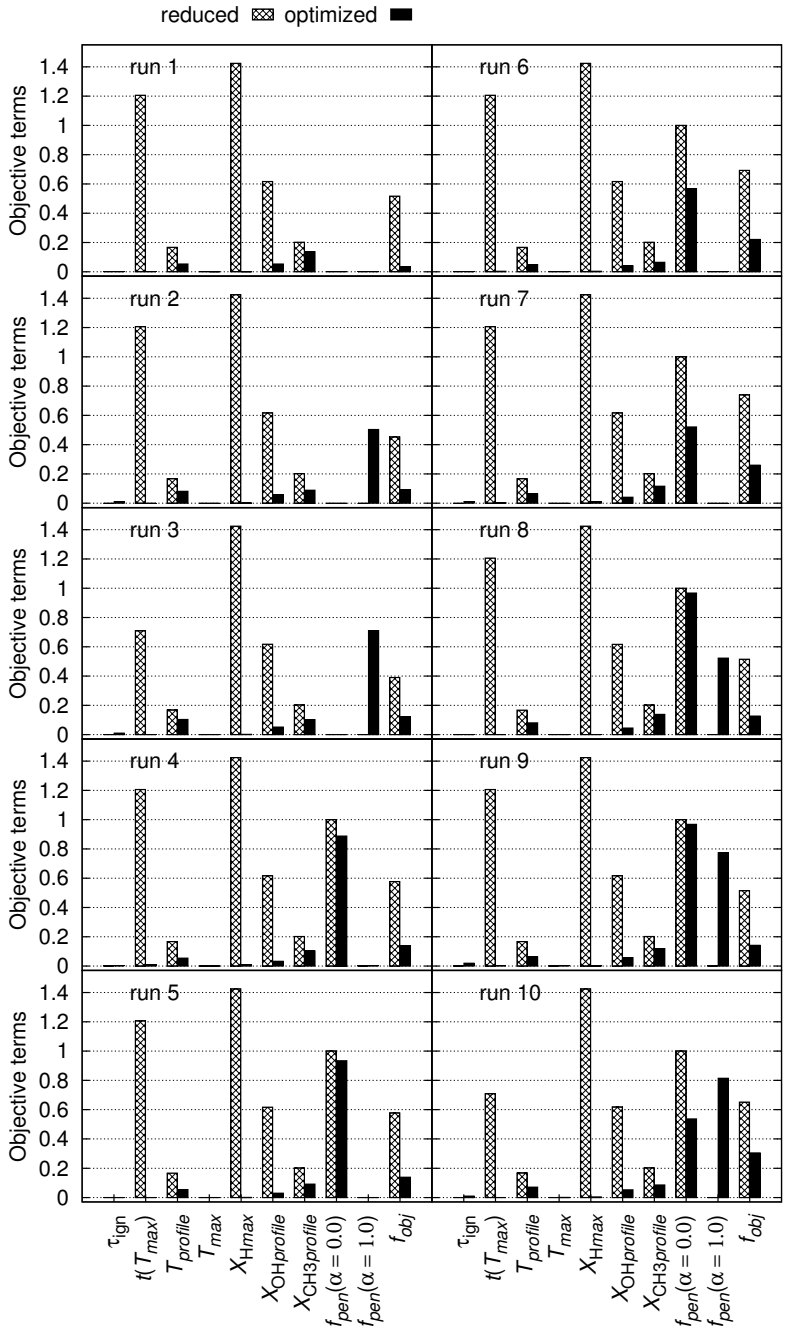

FIGURE 5.43: Values of single objective-function terms, before (reduced) and after the optimization (cf. Table 5.11)

deviation can be adjusted straight forward via the weights of the penalty terms.

To illustrate the influence of the penalty term parameters on the objective function evolution, the overall objective function, the objective-function term $f(X_{\mathrm{H,max}})$ and the penalty terms for runs 2 and 8 are shown in Figs. 5.44 and 5.46. The aim of the penalty term for run 2 was to maintain the faithfulness to the original reaction rates with a small sharpness value in Eq. 7 ($\sigma = 4$). The penalty term of run 2 starts from 0.0 and

converges relatively fast, which helps the overall objective function to converge along with the accuracy.

Run	Standard deviation	mean	N_r
1	1.092	1.063	248
2	0.817	1.022	248
3	0.897	1.095	248
4	1.278	1.049	248
5	1.323	1.065	247
6	1.548	0.813	226
7	1.836	0.977	221
8	0.757	1.010	248
9	0.728	1.018	248
10	1.324	0.693	227

TABLE 5.13: Overview of standard deviation, mean and the number of remaining reactions for ten optimization runs for the reactions of *tert*-butanol.

The evolution of the objective function terms for the case where the penalty term features two conflicting goals, aiming to either remove unnecessary reactions by driving the rate coefficients to zero and to maintain the original value of rate coefficients at the same time (cf. Table 5.12), is illustrated for run 8 in Figs. 5.45 and 5.46. The behavior of the penalty term which prefers values of 1.0 (Fig. 5.46, bottom) is similar to that from run 2 (Fig. 5.44, bottom).

The penalty term that prefers values of 0.0 is comparable to that from run 7, albeit with significantly lower weight. Therefore, the penalty term from run 2 does not significantly contribute to the overall convergence of the objective function (Fig. 5.45).

The standard deviation of the resulting normalized rate constants for all runs with $\alpha_{\text{ref}} = 0.0$ increases when the weight for the corresponding penalty term increases and their probability density (Fig. 5.47) is flattened. For the runs 2, 8, and 9, the standard deviation decreases as the weights of the penalty terms decrease and their probability density is narrower. The value of α is not biased in run 1; however its standard deviation and the mean are close to 1. The plateau region of the penalty function (Fig. 4.9 left) in runs 6, 7, and 10 is responsible for a not-constrained change of larger α values, while very small α values are steeply directed towards α_{ref}.

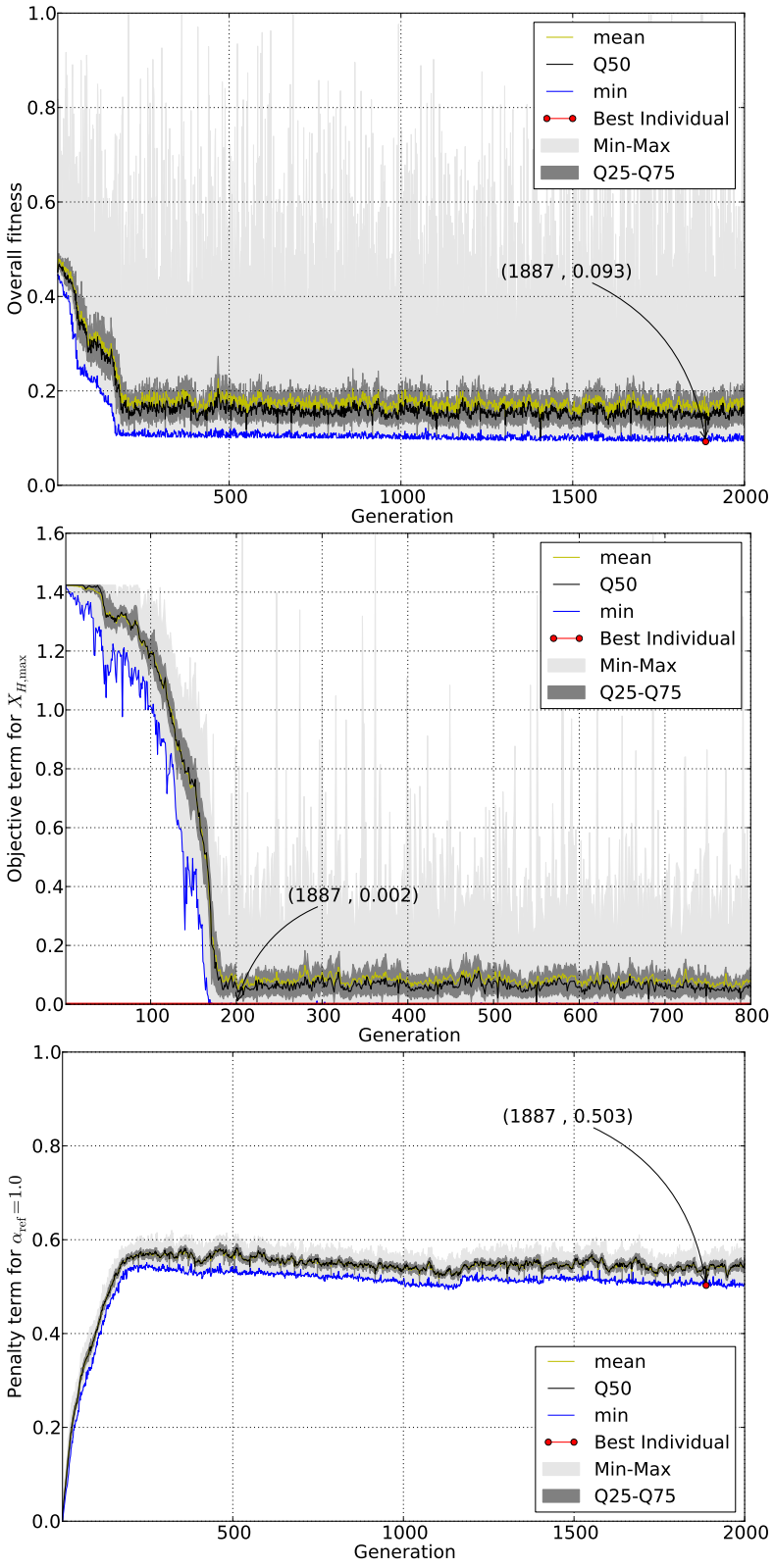

FIGURE 5.44: Evolution of the overall objective function value (top), the objective-function term $f(X_{\mathrm{H,max}})$ (center), and the penalty function term which constraints the change in rate coefficients (bottom) for run 2 (cf. Table 5.12).

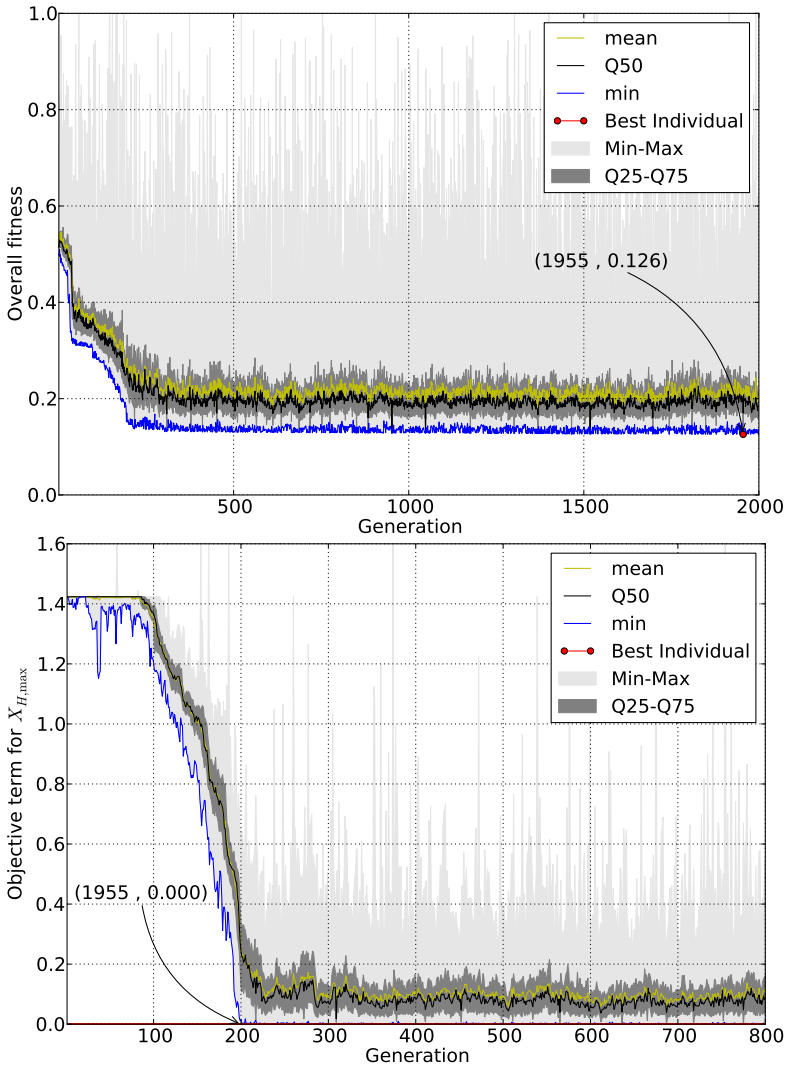

FIGURE 5.45: Evolution of the objective function value (top) and the objective-function term $f(X_{\mathrm{H,max}})$ (bottom) for run 8 (cf. Table 5.12).

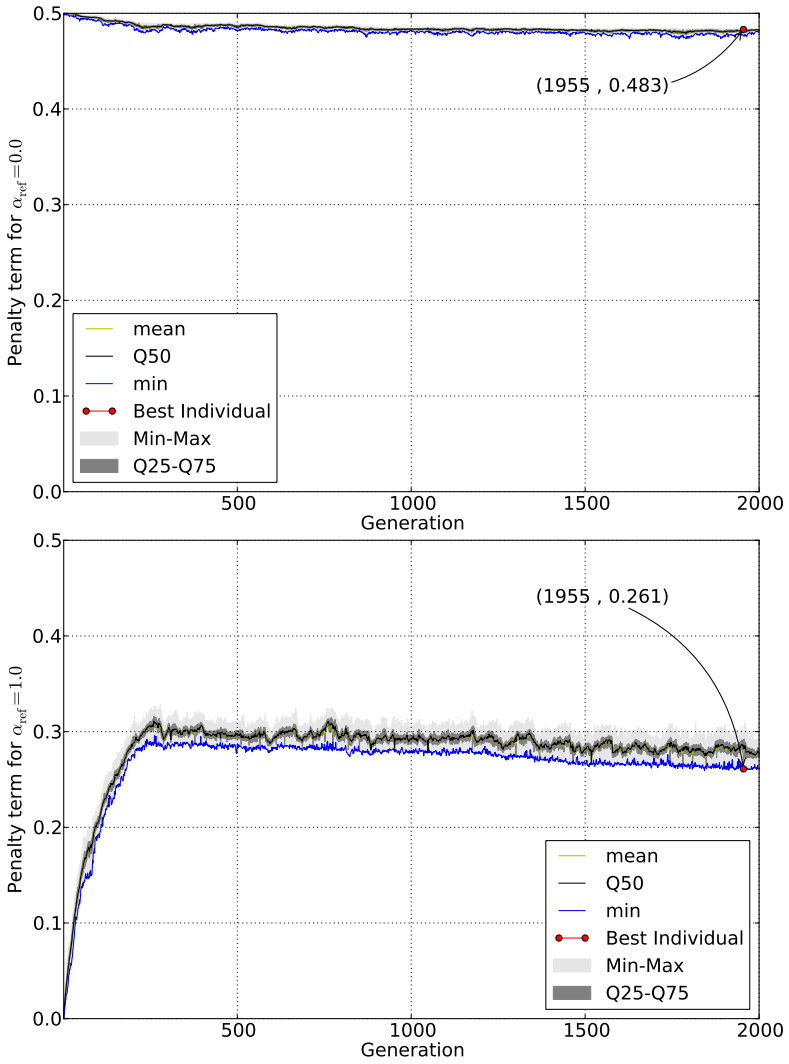

FIGURE 5.46: Evolution of the penalty-function term which drives the rate coefficients towards zero (top) to achieve a further reduction and the penalty-function term which constraints the change in rate coefficients (bottom) for run 8 to maintain near original rate constants (cf. Table 5.12).

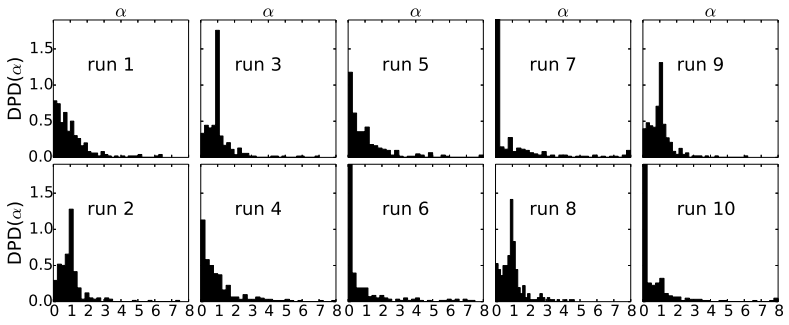

FIGURE 5.47: Discrete probability density of the normalized rate constants for the best individual from the tert-butanol mechanism optimization runs (cf. Table 5.11). The left-most bar relates to removed reactions.

The tendency towards further reduction cannot be recognized from the means of runs 6 and 7 (both means are close to 1) but the reduction trend is more visible from their corresponding discrete probability densities (Fig. 5.47). It can be also seen in Fig 5.47. that high weights in runs 6 and 7 force the values of α towards zero. Although the penalty weight for run 6 is smaller than the weight for run 7, the mean for run 7 is greater than the mean of run 6, indicating that the bias towards $\alpha = 0.0$ is not crucial for the distribution of α. For runs with higher weights towards 0.0 (runs 6, 7, 10, and, less obviously, 5) in Fig 5.47 we see that the bias towards 0.0 is somewhat compensated by an increased standard deviation.

From that, we conclude that the reduction requires significant modification of the original system if the accuracy is to be retained. The mean and the standard deviation for the runs with opposed penalty terms (8, 9, and 10) are consistent with those for runs with single penalty terms, and while their accuracy is retained, the reduction effect is not significant. Runs with small weights of the penalty terms which direct α values towards 0.0 (runs 4 and 5) were not able to reduce the mechanism further.

The highest degree of further reduction was achieved in run 7 where the penalty for the size of the mechanism had the highest weight ($w_i = 6.0$). In this case, the penalty function increased the evolution pressure towards further elimination of 27 reactions during the optimization. The optimization run took about 60 hours for 2000 generations on 48 AMD Opteron 2.6 GHz cores. The evolution of the overall objective function value for a population size of 96 is displayed in Fig. 5.48 (top) for the simulation run 7 (Table 5.12), showing a significant kink in convergence at generation 375 and overall slow convergence. The behavior of the accuracy criteria is illustrated in Fig. 5.48 (center) as evolution of the peak value of atomic hydrogen, which converged already in generation 375. At this generation, the mechanism consisted of 246 reactions. From this generation on, only the highly-weighted penalty criterion was subject to the optimization, reducing the mechanism to 221 reactions in generation 1998 (Fig. 5.48, bottom) without further improvement to accuracy. The optimization was terminated after 2000 generations.

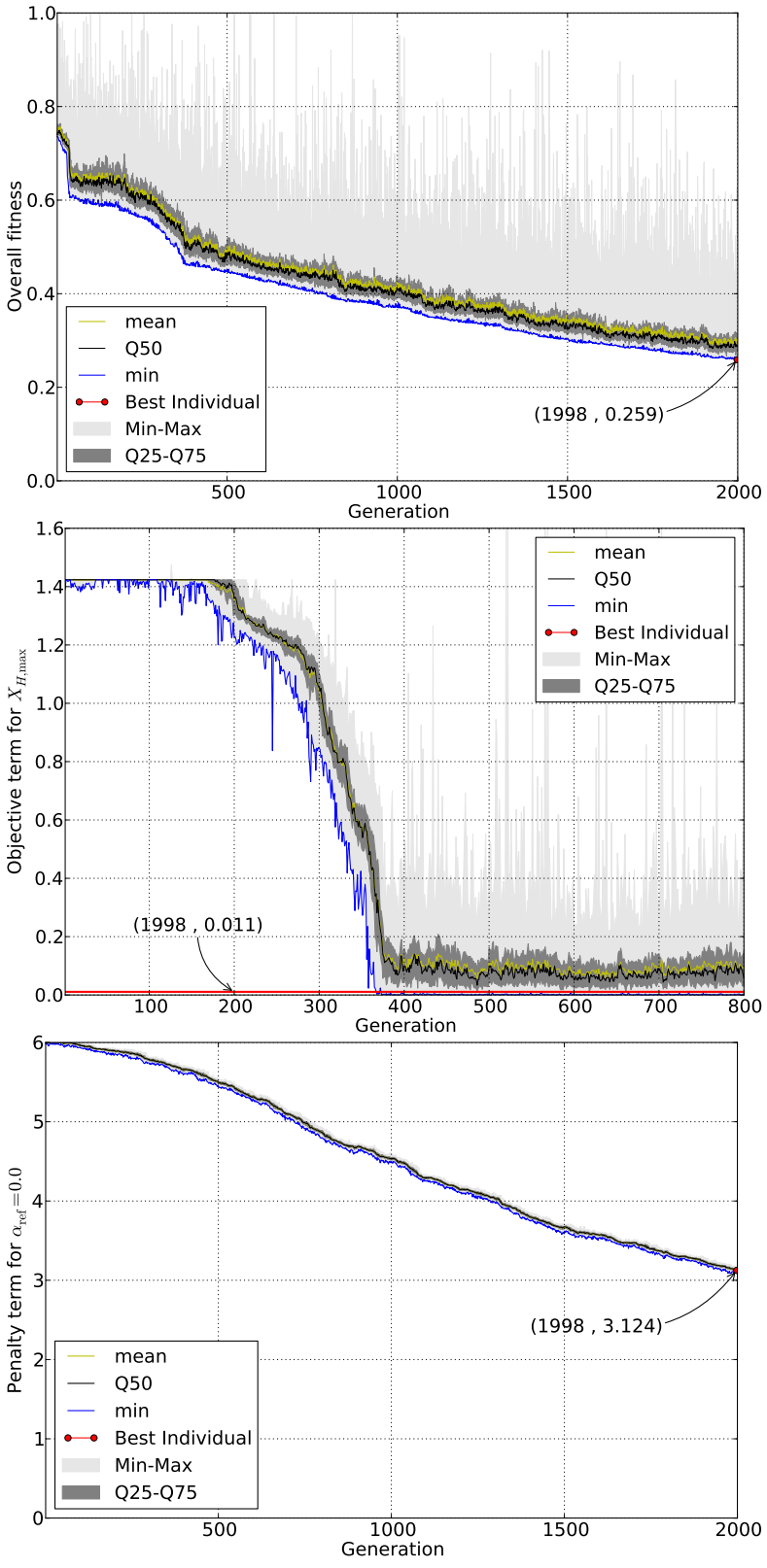

FIGURE 5.48: Evolution of: Overall objective function (top), the objective-function term $f_{\mathrm{H,max}}$ (center) and the penalty-function term (bottom) for the *tert*-butanol mechanism run 7 which lead to further elimination of 27 reactions. (cf. Table 5.12).

Figure 5.42 illustrates the performance of the full, the reduced, and the optimized tert-butanol mechanism for runs 1, 2, and 7 showing a significant improvement of the optimized mechanism over the un-modified reduced mechanism for any case. This demonstrates that both objectives, accuracy and further reduction, can be achieved at the same time.

5.4.3 Optimization Outside of the Reduction Conditions

The optimization of the reduced methane mechanism under six operating conditions different than that for which the mechanism was reduced for, with a minimum deviation from the original reaction rates, is demonstrated in this section. The following material has been published in International Journal of Chemical Kinetics [162] and reused with permission.

The mechanism used in this study is the GRI-Mech 3.0, which is an optimized detailed reaction mechanism developed for a description of methane and natural gas combustion, including NO formation [163]. Prior to the optimization, the GRI-Mech 3.0 had been reduced to 52 reactions and 26 species by removing 273 reactions and 27 species for a homogeneous combustion at atmospheric pressure, stoichiometric methane/air mixture and an initial temperature of 1400 K. The reduction criteria were the ignition delay time, final temperature, number of reactions, and the computational time required for the solution of a homogeneous reactor problem [161]. The computational time and the number of reactions were taken as the reduction criteria to avoid possible stiffness and numerical instabilities that may occur due to eliminating reactions.

The result is a reduced mechanism that is small in size and fast in computation for an intended application. The reduction had successfully preserved the ignition delay times and the final temperature predictions, but the predictions of intermediate species concentrations were disturbed. Following results show significant improvements of the intermediate species predictions by optimizing the rate coefficients of the remaining reactions in the reduced mechanism under various operating conditions (cf. Table 5.14).

The objective function incorporates the ignition delay time, the temperature profile, the maximum value of OH mole fraction, the hydrogen-atom mole fraction profile and its maximum value (Table 5.15). Atomic hydrogen was chosen for its strong impact on laminar flame speed [23]. A penalty function was set up to constrain the change in rate coefficients. The optimization was performed using the same accuracy criteria for each condition.

c	ϕ	T_i/K	p/MPa
1	1	1400	0.1
2	0.67	1400	0.1
3	2	1400	0.1
4	1	1400	1
5	0.67	1400	1
6	2	1400	1

TABLE 5.14: Operating conditions for which the reduced GRI-Mech 3.0 mechanism was optimized.

Property	w_i	Normalization	σ
τ_i	1.0	4.5	4
T_{profile}	1.0	4.9	25
$X_{\text{H,max}}$	1.0	4.5	4
$X_{\text{OH,max}}$	1.0	4.5	4
$X_{\text{H,profile}}$	1.0	4.9	25
$t(T_{\text{max}})$	1.0	4.5	4
$\alpha_{i\text{ref}} = 1.0$	1.0	4.7	5

TABLE 5.15: Objective function parameters for optimization of reduced GRI-Mech 3.0.

The overall objective-function value evolution for a population of 48 chromosomes is illustrated in Fig. 5.49, showing the convergence of the optimization where satisfactory results were achieved after approximately 100 generations (The best individual within 1000 generations appeared in generation 984). The mechanisms performance is shown in Figs. 4 and 5 for the reactor calculations under various operating conditions. For equivalence ratios ϕ of 1 and 0.67 under atmospheric (Fig. 5.50) and elevated pressure (Fig. 5.51), the profiles of temperature and OH, CO_2, and H_2O mole fractions were almost completely restored to the results from the full mechanism. For $\phi = 2$ these profiles were also improved, but not completely restored, implying that the reduction removed reactions that are important at high equivalence ratios.

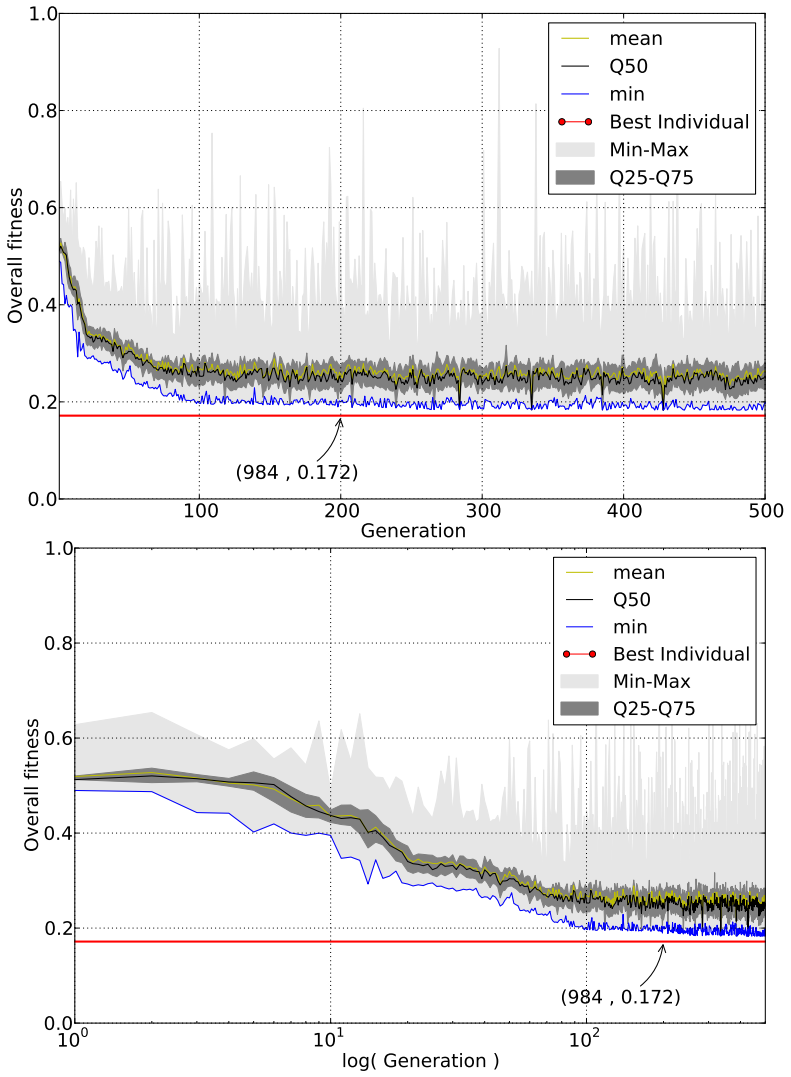

FIGURE 5.49: Evolution of the overall fitness for the reduced methane/air mechanism optimization. Red line denotes the objective function value of the best individual which was found over 1000 generations.

The performance of the reduced and the optimized GRI-Mech 3.0 is shown in Fig. 5.50 and Fig. 5.51.

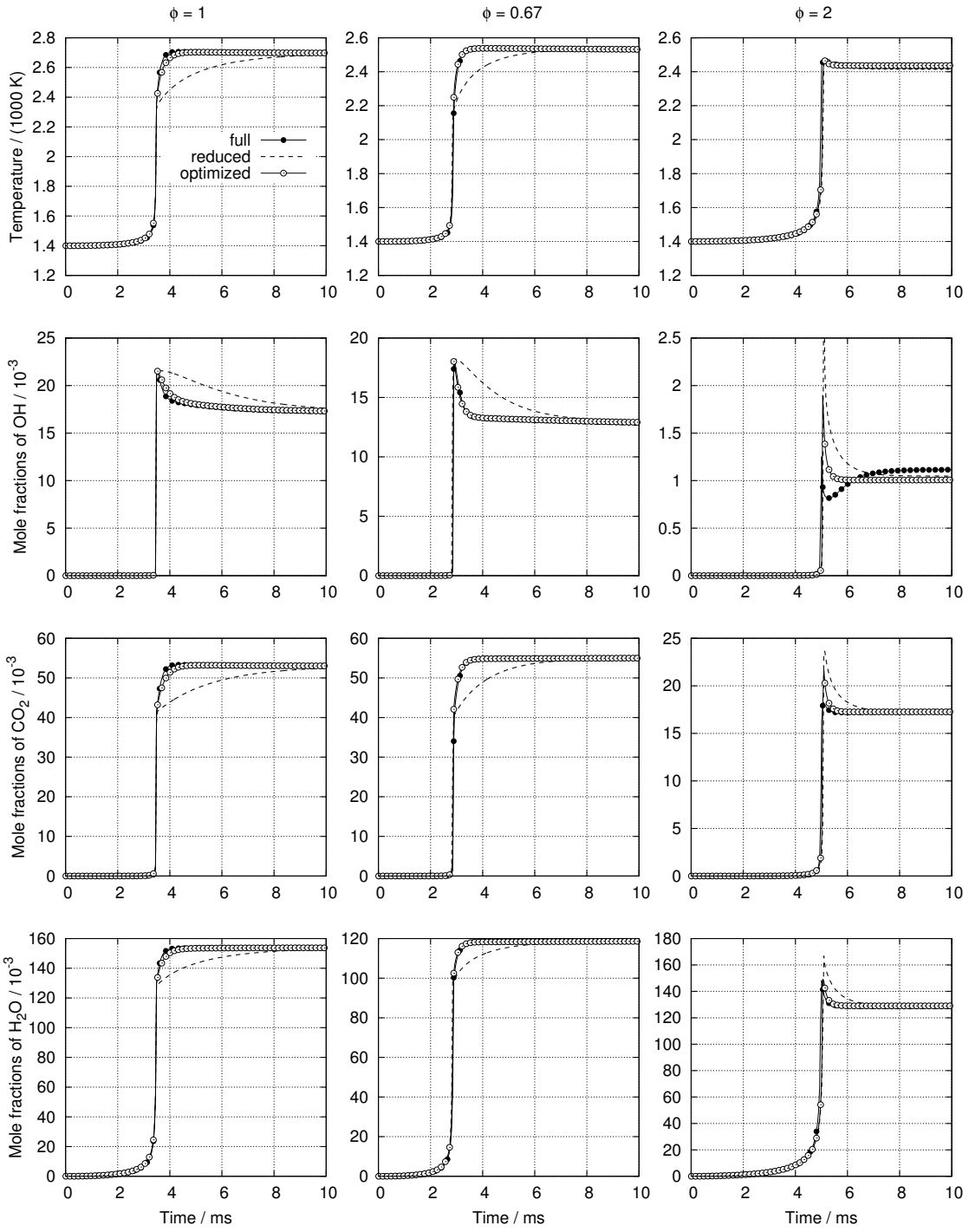

FIGURE 5.50: Auto ignition with the full, reduced, and optimized GRI-Mech 3.0 for $p = 1MPa$, $\phi = 1$(left), $\phi = 0.67$ (center), and $\phi = 2$ (right).

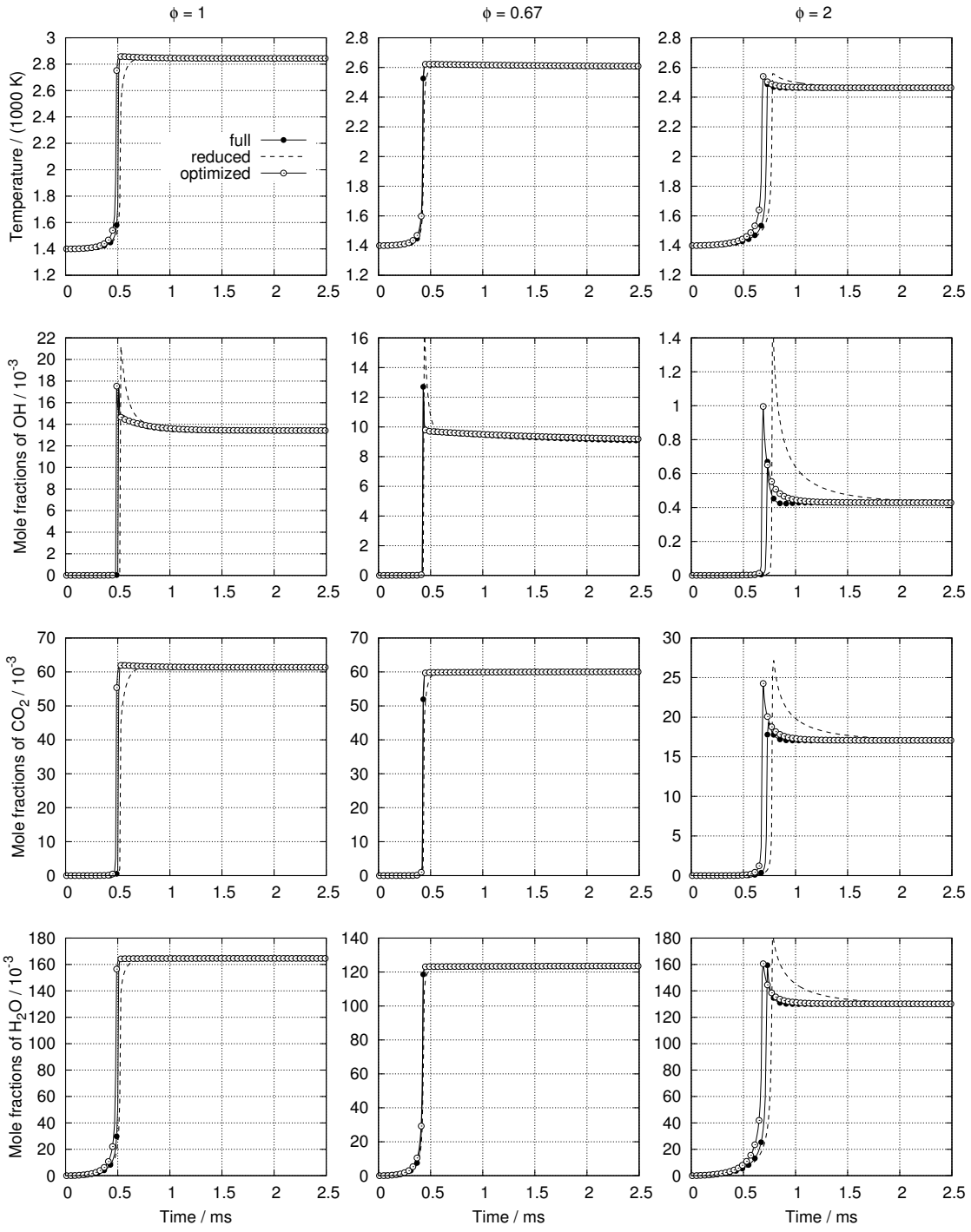

FIGURE 5.51: Auto ignition with the full, reduced, and optimized GRI-Mech 3.0 for $p = 1MPa$, $\phi = 1$(left), $\phi = 0.67$ (center), and $\phi = 2$ (right).

Figure 5.52 shows the behavior of the objective function terms for the optimized mechanism for six operating conditions. Although the objective function is minimized for all the conditions, no significant improvement is obtained for the high equivalence ratio cases 3 and 6. A mismatch between the optimized and the reference mechanism can be seen for OH profile for $\phi = 2$ (Fig. 5.50). However, the OH profile was not considered

by the objective function but only its maximum value, which is significantly improved (Fig. 5.52). Due to the fact that the objective function is a linear combination of single objective function terms, the global minimum of the overall objective function will normally deviate from the global minima of its elements.

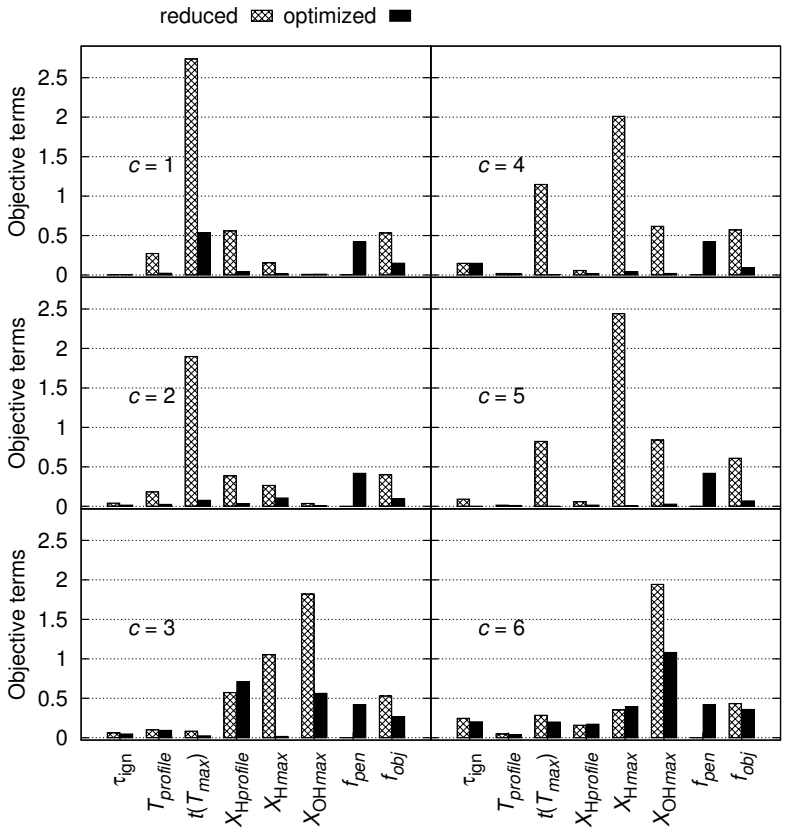

FIGURE 5.52: Values of single objective-function terms (cf. Table 5.15) for conditions given in Table 5.14.

The reduction and optimization of the reaction mechanisms have been carried out for homogeneous reactor simulations only. This may raise the question of how well such mechanisms can work for phenomena that are affected by diffusive transport. To demonstrate the optimization effects on combustion phenomena not considered by the optimization, laminar flame speeds that result from these reduced and optimized mechanisms are shown. The reduced and then optimized methane combustion mechanisms (based on GRI 3.0) were tested for a freely propagating laminar flame at two pressures (1 MPa, 0.1 MPa) and five equivalence ratios (0.5, 0.67, 1, 1.5, 2). The resulting laminar flame speeds are shown in Figure 5.53.

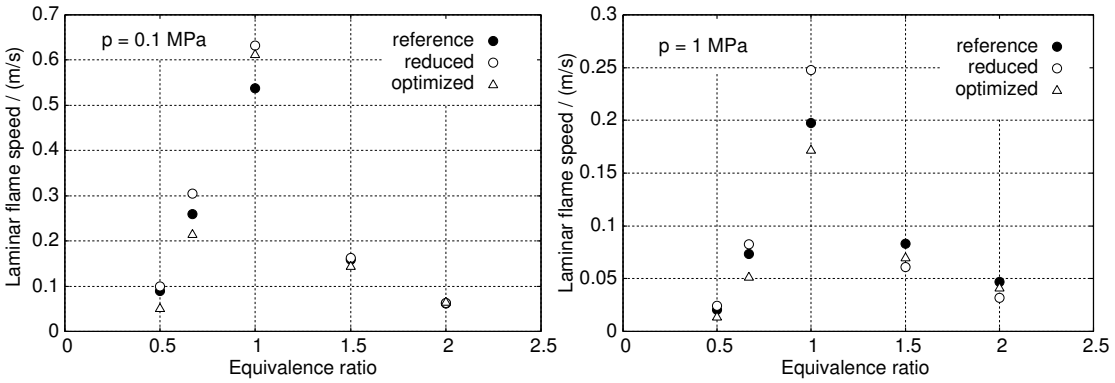

FIGURE 5.53: Laminar flame speed predictions for the full GRI 3.0 mechanism (reference) and the reduced and then optimized mechanisms as a function of equivalence ratio.

The results show that for the present cases, the mechanism reduction introduces an error of approximately 10% which is reduced to 5% for the optimized mechanisms. A further error reduction is expected when including the laminar flame speed in the objective function for reduction and optimization (demonstrated for ethylene flame).

5.4.4 Statistical Interpretation of Multiple Optimization Runs

This section compares repeated optimization runs to analyse how far different optimisation runs for the same target function can vary from each other. In particular, the following questions are addressed: a) are the results of the present GA-based search for the reduced and/or optimized mechanism reproducible, and b) can the real-coded optimization with the help of the penalty function reduce the mechanism to the same extent as the integer-coded mechanism reduction can?

To demonstrate the reproducibility of the algorithm's convergence, each mechanism manipulation run is repeated 50 times. To address the reduction efficiencies, the reduction with the size-penalty function (in further text called penalty function) within the real-coded optimization frame is compared to the integer-coded reduction. The workflow of this study is illustrated in Figure 5.54.

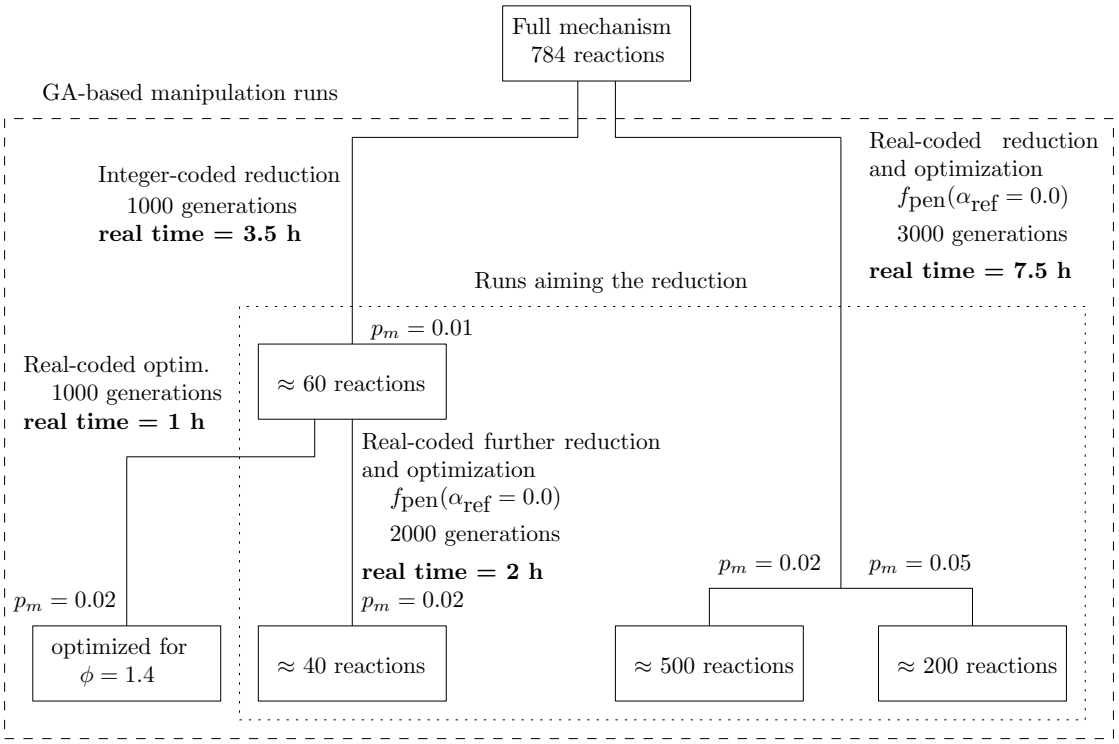

FIGURE 5.54: Schematic representation of the workflow for testing the reproducibility of the optimization results and the extent of reduction achieved with the real-coded GA in comparison to the integer-coded reduction. Each run is performed 50 times. Numbers of reactions are the average numbers of the remaining reactions in the reduced/optimized mechanisms obtained from 50 runs.

As the reference mechanism, the USC Mech Version II [190] with 784 reactions is used. The mechanism is reduced and optimized for a homogeneous constant-pressure reactor with a stoichiometric ethylene/air mixture, atmospheric pressure and initial temperature $T_{\text{in}} = 1300$ K. (The conditions were only different where the mechanism was reduced for $\phi = 1.0$ and then optimized for $\phi = 1.4$, see Fig. 5.54.)

The following GA-based manipulations are applied to this mechanism (see Fig. 5.54):

I Two-step method:

1) Integer-coded reduction (1000 generations)
2) Real-coded optimization of the reduced mechanisms from 1):
   a) with the penalty function to reduce this mechanism further (2000 generations),
   b) for a different equivalence ratio, without the penalty function (1000 generations),

II Single-step method:

Real-coded optimization of the full mechanism with the penalty function aiming to reduce the full mechanism to the same extent as the integer-coded

procedure did. These optimization runs are done with two different mutation rates ($p_m = 0.02$ and $p_m = 0.05$, see Fig. 5.54). The number of generations for these runs was 3000, which is equal to the overall number of generations needed to achieve the results of the integer-code reduction (1) and the optimization run (2a) together. (It should be pointed out, though, that the cost of a single generation varies for the different mechanisms.)

Addressing the question whether the real-coded optimization (with the penalty function) can reduce the mechanism as the integer-coded reduction can, is to highlight the efficiencies and the differences between the integer- and the real-coded approaches for elimination of the reactions. Although the integer-coded algorithm is highly efficient in eliminating redundant reactions (as it simply sets the rates to 1 and 0), the potential of the real-coded approach with the penalty function to reduce the mechanism should be investigated as an alternative reduction technique as well because using only one search algorithm may simplify the reduction/optimization workflow.

Each of these manipulations was performed 50 times to obtain a statistically relevant number of points. Each run was performed on one computer node with 48 AMD Opteron 2.6 GHz cores. The parameters of the reduction and optimization setups are given in Tables 5.16–5.18. The objective function terms and their weights for the real-coded runs with the penalty function (Table 5.17) are chosen according to the following criteria:

a) The size of the resulting reduced and optimized mechanism should be similar for both approaches. For the real-coded further reduction, the penalty function with the weight $w_i = 3.0$ was applied to a reduced mechanism containing roughly 60 reactions (Fig. 5.60). The new weighting factor w_i of the penalty function applied on the full mechanism was then estimated based on the extent of the reduction obtained by the integer-coded reduction and the penalty-function weight of the subsequent real-coded further reduction. The relation between the penalty function and the number of reactions in the mechanism is defined by Eq. 4.10:

$$\left(\frac{\sum_{i=1}^{N_r} f_{\text{pen},i}}{N_r} \right) \cdot w_i = f_{\text{pen}} \cdot w_i.$$

A new weighting factor for the penalty term should provide roughly the same reduction pressure on the full mechanism, as the factor $w_i = 3.0$ did on the reduced mechanism. Therefore, the following proportion was used:

$$\frac{3}{60} = \frac{w_i}{784},$$

which yields the weighting factor $w_i = 39.2$ for the full mechanism (rounded to 39 in the setup). This ensures that the objective functions of the real-coded reduction setups aim at the same optimum.

b) The contributions of single terms to the overall objective function, which should be the same for all three setups (50% for the accuracy and 50% for the size, see Table 5.17.

That way, the reduction setups are made comparable. The objective function for the integer-coded reduction of the full mechanism is given in Table 5.16.

Property	w_i	Normalization	σ	λ
N_r	4.0	4.5	6.0	0.75
τ_i	2.0	4.5	6.0	-
T_{profile}	2.0	4.9	25.0	-
$X_{\text{H,profile}}$	2.0	4.9	25.0	-

TABLE 5.16: Terms of the objective function for the integer-coded reduction of the full USC Mech Version II.

Tables 5.17, and 5.18 list the objective function terms of the real-coded optimization runs.

Property	w_i(reduced)	w_i(detailed)	Normalization	σ
τ_i	1.0	13.0	4.5	6.0
T_{profile}	1.0	13.0	4.9	25.0
$X_{\text{H,profile}}$	1.0	13.0	4.9	25.0
$\alpha_{i\text{ref}} = 0.0$	3.0	39.0	4.7	25.0

TABLE 5.17: Terms of the objective function for the real-coded further reduction and optimization of the reduced and the detailed USC Mech Version II.

Property	w_i	Normalization	σ
τ_i	1.0	4.5	6.0
T_{profile}	1.0	4.9	25.0
$X_{\text{H2,profile}}$	1.0	4.9	25.0
$X_{\text{CO2,profile}}$	1.0	4.7	25.0

TABLE 5.18: Terms of the objective function for the real-coded optimization of the reduced Mech Version II for a different equivalence ratio and accuracy terms.

Integer-coded Reduction

The integer-coded reduction method (Fig. 5.55) shows a small amount of statistical noise (the standard deviation of the overall fitness minima from 50 runs $\sigma = 0.002$ is small and constant compared to the mean value of 0.009), implying that the results of the integer-coded reduction algorithm are reproducible in the sense that a similar fitness is achieved - which does not necessarily mean that the reduction leads to the same remaining reactions.

Real-coded Further Reduction

The real-coded further reduction starts with the reduced mechanisms resulting from the preceeding integer-coded reduction, where the reactions were physically removed and cannot be inserted back to the mechanisms during the optimization.

The real-coded further reduction of the already reduced mechanisms exhibit the highest statistical noise with respect to the other optimization runs, namely: the integer-coded reduction (Fig. 5.56), the real-coded optimization without the penalty term (Fig.5.59) and the real-coded reduction of the full mechanism (Figs. 5.58 and 5.59), which will be discussed later. This is an interesting observation, as it shows the influence the size-penalty function has on the overall convergence behavior of the algorithm. Figure 5.56 show the scattering and the mean of the overall fitness minima from 50 randomly seeded real-coded runs with the size-penalty function. The input mechanisms result from the integer-coded reduction.

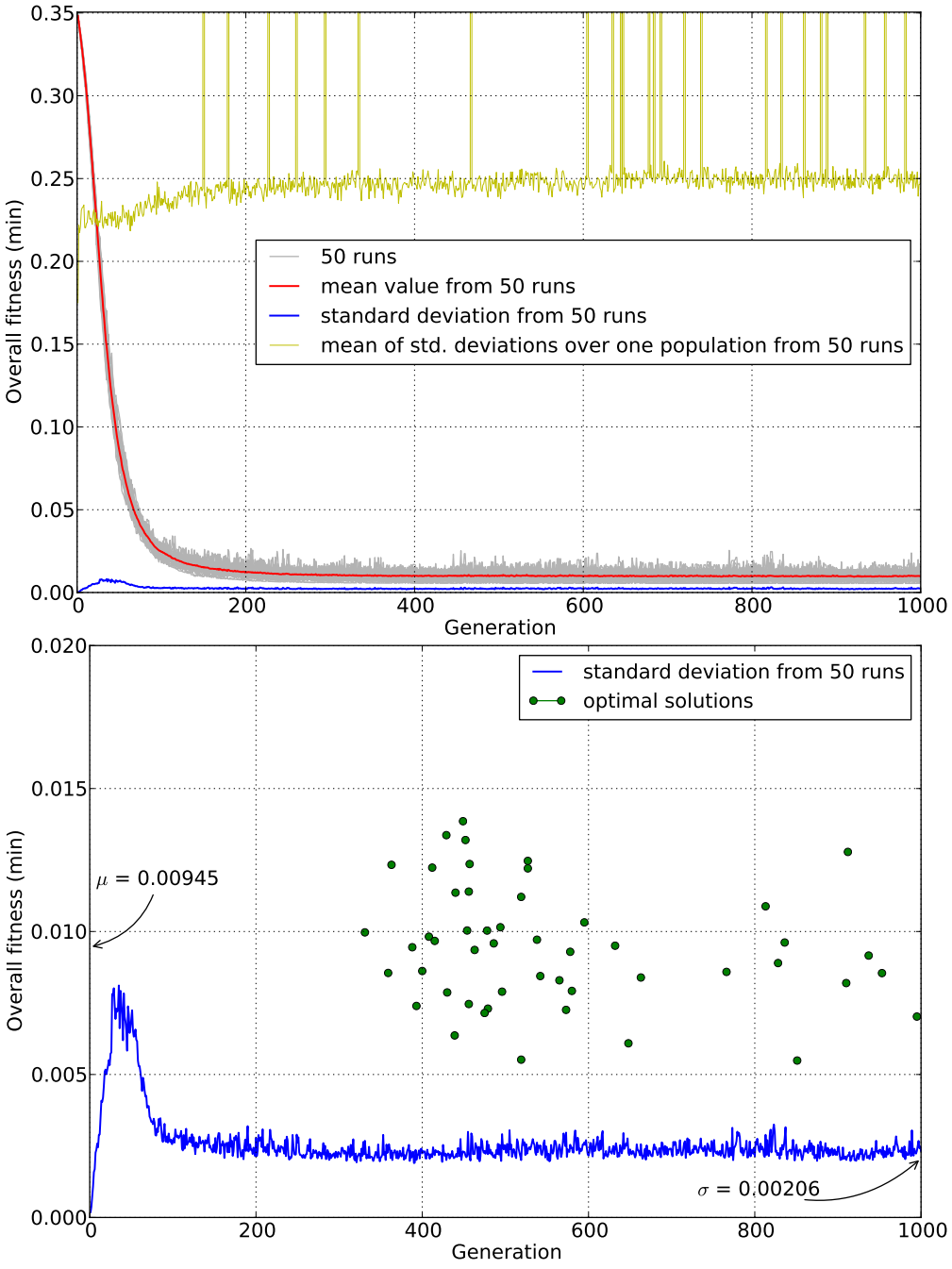

FIGURE 5.55: Top: The mean of the overall fitness minima from 50 randomly-seeded integer-coded reduction runs. Bottom: The standard deviation of the overall fitness minima from 50 runs, the optimal solutions from each run at the time when they were first found, and the mean μ and the standard deviation σ of their fitness.

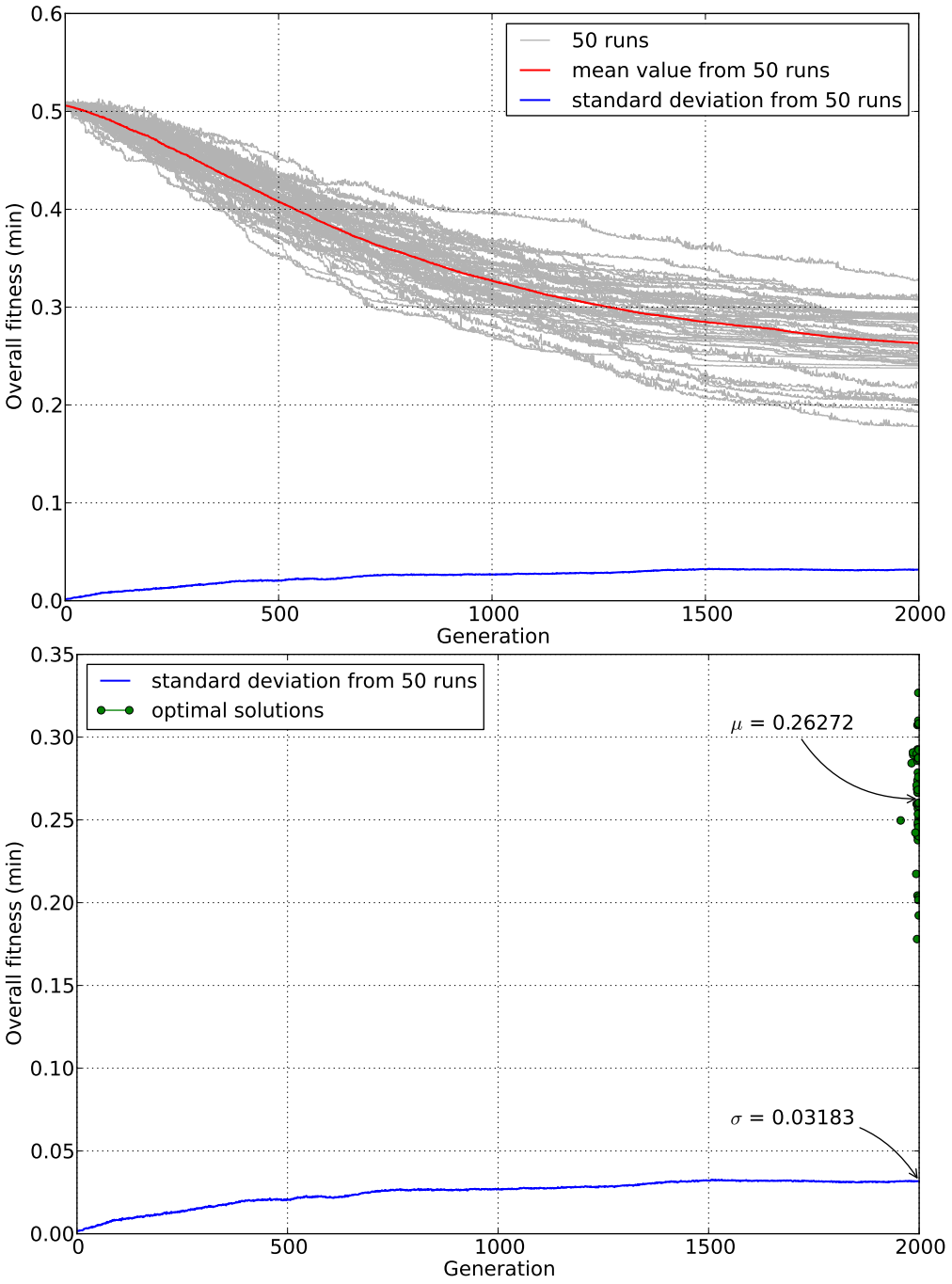

FIGURE 5.56: Top: The mean of the overall fitness minima from 50 randomly-seeded real-coded runs with the penalty function. The input mechanisms result from the integer-coded reduction. Bottom: The standard deviation of the overall fitness minima from 50 runs, the optimal solutions from each run at the time when they were first found, and the mean μ and the standard deviation σ of their fitness.

The algorithm was only able to lower the objective function to about a half of its initial value (from 0.5 to $\approx$ 0.26) within 2000 generations. However, despite this scattering, the standard deviation is an order of magnitude lower than the mean ($\sigma = 0.03$ with respect to the mean $\mu = 0.26$) and remains constant for the last 500 generations.

For this case, high statistical noise is expected for the following reasons: The penalty function adds complexity to the objective function by enabling each reaction to directly contribute to the overall fitness. This additional dimension of the objective function contributes to the statistical noise of the algorithm. It should be noted however, that the asymptotic solution has not been achieved within the given number of generations for all the cases featuring the penalty function. Furthermore, for the real-coded reduction of the already reduced mechanisms, the input mechanisms are different at the start (since they result from 50 corresponding integer-coded reduction runs) and the eliminated reactions cannot be retreived by the optimizer, which reduces the degree of freedom for optimizing such mechanisms. Therefore, we assume that some runs may never achieve the same good fitness as others - so that real convergence to the best possible fitness could not be achieved. In other words, where the reduction seems very effective in terms of the size of the resulting mechanism (from 784 to around 60 reactions), each run is likely to be stuck in a local optimum and cannot reach a global optimum even after an infinite number of iterations. Therefore, the input mechanisms may not have the same degree of freedom when altering/eliminating their remaining reaction rates. This is a real disadvantage of the two-step approach (first integer reduction, then real reduction) that needs to be considered when the two-step approach is taken. On the other hand, the standard deviation remains constant for the last 500 generations for the runs reducing already reduced mechanisms (Fig. 5.56). Because this particular case has the highest statistical noise, it will be further addressed later in this section.

Real-coded Optimization Without the Size-Penalty Term

The subsequent real-coded optimization of the reduced mechanism (without the penalty function) for different operating conditions (equivalence ratio) exhibits a similar behavior (Fig. 5.57) as the integer-coded reduction, even though the starting values of the objective functions for 50 runs were significantly different. The statistical noise for this real-coded case is quite high (the standard deviation of the overall fitness minima from 50 runs is 0.004 and the mean is 0.006). Nevertheless, the real-coded optimization of the mechanism quickly achieved a small value of the objective function for the different equivalence ratio. However, it must be provided that the reactions crucial for describing the target phenomena are not eliminated during the previous reduction.

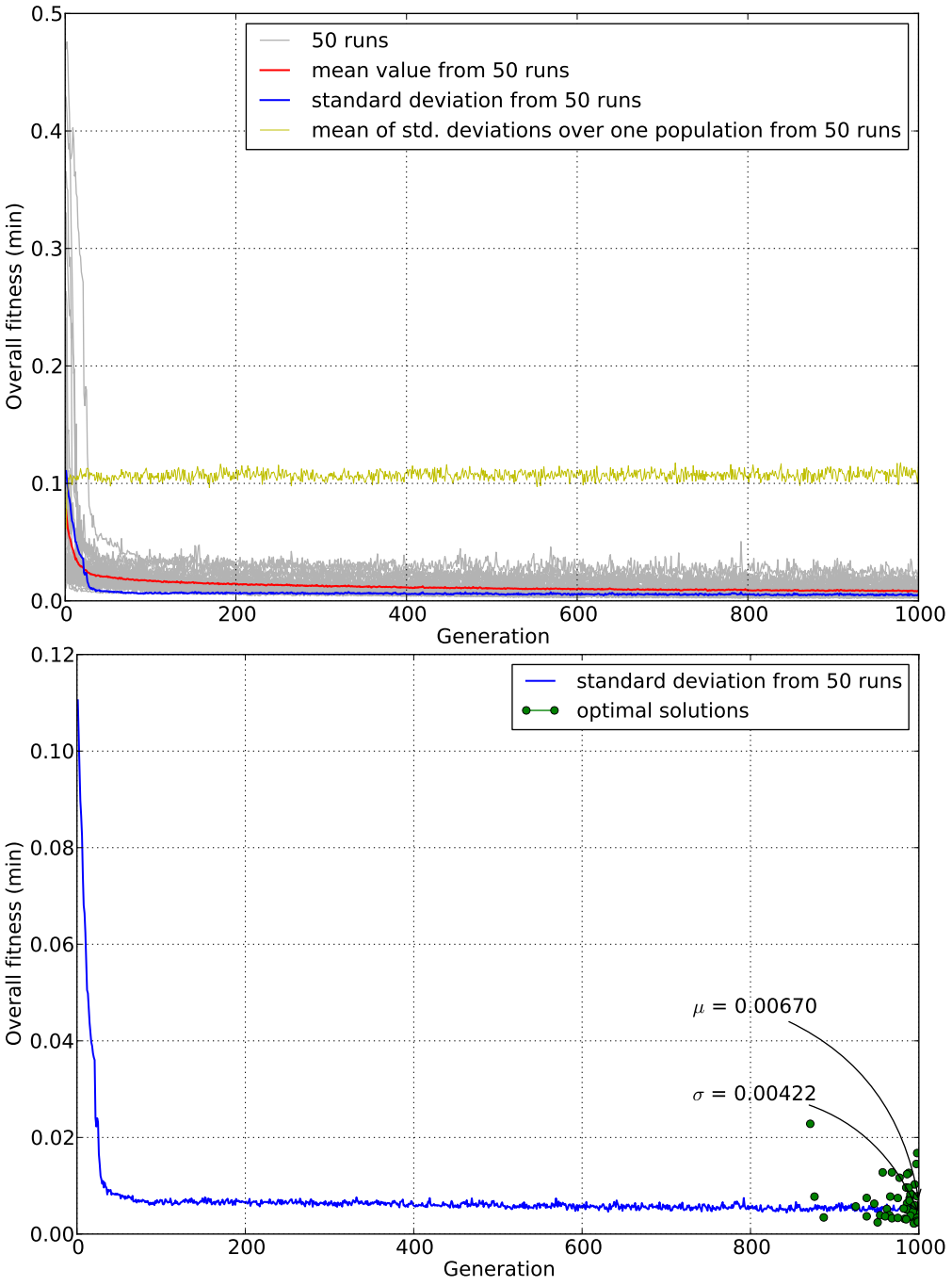

FIGURE 5.57: Top: The mean of the overall fitness minima from 50 randomly-seeded real-coded runs aiming to optimize the mechanism's accuracy for a different equivalence ratio. Bottom: The standard deviation of the overall fitness minima from 50 runs, the optimal solutions from each run at the time when they were first found, and the mean μ and the standard deviation σ of their fitness.

Real-coded Reduction of the Full Mechanism

The real-coded reduction of the full mechanism was performed twice (by using two different mutation rates). The input mechanism for the following real-coded optimization and reduction runs is the detailed mechanism and is the same for all the 50 runs. Figure 5.58 shows the overall fitness of 50 runs, its mean and the standard deviation within 3000 generations for the mutation rate $p_m = 0.02$. The statistical noise for this case is relatively small (standard deviation $\sigma = 0.013$ with respect to the mean of $\mu = 0.159$ is small and constant for the last 1000 generations). Furthermore, the overall fitness has significantly decreased from 0.5 to ≈ 0.16 even though the asymptotic solution was not reached.

The higher mutation rate, $p_m = 0.05$ instead of the previously used $p_m = 0.02$, significantly enhanced the convergence speed and decreased the statistical noise at the end of the evolution even though the complete convergence was not achieved (Fig. 5.59). This is expected because not only the mutation enables the algorithm to find a new better local minima faster but it influences the penalty function directly by finding new (smaller) gene values. However, one should be careful with the mutation rate, as a too-high mutation rate may reduce the GA to a random search and hence reduce the rate of convergence again. The overall fitness for this case was reduced from initial value of 0.5 to ≈ 0.045 within 3000 generations. The statistical noise is noticeably smaller than in the previously discussed cases ($\sigma = 0.006$ with respect to the mean $\mu = 0.045$).

Real-coded reduction runs of the full mechanisms exhibit a relatively small statistical noise, although the algorithm did not aproach an asymptotic solution within a given number of generations (Figs. 5.58 and 5.59). A relatively small statistical noise for these two cases and a better convergence of these runs towards one global minimum is due to the following reasons: The input mechanisms were the same for all the runs, and their degree of freedom in altering (removing) the reaction rates was not previously reduced.

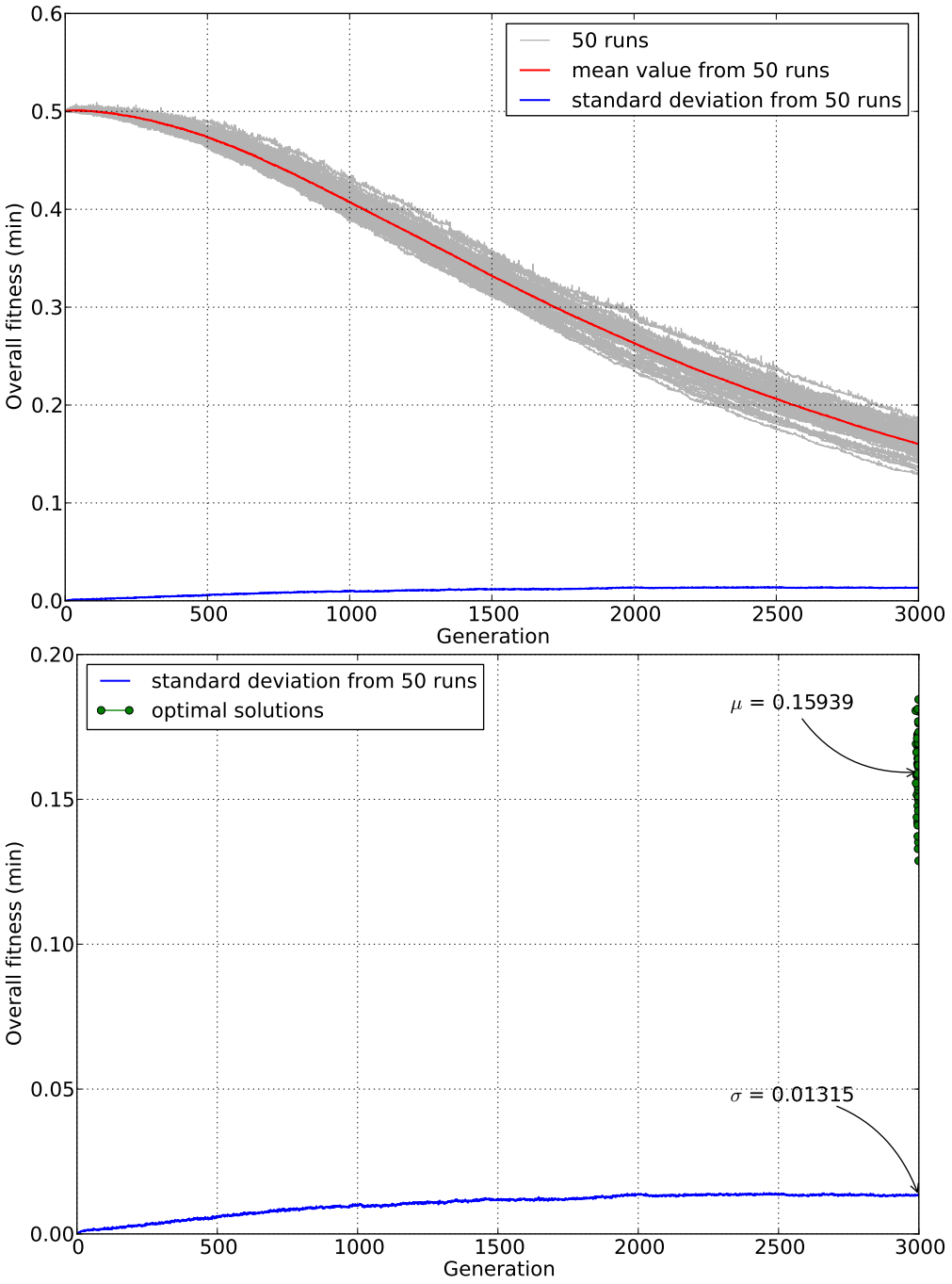

FIGURE 5.58: Top: The mean of the overall fitness minima from 50 randomly-seeded real-coded reductions of the full mechanism with the penalty function and the mutation rate $p_m = 0.02$. Bottom: The standard deviation of the overall fitness minima from 50 runs, the optimal solutions from each run at the time when they were first found, and the mean μ and the standard deviation σ of their fitness.

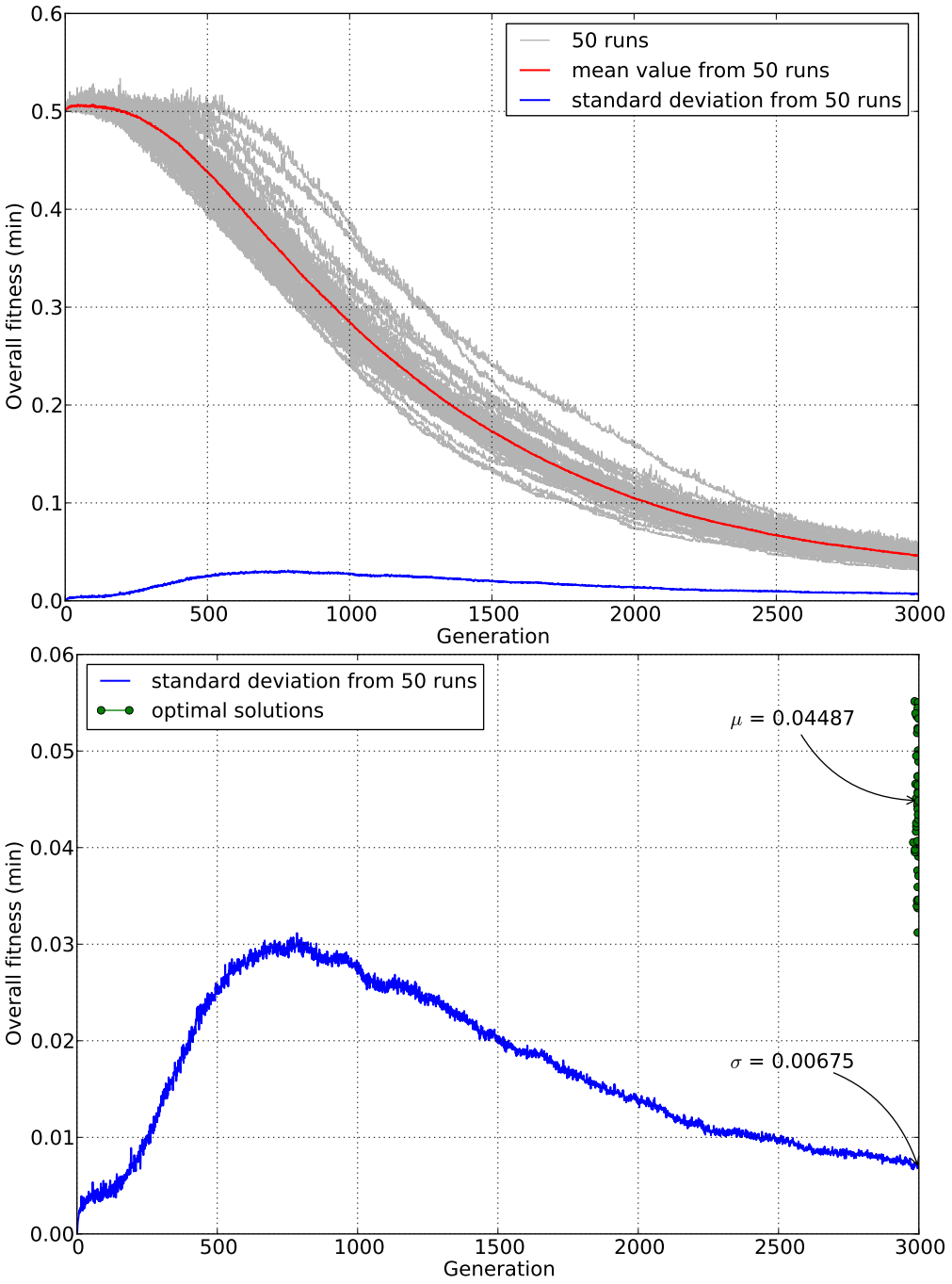

FIGURE 5.59: Top: The mean of the overall fitness minima from 50 randomly-seeded real-coded reductions of the full mechanism with the penalty function and the mutation rate $p_m = 0.05$. Bottom: The standard deviation of the overall fitness minima from 50 runs, the optimal solutions from each run at the time when they were first found, and the mean μ and the standard deviation σ of their fitness.

Overall, the real-coded reduction of the full mechanism has generally converged much faster towards a good fitness, reached a much better fitness value (≈ 0.044 for $p_m = 0.05$) after 3000 generations, and still converges further. Therefore, this algorithm can be expected to find the global optimum (best fitness) after an infinite number of generations.

Such behavior is (near) impossible for the combined integer- and real-coded approach, that is likely to get stuck in local optima. (It should however be pointed out that the two step approach may be easier to use where reduced mechanisms of a specific size are sought.) The efficiency of the real-coded algorithms in reducing the mechanisms is further addressed in the following.

Extent of the Reduction

The integer-coded reduction results in a high extent of the reduction of the mechanisms within a relatively short time (Fig. 5.60), which makes the integer-coded reduction efficient in obtaining very small mechanisms quickly.

Since the objective function is a linear combination of the conflicting criteria (number of reactions and the accuracy), a few Pareto-efficient solutions can be identified (Fig. 5.61) as those solutions that cannot get smaller in size without decreasing their accuracy (for the same value of the overall fitness). Identifying the Pareto-efficient front may provide an information whether the mechanism has multiple equally good reduced versions (lying on the front under which no further reduction is possible without destroying the chemical meaning of the mechanism) or the mechanism has one unique reduced version (a global optimum).

Figure 5.62 shows, for each of the reactions from the full mechanism, in how many reduced mechanisms the reaction occurs. This gives an idea about the most dominant reactions that cannot be removed (as they occur in all the mechanisms, regardless the differences between the reduced mechanisms). Analogously, there is a large number of reactions that can be safely removed as they do not occur in any of the reduced mechanisms (for the conditions and the criteria the mechanisms were reduced for).

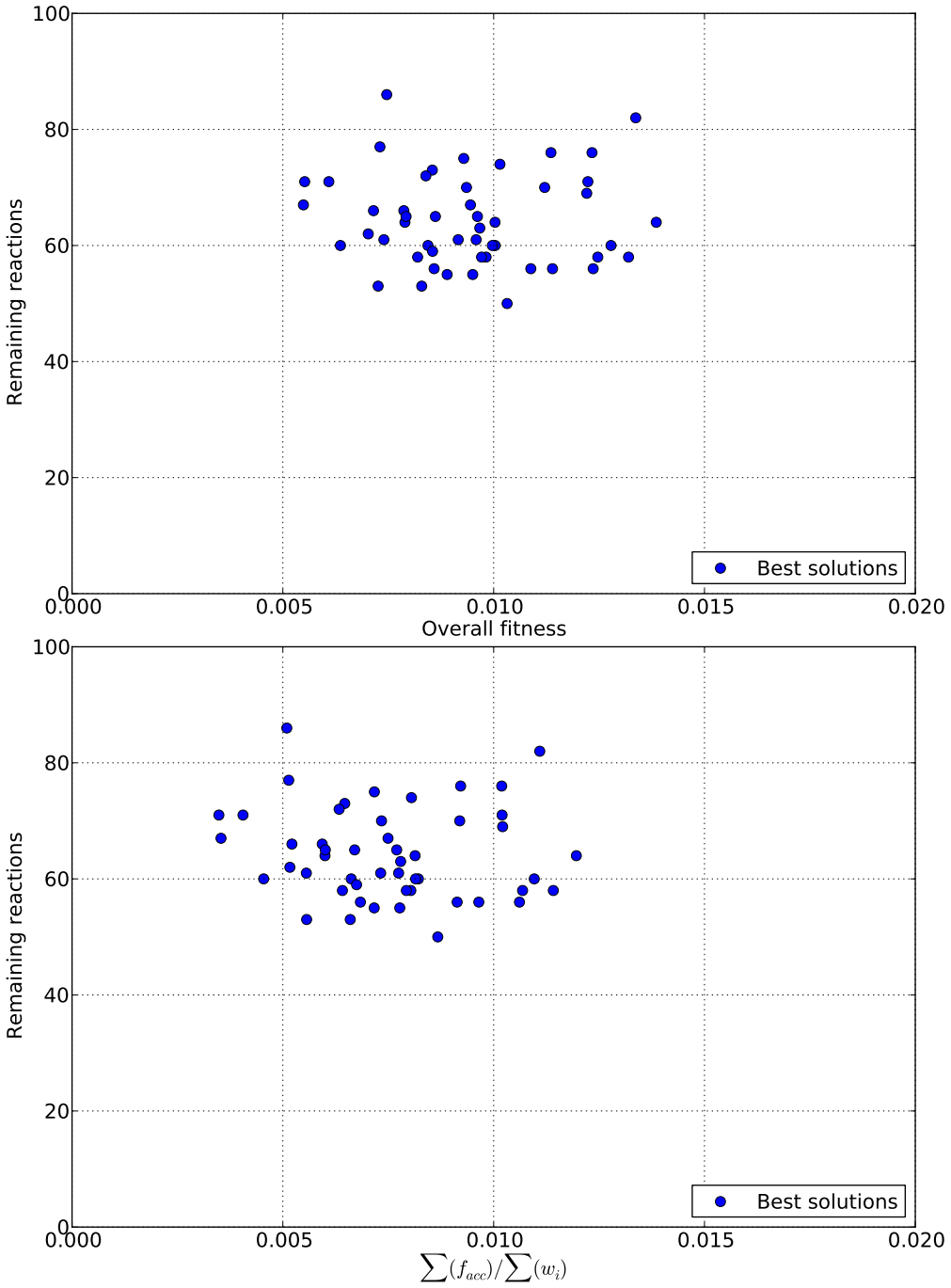

FIGURE 5.60: Top: Number of remaining reactions with respect to the overall fitness of the integer-coded reduction runs. Bottom: Number of remaining reactions with respect to the accuracy of the resulting reduced mechanisms.

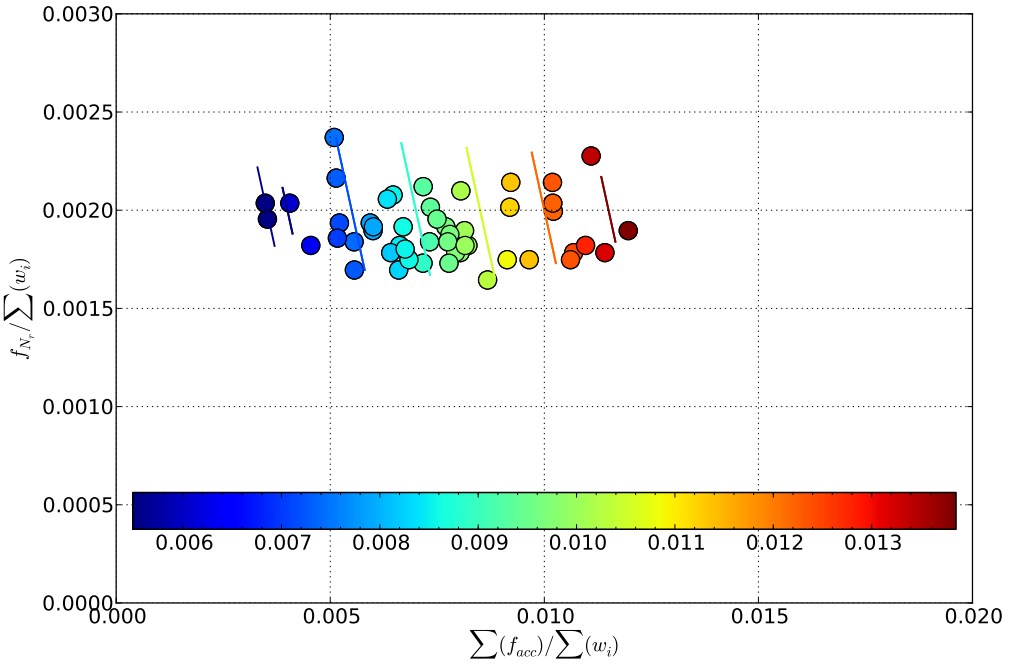

FIGURE 5.61: Size criteria with respect to the accuracy criteria of the integer-coded reduction runs. Colormap is the overall fitness of the solutions. Isolines indicate the expected Pareto front.

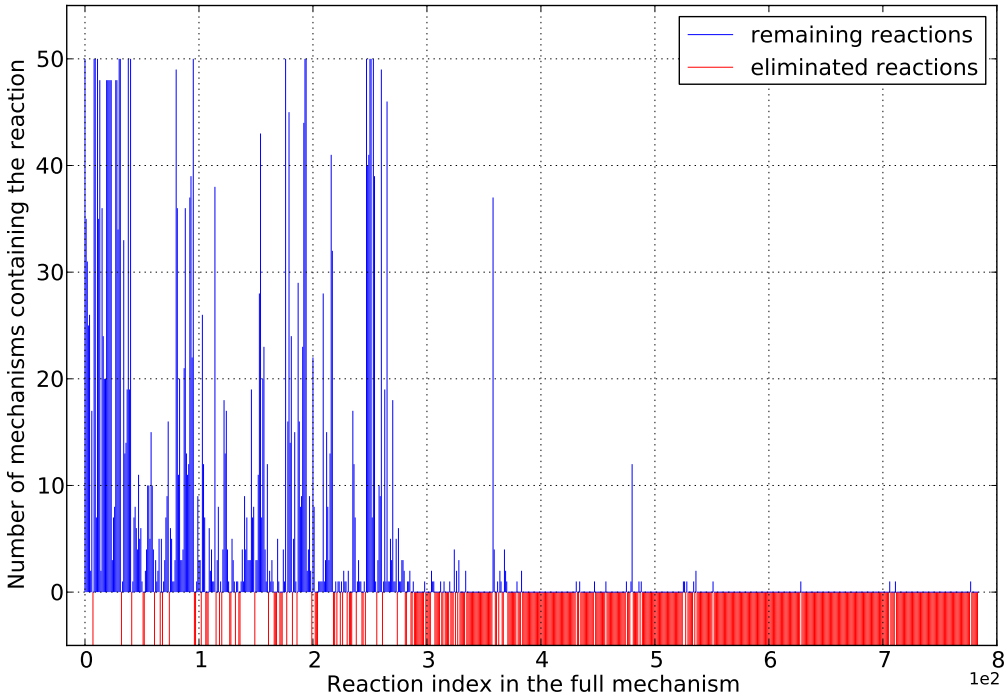

FIGURE 5.62: Frequency of occurrence for each reaction of the full mechanism in the reduced mechanisms (from 50 integer-coded reductions).

The influence of the penalty function on the size of the resulting mechanisms is shown in Figs. 5.63 and 5.64. The number of the remaining reactions for the cases reduced with the penalty function was determined after removing the reactions that have the rates smaller than a given value ϵ. This value is introduced because the convergence of the penalty function is very slow (in these cases, the convergence was not achieved, but a higher fitness level was achieved already) and many reaction rates are driven to values that are very small but they have not reached zero yet.

Although this approach has shown to be useful for cutting-off the very small rates that did not fully converge to zero, one must be aware that there may be reactions that can destroy the mechanism's performance if removed. These reactions may be as small as their unimportant counterparts, but their removal may decrease the accuracy or even the numerical stability of the mechanism. To demonstrate such a behavior, the mechanisms' accuracy is evaluated for several different values of ϵ (Figs. 5.63 and 5.64) and compared to the accuracies of the corresponding resulting optimized mechanisms (shaded regions in Figs. 5.63 and 5.64) without cutting-off the reactions against ϵ. In Fig. 5.63, removing the reaction rates up to $\epsilon = 10^{-3}$ did not affect the accuracy at all, a slightly bigger difference is observed for $\epsilon = 2 \cdot 10^{-3}$, while removing the reactions with rates below $\epsilon = 5 \cdot 10^{-3}$ destroyed a significant amount of the mechanisms.

A similar observations can be made for the real-coded reduction of the full mechanism (Fig. 5.64). The full mechanisms, however, exhibit a higher degree of freedom in eliminating reactions, therefore only a small number of mechanisms were destroyed by eliminating the reactions with $\epsilon = 5 \cdot 10^{-3}$. Such a behavior can be explained by the following: In a mechanism, there are reactions with the rates that can be drawn to a very small value by the penalty function, but cannot be reduced further or eliminated (because of the accuracy criteria). Unimportant reactions will be drawn to very small values just as well, but their removal will not influence the accuracy. Both types of reactions may have comparably the same rates at a certain point of the evolution (before the complete convergence). If the algorithm does not fully converge (like in the present cases), it is impossible to distinguish between these reactions (i.e. to determine apriori which reactions can be safely removed). However, a significant reduction can be achieved against an appropriate ϵ value provided that the accuracy will not be decreased.

Since the present number of generations was not sufficient for the penalty function to converge, the runs with the already reduced mechanisms (Fig. 5.56) are allowed to run for 10000 generations later in this section.

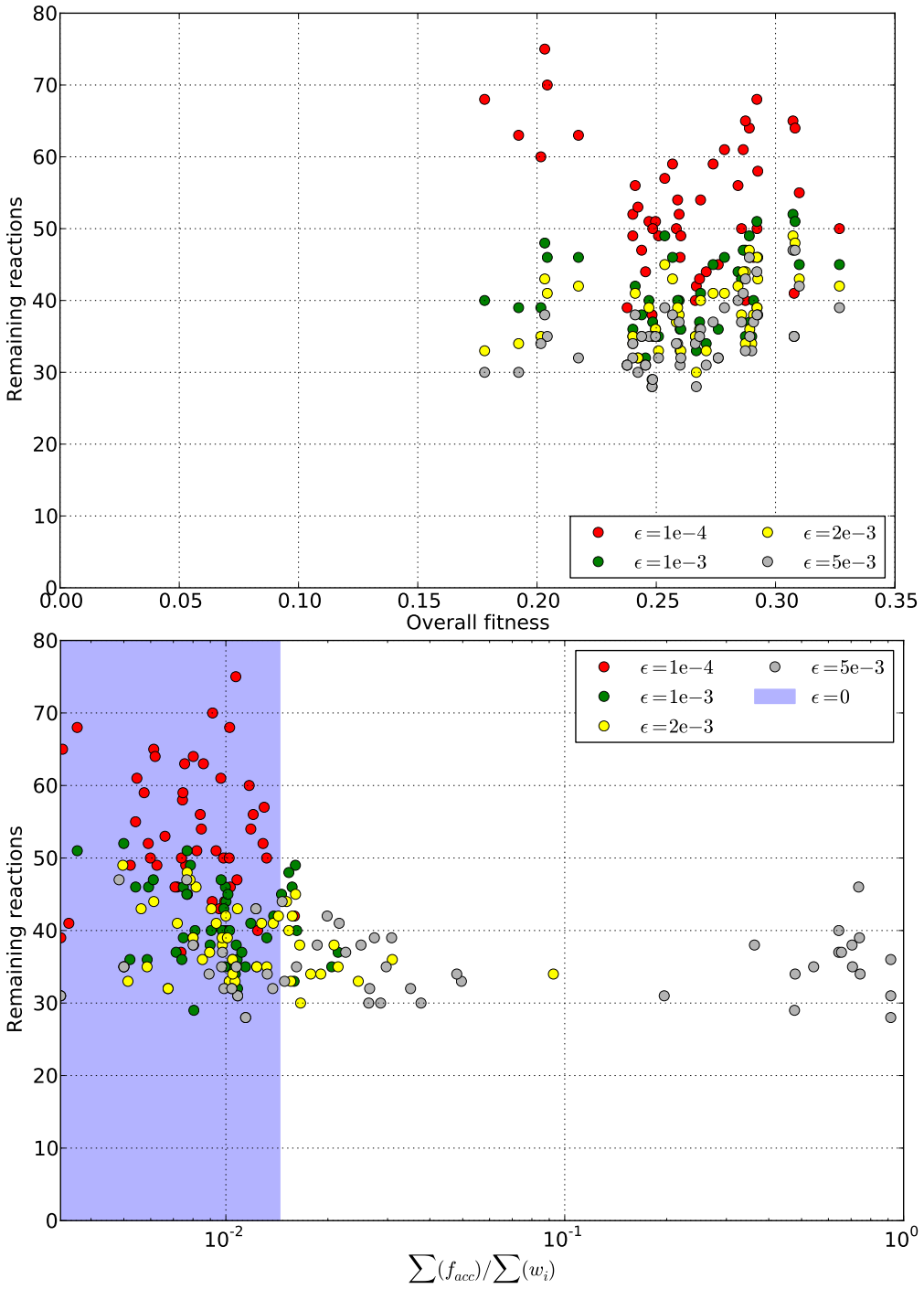

FIGURE 5.63: Top: Number of remaining reactions (after clipping the rate values below ϵ) with respect to the overall fitness of the real-coded runs. Bottom: Number of remaining reactions with respect to the accuracy of the resulting optimized mechanisms.

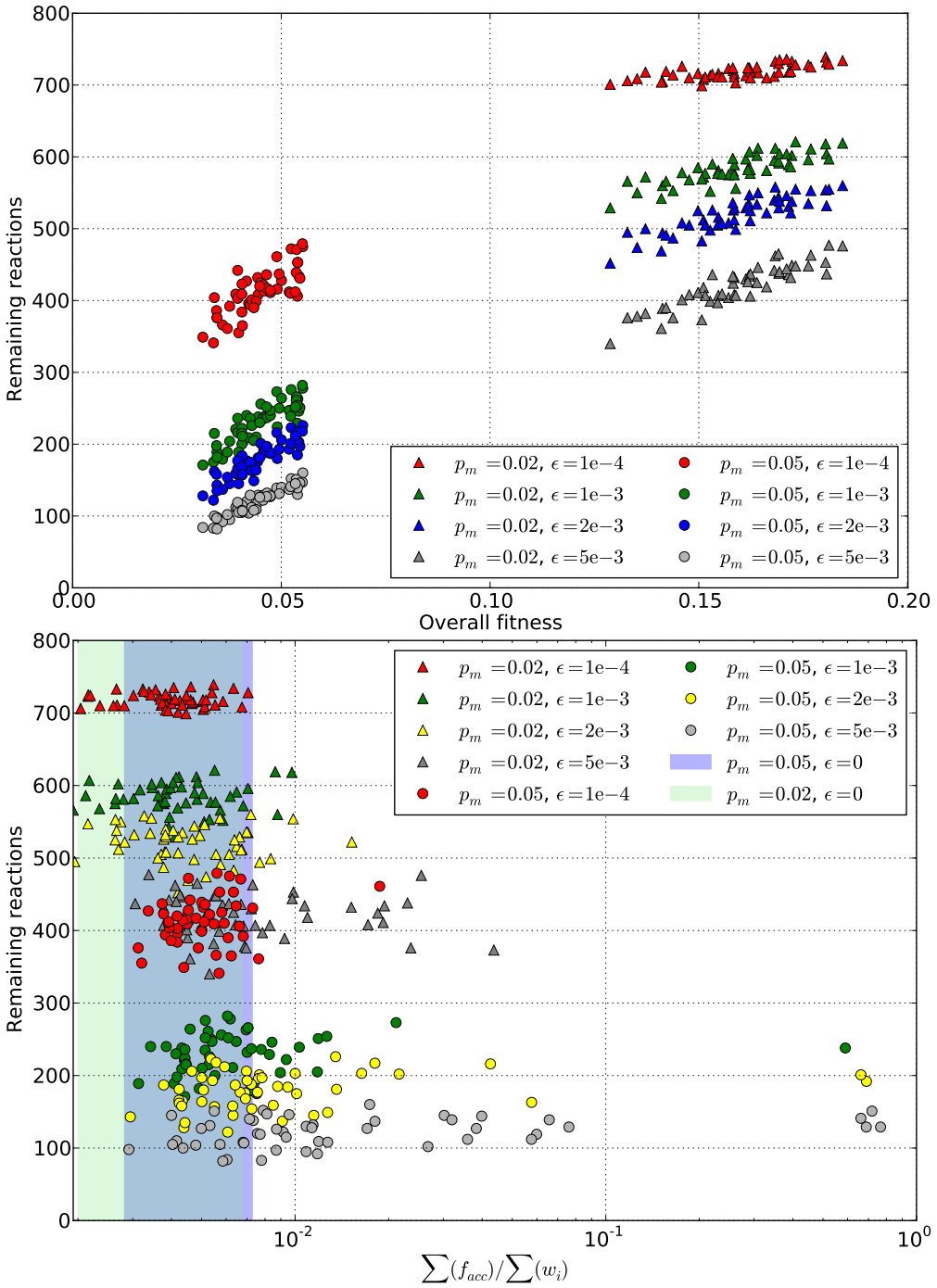

FIGURE 5.64: Top: Number of remaining reactions (after clipping the rate values below ϵ) with respect to the overall fitness of the real-coded reductions of the detailed mechanism with two mutation rates. Bottom: Number of remaining reactions with respect to the accuracy of the resulting mechanisms.

In general, the real-coded optimization with the penalty function can be used instead of the integer-coded reduction or the combined approach (see Fig. 5.54) to reduce the detailed mechanism. However, the real-coded reduction is time-consuming if applied to the detailed mechanism directly as it requires a large number of generations to reach the asymptotic solution. One obvious reason is that the full mechanism (only with different reaction rates) is calculated each time the fitness function is called during the whole evolution. For the integer-coded reduction, the full mechanism is calculated only once as a reference and in the initial population (see Section 4.1.1).

Furthermore, the reactions rates during the real-coded reduction are gradually driven to zero, which means that many generations may be needed before the rates actually reach zero. The real-coded reduction needs significantly larger number of generations before it reaches the same extent of reduction as the integer-coded reduction does, while the integer-coded reduction finds the solution within a reasonably small number of generations and its extent of the reduction is significant. For example, the real-coded reduction with the penalty function could not fully reach an asymptotic solution and a large extent of reduction within the given number of generations for the test-cases discussed in this section (see Figs. 5.56 and 5.58) – while having a better fitness already.

A steady approaching to an asymptotic solution of the real-coded reduction can be observed, for example, in Fig. 5.18 (Section 5.3), where the algorithm was allowed to run for 10000 generations. This is normally prohibitive in terms of the available runtime and memory for large (detailed) mechanisms. Therefore, the present integer-coded reduction method is far more efficient for the reduction of the large (detailed) mechanisms than the real-coded method is, when a significant reduction should be achieved quickly and the mechanism is large. The real-coded optimization with the penalty function, aiming to reduce the already reduced mechanism, can however be a useful approach when the accuracy is to be restored and the computational cost of the mechanism can be reduced further at the same time.

Convergence Behavior of the Penalty Function – Further Reduction

The number of generations defined by the previously discussed workflow was not sufficient for the algorithm to aproach an asymptotic solution. To address the convergence behavior and the statistical noise observed in Fig. 5.56, the same runs are repeated and allowed to run for 10000 generations (the input mechanisms are those resulting from the preceeding integer-coded reduction). The aim of choosing this large number of generations is to test if the significant statistical noise observed for 2000 generations occurs because the algorithm did not converge at that point. Figure 5.65 shows the mean

and the standard deviation of the overall fitness minima within 10000 generations. The standard deviation has only slightly decreased from 2000 generations, remaining almost constant for the rest of the evolution ($\sigma = 0.029$ and $\mu = 0.227$). However, the overall fitness (Fig. 5.65, top) shows evident "jumps" towards the smaller values indicating that the algorithm is still jumping from one local minima into another, in its search for the global minimum.

Another reason for the high statistical noise is that the input mechanisms are different for each of the 50 runs, as they result from the corresponding integer-coded reduction runs. To evaluate the contribution of the different input mechanisms to the statistical noise, additional 50 optimization runs were performed for the same input mechanism. The numerical and the GA setup was the same as for the previously discussed case (Table 5.17). Figure 5.66 shows that a smaller statistical noise is achieved if the input mechanism was kept the same for all the runs ($\sigma = 0.013$ and $\mu = 0.16$). The standard deviation is reduced by a factor of two when the same mechanism was used. However, the penalty function still exhibits a significant amount of the statistical noise and the runs did not converge to one global minimum. The overall fitness that is achieved remains about 3 times poorer than the fitness achieved with the real-coded optimization and reduction after 3000 generations already.

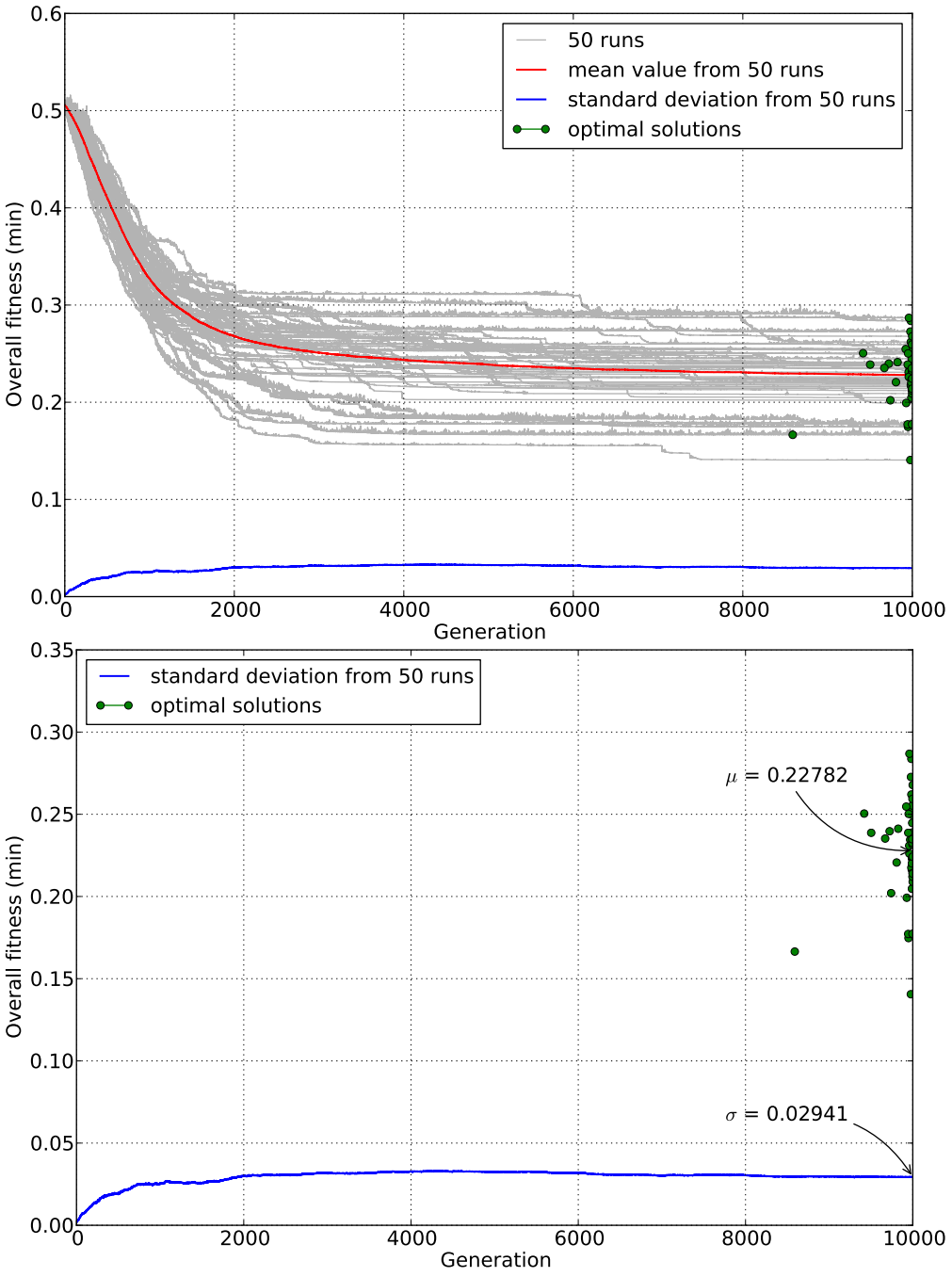

FIGURE 5.65: Top: The mean of the overall fitness minima from 50 randomly-seeded real-coded reductions of the already reduced mechanisms. Bottom: The standard deviation of the overall fitness minima from 50 runs, the optimal solutions from each run at the time when they were first found, and the mean μ and the standard deviation σ of their fitness.

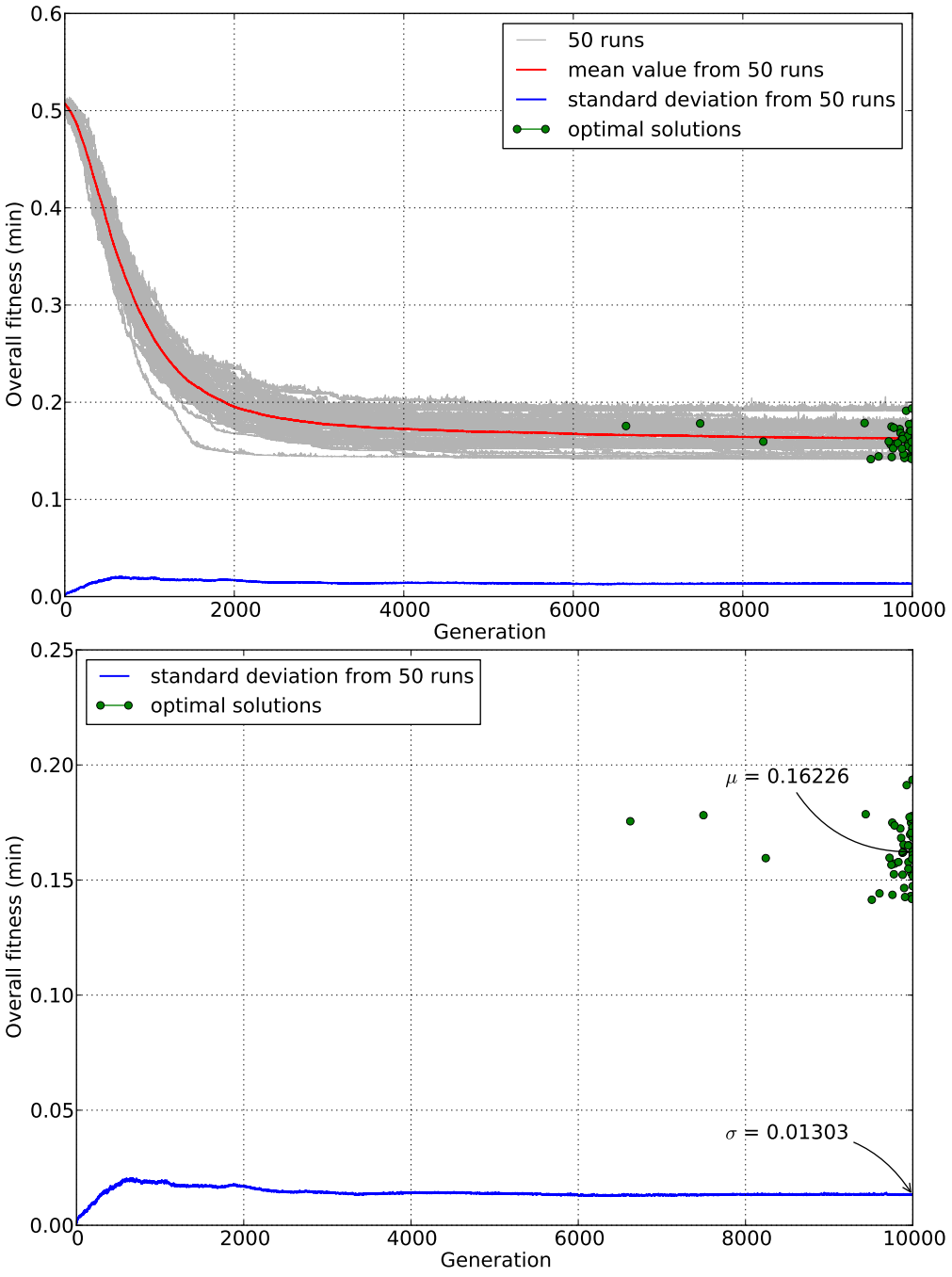

FIGURE 5.66: Top: The mean of the overall fitness minima from 50 randomly-seeded real-coded reductions of one already reduced mechanism. Bottom: The standard deviation of the overall fitness minima from 50 runs, the optimal solutions from each run at the time when they were first found, and the mean μ and the standard deviation σ of their fitness.

The long evolution and a closer aproaching to an asymptotic solution helped distinguishing between the reactions that can be eliminated (even though they were not zero yet) and those that became very small but their removal would damage the mechanism's chemical performance. Figures 5.67 and 5.68 show the accuracy of the mechanisms with respect to the number of the remaining reactions, which results from removing reactions that fall below the cut-off value ϵ. The number of the remaining reactions is almost constant for all the given values of ϵ, but a strong perturbation of accuracy is caused already with $\epsilon = 2 \cdot 10^{-3}$ and most of the mechanisms were destroyed with $\epsilon = 5 \cdot 10^{-3}$ even though the reduction extent was not significant. An almost-constant number of the remaining reactions and a clear separation of the destroyed mechanisms for given values of ϵ imply that, the reactions that can be removed already achieved the rates well below $\epsilon = 10^{-4}$, and those that are small but cannot be removed are around the $\epsilon = 10^{-4}$ of the rate limit.

The real-coded runs with the penalty function aiming at elimination of the reactions highlight the following properties of the penalty approach: The penalty function adds an additional dimension to the objective function (that normally contains only the performance of the mechanisms) as it influences each individual rate, thus increasing the complexity of the overall objective. The mutation (which is responsible for altering the single genes) contributes to the convergence not only by jumping faster from one local minimum into another, but it influences the objective function directly (through the penalty term). Therefore, the penalty function analysis should be done in combination with the mutation analysis to estimate the optimal combination of the parameters that would speed up the convergence of the real-coded reduction. Although the penalty function has proven to be a useful tool for dealing with the mechanisms that still remain relatively large even after the integer-coded reduction (see Section 5.3), one should note that achieving a great extent of the further reduction is time-consuming and depends on the mechanism's degree of freedom in altering (removing) its reaction rates. Section 6.2 offers some recommendations for further investigation and improvement of the penalty-function efficiency.

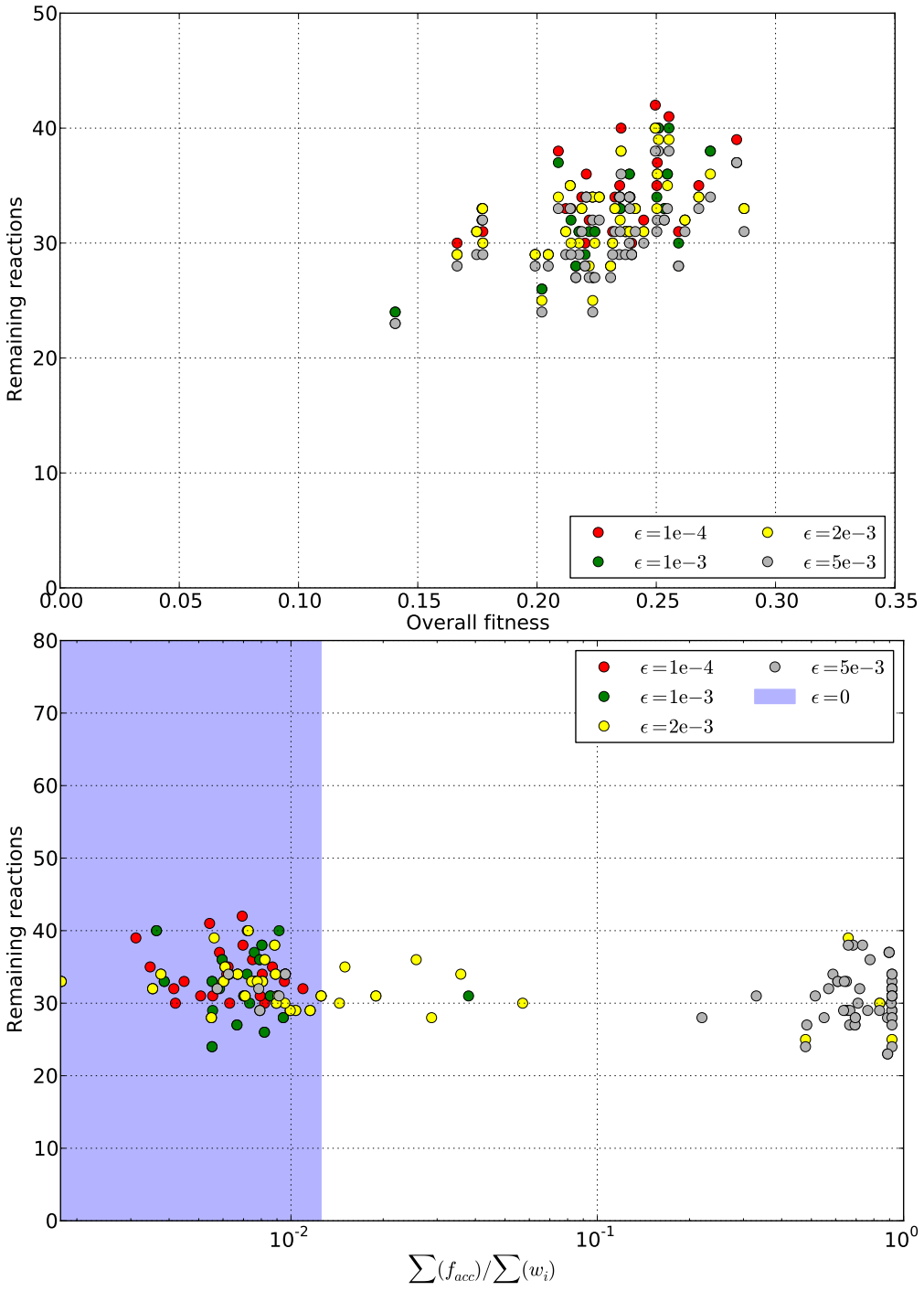

FIGURE 5.67: Top: Number of remaining reactions (after clipping the rate values below ϵ) with respect to the overall fitness of the real-coded runs. Bottom: Number of remaining reactions with respect to the accuracy of the resulting optimized mechanisms.

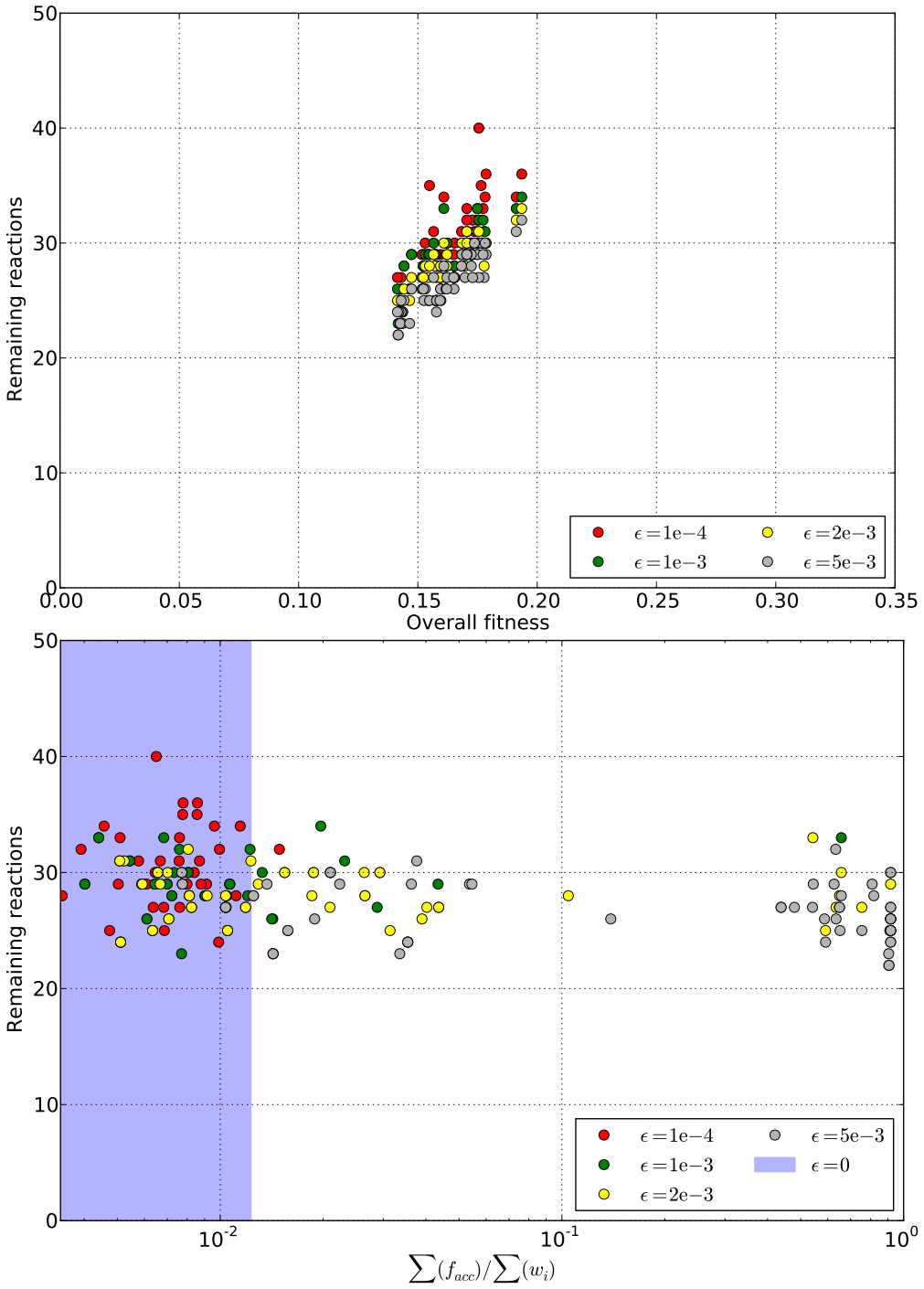

FIGURE 5.68: Top: Number of remaining reactions (after clipping the rate values below ϵ) with respect to the overall fitness of the real-coded runs. Bottom: Number of remaining reactions with respect to the accuracy of the resulting optimized mechanisms.

Summary

This subsection addressed the convergence behavior of the integer-coded reduction, the real-coded optimization and reduction of the reduced mechanisms and the real-coded-optimization and reduction of the full mechanism. The mechanism used for this study is USC Mech Version II [190] with 784 reactions. The results are summarized in the following.

Integer-coded reduction has a very small statistical noise ($\sigma = 0.002$ and $\mu = 0.009$, Fig. 5.55) and achieves a small value of objective function quickly, thus leading to very small mechanisms within reasonably small number of generations. Successive optimization of the integer-coded reduced mechanisms exhibits a higher amount of the statistical noise ($\sigma = 0.03$ and $\mu = 0.26$, Fig. 5.56) and the runs do not converge to the same optimum even within 10000 generations ($\sigma = 0.029$ and $\mu = 0.227$, Fig. 5.65). In case where the input reduced mechanism for the real-coded further reduction was the same in 50 runs, the statistical noise was reduced by a factor of two ($\sigma = 0.013$ and $\mu = 0.16$, Fig. 5.66) in comparison to the case where the input mechanisms were different (Fig. 5.65). However, the runs did not converge to the same optimum. This is because the integer-coded reduction removes reactions that may be important for the optimization step, but can no longer be retreived, i.e. certain degree of freedom is removed from the mechanisms to be optimized.

The real-coded optimization with the size-penalty term was applied to the full mechanism with two different mutation rates ($p_m = 0.02$ and $p_m = 0.05$) within 3000 generations. Even though the asymptotic solution was not reached, the objective function was significantly decreased and the statistical noise is quite small for both mutation rates. More specifically, for $p_m = 0.02$, the overall fitness has decreased from 0.5 to ≈ 0.16 with the standard deviation $\sigma = 0.013$ and the mean $\mu = 0.159$ (Fig. 5.58).

Higher mutation rate, $p_m = 0.05$, increased the convergence speed and significantly decreased the overall fitness from initial value of 0.5 to ≈ 0.045 (Fig. 5.59). As a result of a better convergence, the statistical noise is noticeably small ($\sigma = 0.006$ with respect to $\mu = 0.045$).

The real-coded reduction of the full mechanisms generally exibits a better statistical and convergence behavior (optimal solutions from the observed 50 runs are very close to each other) than the previously discussed two-step approach, which makes a strong case for further investigating and improving a real-coded reduction and optimization method.

For easier comparison, Figure 5.69 shows the mean values of fitness from 50 runs of three cases: real-coded reduction of the full mechanism from Fig. 5.59, real-coded further reduction of already reduced (different) mechanisms from Fig. 5.65 and the real-coded further reduction of one already reduced mechanism from Fig. 5.66, within 3000 generations (which is how long the full-mechanism real-coded reduction took).

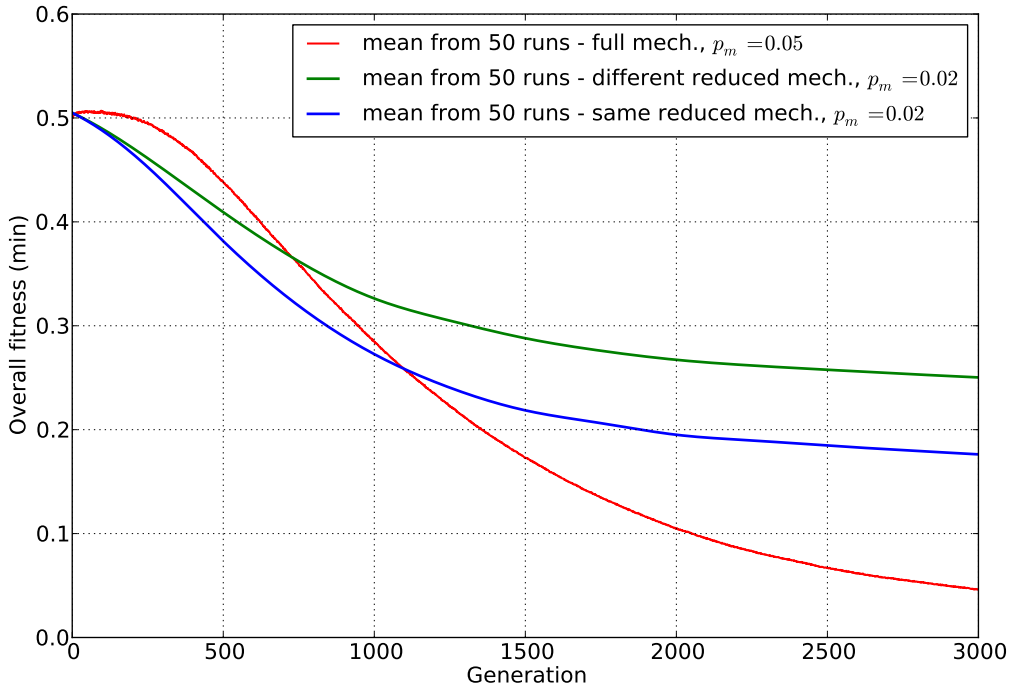

FIGURE 5.69: Mean values of the overall fitness of different real-coded optimization runs with the penalty function.

Although this comparison is not absolutely fair (different optimization processes and the mechanisms are used), it must be noticed that the real-coded reduction of the full mechanism reached the best fitness value quicker than the two-step approaches.

Integer-coded reduction leads to small mechanisms quickly, with a small amount of statistical noise. However, due to eliminating reactions, the subsequent optimization (aiming to further reduce the mechanisms) cannot recover the lost reactions, thus resulting in a relatively poor fitness value. Therefore, the two-step approach is a method of choice when small mechanisms should be obtained quickly.

However, the algorithmic behavior of the real-coded algorithm applied to a full mechanism is generally more consistent, has a small statistical noise, leads to a better fitness value than the real-coded reduction of the already reduced mechanisms does and the runs are able to closely approach one minimal value (Fig. 5.59). For these reasons, the real-coded reduction should be further investigated and enhanced to be able to reduce

and optimize the large mechanisms quicker than the current two-step approach can, which was in the focus of the thesis.

Chapter 6

Summary and Outlook

6.1 Summary

The focus of the research conducted within the scope of this thesis is the development of an automatic method for the reduction of detailed reaction mechanisms and their optimization. As the reaction mechanism is a set of elementary reactions and their relevance for a particular simulation depends on specific operating conditions, the reduction problem can be considered as a search problem where the aim is to find a subset of reactions that satisfy specified user-defined criteria just as well as the detailed set would do.

In this context, the genetic algorithm is the method of choice and the first part of the research is dedicated to developing a genetic algorithm-based reduction technique. The algorithm finds a smallest possible subset of relevant reactions by minimizing the objective function which contains the criteria the reduced mechanism must satisfy with respect to its detailed version. The objective function evaluates the performance of the candidate solution (submechanism) with respect to the its detailed version in predicting the combustion phenomena of interest. The mechanism evaluation is conducted by simulating the reacting case of interest, for example a homogeneous reactor (zero-dimensional model) or a laminar flame (one-dimensional model). These models are calculated using the chemical kinetics library Cantera [55]. The overall objective function used for the reduction purpose involves both the accuracy and the cost criteria. The accuracy criterion is based on the difference between the calculated properties resulting from the detailed (reference) mechanism and the reduced mechanism.

Depending on the nature of the optimization target, a set of different normalization functions is offered to faciliate incorporation of different properties (e.g. ignition delay

time, temperature, relevant species concentrations, laminar flame speed) into one single objective function. The cost criteria include the computational time for the candidate solution and the number of remaining reactions (which we aim to minimize). Different expressions used for normalization of single criteria enable a simultaneous minimization of both the accuracy and the cost (which are conflicting criteria) within one single objective function and allow the user to achieve a desired trade-off between the accuracy and the computational cost of the reduced mechanism. Important aspects of the reduction method are demonstrated in Chapter 5 for several different mechanisms.

Where the accuracy of the reduced mechanism is sacrificed for its computational cost, tuning of the rate coefficients of the remaining reactions can largely restore the accuracy of the reduced mechanism without increasing its computational cost. Optimization of the rate coefficients is achieved in the second part of this research by finding the optimal values of the rate coefficients (in this work, the pre-exponential factors) which give the minimal value of the objective function. The genetic algorithm-based optimization uses a similar searching technique, albeit with differently defined operators and additional aspects of the objective function. Although the accuracy of the mechanism is a primary goal of the optimization, and the physical uncertainties of the reaction rates (from the literature or chemical databases) are not primarily considered in this work, it was made possible to constrain the individual reaction rates by their prescribed uncertainty factors.

As the consideration of the uncertainties would require tremendous effort in finding the data (many of them being highly uncertain anyway), this work advocates constraining the reaction rate alterations during the optimization with the penalty function defined within the overall objective function. The penalty function used in this context keeps the reaction rates as close as possible to their nominal values, in case where the physical meaning of the reaction rates is important. This approach is not typical for standard use of genetic algorithms as it not only considers the performance of the model, but controls the properties of the model as well. The penalty function approach has been demonstrated in Section 5.1 for the hydrogen mechanism (where the kinetic data are known) and compared to the optimization using fixed uncertainty ranges for single reactions. The same formulation of the penalty function can alternatively be used for a further reduction of the mechanism and its optimization at the same time, which is demonstrated in Section 5.3 on a reduced mechanism for *tert*-butanol combustion.

The efficiency of the penalty-function approach for reducing the detailed mechanism is further investigated in Section 5.4.4. It is shown that, although the penalty function is a useful tool for simultaneous further reduction and optimization, it requires a large number of generations to reach the complete convergence. Therefore, if a quick finding

a small mechanism from a large detailed mechanism is desired, the integer-coded reduction (and if needed, the subsequent optimization) is a good method of choice. On the other hand, the real-coded reduction of the full mechanism shows a better algorithmic behavior (small statistical noise, smaller resulting fitness value than that obtained by the real-coded reduction of the already reduced mechanisms). The extent of the reduction achieved by the real-coded reduction of large mechanisms is still a drawback of this approach if a small resulting mechanism is desired, but due to its overall algorithmic behavior, the real-coded reduction makes a good case for further investigation and improvement so that it can be used as the only reduction and optimization step.

The genetic algorithm-based reduction/optimization method is made to run in parallel on a desired number of computational cores. The method is reproducible and robust with respect to stiff or non-converging mechanisms that may occur during the search.

6.2 Recommendations for the Future Work

Since there is no research that can be considered finished, this work can also be further improved or continued in several ways. In this section, several recommendations for extending the genetic algorithm-based method for manipulation of reactions mechanisms will be highlighted.

Choice of the Optimization Targets

As the performance of the resulting reduced and/or optimized mechanism greatly depends on the appropriate definition of the optimization targets, it is important to make the right choice of the optimization targets. The right choice of the reduction and optimization targets is essential to obtaining a useful simplified/optimized mechanism for its further application in complex CFD simulations. The main motivation is the difference between the models (zero-dimensional reactors and one-dimensional laminar flames) used for the reduction and/or optimization and the more complex CFD models. Defining an appropriate optimization target is therefore a non-trivial task. However, it is important to find out from which characteristics of the reduced/optimized mechanism a given CFD problem-specific requirements would benefit. Different CFD simulations may have different demands and aims, for example, some require very small number of reactions, a less stiff mechanism or even a mechanism that is not very accurate in terms of predicting specific chemical behaviors, but is robust enough to avoid numerical instability. The correlation between the targets used for reducing/optimizing a large mechanism for a zero-dimensional homogeneous reactor model and prediction ability of

the same mechanism for a laminar flame (even one-dimensional) should be attempted next as an improvement of the present algorithm.

Overall Objective Function Formulation

The present overall objective function described by Eq. 4.1 in Section 4 is a linear combination of single objective functions defined for each of the operating conditions, each of which is a linear combination of chosen optimization targets. Although this formulation is shown to be relatively easy to implement and tune to provide the best possible trade-off even if the targets are conflicting, there is still room for improvement. For example, if the mechanism is missing some reactions relevant for a specific condition among the set of conditions (see Section 5.4.3), yet the optimizer is trying to meet the criteria set for it (and it will find the global minimum of the function), the global minimum of the overall objective function will not necessarily be the minimum of all its terms.

Although the application of the reduced mechanism to the conditions it has not been reduced for is generally not recommended, it still may provide some insight into the ability of the reduction/optimization method. While the present formulation of the objective function is shown to perform well due to the specific expressions used for normalizing its single terms (Section 4.1.2), it may be worth to attempt to improve its definition further and test other non-linear combinations of single function terms.

Optimization of all the Arrhenius Parameters

Extending the mechanism representation as a chromosome to account for the temperature exponent and the activation energy for the optimization is probably the most logical next step in improving the overall optimization. Many reported studies take the latter two into account. This would require different type of mapping of the reactions into a chromosome (including all types of the reactions, see Section 2.5.2) and some interesting aspects regarding the treatment of different rate parameters (pre-exponential factor, temperature exponent and activation energy) during the evolution are worth investigating. Altering of the latter two parameters may increase a degree of freedom for optimizing large mechanisms as they contain a large number of reactions with only the pre-exponential factor defined (temperature exponent and activation energy are set to zero). These reaction rates are very uncertain (their coefficients result from mere fitting), which may allow the modeler to freely adjust their rates and improve the overall behavior of such a mechanism, without destroying any chemical knowledge (where this appears important).

Uncertainty Consideration from the Database

In the present work, the uncertainty was not the main issue considered during the optimization, but in cases where it was important (Section 5.1), the uncertainty factors were pre-defined for each reaction within the setup file. That approach does not require much effort for relatively small mechanisms, but it may require significant (and unnecessary) effort for large mechanisms. If specifying the rate uncertainty reported in the literature is of interest when optimizing the mechanism, and the penalty function approach is not desired as an alternative, then enabling the optimizer to read the uncertainty data directly from the database may be an option. As this approach may require tremendous effort in implementing these databases (possibly converting them into appropriate format) as well, an alternative formulation for the penalty function is worth considering. For example, it would be interesting to test a penalty function, which constraints the reaction rates according to their reported standard deviations, when these are available.

Mechanism Generation

Clearly, for the mechanisms that are not (fully) developed and where is little known about their actual chemistry, the mechanisms' optimization may get us closer to constructing the mechanism. For example, if there are some available experimental data that can be used as a reference and possible reaction steps are listed, the reduction/optimization approach may be used to find the relevant reaction rates that reproduce the observed behavior of the system. Of course, this has to be done in combination with thermodynamic and transport data (if available) of the species involved and the experimental findings. One example of such a mechanism is the formation of iron-oxide nanoparticles from an iron-pentacarbonyl doped hydrogen flame [199], where only the iron-pentacarbonyl decomposition chemistry and some species are known from the literature, but the iron-oxide formation submechanism is not fully established and there are not many experimental data either.

Real-coded Reduction

Section 5.4.4 tackles the potential of the real-coded algorithm to reduce the (detailed) reaction mechanism and the possibility of simplifying the reduction/optimization workflow by using the real-coded algorithm only. The present formulation of the penalty function, although quite useful, still exhibits a slow convergence behavior and it takes a large number of generations (long runtime of the algorithm) to make a significant

reduction, thus making the current integer-coded reduction way more efficient approach to a quick elimination of the reactions.

On the other hand, as shown in Section 5.4.4, the real-coded algorithm should be further investigated and improved to be able to replace the combined approach, i.e. to reduce and optimize the mechanisms directly (without the integer-coded elimination). The efficiency of the real-coded algorithm should be further addressed by performing the convergence analysis of the penalty function with varying the mutation rate and/or the population size to find the optimal combination of the parameters that provide the best efficiency of the real-coded reduction and optimization. This analysis should be performed for a statistically relevant number of the optimization runs (samples). It would be also interesting to find a new formulation of the objective function that would be able to draw the reactions towards zero in a much faster manner.

Another important question regarding the current penalty function approach for eliminating reactions is how to automatically distinguish between the very small reaction rates that can be removed (even before they converge to zero) and the rates that are driven to a very small value but cannot be removed. For the long runs made in Section 5.4.4, it was possible to make a clear separation of such reactions by finding a threshold value under which the reactions (although with very small rates) cannot be removed from the mechanism. However, developing a method for an automatic recognition of such reactions and an automatic determination of the cut-off value under which the reactions cannot be removed is still an open question that should be addressed by future work.

Appendix A

Mixture-averaged and multicomponent transport model

In chemically reacting-flow phenomena, species production and consumption is frequently balanced by convective, diffusive and conductive transport. Althoug these effects of transport are neglected for homogeneous kinetically controlled systems (perfectly stirred and plug-flow reactors, see Chapter 2), in other important systems (flames and chemical vapor deposition systems), transport of energy and species control the reaction rate. Evaluation of the transport effects of species, momentum and energy in a multicomponent gas-phase reacting flow includes calculating coefficients of molecular diffusion, thermal conductivity and termal diffusion.

For most simulations, these properties can be obtained from pure-species properties by employing the mixture averaging rules (Chapter 2). However, for some applications, the mixture averaging rules may not adequately address the solution of transport properties. Therefore, many software-packages (e.g. CHEMKIN [77] or Cantera [55]) offer a possibility to chose between both the mixture-averaged and the full multicomponent approach to solving transport properties. The multicomponent evaluation is generally more accurate than the relatively simpler mixture-averaged approach. The mixture-averaged formulation is only correct asymptotically in some special cases, e.g. for a binary mixture, or for diffusion of trace amounts of species into a nearly pure species, or for systems in which all species except one move with nearly the same diffusion velocity [19]. Expressions for calculating transport coefficients for reacting-cases simulations are usually based on Chapman-Enskog theory extended to account for transport properties in multicomponent systems [19, 34].

A.1 Mixture-averaged transport formulation

In this approach, mixture properties are determined using the pure species properties. The viscosity is calculated according to the semi-empirical formula from Wilke modified by Bird et al. [19]:

$$\eta = \sum_{k=1}^{N_s} \frac{X_k \eta_k}{\sum_{j=k}^{N_s} X_j \Phi_{kj}}, \tag{A.1}$$

where

$$\Phi_{kj} = \frac{1}{\sqrt{8}} \left(1 + \frac{M_k}{M_j}\right)^{-\frac{1}{2}} \left(1 + \left(\frac{\eta_k}{\eta_j}\right)^{\frac{1}{2}} \left(\frac{M_j}{M_k}\right)^{\frac{1}{4}}\right)^2, \tag{A.2}$$

and η_k is a pure-species viscosity given by the standard kinetic theory expression [67]:

$$\eta_k = \frac{5}{16} \frac{\sqrt{\pi m_k k_B T}}{\pi \sigma_k^2 \Omega^{(2,2)^*}}, \tag{A.3}$$

where σ_k is a Lennard-Jones collision diameter, m_k is the molecular mass of species k, k_B is the Boltzmann's constant, T is the temperature and $\Omega^{(2,2)^*}$ is the collision integral determined by a quadratic interpolation of the tables based on Stockmayer potentials given by Monchick and Mason [120].

The mixture-averaged thermal conductivity is calculated from the pure species thermal conductivities λ_k as:

$$\lambda = \frac{1}{2} \left(\sum_{k=1}^{N_s} X_k \lambda_k + \frac{1}{\sum_{k=1}^{N_s} X_k / \lambda_k} \right). \tag{A.4}$$

The pure-species thermal conductivity consists of translational, rotational, and vibrational contributions [192]:

$$\lambda_k = \frac{\eta_k}{M_k} \left(f_{\text{trans}} C_{v,\text{trans}} + f_{\text{rot}} C_{v,\text{rot}} + f_{\text{vib}} C_{v,\text{vib}} \right), \tag{A.5}$$

where $f_{\text{trans}} = \frac{5}{2}$.

The mixture-averaged formulation calculates the diffusion coefficient D_{km} for species k that diffuses into a mixture of other gas components as:

$$D_{km} = \frac{1 - Y_k}{\sum_{j \neq k}^{N_s} X_j / D_{jk}}, \tag{A.6}$$

where D_{jk} is the binary diffusion coefficient of species k into species j given in terms of pressure P and temperature T:

$$D_{jk} = \frac{3}{16} \frac{\sqrt{2\pi k_B^3 T^3 / m_{jk}}}{P\pi\sigma_{jk}^2 \Omega^{(1,1)^*}}, \tag{A.7}$$

where m_{jk} is the reduced molecular mass for the species pair (j, k):

$$m_{jk} = \frac{m_j m_k}{m_j + m_k} \tag{A.8}$$

and σ_{jk} is the reduced collision diameter:

$$\sigma_{jk} = \frac{1}{2} \left(\sigma_j + \sigma_k \right). \tag{A.9}$$

The collision integral $\Omega^{(1,1)^*}$ is based on Stockmayer potentials and is obtained from the look-up tables based on the reduced temperature $T_{jk}^* = k_B T / \varepsilon_{jk}$ where $\varepsilon_{jk} = \sqrt{\left(\varepsilon_j / k_B\right)\left(\varepsilon_k / k_B\right)}$ is the reduced Lennard-Jones potential well depth.

The diffusion velocity of species k in the mixture-average formulations is related to the species gradients by a Fickian formula as:

$$\mathbf{V}_k = \frac{1}{X_k} D_{km} \mathbf{d}_k - \frac{D_k^T}{\rho Y_k T} \nabla T. \tag{A.10}$$

A.2 Multicomponent transport properties

The multicomponent approach to determining the diffusion coefficients, thermal conductivities and thermal diffusion coefficients is based on solving a system of equations defined by a so-called L matrix. The L matrix consists of nine sub-matrices and it is formulated as:

$$\begin{pmatrix} L^{00,00} & L^{00,10} & 0 \\ L^{10,00} & L^{10,10} & L^{10,01} \\ 0 & L^{01,10} & L^{01,01} \end{pmatrix} \begin{pmatrix} a_{00}^1 \\ a_{10}^1 \\ a_{01}^1 \end{pmatrix} = \begin{pmatrix} 0 \\ X \\ X \end{pmatrix}. \tag{A.11}$$

The vector on the right-hand side consists of the mole fraction vectors X_k of the component k. The diffusion coefficients are calculated in terms of the inverse of the $L^{00,00}$ block as:

$$D_{jk} = X_j \frac{16 T \bar{M}}{25 p m_k} \left(P_{jk} - P_{jj} \right), \tag{A.12}$$

where $(P) = \left(L^{00,00}\right)^{-1}$.

Thermal conductivities are calculated in terms of the solution to the system of equations:

$$\lambda_{0,\text{trans.}} = -4 \sum_{k=1}^{N_s} X_k a^1_{k10} \tag{A.13}$$

$$\lambda_{0,\text{int.}} = -4 \sum_{k=1}^{N_s} X_k a^1_{k01} \tag{A.14}$$

$$\lambda_0 = \lambda_{0,\text{trans.}} + \lambda_{0,\text{int.}} \tag{A.15}$$

Thermal diffusion coefficients are calculated from:

$$D^T_k = \frac{8 m_k X_k}{5R} a^1_{k00}. \tag{A.16}$$

The L matrix components are given by Dixon-Lewis [39]:

$$
\begin{aligned}
L_{ij}^{00,00} &= \frac{16T}{25p}\sum_{l=1}^{N_s}\frac{X_l}{m_j\mathcal{D}_{jl}}\left\{m_kX_k(1-\delta_{jl})-m_jX_j(\delta_{jk}-\delta kl)\right\}\\
L_{jk}^{00,10} &= \frac{8T}{5p}\sum_{l=1}^{N_s}X_kX_l(\delta_{jk}-\delta jl)\frac{m_l\left(1.2C_{kl}^{*}-1\right)}{\left(m_k+m_l\right)\mathcal{D}_{kl}}\\
L_{jk}^{10,00} &= L_{kj}^{00,10}\\
L_{jk}^{01,00} &= L_{kj}^{00,01}=0\\
L_{jk}^{10,10} &= \frac{16T}{25p}\sum_{l=1}^{N_s}\frac{m_j}{m_k}\frac{X_jX_l}{(m_i+m_k)^2\mathcal{D}_{jl}}\\
&\quad\times\{(\delta_{kl}-\delta_{jk})\left[\frac{15}{2}m_k^2+\frac{25}{4}m_l^2-3m_l^2B_{jl}^{*}\right]\\
&\quad-4m_km_lA_{jl}^{*}(\delta_{kl}-\delta_{jk})\left[1+\frac{5}{3\pi}\left(\frac{C_{j,\mathrm{rot.}}}{R\xi_{jl}}+\frac{C_{l,\mathrm{rot.}}}{R\xi_{lj}}\right)\right]\}\\
L_{jj}^{10,10} &= -\frac{16m_jX_j^2}{R\mu_j}\left(1+\frac{10C_{j,\mathrm{rot.}}}{R\xi_{jj}}\right)-\frac{16T}{25p}\sum_{l\neq j}^{N_s}\frac{X_jX_l}{(m_j+m_l)^2\mathcal{D}_{jl}}\\
&\quad\times\{\frac{15}{2}m_j^2+\frac{25}{4}m_l^2-3m_l^2B_{jl}^{*}+4m_jm_lA_{jl}^{*}\\
&\quad\times\left[1+\frac{5}{3\pi}\left(\frac{C_{j,\mathrm{rot.}}}{R\xi_{jl}}+\frac{C_{l,\mathrm{rot.}}}{R\xi_{lj}}\right)\right]\}\\
L_{jk}^{10,01} &= \frac{32T}{5\pi pC_{k,\mathrm{int.}}}\sum_{l=1}^{N_s}\frac{m_kA_{kl}^{*}}{(m_k+m_l)\mathcal{D}_{kl}}(\delta_{jl}+\delta_{jk})X_kX_l\frac{C_{k,\mathrm{rot.}}}{R\xi_{kl}}\\
L_{jj}^{10,01} &= \frac{16m_jX_j^2}{3\pi\mu_jC_{j,\mathrm{int.}}}\frac{C_{j,\mathrm{rot.}}}{R\xi_{jj}}+\frac{32TR}{5\pi pC_{j,\mathrm{int.}}}\sum_{l\neq j}^{N_s}\frac{m_jA_{jl}^{*}}{(m_j+m_l)\mathcal{D}_{jl}}X_jX_l\frac{C_{j,\mathrm{rot.}}}{R\xi_{jl}}\\
L_{jk}^{01,10} &= L_{kj}^{10,01}\\
L_{jj}^{01,10} &= -\frac{8R^2}{\pi C_{j,\mathrm{int.}}^2}\frac{m_jX_j^2}{R\mu_j}\frac{C_{j,\mathrm{rot.}}}{R\xi_{jj}}\\
&\quad-\frac{4RT}{C_{j,\mathrm{int.}}p}\left(\sum_{l=1}^{N_s}\frac{X_jX_l}{\mathcal{D}_{jl}}+\sum_{l\neq j}^{N_s}\frac{12X_jX_lm_jA_{jl}^{*}C_{j,\mathrm{rot.}}}{5\pi C_{j,\mathrm{int.}}m_l\mathcal{D}_{jl}\xi_{jj}}\right)\\
L_{jk}^{01,01} &= 0\ (j\neq k)
\end{aligned}
$$

where T is the temperature, p is the pressure, X_k is the mole fraction of component k, D_{ik} are the binary diffusion coefficients and m_i is the molecular mass of component i, R is the universal gas constant, η_k are the pure species viscosities, A_{jk}^{*},B_{jk}^{*} and C_{jk}^{*} are the ratios of collision integrals defined as:

$$A^*_{jk} = \frac{1}{2}\frac{\Omega^{(2,2)}_{jk}}{\Omega^{(1,1)}_{jk}} \tag{A.17}$$

$$B^*_{jk} = \frac{1}{3}\frac{5\Omega^{(1,2)}_{jk} - \Omega^{(1,3)}_{jk}}{\Omega^{(1,1)}_{jk}} \tag{A.18}$$

$$C^*_{jk} = \frac{1}{3}\frac{\Omega^{(1,2)}_{jk}}{\Omega^{(1,1)}_{jk}} \tag{A.19}$$

The rotational and internal contributions to the species molecular heat capacities are $c_{k,\mathrm{rot}}$ and $c_{k,\mathrm{int}}$. For a linear molecule,

$$\frac{c_{k,\mathrm{rot}}}{k_B} = 1,$$

and for a non-linear molecule

$$\frac{c_{k,\mathrm{rot}}}{k_B} = \frac{3}{2},$$

where k_B is the Boltzmann constant. The internal contribution to the heat capacity is calculated from:

$$\frac{c_{k,\mathrm{int}}}{k_B} = \frac{c_p}{k_B} - \frac{3}{2}.$$

Appendix B

Solution Schemes

There are two main issues associated with with error control through time step selection for numerical solution of differential equations: accuracy and the stability. Accuracy requires a time step that is sufficiently small so that the numerical solution is close to the true solution. Numerical methods usually measure the accuracy in terms of the local truncation error, which depends on the details of the method and the time step. Stability requires a time step that is sufficiently small that numerical errors are damped, and not amplified. A problem is called stiff when the time step required to maintain stability is much smaller than the time step required to deliver accuracy (if stability were not an issue). Generally speaking, implicit methods have very much better stability properties than explicit methods, and thus are much better suited to solving stiff problems. Since most chemical kinetic problems are stiff, implicit methods are usually the method of choice [74].

Explicit (Forward Euler) Schemes

Consider the general first-order differential equation:

$$\frac{dy}{dt} = f(y,t), \tag{B.1}$$

where the initial condition is $y(0) = y_0$ and the function $f(y,t)$ is nonlinear.

The explicit method approximates the time derivative with a first-order finite difference [6, 74]:

$$\frac{y_{n+1} - y_n}{h_n} = f\left(t_n, y_n\right). \tag{B.2}$$

Given a solution at time level t_n, the solution at time t_{n+1} is determined explicitly as:

$$y_{n+l} = y_n + h_n f\left(t_n, y_n\right), \tag{B.3}$$

where the time step is $h_n = t_{n+1} - t_n$ and the right-hand-side function f is evaluated at t_n and y_n. The explicit method is easy to implement, but suffers from stability restrictions.

Implicit (Backward Euler) Scheme

The simplest implicit method is the backward Euler method formulated as [6, 74]:

$$\frac{y_{n+1} - y_n}{h_n} = f\left(t_{n+1}, y_{n+1}\right). \tag{B.4}$$

If $f\left(t_{n+1}, y_{n+1}\right)$ is nonlinear then the equation must be solved iteratively to determine y_{n+1}. Due to the strong stability, the time step for the implicit method is chosen primarily to maintain the accuracy. Although the implicit methods resolve the stability problems associated with stiffness, they are more complicated to implement because more work at each time step is required to solve a system of equations, which is typically nonlinear. For stiff problems, the iterative solution is usually accomplished with a modified Newton method [74, 77].

Bibliography

[1] A. Aldawood, S. Mosbach, M. Kraft, and A. Amer. Multiobjective optimization of a kinetics-based HCCI model using engine data. *SAE Technical Paper*, pages 01–1783, 2011.

[2] E. Alexandre and V. Giovangigli. Thermal diffusion effects in hydrogen-air and methane-air flames. *Combustion Theory and Modelling*, 2(4):349–372, 1998.

[3] I. Ali and M. Basit. Significance of hydrogen content in fuel combustion. *International Journal of Hydrogen Energy*, 18(12):1009–1011, 1993.

[4] I. P. Androulakis. Kinetic mechanism reduction based on an integer programming approach. *AIChE Journal*, 46(2):361–371, 2000.

[5] I. P. Androulakis, J. M. Grenda, and J. W. Bozzelli. Time-integrated pointers for enabling the analysis of detailed reaction mechanisms. *AIChE Journal*, 50(11):2956–2970, 2004.

[6] U. Ascher and L. Petzold. *Computer Methods for Ordinary Differential Equations and Differential-Algebraic Equations*. Society for Industrial and Applied Mathematics, 1998.

[7] T. Bäck. Optimal mutation rates in genetic search. In *Proceedings of the Fifth International Conference on Genetic Algorithms*, pages 2–8, 1993.

[8] T. Bäck and H.-P. Schwefel. An overview of evolutionary algorithms for parameter optimization. *Evolutionary computation*, 1(1):1–23, 1993.

[9] I. Banerjee and I. G. Ierapetritou. Development of an adaptive chemistry model considering micromixing effects. *Chemical Engineering Science*, 58(20):4537–4555, 2003.

[10] F. Battin-Leclerc, J. Simmie, and E. Blurock. *Cleaner Combustion: Developing Detailed Chemical Kinetic Models*. Green Energy and Technology. Springer London, 2013.

[11] D. L. Baulch, C. T. Bowman, C. J. Cobos, R. A. Cox, T. Just, J. A. Kerr, M. J. Pilling, D. Stocker, J. Troe, W. Tsang, et al. Evaluated kinetic data for combustion modeling: supplement II. *Journal of physical and chemical reference data*, 34(3):757–1397, 2005.

[12] D. L. Baulch, C. Cobos, R. A. Cox, C. Esser, P. Frank, T. Just, J. A. Kerr, M. J. Pilling, J. Troe, R. W. Walker, et al. Evaluated kinetic data for combustion modelling. *Journal of Physical and Chemical Reference Data*, 21(3):411–734, 1992.

[13] D. L. Baulch, C. J. Cobos, R. A. Cox, P. Frank, G. Hayman, T. Just, J. A. Kerr, T. Murrells, M. J. Pilling, J. Troe, et al. Summary table of evaluated kinetic data for combustion modeling: Supplement 1. *Combustion and flame*, 98(1):59–79, 1994.

[14] S. W. Benson. *The foundations of chemical kinetics.* McGraw-Hill series in advanced chemistry. McGraw-Hill, 1960.

[15] S. W. Benson. *Thermochemical kinetics: methods for the estimation of thermochemical data and rate parameters.* Wiley-Interscience. Wiley, 1976.

[16] S. W. Benson and H. E. O'Neal. *Kinetic data on gas phase unimolecular reactions.* NSRDS-NBS. U.S. National Bureau of Standards; for sale by the Supt. of Docs., U.S. Govt. Print. Off., 1970.

[17] G. S. G. Beveridge and R. S. Schechter. *Optimization: theory and practice.* McGraw-Hill chemical engineering series. McGraw-Hill, 1970.

[18] B. Bhattacharjee, D. A. Schwer, P. I. Barton, and W. H. Green. Optimally-reduced kinetic models: reaction elimination in large-scale kinetic mechanisms. *Combustion and Flame*, 135(3):191–208, 2003.

[19] R. B. Bird. Transport phenomena. *Applied Mechanics Reviews*, 55(1):R1–R4, 2002.

[20] T. Blickle and L. Thiele. *A comparison of selection schemes used in genetic algorithms.* TIK-Report, Zürich, 1995.

[21] T. Blickle and L. Thiele. A mathematical analysis of tournament selection. In *Proceedings of the 6th International Conference on Genetic Algorithms*, pages 9–16, San Francisco, CA, USA, 1995. Morgan Kaufmann Publishers Inc.

[22] M. Bodenstein. Eine Theorie der photochemischen Reaktionsgeschwindigkeiten. *Z. phys. Chem*, 85(329):0022–3654, 1913.

[23] H. Bongers and L. P. H. De Goey. The effect of simplified transport modeling on the burning velocity of laminar premixed flames. *Combustion science and technology*, 175(10):1915–1928, 2003.

[24] R. Bounaceur, V. Warth, P. A. Glaude, F. Battin-Leclerc, G. Scacchi, G.-M. Côme, T. Faravelli, and E. Ranzi. Chemical lumping of mechanisms generated by computer. application to the modelling of normal butane oxidation. *Journal de chimie physique*, 93(9):1472–1491, 1996.

[25] M. J. Brown, D. B. Smith, and S. C. Taylor. Influence of uncertainties in rate constants on computed burning velocities. *Combustion and flame*, 117(3):652–656, 1999.

[26] A. Burcat. Thermodynamic database. http://garfield.chem.elte.hu/Burcat/burcat.html.

[27] A. Burcat. Thermochemical data for combustion calculations. In *Combustion chemistry*, pages 455–473. Springer, 1984.

[28] A. Burcat and B. Ruscic. Third millenium ideal gas and condensed phase thermochemical database for combustion with updates from active thermochemical tables. Argonne National Laboratory report ANL-05/20, 2005.

[29] V. Bykov and U. Maas. Problem adapted reduced models based on reactiondiffusion manifolds (redims). *Proceedings of the Combustion Institute*, 32(1):561–568, 2009.

[30] L. Cai and H. Pitsch. Mechanism optimization based on reaction rate rules. *Combustion and Flame*, 161(2):405–415, 2014.

[31] L. Cai and H. Pitsch. Optimized chemical mechanism for combustion of gasoline surrogate fuels. *Combustion and Flame*, 162(5):1623–1637, 2015.

[32] H.-H. Carstensen and A. M. Dean. The kinetics of pressure-dependent reactions. *Comprehensive Chemical Kinetics*, 42:101–184, 2007.

[33] H. Chelliah, C. Law, T. Ueda, M. Smooke, and F. Williams. An experimental and theoretical investigation of the dilution, pressure and flow-field effects on the extinction condition of methane-air-nitrogen diffusion flames. *Symposium (International) on Combustion*, 23(1):503–511, 1991.

[34] C. F. Curtiss and J. O. Hirschfelder. Transport properties of multicomponent gas mixtures. *The Journal of Chemical Physics*, 17(6):550–555, 1949.

[35] C. F. Curtiss and J. O. Hirschfelder. Integration of stiff equations. *Proc. Nat. Acad. Sci. U.S.A.*, 38:235–243, 1952.

[36] K. A. De Jong. *An Analysis of the Behavior of a Class of Genetic Adaptive Systems*. PhD thesis, Department of Computer and Communication Sciences, University of Michigan, Ann Arbor, 1975.

[37] K. A. De Jong. Adaptive system design: A genetic approach. *IEEE Transactions on System, Man and Cybernetics*, 10:566–574, 1980.

[38] K. Deb and S. Agrawal. Understanding interactions among genetic algorithm parameters. *Foundations of genetic algorithms*, 5:265–286, 1998.

[39] G. Dixon-Lewis. Flame structure and flame reaction kinetics. ii. transport phenomena in multicomponent systems. *Proceedings of the Royal Society of London A: Mathematical, Physical and Engineering Sciences*, 307(1488):111–135, 1968.

[40] Y. Dong, A. T. Holley, M. G. Andac, F. N. Egolfopoulos, S. G. Davis, P. Middha, and H. Wang. Extinction of premixed H2/air flames: Chemical kinetics and molecular diffusion effects. *Combustion and Flame*, 142(4):374–387, 2005.

[41] S. Dunn. Hydrogen futures: toward a sustainable energy system. *International Journal of Hydrogen Energy*, 27(3):235–264, 2002.

[42] L. Elliott, D. B. Ingham, A. G. Kyne, N. S. Mera, M. Pourkashanian, and C. W. Wilson. A real coded genetic algorithm for the optimisation of reaction rate parameters for chemical kinetic modelling in a perfectly stirred reactor. In *GECCO Late Breaking Papers*, pages 138–145, 2002.

[43] L. Elliott, D. B. Ingham, A. G. Kyne, N. S. Mera, M. Pourkashanian, and C. W. Wilson. Incorporation of physical bounds on rate parameters for reaction mechanism optimization using genetic algorithms. *Combustion Science and Technology*, 175(4):619–648, 2003.

[44] L. Elliott, D. B. Ingham, A. G. Kyne, N. S. Mera, M. Pourkashanian, and C. W. Wilson. Multiobjective genetic algorithm optimization for calculating the reaction rate coefficients for hydrogen combustion. *Industrial & engineering chemistry research*, 42(6):1215–1224, 2003.

[45] L. Elliott, D. B. Ingham, A. G. Kyne, N. S. Mera, M. Pourkashanian, and C. W. Wilson. Genetic algorithms for optimisation of chemical kinetics reaction mechanisms. *Progress in Energy and Combustion Science*, 30(3):297–328, 2004.

[46] L. Elliott, D. B. Ingham, A. G. Kyne, N. S. Mera, M. Pourkashanian, and C. W. Wilson. Reaction mechanism reduction and optimization using genetic algorithms. *Industrial & Engineering Chemistry Research*, 44(4):658–667, 2005.

[47] E. M. Fisher, B. A. Williams, and J. W. Fleming. Determination of the strain in counterflow diffusion flames from flow conditions. *Chemical and physical processes in combustion*, pages 191–194, 1997.

[48] D. B. Fogel and J. W. Atmar. Comparing genetic operators with gaussian mutations in simulated evolutionary processes using linear systems. *Biological Cybernetics*, 63(2):111–114, 1990.

[49] R. Fournet, V. Warth, P. A. Glaude, F. Battin-Leclerc, G. Scacchi, and G. M. Cme. Automatic reduction of detailed mechanisms of combustion of alkanes by chemical lumping. *International Journal of Chemical Kinetics*, 32(1):36–51, 2000.

[50] M. Frenklach, H. Wang, and M. J. Rabinowitz. Optimization and analysis of large chemical kinetic mechanisms using the solution mapping method - combustion of methane. *Progress in Energy and Combustion Science*, 18(1):47–73, 1992.

[51] R. G. Gilbert, K. Luther, and J. Troe. Theory of thermal unimolecular reactions in the fall-off range. II. Weak collision rate constants. *Berichte der Bunsengesellschaft für physikalische Chemie*, 87(2):169–177, 1983.

[52] I. Glassman and R. Yetter. *Combustion*. Elsevier Science, 2008.

[53] D. E. Goldberg. *Genetic Algorithms in Search, Optimization and Machine Learning*. Addison-Wesley Longman Publishing Co., Inc., Boston, MA, USA, 1st edition, 1989.

[54] D. E. Goldberg and K. Deb. A comparative analysis of selection schemes used in genetic algorithms. *Foundations of genetic algorithms*, 1:69–93, 1991.

[55] D. G. Goodwin. Cantera: An object-oriented software toolkit for chemical kinetics, thermodynamics, and transport processes. http://code.google.com/p/cantera, 2009.

[56] D. A. Goussis and S. H. Lam. Twenty-fourth symposium on combustion a study of homogeneous methanol oxidation kinetics using CSP. *Symposium (International) on Combustion*, 24(1):113–120, 1992.

[57] J. F. Grcar, R. J. Kee, M. D. Smooke, and J. A. Miller. A hybrid newton/time-integration procedure for the solution of steady, laminar, one-dimensional, premixed flames. *Symposium (International) on Combustion*, 21(1):1773–1782, 1988.

[58] J. Griffiths. Reduced kinetic models and their application to practical combustion systems. *Progress in Energy and Combustion Science*, 21(1):25–107, 1995.

[59] E. Hairer, S. Nørsett, and G. Wanner. *Solving Ordinary Differential Equations II: Stiff and Differential-Algebraic Problems*. Lecture Notes in Economic and Mathematical Systems. Springer, 1996.

[60] S. D. Harris, L. Elliott, D. B. Ingham, M. Pourkashanian, and C. W. Wilson. The optimisation of reaction rate parameters for chemical kinetic modelling of combustion using genetic algorithms. *Computer methods in applied mechanics and engineering*, 190:1065–1090, 2000.

[61] K. He, I. P. Androulakis, and M. G. Ierapetritou. On-the-fly reduction of kinetic mechanisms using element flux analysis. *Chemical Engineering Science*, 65(3):1173–1184, 2010.

[62] K. He, M. G. Ierapetritou, and I. P. Androulakis. A graph-based approach to developing adaptive representations of complex reaction mechanisms. *Combustion and Flame*, 155(4):585–604, 2008.

[63] K. Héberger, S. Kemény, and T. Vidóczy. On the errors of arrhenius parameters and estimated rate constant values. *International journal of chemical kinetics*, 19(3):171–181, 1987.

[64] F. Herrera, M. Lozano, and J. L. Verdegay. Tackling real-coded genetic algorithms: Operators and tools for behavioural analysis. *Artif. Intell. Rev.*, 12(4):265–319, Aug. 1998.

[65] J. Hesser and R. Männer. Towards on optimal mutation probability for genetic algorithms. In *Proceedings of Parallel Problem Solving from Nature Conference*, pages 23–32, 1990.

[66] R. Hinterding. Gaussian mutation and self-adaption for numeric genetic algorithms. In *Evolutionary Computation, 1995., IEEE International Conference on*, volume 1, pages 384–389. IEEE, 1995.

[67] J. O. Hirschfelder. Some remarks on the theory of flame propagation. *Symposium (International) on Combustion*, 9(1):553–559, 1963.

[68] J. O. Hirschfelder and C. F. Curtiss. The theory of flame propagation. *The Journal of Chemical Physics*, 17(11):1076–1081, 1949.

[69] J. O. Hirschfelder, C. F. Curtiss, R. B. Bird, and M. G. Mayer. *Molecular theory of gases and liquids*, volume 26. Wiley New York, 1954.

[70] J. H. Holland. *Adaptation in natural and artificial systems: an introductory analysis with applications to biology, control, and artificial intelligence.* University of Michigan Press, 1975.

[71] H. Huang, M. Fairweather, J. Griffiths, A. Tomlin, and R. Brad. A systematic lumping approach for the reduction of comprehensive kinetic models. *Proceedings of the Combustion Institute*, 30(1):1309–1316, 2005.

[72] K. J. Hughes, M. Fairweather, J. F. Griffiths, R. Porter, and A. S. Tomlin. The application of the QSSA via reaction lumping for the reduction of complex hydrocarbon oxidation mechanisms. *Proceedings of the Combustion Institute*, 32(1):543–551, 2009.

[73] B. Johnston, M. C. Mayo, and A. Khare. Hydrogen: the energy source for the 21st century. *Technovation*, 25(6):569–585, 2005.

[74] R. Kee, M. Coltrin, and P. Glarborg. *Chemically Reacting Flow: Theory and Practice*. Wiley, 2005.

[75] R. J. Kee and J. A. Miller. Computational modeling of flame structure. *Physica D: Nonlinear Phenomena*, 12(13):198–211, 1984.

[76] R. J. Kee, F. M. Rupley, J. A. Miller, M. E. Coltrin, J. F. Grcar, E. Meeks, H. K. Moffat, A. E. Lutz, G. Dixon-Lewis, M. D. Smooke, and J. Warnatz. OPPDIF, CHEMKIN collection, release 3.5, reaction design. *Inc., San Diego, CA*, 1999.

[77] R. J. Kee, F. M. Rupley, J. A. Miller, M. E. Coltrin, J. F. Grcar, E. Meeks, H. K. Moffat, A. E. Lutz, G. Dixon-Lewis, M. D. Smooke, J. Warnatz, G. H. Evans, R. S. Larson, R. E. Mitchell, L. R. Petzold, W. C. Reynolds, M. Caracotsios, W. E. Stewart, P. Glarborg, C. Wang, C. L. McLellan, O. Adigun, W. G. Houf, C. P. Chou, S. F. Miller, P. Ho, P. D. Young, D. J. Young, D. W. Hodgson, M. V. Petrova, and K. V. Puduppakkam. CHEMKIN Release 4.1. Reaction Design, San Diego, CA, 2006.

[78] K. Knig and U. Maas. On-demand generation of reduced mechanisms based on hierarchically extended intrinsic low-dimensional manifolds in generalized coordinates. *Proceedings of the Combustion Institute*, 32(1):553–560, 2009.

[79] A. A. Konnov. Remaining uncertainties in the kinetic mechanism of hydrogen combustion. *Combustion and flame*, 152(4):507–528, 2008.

[80] M. A. Kramer, H. Rabitz, J. M. Calo, and R. J. Kee. Sensitivity analysis in chemical kinetics: Recent developments and computational comparisons. *International Journal of Chemical Kinetics*, 16(5):559–578, 1984.

[81] J. C. W. Kuo and J. Wei. Lumping analysis in monomolecular reaction systems. analysis of approximately lumpable system. *Industrial & Engineering Chemistry Fundamentals*, 8(1):124–133, 1969.

[82] K. K. Kuo. *Principles of combustion*. Wiley New York et al., 1986.

[83] S. H. Lam. Singular perturbation for stiff equations using numerical methods. In C. Casci and C. Bruno, editors, *Recent Advances in the Aerospace Sciences: In Honor of Luigi Crocco on His Seventy-fifth Birthday*, pages 3–19. Springer US, Boston, MA, 1985.

[84] S. H. Lam. Using CSP to understand complex chemical kinetics. *Combustion Science and Technology*, 89(5-6):375–404, 1993.

[85] S. H. Lam. Model reductions with special CSP data. *Combustion and Flame*, 160(12):2707–2711, 2013.

[86] S. H. Lam and D. A. Goussis. Understanding complex chemical kinetics with computational singular perturbation. *Symposium (International) on Combustion*, 22(1):931–941, 1989.

[87] S. H. Lam and D. A. Goussis. Sensitivity analysis of complex simulations using basis vectors. In R. Vichnevetsky and J. H. Miller, editors, *Proceedings of the 13th IMACS World Congress on Computation and Applied Mathematics*, volume 3, pages 1992–1994. Criterion Press, Dublin, Ireland, 1991.

[88] S. H. Lam and D. A. Goussis. The CSP method for simplifying kinetics. *International Journal of Chemical Kinetics*, 26(4):461–486, 1994.

[89] C. K. Law. *Combustion Physics*. Cambridge University Press, 2006.

[90] C. K. Law. Combustion at a crossroads: Status and prospects. *Proceedings of the Combustion Institute*, 31(1):1–29, 2007.

[91] C. K. Law, C. J. Sung, H. Wang, and T. Lu. Development of comprenhensive detailed and reduced reaction mechanisms for combustion modeling. *AIAA Journal*, 41(9):1629–1646, 2003.

[92] G. Li and H. Rabitz. A general analysis of exact lumping in chemical kinetics. *Chemical Engineering Science*, 44(6):1413–1430, 1989.

[93] G. Li, H. Rabitz, and J. Tóth. A general analysis of exact nonlinear lumping in chemical kinetics. *Chemical Engineering Science*, 49(3):343–361, 1994.

[94] G. Li, A. S. Tomlin, H. Rabitz, and J. Tóth. A general analysis of approximate nonlinear lumping in chemical kinetics. i. unconstrained lumping. *The Journal of Chemical Physics*, 101(2):1172–1187, 1994.

[95] J. Li, Z. Zhao, A. Kazakov, and F. L. Dryer. An updated comprehensive kinetic model of hydrogen combustion. *International Journal of Chemical Kinetics*, 36(10):566–575, 2004.

[96] F. A. Lindemann, S. Arrhenius, I. Langmuir, N. R. Dhar, J. Perrin, and W. C. M. Lewis. The radiation theory of chemical action. *Trans. Faraday Soc.*, 17:598–606, 1922.

[97] L. A. Lovachev. Chemical kinetics in flames a review. *Combustion Science and Technology*, 25(1-2):49–69, 1981.

[98] T. Løvås. Automatic generation of skeletal mechanisms for ignition combustion based on level of importance analysis. *Combustion and Flame*, 156(7):1348–1358, 2009.

[99] T. Lu, Y. Ju, and C. K. Law. Complex csp for chemistry reduction and analysis. *Combustion and Flame*, 126(1):1445–1455, 2001.

[100] T. Lu and C. K. Law. A directed relation graph method for mechanism reduction. *Proceedings of the Combustion Institute*, 30(1):1333–1341, 2005.

[101] T. Lu and C. K. Law. Linear time reduction of large kinetic mechanisms with directed relation graph: n-heptane and iso-octane. *Combustion and Flame*, 144(12):24–36, 2006.

[102] T. Lu and C. K. Law. On the applicability of directed relation graphs to the reduction of reaction mechanisms. *Combustion and Flame*, 146(3):472–483, 2006.

[103] T. Lu and C. K. Law. Diffusion coefficient reduction through species bundling. *Combustion and Flame*, 148(3):117–126, 2007.

[104] T. Lu and C. K. Law. Strategies for mechanism reduction for large hydrocarbons: n-heptane. *Combustion and Flame*, 154(12):153–163, 2008.

[105] T. Lu and C. K. Law. Toward accommodating realistic fuel chemistry in large-scale computations. *Progress in Energy and Combustion Science*, 35(2):192–215, 2009.

[106] U. Maas and S. Pope. Simplifying chemical kinetics: Intrinsic low-dimensional manifolds in composition space. *Combustion and Flame*, 88(3):239–264, 1992.

[107] A. Massias, D. Diamantis, E. Mastorakos, and D. A. Goussis. An algorithm for the construction of global reduced mechanisms with CSP data. *Combustion and Flame*, 117(4):685–708, 1999.

[108] A. Massias, D. Diamantis, E. Mastorakos, and D. A. Goussis. Global reduced mechanisms for methane and hydrogen combustion with nitric oxide formation constructed with CSP data. *Combustion Theory and Modelling*, 3(2):233–257, 1999.

[109] S. Mathur, P. Tondon, and S. Saxena. Thermal conductivity of binary, ternary and quaternary mixtures of rare gases. *Molecular Physics*, 12(6):569–579, 1967.

[110] Z. Michalewicz. *Genetic Algorithms + Data Structures = Evolution Programs*. Springer-Verlag, AI Series, New York, 1996.

[111] B. L. Miller and D. E. Goldberg. Genetic algorithms, tournament selection, and the effects of noise. *Complex Systems*, 9(3):193–212, 1995.

[112] J. A. Miller, M. C. Branch, W. J. McLean, D. W. Chandler, M. D. Smooke, and R. J. Kee. The conversion of HCN to NO and N2 in H2-O2-HCN-Ar flames at low pressure. In *Symposium (International) on Combustion*, volume 20(1), pages 673–684. Elsevier, 1985.

[113] J. A. Miller and G. A. Fisk. Combustion chemistry. *Chem. Eng. News*, 65:22–46, 1987.

[114] J. A. Miller, R. J. Kee, and C. K. Westbrook. Chemical kinetics and combustion modeling. *Annual Review of Physical Chemistry*, 41(1):345–387, 1990.

[115] J. A. Miller, R. E. Mitchell, M. D. Smooke, and R. J. Kee. Toward a comprehensive chemical kinetic mechanism for the oxidation of acetylene: comparison of model predictions with results from flame and shock tube experiments. In *Symposium (International) on Combustion*, volume 19(1), pages 181–196. Elsevier, 1982.

[116] J. A. Miller, M. D. Smooke, R. M. Green, and R. J. Kee. Kinetic modeling of the oxidation of ammonia in flames. *Combustion Science and Technology*, 34(1-6):149–176, 1983.

[117] M. Mitchell. *An Introduction to Genetic Algorithms*. The MIT Press, 1996.

[118] A. Mitsos, G. M. Oxberry, P. I. Barton, and W. H. Green. Optimal automatic reaction and species elimination in kinetic mechanisms. *Combustion and Flame*, 155(12):118–132, 2008.

[119] M. Momirlan and T. Veziroglu. The properties of hydrogen as fuel tomorrow in sustainable energy system for a cleaner planet. *International Journal of Hydrogen Energy*, 30(7):795–802, 2005.

[120] L. Monchick and E. A. Mason. Transport properties of polar gases. *The Journal of Chemical Physics*, 35(5):1676–1697, 1961.

[121] C. J. Montgomery, C. Yang, A. R. Parkinson, and J.-Y. Chen. Selecting the optimum quasi-steady-state species for reduced chemical kinetic mechanisms using a genetic algorithm. *Combustion and Flame*, 144(12):37–52, 2006.

[122] T. Nagy and T. Turányi. Reduction of very large reaction mechanisms using methods based on simulation error minimization. *Combustion and Flame*, 156(2):417–428, 2009.

[123] T. Nagy and T. Turányi. Uncertainty analysis of varying temperature chemical kinetic systems. *Procedia-Social and Behavioral Sciences*, 2(6):7757–7758, 2010.

[124] T. Nagy and T. Turányi. Uncertainty of arrhenius parameters. *International Journal of Chemical Kinetics*, 43(7):359–378, 2011.

[125] T. Nagy and T. Turányi. Determination of the uncertainty domain of the Arrhenius parameters needed for the investigation of combustion kinetic models. *Reliability Engineering & System Safety*, 107:29–34, 2012.

[126] H. N. Najm, B. J. Debusschere, Y. M. Marzouk, S. Widmer, and O. P. Le Matre. Uncertainty quantification in chemical systems. *International Journal for Numerical Methods in Engineering*, 80(6-7):789–814, 2009.

[127] K. E. Niemeyer and C. Sung. DRGEP-based mechanism reduction strategies: graph search algorithms and skeletal primary reference fuel mechanisms. In *49th AIAA Aerospace Sciences Meeting including the New Horizons Forum and Aerospace Exposition*, page 508, 2011.

[128] K. E. Niemeyer and C.-J. Sung. On the importance of graph search algorithms for DRGEP-based mechanism reduction methods. *Combustion and Flame*, 158(8):1439–1443, 2011.

[129] K. E. Niemeyer, C.-J. Sung, and M. P. Raju. Skeletal mechanism generation for surrogate fuels using directed relation graph with error propagation and sensitivity analysis. *Combustion and Flame*, 157(9):1760–1770, 2010.

[130] M. O' Conaire, H. J. Curran, J. M. Simmie, W. J. Pitz, and C. K. Westbrook. A comprehensive modeling study of hydrogen oxidation. *International Journal of Chemical Kinetics*, 36(11):603–622, 2004.

[131] G. Ochoa, I. Harvey, and H. Buxton. On recombination and optimal mutation rates. In *Proceedings of Genetic and Evolutionary Computation Conference*, pages 488–495, 1999.

[132] M. S. Okino and M. L. Mavrovouniotis. Simplification of mathematical models of chemical reaction systems. *Chemical reviews*, 98(2):391–408, 1998.

[133] P. Papas, J. W. Fleming, and R. S. Sheinson. Extinction of non-premixed methane- and propane-air counterflow flames inhibited with CF4, CF3H and CF3Br. In *Symposium (International) on Combustion*, volume 26(1), pages 1405–1411. Elsevier, 1996.

[134] P. Pepiot-Desjardins and H. Pitsch. An automatic chemical lumping method for the reduction of large chemical kinetic mechanisms. *Combustion Theory and Modelling*, 12(6):1089–1108, 2008.

[135] P. Pepiot-Desjardins and H. Pitsch. An efficient error-propagation-based reduction method for large chemical kinetic mechanisms. *Combustion and Flame*, 154(12):67–81, 2008.

[136] F. Perini. *Optimally reduced reaction mechanisms for Internal Combustion Engines running on biofuels*. PhD thesis, Universitá di Modena e Reggio Emilia, 2011.

[137] F. Perini, J. L. Brakora, R. D. Reitz, and G. Cantore. Development of reduced and optimized reaction mechanisms based on genetic algorithms and element flux analysis. *Combustion and Flame*, 159(1):103–119, 2012.

[138] M. J. Pilling and P. W. Seakins. *Reaction kinetics*. Oxford University Press, 1996.

[139] T. Poinsot and D. Veynante. *Theoretical and Numerical Combustion*. Edwards, 2005.

[140] W. Polifke, W. Geng, and K. Döbbeling. Optimization of rate coefficients for simplified reaction mechanisms with genetic algorithms. *Combustion and Flame*, 113(1):119–134, 1998.

[141] F. Proch, M. Rieth, A. Rittler, and A. Kempf. Highly-resolved numerical simulation of the turbulent combustion process in experimental burners. In K. Binder, M. Müller, M. Kremer, and A. Schnurpfeil, editors, *Proceedings*, volume 48 of *NIC Symposium*, pages 373–380. Forschungszentrum Jülich, 2016.

[142] H. Rabitz, M. Kramer, and D. Dacol. Sensitivity analysis in chemical kinetics. *Annual review of physical chemistry*, 34(1):419–461, 1983.

[143] E. Ranzi, M. Dente, A. Goldaniga, G. Bozzano, and T. Faravelli. Lumping procedures in detailed kinetic modeling of gasification, pyrolysis, partial oxidation and combustion of hydrocarbon mixtures. *Progress in Energy and Combustion Science*, 27(1):99–139, 2001.

[144] E. Ranzi, T. Faravelli, P. Gaffuri, and A. Sogaro. Low-temperature combustion: Automatic generation of primary oxidation reactions and lumping procedures. *Combustion and Flame*, 102(1):179–192, 1995.

[145] Z. Ren and S. B. Pope. The use of slow manifolds in reactive flows. *Combustion and flame*, 147(4):243–261, 2006.

[146] J. Revel, J. C. Boettner, M. Cathonnet, and J. S. Bachman. Derivation of a global chemical kinetic mechanism for methane ignition and combustion. *J. Chim. Phys. Phys. Chim. Biol.*, 91(4):365–382, 1994.

[147] S. Rolland and J. M. Simmie. The comparison of detailed chemical kinetic mechanisms: Application to the combustion of methane. *International Journal of Chemical Kinetics*, 36(9):467–471, 2004.

[148] M. D. Rumminger, D. Reinelt, V. Babushok, and G. T. Linteris. Numerical study of the inhibition of premixed and diffusion flames by iron pentacarbonyl1. *Combustion and Flame*, 116(12):207–219, 1999.

[149] B. Ruscic, J. E. Boggs, A. Burcat, A. G. Császár, J. Demaison, R. Janoschek, J. M. L. Martin, M. L. Morton, M. J. Rossi, J. F. Stanton, P. G. Szalay, P. R. Westmoreland, F. Zabel, and T. Bérces. IUPAC critical evaluation of thermochemical properties of selected radicals. Part I. *Journal of physical and chemical reference data*, 34(2):573–656, 2005.

[150] C. Saggese, A. Frassoldati, A. Cuoci, T. Faravelli, and E. Ranzi. A lumped approach to the kinetic modeling of pyrolysis and combustion of biodiesel fuels. *Proceedings of the Combustion Institute*, 34(1):427–434, 2013.

[151] A. Saltelli, M. Ratto, S. Tarantola, and F. Campolongo. Sensitivity analysis for chemical models. *Chemical Reviews*, 105(7):2811–2828, 2005. PMID: 16011325.

[152] R. Sankaran, E. R. Hawkes, J. H. Chen, T. Lu, and C. K. Law. Structure of a spatially developing turbulent lean methaneair Bunsen flame. *Proceedings of the Combustion Institute*, 31(1):1291–1298, 2007.

[153] S. M. Sarathy, S. Vranckx, K. Yasunaga, M. Mehl, P. Oßwald, W. K. Metcalfe, C. K. Westbrook, W. J. Pitz, K. Kohse-Höinghaus, R. X. Fernandes, and H. J.

Curran. A comprehensive chemical kinetic combustion model for the four butanol isomers. *Combustion and Flame*, 159(6):2028–2055, 2012.

[154] D. A. Schwer, P. Lu, and W. H. Green Jr. An adaptive chemistry approach to modeling complex kinetics in reacting flows. *Combustion and Flame*, 133(4):451–465, 2003.

[155] P. W. Seakins. Product branching ratios in simple gas phase reactions. *Annu. Rep. Prog. Chem., Sect. C: Phys. Chem.*, 103:173–222, 2007.

[156] I. Sedyó, T. Nagy, I. G. Zsély, and T. Turányi. Uncertainty of the arrhenius parameters of important elementary reactions of the hydrogen- oxygen system. In *Proceedings of the European Combustion Meeting*, 2011. Paper 163.

[157] R. Shaw, G. Brownbridge, S. Mosbach, M. Kraft, and T. Løvås. Using timescale analysis for optimising large chemical mechanisms. *Preprint series of the Cambridge Centre of Computational Chemical Engineering*, 112, 2012.

[158] D. A. Sheen and H. Wang. Combustion kinetic modeling using multispecies time histories in shock-tube oxidation of heptane. *Combustion and Flame*, 158(4):645–656, 2011.

[159] D. A. Sheen and H. Wang. The method of uncertainty quantification and minimization using polynomial chaos expansions. *Combustion and Flame*, 158(12):2358–2374, 2011.

[160] D. A. Sheen, X. You, H. Wang, and T. Løvås. Spectral uncertainty quantification, propagation and optimization of a detailed kinetic model for ethylene combustion. *Proceedings of the Combustion Institute*, 32(1):535–542, 2009.

[161] N. Sikalo, O. Hasemann, C. Schulz, A. Kempf, and I. Wlokas. A genetic algorithm-based method for the automatic reduction of reaction mechanisms. *International Journal of Chemical Kinetics*, 46(1):41–59, 2014.

[162] N. Sikalo, O. Hasemann, C. Schulz, A. Kempf, and I. Wlokas. A genetic algorithm–based method for the optimization of reduced kinetics mechanisms. *International Journal of Chemical Kinetics*, 47(11):695–723, 2015.

[163] G. P. Smith, D. M. Golden, M. Frenklach, B. Eiteener, M. Goldenberg, C. T. Bowman, R. K. Hanson, W. C. Gardiner, V. V. Lissianski, and Z. W. Qin. GRI-Mech 3.0, 2000.

[164] M. D. Smooke. Solution of burner-stabilized premixed laminar flames by boundary value methods. *Journal of Computational Physics*, 48(1):72–105, 1982.

[165] M. D. Smooke, J. A. Miller, and R. J. Kee. Determination of adiabatic flame speeds by boundary value methods. *Combustion Science and Technology*, 34(1-6):79–90, 1983.

[166] M. D. Smooke, H. Rabitz, Y. Reuven, and F. L. Dryer. Application of sensitivity analysis to premixed hydrogen-air flames. *Combustion Science and Technology*, 59(4-6):295–319, 1988.

[167] B. D. Solomon and A. Banerjee. A global survey of hydrogen energy research, development and policy. *Energy Policy*, 34(7):781–792, 2006.

[168] W. M. Spears and K. A. De Jong. On the virtues of parameterized uniform crossover. In *In Proceedings of the Fourth International Conference on Genetic Algorithms*, 1991.

[169] A. Stagni, A. Cuoci, A. Frassoldati, T. Faravelli, and E. Ranzi. Lumping and reduction of detailed kinetic schemes: an effective coupling. *Industrial & Engineering Chemistry Research*, 53(22):9004–9016, 2014.

[170] P. H. Stewart, C. W. Larson, and D. M. Golden. Pressure and temperature dependence of reactions proceeding via a bound complex. 2. application to $2CH_3 \rightarrow C_2H_5 + H$. *Combustion and Flame*, 75(1):25–31, 1989.

[171] W. Sun, Z. Chen, X. Gou, and Y. Ju. A path flux analysis method for the reduction of detailed chemical kinetic mechanisms. *Combustion and Flame*, 157(7):1298–1307, 2010.

[172] G. Syswerda. Uniform crossover in genetic algorithms. In J. Shaffer, editor, *Proceedings of the Third International Conference on Genetic Algorithms*. Morgan Kaufmann Publishers, Inc., 1989.

[173] A. S. Tomlin. The role of sensitivity and uncertainty analysis in combustion modelling. *Proceedings of the Combustion Institute*, 34(1):159–176, 2013.

[174] A. S. Tomlin, M. J. Pilling, T. Turányi, J. H. Merkin, and J. Brindley. Mechanism reduction for the oscillatory oxidation of hydrogen: sensitivity and quasi-steady-state analyses. *Combustion and Flame*, 91(2):107–130, 1992.

[175] A. S. Tomlin and T. Turányi. Mechanism reduction to skeletal form and species lumping. In F. Battin-Leclerc, M. J. Simmie, and E. Blurock, editors, *Cleaner Combustion: Developing Detailed Chemical Kinetic Models*, pages 447–466. Springer London, London, 2013.

[176] A. S. Tomlin, T. Turányi, and M. J. Pilling. Mathematical tools for the construction, investigation and reduction of combustion mechanisms. In M. J. Pilling, editor, *Low-Temperature Combustion and Autoignition*, volume 35 of *Comprehensive Chemical Kinetics*, pages 293–437. Elsevier, 1997.

[177] J. Troe. Predictive possibilities of unimolecular rate theory. *Journal of Physical Chemistry*, 83(1):114–126, 1979.

[178] J. Troe. Theory of thermal unimolecular reactions in the fall-off range. I. Strong collision rate constants. *Berichte der Bunsengesellschaft für physikalische Chemie*, 87(2):161–169, 1983.

[179] T. Turányi. Sensitivity analysis of complex kinetic systems. Tools and applications. *Journal of Mathematical Chemistry*, 5(3):203–248, 1990.

[180] T. Turányi. The role of sensitivity analysis in the corroboration of models and its links to model structural and parametric uncertainty applications of sensitivity analysis to combustion chemistry. *Reliability Engineering & System Safety*, 57(1):41–48, 1997.

[181] T. Turányi, T. Nagy, I. G. Zsély, M. Cserháti, T. Varga, B. Szabó, I. Sedyó, P. Kiss, A. Zempléni, and H. Curran. Determination of rate parameters based on both direct and indirect measurements. *International Journal of Chemical Kinetics*, 44(5):284–302, 2012.

[182] T. Turányi and A. S. Tomlin. *Analysis of Kinetic Reaction Mechanisms*. Springer, 2014.

[183] T. Turányi, L. Zalotai, S. Dóbé, and T. Bérces. Effect of the uncertainty of kinetic and thermodynamic data on methane flame simulation results. *Physical Chemistry Chemical Physics*, 4(12):2568–2578, 2002.

[184] M. Valorani, F. Creta, F. Donato, H. N. Najm, and D. A. Goussis. Skeletal mechanism generation and analysis for n-heptane with CSP. *Proceedings of the Combustion Institute*, 31(1):483–490, 2007.

[185] M. Valorani, F. Creta, D. Goussis, J. Lee, and H. Najm. An automatic procedure for the simplification of chemical kinetic mechanisms based on CSP. *Combust. Flame*, 146:29–51, 2006.

[186] L. Varga, B. Szabó, I. G. Zsély, A. Zempléni, and T. Turányi. Numerical investigation of the uncertainty of arrhenius parameters. *Journal of mathematical chemistry*, 49(8):1798–1809, 2011.

[187] P. K. Venkatesh. Damped pseudospectral functional forms of the falloff behavior of unimolecular reactions. *The Journal of Physical Chemistry A*, 104(2):280–287, 2000.

[188] P. K. Venkatesh, A. Y. Chang, A. M. Dean, M. H. Cohen, and R. W. Carr. Parameterization of pressure-and temperature-dependent kinetics in multiple well reactions. *AIChE journal*, 43(5):1331–1340, 1997.

[189] H. Wang and M. Frenklach. Detailed reduction of reaction mechanisms for flame modeling. *Combustion and Flame*, 87(3):365–370, 1991.

[190] H. Wang, X. You, A. V. Joshi, S. G. Davis, A. Laskin, F. Egolfopoulos, and C. K. Law. USC Mech version II. high-temperature combustion reaction model of H2/CO/C1-C4 compounds. http://ignis.usc.edu/USC_Mech_II.htm, 2007.

[191] Q.-D. Wang, Y.-M. Fang, F. Wang, and X.-Y. Li. Systematic analysis and reduction of combustion mechanisms for ignition of multi-component kerosene surrogate. *Proceedings of the Combustion Institute*, 34(1):187–195, 2013.

[192] J. Warnatz, U. Maas, and R. W. Dibble. *Combustion: Physical and Chemical Fundamentals, Modeling and Simulation, Experiments, Pollutant Formation*. Springer Science & Business Media, 2006.

[193] C. K. Westbrook and F. L. Dryer. Simplified reaction mechanisms for the oxidation of hydrocarbon fuels in flames. *Combustion Science and Technology*, 27(1-2):31–43, 1981.

[194] C. K. Westbrook and F. L. Dryer. Chemical kinetic modeling of hydrocarbon combustion. *Progress in Energy and Combustion Science*, 10(1):1–57, 1984.

[195] F. Westley. Table of recommended rate constants for chemical reactions occurring in combustion. no. NSRDS-NBS-67. Technical report, DTIC Document, 1980.

[196] D. L. Whitley. The GENITOR algorithm and selection pressure: Why rank-based allocation of reproductive trials is best. In J. Schaffer, editor, *Proceedings of the Third International Conference on Genetic Algorithms*, volume 89, pages 116–123. Morgan Kaufmann Publishers, San Mateo, CA, 1989.

[197] C. R. Wilke. A viscosity equation for gas mixtures. *The Journal of Chemical Physics*, 18(4):517–519, 1950.

[198] F. A. Williams. *Combustion Theory: The Fundamental Theory of Chemically Reacting Flow Systems*. Combustion science and engineering series. Perseus Books Group, 1985.

[199] I. Wlokas, A. Faccinetto, B. Tribalet, C. Schulz, and A. Kempf. Mechanism of iron oxide formation from iron pentacarbonyl-doped low-pressure hydrogen/oxygen flames. *International Journal of Chemical Kinetics*, 45(8):487–498, 2013.

[200] Y. Xin, D. A. Sheen, H. Wang, and C. K. Law. Skeletal reaction model generation, uncertainty quantification and minimization: Combustion of butane. *Combustion and Flame*, 161(12):3031–3039, 2014.

[201] Z. Yang, B. Yang, and H. Wang. The influence of h-atom diffusion coefficient on laminar flame simulation. In *Proceedings of the Second Joint Meeting of the U.S. Sections of the Combustion Institute*. Berkeley, CA, March 2001. Paper 237.

[202] G. H. Yeoh and K. K. Yuen. *Computational fluid dynamics in fire engineering: Theory, modelling and practice*. Butterworth-Heinemann, 2009.

[203] R. A. Yetter, F. L. Dryer, and H. Rabitz. A comprehensive reaction mechanism for carbon monoxide/hydrogen/oxygen kinetics. *Combustion Science and Technology*, 79(1-3):97–128, 1991.

[204] J. Zádor, C. A. Taatjes, and R. X. Fernandes. Kinetics of elementary reactions in low-temperature autoignition chemistry. *Progress in energy and combustion science*, 37(4):371–421, 2011.

[205] J. Zádor, I. G. Zsely, and T. Turányi. Local and global uncertainty analysis of complex chemical kinetic systems. *Reliability Engineering & System Safety*, 91(10):1232–1240, 2006.

[206] J. Zádor, I. G. Zsely, T. Turányi, M. Ratto, S. Tarantola, and A. Saltelli. Local and global uncertainty analyses of a methane flame model. *The Journal of Physical Chemistry A*, 109(43):9795–9807, 2005.

[207] S. Zhang, I. P. Androulakis, and M. G. Ierapetritou. A hybrid kinetic mechanism reduction scheme based on the on-the-fly reduction and quasi-steady-state approximation. *Chemical Engineering Science*, 93(0):150–162, 2013.

[208] X. Zheng, T. Lu, and C. Law. Experimental counterflow ignition temperatures and reaction mechanisms of 1,3-butadiene. *Proceedings of the Combustion Institute*, 31(1):367–375, 2007.

[209] J. Zhong, X. Hu, M. Gu, and J. Zhang. Comparison of performance between different selection strategies on simple genetic algorithms. In *Computational Intelligence for Modelling, Control and Automation, 2005 and International Conference on Intelligent Agents, Web Technologies and Internet Commerce*, volume 2, pages 1115–1121. IEEE, 2005.

[210] I. G. Zsély, T. Nagy, J. M. Simmie, and H. J. Curran. Reduction of a detailed kinetic model for the ignition of methane/propane mixtures at gas turbine conditions using simulation error minimization methods. *Combustion and Flame*, 158(8):1469–1479, 2011.

[211] I. G. Zsély, J. Zádor, and T. Turányi. Uncertainty analysis backed development of combustion mechanisms. In *Proc Combust Inst*, volume 30, pages 1273–1281, 2005.

[212] I. G. Zsély, J. Zádor, and T. Turányi. Uncertainty analysis of NO production during methane combustion. *International Journal of Chemical Kinetics*, 40(11):754–768, 2008.